Biosensors for detection of colorectal cancer

Shazana Hilda Binti Shamsuddin

Submitted in accordance with the requirements for the degree of
Doctor of Philosophy

The University of Leeds

School of Biomedical Sciences

Faculty of Biological Sciences

November 2018

Declaration

The candidate confirms that the work submitted is her own and that appropriate credit has been given where reference has been made to the work of others.

This copy has been supplied on the understanding that it is copyright material and that no quotation from the thesis may be published without proper acknowledgement

The right of Shazana Hilda Binti Shamsuddin to be identified as Author of this work has been asserted by her in accordance with the Copyright, Designs and Patents Act 1988.

i

Acknowledgement

First and foremost, I would like to express my deepest gratitude to the Almighty Allah for His countless blessing that has brought me this far. I gratefully acknowledge the financial support from the Ministry of Higher Education of Malaysia and Universiti Sains Malaysia for this research. This PhD would not have been possible without the support of many people. My deepest thanks go to my wonderful supervisor, Professor Paul Millner for the exceptional supervision and for being a very supportive and encouraging throughout my study in Leeds. He has the unique ability to calm me when I am worried and inspire me when I am doubtful. There is no words that can describe how much gratitude I owe you. I hope that one day, I can mentor someone in the way Paul has mentored me.

Special thanks go to my co-supervisors, Prof. Michael McPherson and Dr. Darren Tomlinson and the BSTG team particularly Anna, Tom and Cristian for their invaluable technical expertise and support in Affimer production. I am also highly indebted to Prof. David Jayne and his team member at the Leeds Institute of Medical Research, St James Hospital for giving me the opportunity to use their tissue culture facilities. Many thanks to Dr. Iain Manfield for his technical advices in SPR and Dr. Tim Gibson and Mr. Duncan Sharp for their kind assistance in the electrochemistry experiments. Within the Millner's group I wish to thank members both past and present for making this PhD journey enjoyable. Special thanks to Sherry and Eiman, who keep me sane and made my day colourful when the going gets tough. To my writing buddy, Shafa, I am grateful we are completing this journey together.To my dearest best friends, Janet,Yana and Raisah, thank you for your understanding and endless supports.

I would like to express my sincerest gratitude to my wonderful parents, Shamsuddin Harun and Norvaiti Burhan Nordin for their unwavering supports and unmeasureable love that they have given me. To my biggest supporters, Makcik Norisham, my siblings (Abang,Achik,Adik and Haziq), nieces, nephew and my family in-law, thank you for being very patient and for positive encouragements over the past four years. And finally, to the most important person who is the reason I took this journey, my dearest husband, Mohd Zulkifli, thank you for letting me spread my wings and discover this remarkable journey. Without your sacrifices and blesses, I will never be able to complete this journey alone. I dedicate this PhD to all of you especially to my late-mama who is the reason I pursue study in cancer research.

Abstract

Morbidity and mortality rates of colorectal cancer (CRC) remain among the highest in cancer cases due to late detection. Conventional diagnostics are complicated, often invasive and time-consuming with variable sensitivity and specificity. Carcinoembryonic antigen (CEA) is the only validated blood biomarker routinely used for prognostic screening of advanced CRC. Therefore, development of a highly sensitive, specific and rapid diagnosis device, such as a biosensors is needed. Most biosensors developed currently are antibody-based which restricts their commercialisation due to stability, cost and variability batch-to-batch. The main aim of this study was to develop impedimetric biosensors that are inexpensive and with simple fabrication using anti-CEA Affimers as novel bioreceptors. Initially, the anti-CEA Affimers were selected from a phage display library and characterized for specificity binding against CEA. Ultimately, anti-CEA Affimer-based biosensors were fabricated on DropSens screen printed gold electrodes coated with a novel non-conducting polymer layer, polyoctopamine (POct), for CEA detection. Electrochemical characterisation of developed biosensors was performed via cyclic voltammetry, electrochemical impedance spectroscopy and protein blotting. Newly constructed CEA immunosensors with anti-CEA IgG covalently immobilised onto the POct coated electrode surface were developed in parallel as a comparison. A highly sensitive and specific anti-CEA Affimer-based biosensor was successfully developed that is superior to the monoclonal based CEA immunosensor when both were interrogated in buffer or in diluted human serum. A polyclonal based CEA immunosensor showed equivalent sensitivity to the Affimer-based biosensors with limit of detection (LOD) at 1 fM and wide dynamic range (1 fM − 100 nM). This LOD was significantly lower than the basal clinical levels of 25 pM (i.e. $\geq$ 5 ng/ml). Overall, this label-free Affimer-based biosensor has strong potential to be developed as point-of-care device for CEA detection as it required small sample volumes (10 µl) and had rapid response time (5 min). Additionally, the newly discovered polyoctopamine polymer base layer has proved its generic application in immobilising different types of bioreceptors.

Table of Contents

List of Figures

List of Tables

List of Equations

Abbreviations

Ab	Antibody
AC	Alternating current
BCA	Bicinchoninic acid
Cdl	Double layer capacitance
CDR	complementarity-determining regions
CEA	Carcinoembryonic antigen
CPE	Constant phase element
CRC	Colorectal cancer
CV	Cyclic voltammetry
DC	Direct current
DMSO	Dimethyl sulfoxide
DNA	Deoxyribonucleic acid
E	Potential
ECL	Enhanced chemiluminescence
EIS	Electrochemical impedance spectroscopy
ELISA	Enzyme linked immunosorbent assay
FIT	Faecal immunochemical test
GCE	Glassy carbon electrode
gFOBT	guaiac faecal occult blood test
HRP	Horseradish peroxidase
I	Current
IgG	Immunoglobulin
IHP	Inner Helmholtz plane
LOD	Limit of detection
mAb	Monoclonal antibody
mRNA	messenger RNA
NABP	Non-antibody binding proteins
NHS	N-hydroxysuccinimide ester
OHP	Outer Helmholtz plane
pAb	Polyclonal antibody
PBS	Phosphate buffer saline
PCR	Polymerase chain reaction
PEG	Polyethylene glycol
POC	Point-of-care
POct	Polyoctopamine
Ptyr	Polytyramine
QCM	Quartz crystal microbalance
Rct	Charge transfer resistance
Rp	Polarization resistance
Rs	Solution resistance
SAM	Self-assembled monolayer
scFv	Single chain variable fragment
SPGE	Screen printed gold electrode

sulfo-SMCC	Sulfosuccinimidyl 4-(N-maleimidomethyl) cyclohexane-1-carboxylate
SPR	Surface plasmon resonance
TCEP	Tris (2-carboxyethyl) phosphine
VR	Variable region
ySUMO	yeast SUMO
$|Z|$	Total impedance
Z'	Real impedance
$-Z''$	Imaginary impedance
Z_W	Warburg impedance

Chapter One

Introduction

Chapter 1 : Introduction

1.1 Overview

According to the latest global statistic in cancer, colorectal cancer (CRC) is the fourth leading cause of cancer-related death and the third most common diagnosed malignancy (Ferlay et al., 2015). The CRC incidence and mortality rates are rising in low-income and developing countries whilst remaining high in well-developed countries (Arnold et al., 2017). Late detection due to current modalities of diagnostics (e.g. colonoscopy and faecal immunochemical test) which are time-consuming, often invasive and expensive, require centralised laboratories as well as showing variable sensitivity and specificity. These have been factors identified as major contributors to the high incidence and mortality rates. CRC in many cases is detected at an advanced stage and determination of carcinoembryonic antigen (CEA) level, a prognostic blood biomarker for CRC, through enzyme-linked immunosorbent assay (ELISA) is routinely utilised in clinical practice. Although ELISA is considered a highly sensitive technique, this technique has inherent limitations as described earlier including being time-consuming and laboratory dependant. The drawbacks seen in current CRC diagnostics have triggered more research in the development of biosensors for cancer diagnosis.

There are plenty of CEA biosensors that have been developed but all of them remain in their early stage. In addition, the implementation of these biosensors into commercialise devices is still far from realisation. This is because most of the biosensors constructed at present are built in an antibody-based format with complex fabrication and are expensive in the type of material used for the electrode. Moreover, majority of the developed biosensor constructs are impractical for a point-of-care (POC) approach and more suitable for laboratory-based applications. Although antibodies and their derivatives have been extensively used as bioreceptors in biomedical and biotechnological applications, their complex protein structure, batch-to-batch variability, expensive and slow production and complex chemical modification needed for oriented immobilisation in biosensor construction have rendered them of limited usefulness in POC biosensor applications.

Therefore, a shift in research direction was observed in the past few years with emerging research focusing on the development of non-antibody binding proteins

(NABP) as alternative bioreceptors to overcome the shortcomings of antibodies. The use of Affimer as bioreceptors in biochemical and biomedical research recently have shown promising results (Tiede et al., 2017). However, their application as biorecognition elements in the fabrication of biosensor is still limited. There is a consensus within the field of biosensors that oriented immobilisation correlates with high sensitivity detection of target analyte (Sharma et al., 2016c, Welch et al., 2017). With the ease of modification by incorporating a single cysteine residue at the C-terminus of an Affimer, site-directed immobilisation onto sensor surface can easily be achieved. Additionally, electrochemical biosensors are known for having the advantage of being inexpensive, robust, highly sensitive and practical for POC approach, such as the commercial glucose biosensor compared to other type of biosensors (Rushworth et al., 2013b). Hence, the work in this thesis was exclusively focused on the possibility of using anti-CEA Affimers as novel bioreceptors in developing label-free and sensitive impedimetric biosensors for CEA detection. To achieve the practicality of a POC device and inexpensive biosensor device, a commercial DropSens screen printed gold electrode, was selected as the electrode on which to base the biosensors.

1.2 Epidemiology of colorectal cancer

Colorectal cancer (CRC) is an abnormal growth of tissue derived from the epithelial cells lining either the colon or the rectum. In 2012, approximately 1.36 million new cases were forecast to be diagnosed with CRC and 694,000 death cases were reported worldwide (Ferlay et al., 2015). Despite improvements made in cancer treatment, advanced technologies in cancer diagnostics and augmentation of cancer awareness, the incidence and mortality rates of CRC still remain high.

CRC can be categorized into two types. The first category is known as sporadic CRC and involves a multi-step process and multiple genetic alteration (Tanaka, 2009). The second is known as familial/hereditary type and is caused by inheritance of known CRC genes such as adenomatous polyposis coli (APC), familial adenomatous polyposis (FAP), hereditary non-polyposis colorectal cancer (HNPCC), as well as unknown inherited CRC genes (Tanaka, 2009). Hereditary CRC often occurs at a younger age, whilst sporadic CRC is the predominant type of CRC, which accounts for ~70% of all CRC. This normally occurs in older people above 50 years of age. As mentioned earlier, tumorigenesis of sporadic CRC involves multistep genetic mutations that begin by causing hyperproliferation and lead to the development of adenomatous polyps, followed by severe dysplasia which later progresses into adenocarcinoma and eventually metastazises to distant organs.

1.3 Biomarkers of colorectal cancer

Many CRC cases are diagnosed at an advanced stage and the majority of CRC incidences are non-hereditary and sporadic which makes early detection crucial. In addition, late diagnosis is commonly associated with poor prognosis and one of the main factor for high mortality rates. The most effective and precise way of achieving early detection is through determination of CRC biomarkers. In general, genetic and protein biomarkers can exist as biomolecules that are found in either the blood, body fluids or tissues and whose change in the concentration reflect the pathological process (Langan et al., 2013). They can be further categorized as molecular diagnostic (used for risk stratification and early detection), predictive (prediction of treatment response), prognostic (indicators of the likely progression of tumour) and surveillance (for monitoring the tumour recurrence) biomarkers (Gonzalez-Pons and Cruz-Correa, 2015).

Although promising candidate biomarkers have been proposed for CRC detection, only a few biomarkers have been approved for clinical practice to date, including tumour, stool and blood biomarkers. Hence, a detailed description in this section will only focus on the validated biomarkers of CRC that are routinely utilised. The detection of CRC biomarkers is normally evaluated from the blood or stool samples. These biomarkers can be further categorised into nucleic acid based (i.e., DNA, mRNA and miRNA) and protein based (i.e., carcinoembryonic antigen (CEA) and carbohydrate antigen 19-9 (CA 19-9).

1.3.1   Nucleic acid based biomarkers

1.3.1.1   DNA biomarkers

In general, there are three main molecular mechanisms that have been identified involved in CRC carcinogenesis either via mutation or methylation of DNA including chromosomal instability (CIN), microsatellite instability (MSI), and the CpG island methylator phenotype (CIMP) (Ross et al., 2010). DNA methylation occurs when a methyl group is added to the 5-carbon position on cytosines nucleotide within the CpG dinucleotides without altering the DNA sequence but consequently affects gene expression. DNA hypermethylation that occurs in the CpG islands near the promoter region will result in gene silencing, whilst, DNA hypomethylation in the same region will result in overexpression of the gene and genomic instability (Pritchard and Grady, 2011). All of the validated genetic biomarkers for CRC detection outlined here undergo either one of these molecular processes or combination of both.

KRAS, a member of the RAS-family, is a downstream effector of the endothelial growth factor receptor (EGFR) pathway and is known as a proto-oncogene which play roles in cellular proliferation and differentiation, notably in CRC (Deschoolmeester et al., 2010). Mutations in *KRAS,* which accounts for 40% of CRC cases, have been clinically used as a negative predictive biomarker for anti-EGFR monoclonal antibody therapy in metastatic CRC (Reimers et al., 2013, Lech et al., 2016).

Meanwhile, *BRAF*, a member of the RAF kinase family, is an immediate downstream effector of *KRAS* in the RAS/RAF/MAPK signaling pathway that encodes a serine/threonine protein kinase which regulates cell proliferation and differentiation (Reimers et al., 2013). Activation of the *BRAF* mutation, which accounts for 5-15% of CRC cases is commonly associated with a worst clinical outcome and is frequently found in sporadic *MSI*-high tumours (Deschoolmeester et al., 2010). Similar to *KRAS*, *BRAF* is

also clinically used as second predictive biomarker in the detection of resistance to anti-EGFR monoclonal antibody therapy in metastatic CRC patients as well as for exclusion criteria for Lynch syndrome to distinguish between familial and sporadic CRC (Deschoolmeester et al., 2010, Reimers et al., 2013).

Microsatellite instability (*MSI*), a well-known biomarker that is exclusively derived from tumours of the Lynch syndrome (also known as hereditary non-polyposis colorectal cancer), results from inactivation of genes in the DNA mismatch repair (*MMR*) pathway either via aberrant methylation (which causes development of sporadic MSI-CRC due to silencing of the *MLH1* gene) or via germline mutations in the *MMR* genes including *MLH1, MSH2, MSH6 AND PMS2* (Pritchard and Grady, 2011). Due to its specificity, *MSI* has been clinically used as a prognostic biomarker to identify Lynch syndrome in CRC (Reimers et al., 2013, Pritchard and Grady, 2011).

There is a growing consensus in the CRC research that aberrant DNA methylation is normally found in most of the CRC subtypes and has potential to be implemented as diagnostic biomarker for screening of CRC. For instances, methylation of Vimentin (*VIM*) and Septin 9 (*SEPT9)* genes in the blood and faecal samples are clinically used as biomarkers for early CRC detection (Pritchard and Grady, 2011, Yiu and Yiu, 2016, Gonzalez-Pons and Cruz-Correa, 2015). There are currently three commercial real-time PCR based assays available for the detection of methylated *SEPT9* including Epi proColon 2.0 (Epigenomics), ColoVantage™ (Quest Diagnostic), and RealTime ms9 (Abbott). Additionally, the presence of methylated *NDRG4* and *BMP3* genes in faecal CRC samples are clinically utilised as prognostic biomarkers in a multi-target stool test together with status in KRAS mutation and haemoglobin immunoassay (Yiu and Yiu, 2016). This multi-target assays is commercially available and known as the ColoGuard® DNA stool test.

1.3.1.2 mRNA biomarkers

Other than DNA-based biomarkers, extensive studies have investigated the potential of RNA-based biomarkers for CRC detection such as mRNA (Heichman, 2014), microRNA (miRNA) (Wu et al., 2014, Yiu and Yiu, 2016) and long non-coding RNA (lncRNA) (Hauptman et al., 2017) gene transcripts. However, most of these studies are still at the pilot stage and yet to be validated due to inconsistency of results and the stability issue of RNA. Despite these issues, seven mRNA transcripts are the only

validated mRNA-based diagnostic biomarkers that have been approved for CRC screening in the blood sample and were commissioned in 2008 (Heichman, 2014). A commercial blood-based assay, ColoSentry™, is a real-time PCR-based assay which measures multiple gene expression from seven mRNA transcripts including *ANXA3*, *CLEC4D*, *LMNB1*, *PRRG4*, *TNFAIP6*, *VNN1*, and *IL2RB* (Marshall et al., 2010). This test produces a risk assessment for patients potentially at risk of CRC. Individuals been identified at increased risk are recommended for colonoscopy.

1.3.2 Stool biomarkers

One of the main symptoms in colorectal cancer is rectal bleeding or blood in the faeces. Two types of detection are currently used, known as the stool-based and faecal DNA-based tests, which has been outlined earlier. The most commonly used stool biomarker is faecal occult blood that can be detected via the guaiac faecal occult blood test (gFOBT) (Levi et al., 2011). This test is based on the pseudo-peroxidase activity of haem in human faeces as a result of bleeding derived from upper or lower gastrointestinal region (Gonzalez-Pons and Cruz-Correa, 2015). The drawback from this technique is low specificity and sensitivity as the test cannot distinguish the source of bleeding either from cancerous or precancerous lesions. It could also be derived from inflammatory bowel diseases, haemorrhoids or dietary intake. Due to these limitation, an improved test with higher specificity and sensitivity was invented using antibodies to detect human haemoglobin in faeces known as faecal immunochemical test (FIT) or immunochemical faecal occult blood test (iFOBT) (Doubeni et al., 2016), but still suffers from some of the disadvantages listed for gFOBT.

1.3.3 Protein based biomarker

To date, there are only two blood-based protein biomarkers that have been validated for monitoring CRC patients namely, carcinoembryonic antigen (CEA) and carbohydrate antigen 19-9 (CA 19-9) (Lech et al., 2016, Hauptman et al., 2017). Both proteins are a glycoprotein but the relevance of CA 19-9 in diagnosing CRC remains controversial as it shows less sensitivity and specificity for CRC (Hauptman et al., 2017). Therefore, CEA in the blood is the only protein biomarker that is widely utilised at present in clinical routine as a prognostic and surveillance biomarker for CRC detection (Wu et al., 2010, Labianca et al., 2010). In this study, CEA has been selected as a model analyte

to develop biosensors for CRC detection. Further descriptions of CEA will be elaborated in the following **section 1.3.3.1**.

1.3.3.1   CEA as biomarker for CRC

Carcinoembryonic antigen (CEA) is also known as carcinoembryonic antigen-related cell adhesion molecule 5 (CEACAM5) or CD66e which is a member of the CEA family of immunoglobulin superfamily genes (Hatakeyama et al., 2013). There are 12 unique genes encoded in the human and clustered under the CEACAM subgroup. These CEACAM proteins are anchored to the cellular membrane either via glycosylphosphatidylinositol (GPI)-linkage (e.g. CEACAM5 and CEACAM6) or transmembrane domains (e.g., CEACAM1, CEACAM3, CEACAM4, CEACAM19, CEACAM20, and CEACAM21) (Beauchemin and Arabzadeh, 2013, Tchoupa et al., 2014). They generally exhibit one variable IgV-like domain, termed the N domain, followed by either none, or up to six constant IgC2-like domains (identified as A or B) (Hammarström, 1999). Among these proteins, CEACAM1, CEACAM5 and CEACAM6 are well characterised and play significant roles in tumour progression and metastasis. These three proteins differ in the IgC2-like domain where CEACAM1 has three domains (A1-B-A2), CEACAM5 has six domains (A1-B1-A2-B2-A3-B3) and CEACAM6 has two domains (A-B) (Tchoupa et al., 2014).

CEA, which is the main focus of this study, is a highly N-glycosylated oncofetal antigen that was originally found in gastrointestinal cancer tissues (Gold and Freedman, 1965, Thomas et al., 1990). This soluble protein with an isoelectric point of ~4.7 (Casey and Kofinas, 2008) is a homodimer encoded by a 3100 bp mRNA which translates into a 70 KDa protein (Garcia et al., 1991, Kaufman et al., 2000). After undergoing post-translational modification, the molecular weight of full-length CEA protein is 180-200 KDa (Thomas et al., 1990, Hatakeyama et al., 2013). It is comprised of an N-terminal sequence, three highly conserved repeat domains of 178 amino acids and an anchored hydrophobic C-terminal domain (Bjerner et al., 2002) as shown in **Figure 1.1**. CEA is unique compared to the other CEACAMs protein because it is comprised of A3 and B3 domains that mediates the intercellular adhesion process (Blumenthal et al., 2005).
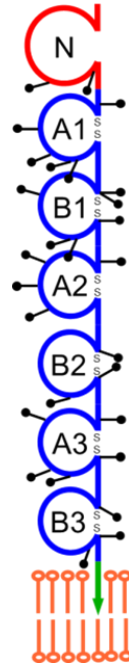
Figure 1.1: Schematic of CEA protein structure

Full-length CEA protein consisted of an N-terminal IgV-like domain (red sphere), six IgC2-like domains (blue spheres; A1 - A3 and B1 - B3) which are stabilized by disulphide bonds and a glycosylphosphatidylinositol (GPI; green arrow) linkage to the cell membrane. N-glycosylation sites are depicted in lollipop form (——●). This schematic is adapted from http://www.carcinoembryonic-antigen.de/human/index.html.

CEA can be found in high abundance during embryonic development in colon epithelial cells as well in pathological conditions like tumours in any endodermal tissue but is in low abundance in the normal colon tissue of adults (Gold and Freedman, 1965, Thomas et al., 1990). It is among the earliest tumour-associated antigens that have been identified and characterized (Gold and Freedman, 1965) and plays a role in several cellular processes, including as an intercellular adhesion molecule connecting the adjacent epithelial cell membranes and disruption of tissue architecture and cell polarization (Hammarström, 1999). Studies have shown that CEA is not only expressed in tumour tissues of adenocarcinomas (e.g. gastric, pancreatic, small intestine, colon, rectal, ovarian, breast, cervical and non-small-cell-lung cancers), but can also be expressed in renal failure patients and in normal lung tissue from smokers (Duffy, 2001, Fakih and Padmanabhan, 2006, Ohwada et al., 1995). Previous studies have demonstrated that elevated levels of CEA were associated with advanced tumour stage in CRC patients (Kim et al., 2009, Su et al., 2012) and the presence of CEA in resected CRC patients was correlated with tumour recurrence (Fakih and Padmanabhan, 2006, Lee and Lee, 2017,

Wu et al., 2010). Hence, CEA has been widely used as a prognostic biomarker after diagnosis and surveillance biomarker for tumour recurrence in post-operative CRC patients (Labianca et al., 2010). The cut-off value for CEA levels in serum considered abnormal is more than 5 ng/ml (Kim et al., 2009).

Apart from being used as a biomarker in tumour progression, several studies also reported that CEA regulates CRC metastasis to the liver by binding to a putative CEA receptor (CEAR) located on the surface of liver Kupffer cells (Lee and Lee, 2017). This interaction triggers secretion of pro-inflammatory cytokines (e.g., interleukin-1β and tumor necrosis factor-α) and upregulation of cell adhesion molecules (e.g., intercellular cell adhesion molecule 1, vascular cell adhesion molecule-1 and E-selectin) that result in increased binding of CRC circulating tumour cells to the endothelium which promotes metastasis (Lee and Lee, 2017).

Meanwhile, increasing evidence in preclinical studies reported that apart from CEA, CEACAM1 and CEACAM6 also regulate tumour progression and metastasis in CRC. Interestingly, the expression of these proteins were not exclusive to CRC but showed over-expression in melanoma and pancreatic cancers as well (Beauchemin and Arabzadeh, 2013). Although many studies showed that these three CEACAMs are often found in the same type of cells or tissues, their specific roles, especially in CRC tumour progression and metastasis have remained elusive. The majority of investigations were performed at cell culture level and preclinical data are mostly derived from transgenic mice models that expressed individual CEACAM protein (Beauchemin and Arabzadeh, 2013). Thus, the functional roles of each CEACAM within the same tumour environment are difficult to investigate. In this context, Affimer technology (Tiede et al., 2014), a synthetic non-antibody binding protein, could possibly overcome these limitations. This is based on recent evidence which demonstrated that Affimers have successfully distinguished closely related SUMO isoforms (Hughes et al., 2017). Affimers will be used as an alternative binding protein in this study and greater detail of this technology is discussed in **Section 1.6.2.2.4.**

1.4 Current diagnostics for colorectal cancer detection

There are several screening modalities that have been implemented in clinical practice for CRC detection which can be categorised into non-invasive and invasive techniques. The non-invasive techniques normally used for screening of early CRC and monitoring tumour recurrence are: the faecal occult blood test (FOBT), PCR-based assays for determination of DNA mutation and methylation, as well as ELISA for CEA protein evaluation. In contrast, the invasive techniques involve radiological examination using double-contrast barium enema (DCBE), flexible sigmoidoscopy, colonoscopy and computed tomography (CT) colonoscopy. However, each test has its own benefits as well as limitations.

The FOBT has several shortcomings such as its low sensitivity for detection of polyps and cancers located in the distal colon, low specificity, since haemoglobins can result from non-cancerous bleeding, and requirement for periodic testing. (Levi et al., 2011, Shah et al., 2014). Additionally, low compliance rates are seen due to patients' reluctance to handle faeces. Although more specific and sensitive faecal tests (i.e., faecal immunochemical test) have been implemented as national bowel screening in the UK, in general, these faecal-based tests are not exclusive to CRC. Further invasive and expensive evaluations via flexible sigmoidoscopy and colonoscopy are still needed. The alternative DNA-based tests from faecal and blood samples (e.g. Epi proColon 2.0, ColoVantage™, RealTime ms9, ColoGuard® and ColonSentry™) provide favourable benefits than the FIT test such as a non-invasive technique, do not require bowel preparation and have better sensitivity for cancer detection compared to FIT. Unfortunately, the multi-target stool DNA assays show high false positive rates and the overall cost of the DNA test is still expensive and might therefore not be suitable as a population wide screening test (Fung et al., 2015). In addition, subsequent confirmatory colonoscopy is needed for positive results which is similar to FIT.

On the other hand, invasive techniques often require bowel preparation prior conducting the examination. The entire colon can be assessed using double-contrast barium enema (DCBE), computed tomography (CT) colonoscopy and colonoscopy (Gonzalez-Pons and Cruz-Correa, 2015, Langan et al., 2013). The radiological examination using DCBE is commonly associated with unacceptably high false negative rates for polyp sizes less than 1cm (Langan et al., 2013). Flexible sigmoidoscopy is a rapid and safe test which can be performed without sedation. It has a lower risk of serious

complications such as perforation and bleeding as compared to the colonoscopy which requires sedation. Moreover, colonoscopy has poor compliance rates and risk of perforation between 1 in 1,000 to 10,000 colonoscopies (Shah et al., 2014), deterioration of cardiopulmonary function, infection and post-polypectomy syndrome (Young and Womeldorph, 2013). Even though colonoscopy is an invasive and expensive technique, it is the gold-standard screening test for CRC detection at present due to its high sensitivity and specificity for identification of polyps and cancers (Young and Womeldorph, 2013). Another alternative to colonoscopy is computed tomography (CT) colonoscopy which differ in terms of the radiation used but has the same limitations as colonoscopy (Shah et al., 2014). Meanwhile, immunoassay analysis of the CEA marker such as enzyme-linked immunoabsorbant assay (ELISA) is commonly used for preoperative screening of advanced CRC patients to determine the appropriate curative treatments and post-surveillance screening for tumour recurrence (Kim et al., 2009, Su et al., 2012).

1.5 Biosensors: Overview

Conventional analytical devices are superior in terms of accuracy and sensitivity but suffer from numerous limitations such as being labour intensive, time-consuming, needing complicated sample preparation and requiring sophisticated and expensive instruments. Analyses are also difficult to perform on-site and with real-time detection. In regards to cancer diagnosis, the conventional methods such as ELISA may take from several hours to a few days starting from the test being made until the results reach the patient. Meanwhile, the gold standard screening for colorectal cancer using colonoscopy normally involves 31 to 62 days waiting time from the date of referral (CRUK, 2018). Hence, the idea of implementing biosensors as new analytical devices comes into plan since substantial research effort to develop biosensors can be seen in the last few decades. The main aim that drives research into biosensor development is to accelerate clinical diagnosis, notably in cancer management. It is a well-known fact that early cancer detection can be curative and can reduce the incidence and mortality rates.

In general, a biosensor is comprised of three essential components that includes a biorecognition element, a transducer and signal processor. **Figure 1.2** illustrates the brief framework of biosensors platform. The biorecognition element is one of the main determinant factors besides the transduction mechanism that defines the type of biosensor which enables the selective response to a particular analyte or a group of analytes. The

range of analytes are wide ranging, from small molecules (e.g., metal ions) to proteins and nucleic acids, and up to microorganisms including bacteria and viruses. The biorecognition element can be categorised into protein-based (e.g., enzyme, cellular receptor protein, antibodies and alternative binding proteins), nucleic-acid based (e.g., oligonucleotides, DNA or RNA aptamer) or whole organism (e.g., viruses or bacteria). A detailed discussion of biorecognition elements that are currently employed in cancer diagnosis is discussed in **section 1.7**.

The binding of target analyte to the biorecognition element on the sensor surface creates a difference in the signal which is converted into a measureable signal via a transducer. This transduction mechanism can be further divided into non-electrochemical (e.g., optical and mechanical) or electrochemical transduction (e.g., voltammetry, amperometry, potentiometry, conductometry and impedimetry) (Tothill, 2009, Rushworth et al., 2013b) depending on the type of transducer material used. Ultimately, a signal processor collects, amplifies, and presents the signal on the readout display. For instance, charge-couple device cameras (CCD) or photomultiplier tubes (PMT) (Bally et al., 2006) are signal processors used in in optical sensing, whilst frequency response analysers (FRA) are typically used in electrochemical sensing (Chang and Park, 2010). The amount of measured signal reflects the concentration of analyte present in the sample, with the response typically being linear or log/linear; i.e. the signal is directly proportional to analyte concentration or is proportional to the log (analyte) concentration.
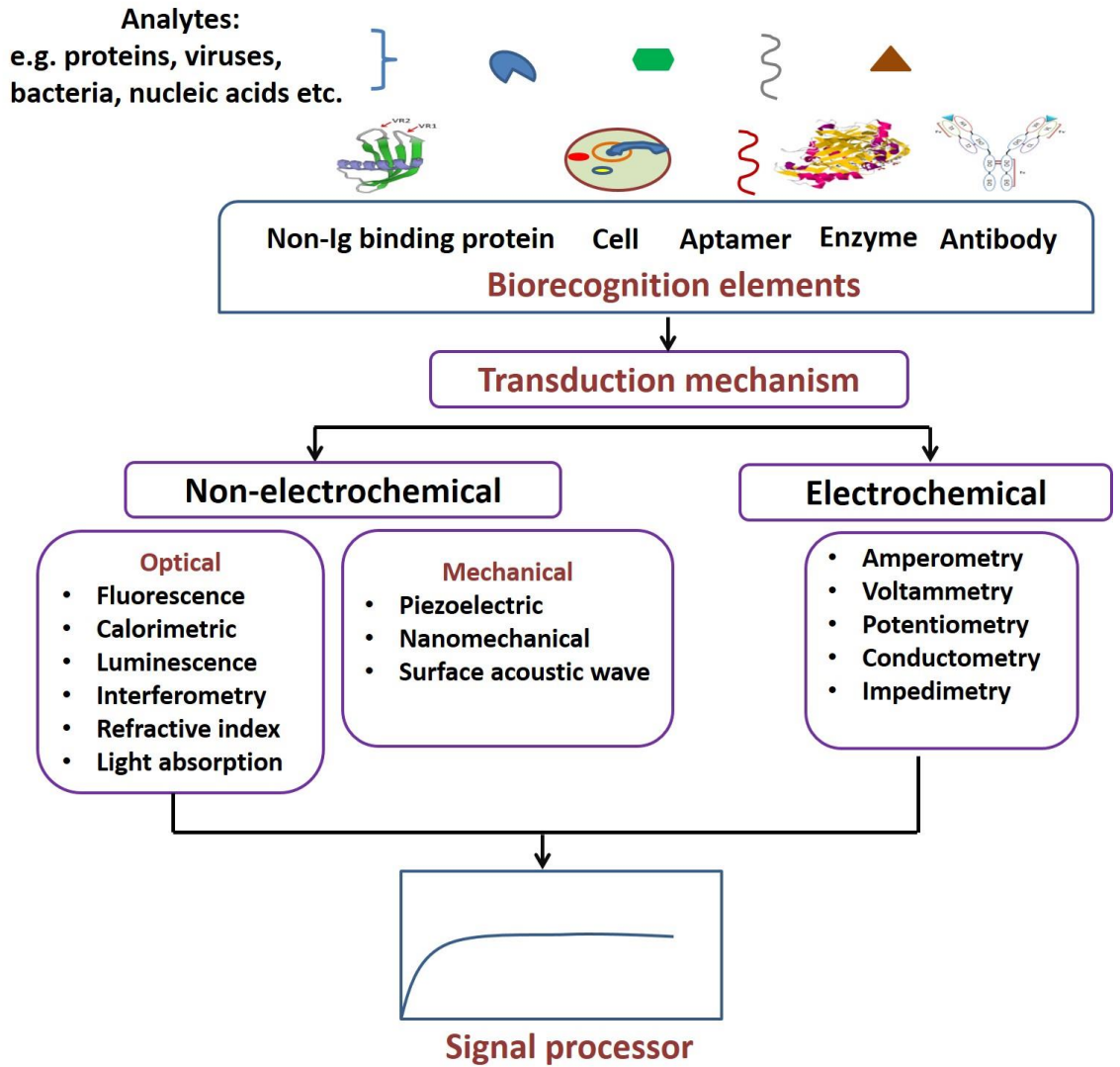
Figure 1.2: Biosensors framework

Schematic showing a brief framework of biosensors platform which in general consists of a biorecognition element, a transducer and a signal processor.

The success of a biosensor system can be measured via several factors. The most critical factors are the sensor's sensitivity and selectivity which are determined from its limit of detection (LOD) and response to interference, respectively. The efficiency of the biosensor system can be evaluated based on the sensor's response time and its linear and dynamic ranges. In order to be successful POC devices, biosensors must be portable, easy to handle and stable at ambient temperature. The majority of biosensors developed nowadays are single use and are frequently applied in the medical sector, for example, the lateral flow devices used in the pregnancy test kit. However, a regenerable biosensor would be an advantage for continuous monitoring of an analyte. Herein, a detailed discussion of non-electrochemical and electrochemical biosensors will be discussed in the next section.

1.5.1 Non-electrochemical biosensors

1.5.1.1 Optical biosensors

Optical biosensors are analytical devices that measure changes in target analyte binding onto the surface of an optical transducer which translates this binding into an electronic signal (Long et al., 2013). This changes varies according to the optical properties of the transducer such as changes in light absorption, refractive index, chromophore intensity (e.g., fluorescence, luminescence), calorimetric, reflectance and light scattering. Based on their optical properties, biosensors can be further classified into labelled and label-free detections. The indirect methods are often known as labelled detection and include fluorescence and luminescence. They are extensively utilised in diagnostic imaging, structural biology study, live cell sensing, biochemical assays (Velasco-Garcia, 2009) and multiplexed assays (e.g., DNA and protein microarray) (Bally et al., 2006). Changes in the chromophore signal (such as change in the emission amplitude) upon analyte binding are normally used to determine the concentration of target molecule in the sample (Velasco-Garcia, 2009). Labelled detection is often associated with higher sensitivity compared to the label-free detection. However, the labelling process can be time-consuming, laborious and expensive. Additionally, the assays normally require sophisticated instrument for data analysis which are only suitable for laboratory-based assay and not feasible for a point-of-care (POC) approach.

In contrast, label-free detection systems such as surface plasmon resonance (SPR), interferometry and Raman spectroscopy offer real-time detection and are predominantly

utilised for biomolecular interaction study, epitope mapping, drug screening and binding kinetics analysis. Amongst these technique, SPR is the most widely studied and extensively used at present. Briefly, SPR is a surface sensitive optical biosensor technique which integrates the total internal reflection of incident light coupled with surface plasmon wave generated on the surface of a thin metallic film. Typically a flat gold film is used but other metals, e.g. silver, are SPR active. The analyte binding can be analysed in real-time by monitoring the change in the SPR angle and light reflected which represents a change in the interfacial refractive index. The sensitivity of the biomolecular interaction is only measured up to 300 nm from the gold surface as optical electric fields diminish rapidly beyond that distance (Nguyen et al., 2015).

Apart from biomolecular interactions, recent advances in SPR technology extend to applications in cancer detection such as the detection of folic acid protein in human serum, a cancer biomarker in numerous epithelial-derived tumours (He et al., 2017) and the detection of prostate-specific antigen (Uludag and Tothill, 2012). Although label-free and real-time detection are desirable features in the application of POC devices, the prism that is used as the optical transducer in SPR biosensor is physically bulky which makes it difficult for miniaturisation and incorporation into POC devices (Velasco-Garcia, 2009) and SPR machines are typically expensive. In addition, complex data analysis, which requires sophisticated software and skilled personnel to interpret the output also limit this type of biosensor to research applications.

1.5.1.2 Mechanical biosensors

Mechanical biosensors are based on detection of the force, motion, mechanical properties and mass in biomolecular interactions (Tamayo et al., 2013). They can be classified into three categories including the quartz crystal microbalance (QCM), surface acoustic wave sensor and microcantilevers (Tamayo et al., 2013). QCM, commonly known as a piezoelectric biosensor, is technically an electromechanical sensor using bulk acoustic waves (Lange et al., 2008). The resonance frequency of the mass changes upon analyte binding the bioreceptor immobilized on the crystal surface is measured and binding of analyte (added mass) causes a frequency downshift (Ranjan et al., 2017). The relationship between added mass and frequency shift is described by the Sauerbrey equation (**Equation 1.1**) as shown below.

$$\Delta m = -C \cdot \Delta f$$

Equation 1.1 : Sauerbrey equation

(Where Δm = mass change at the surface of the crystal; C= constant of crystal ng/cm^2; Δf = frequency shift)

This principle is only valid for measurement of inelastic materials such as metallic coatings, metal oxides and thin absorbed layers, which do not dissipate any energy during oscillation. It is invalid for viscoelastic materials such as cells and polymers, where there is energy loss due to viscous damping during oscillation (Vashist and Vashist, 2011). However, QCM with dissipation (QCM-D) can be used here; in addition to frequency, dissipation (D) is measured when the driving electric potential is turned off. QCM-D biosensors have been widely studied in clinical diagnostics to quantify cancer cells such as leukemia (Shan et al., 2014) and breast cancer cells (Damiati et al., 2018). Although a lot of studies have reported the potential of QCM-D as biosensors, they are time-consuming during detection and non-specific adsorption issues have limited their usage as POC devices.

Meanwhile, surface acoustic wave biosensors have been used for the detection of parathyroid hormone-related peptide (PTHrP), a metastatic protein biomarker for breast and prostate cancer (Crivianu-Gaita et al., 2016), detection of CEA in exhaled breath condensate (Zhang et al., 2015) and quantification of cell viability and growth in suspension cultures and tumour spheroid cultures (Wang et al., 2015). Principally, when analytes bind on the immobilized bioreceptor located on the piezoelectric crystal, a change in the velocity of the surface acoustic wave is detected by an interdigitated transducer (Lange et al., 2008). Thus, the concentration of analyte can be measured from the changes in velocity. Apart from velocity, the device can also measure changes in amplitude and surface resonance generated from the analyte-bioreceptor interactions (Grammoustianou and Gizeli, 2018).

Advances in nanofabrication technologies have allowed the emergence of nanomechanical biosensors which normally exist in the form of cantilevers. Microcantilever surface stress biosensors have shown tremendous success in the detection of circulating tumour cells derived from breast cancer cells (Etayash et al., 2015), real-time detection of liver cancer cells on aptamer-based biosensors (Chen et al., 2016) and pathogen detection and treatment response, notably in the identification of antibiotic

resistance (Ndieyira et al., 2013). In general, mechanical biosensors provides rapid, label-free and real-time detection. They are less sensitive in sensing small molecules but excellent in the detection of large macromolecules and mammalian cells, virus and bacteria.

1.5.2 Electrochemical biosensors

Electrochemical biosensors, are the most developed biosensors at present and dominate the commercial biosensor market. They have been frequently applied in clinical, industrial and environmental fields (Turner, 2013). This is due to their rapid response times, user friendly application, low cost production and miniaturized forms (Rushworth et al., 2013b) . They also offer high specificity and sensitivity. Based on these characteristics, electrochemical biosensors are the main focus of this thesis. In principle, an electrochemical biosensor measures changes that occur in close proximity to the electrode surface where electrons flow between the electrode surface and electrolytes in the solution. The changes can be monitored through several parameters such as electrolyte resistance, adsorption or desorption of electroactive species, charge transfer at the electrode surface, and mass transfer from the bulk solution to the electrode surface (Bahadir and Sezginturk, 2014). Observation and analyses on any of these changes enable determination of the analyte concentration as well as characterisation of the electrochemical reactivity of the analyte interaction on the electrode surface.

Technically, an electrochemical biosensor is based on a three electrode system including a working electrode, a reference electrode and a counter electrode in which all of them are connected to a potentiostat as illustrated in **Figure 1.3**. The working electrode, where the biorecognition elements are attached, serves as the transduction element and is typically a conductive material such as platinum, gold or carbon. Carbon based electrodes have been extensively used as working electrodes in electrochemical biosensors due to their low cost in large scale production and existence in multiple forms (Li and Miao, 2013, McCreery, 2008). Earlier amorphous carbon or glassy carbon was frequently used but more recently graphene and doped-diamond surfaces are becoming more common in electrochemical applications. Graphene and doped-diamond have additional advantages in terms of electrochemical properties including greater chemical stability and resistance to electrode fouling which could be derived from the impurities adsorbed from electrochemical solvents (McCreery, 2008). Additionally, doped-diamond has low chemical reactivity that enables a wider electrochemical potential window (Kraft, 2007).

Meanwhile, gold electrodes which are chemically stable and highly conductive are commonly employed and easily modified via thiol-coupling functionalisation such as self-assembled monolayers (SAM) using alkane-thiols (Billah et al., 2010, Billah et al., 2012, Hays et al., 2006, Jeuken, 2016). The reference electrode plays an important role in maintaining a set potential at the working electrode. The most popular materials used for reference electrodes are silver/silver chloride but the mercury-chloride (saturated-calomel) reference electrode can also be used. The counter electrode often ten times larger than the working electrode, is normally made of inert materials such as gold, platinum or carbon, and is responsible for maintaining the current between working electrode and counter electrode (Lisdat and Schäfer, 2008, Li and Miao, 2013).

The three electrodes can be printed together on a single chip or prepared individually and all electrodes assemble once the measurement is ready to be conducted. The advantage of screen printed electrodes is good result reproducibility due to their fixed electrodes position. However, screen printing normally generates a fairly rough electrode surface which makes oriented and homogeneous immobilisation of bioreceptors difficult to control.
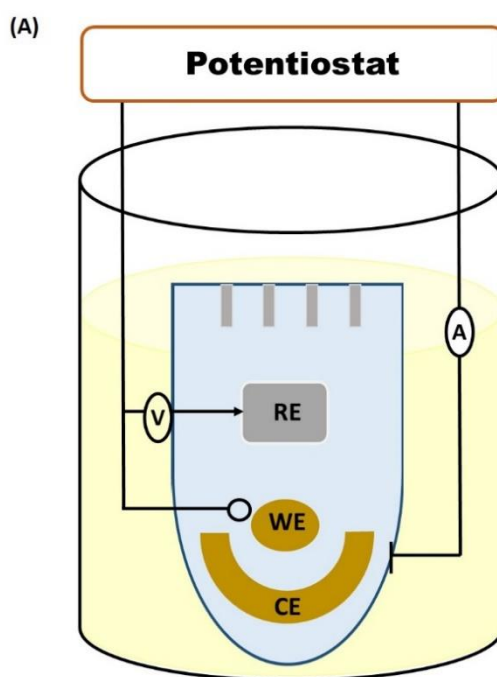
Figure 1.3: Electrochemical cells using three electrode system

(A) Schematic showing the electrochemical cells containing a three electrodes system in a redox mediator solution (i.e., $[Fe(CN)_6]^{3-}/[Fe(CN)_6]^{4-}$) which shown in yellow. All electrodes are connected to a potentiostat. The working electrode (WE) serves as sensing electrode, reference electrode (RE) maintaining the potential during electrochemical reaction and counter electrode (CE) facilitates in controlling the current between WE and CE.

1.5.2.1 Transducer surface modification

The majority of proteins are prone to becoming denatured and inactive when immobilised directly onto bare gold or carbon-based electrodes due to the hydrophobic nature of these electrodes surfaces. Therefore, in most circumstances, surface modification is necessary to immobilise the biorecognition element. However, most carbon based electrodes lack useful reactive groups, whilst SAM-modified gold electrodes are only practical on atomically flat gold surface (Jeuken, 2016). In this regard, several other options for surface modification are available and the most popular choices are conducting and non-conducting polymers. Both types of polymer are typically fabricated by electrochemical deposition. An advantage of using these polymers as a transducer base layer is that the thickness of the polymer is controllable. Additionally, the selection of appropriate solvent, supporting electrolytes and applied charge are all critical in determining the conductivity, resistivity and morphology of the surface (Yarman et al., 2014).

Conducting polymers are synthetic organic polymers that exhibit metallic conductivity or semiconductor properties. The conducting polymers provide electrical conductivity derived from the delocalisation of π-bonded electrons over the polymeric backbone (Ates, 2013). These π-bonds are highly susceptible to electrochemical oxidation and reduction. The inherent high electron affinity and redox activity together with biocompatibility in neutral aqueous solution are some of the factors that contribute to their extensive applications for electrochemical biosensors. Incorporation of nanomaterials (e.g., metal nanoparticles and carbon nanotubes) with conducting polymers often enhances the charge transport properties which results in a faster response time (Naveen et al., 2017). In addition, the presence of nanomaterials in the polymer composite can provide more binding sites for immobilising the biorecognition molecules and can increase biosensor sensitivity (Naveen et al., 2017). The most widely used conducting polymers in the fabrication of electrochemical biosensors are polypyrrole, polyaniline, polythiophene and poly (3,4-ethylenedioxythiophene)(PEDOT) (Aydemir et al., 2016).

Surface modification using non-conducting polymers as a transducer element is also frequently employed, usually in molecular imprinted polymer (MIP)-based electrochemical biosensors (Yarman et al., 2014) and enzyme based biosensors (Yuqing et al., 2004). Despite still being conductive to some extent, non-conducting polymers exhibit high resistivity. The polymer growth is often self-limited and generates thinner

films than with conducting polymers (10 -100 nm) (Yuqing et al., 2004). Hence, the charge transport across the electrode-electrolyte interface is very rapid and contributes to highly sensitive detection. The most frequently used non-conducting polymers are polytyramine (Ahmed et al., 2013), poly-o-phenylenediamines (Gomes et al., 2018) and poly(o-aminophenol) (Tucceri, 2013). Interestingly, certain conducting polymers can transform into non-conducting polymers when over-oxidised during electropolymerisation using high positive potentials, such as over-oxidised polypyrrole (Yarman et al., 2014).

Atomically flat gold electrode surface allows spontaneous chemisorption of thiols and the most popular choice for surface modification on this type of electrode is through formation of self-assembled monolayers (SAMs) using organo-thiols such as 4-aminothiophenol (4-ATP), mercaptohexadecanoic acid (MHDA) and several others (Billah et al., 2012, Millner et al., 2009). The formation of SAMs on the electrode surface is spontaneous and results in an organised array of closely-packed molecules. Surface modification with a SAM allows correct orientation of the immobilised biorecognition element on the transducer surface and can prevent protein denaturation as it provides indirect conjugation of the bioreceptor to the hydrophobic electrode surface. Immobilisation of biorecognition elements onto SAM modified electrodes is widely employed in capacitive biosensors and surface plasmon resonance platforms. Although biosensors modified with SAMs show excellent detection for small analytes (Arya et al., 2018), the SAM layers are unstable for the detection of large analytes like microorganisms (Caygill, 2012, Ahmed, 2015). It is important to highlight that the experimental works involved in this thesis used polytyramine and its biological by-product, polyoctopamine, as non-conducting polymers coated on screen printed gold electrodes. A detailed analysis and discussions of these polymers is presented in **section 4.2**.

1.5.2.2   Immobilisation of the biorecognition element

The immobilisation of biorecognition elements onto a biosensor surface plays a crucial role in producing a highly effective and sensitive biosensor device. Random or oriented immobilisation techniques normally depends on the availability of electrode surface's chemistry and functional group present on the biorecognition element. Direct physical adsorption, via electrostatic or hydrophobic interactions, or matrix entrapment in an electropolymerised film normally yield randomly orientated of biorecognition

elements (Ronkainen et al., 2010, Rushworth et al., 2013b). In contrast, covalent immobilisation via coupling to –SH, -COOH and –NH$_2$ side chain residues or affinity interactions including biotin-avidin and protein A/G interactions generate oriented immobilisation of the biorecognition elements that normally produce a better sensor performance (Sharma et al., 2016c, Welch et al., 2017). In regards to covalent immobilisation, a crosslinker is frequently employed to conjugate the bioreceptors onto the transducer layer. Typically heterobifunctional crosslinkers are used such as sulfosuccinimidyl 4-(N-maleimidomethyl) cyclohexane-1-carboxylate (sulfo-SMCC) and succinimide-maleimide PEG SM(PEG)n, which are amine-to-sulfhydryl crosslinkers, and 1-ethyl-3-(3-dimethyl aminopropyl) carbodiimide- N-hydroxysuccinimide (EDC-NHS), which is a carboxyl-to-amine crosslinker. Selection of an appropriate immobilisation strategy is crucial during biosensor construction as uncontrolled immobilisation will result in hindrance to the binding sites and difficulty in obtaining reproducible sensor output.

1.5.2.3   Electrochemistry at biosensor interfaces

Electrochemical biosensors rely on the electrical signal generated at the electrode-electrolyte interface. Two types of process can take place at this electrode-electrolyte interface which can be categorised into faradaic and non-faradaic processes. In a faradaic process, reversible oxidation or reduction of redox species present in the electrolyte solution facilitates the charge transfer across the electrode surface. This process follows Faraday's law. A transient current can also flow via charge accumulation on the electrode interface without involving the charge transfer process between the electrode interface and electrolyte solution. This phenomenon operates in static conditions and is known as a non-faradaic process, normally used in capacitive and potentiometric biosensors.

In general, there are several variables that play major roles in determining the rate of reaction on the electrode surface. The variables can be derived from the type of electrode materials, including its roughness and surface area as well as any modification of the electrode surface (biological or chemical) also influence electron transfer across the interfacial boundary. Additionally, the applied potential can influence the mass transport of species from bulk solution to the electrode interface either via diffusion, convection or migration (Hammond et al., 2016). Diffusion normally occur in electroanalytical process when redox reaction kinetics are fast at the electrode surface. This generates a concentration gradient of the analyte and other species between the bulk

solution and the electrode surface. In contrast, the electrochemistry is kinetically controlled when the diffusion of redox species is very fast.

An electrode will electrostatically attracts ions of opposite charge in the electrolyte solution that subsequently accumulate at the electrode interface. This generates an electrical double layer which behaves in similar way to a parallel-plate capacitor (**Figure 1.4**). There are several models explaining the electrical double layer theory such as the Helmholtz, Gouy-Chapman and Stern models. Amongst these, the Stern model gives a good correspondence to the real experimental data. The Stern model is a refined model comprising a combination of the Helmholtz and Gouy-Chapman models with inclusion of the theory that ions have a finite size. In this model, the electrical double layer is made of two parts which can be divided into a compact layer and a diffuse layer. The compact layer is a charge free layer containing the Stern plane and inner and outer Helmholtz planes. The closest region to the electrode surface are the Stern and inner Helmholtz planes (IHP) which consists of specifically absorbed ions and solvent molecules. The immediate next layer is filled with solvated ions which non-specifically adsorbed and identified as outer Helmholtz plane (OHP). This layer is then followed by the Debye and diffuse layers which consist of scattered ions and next to it is the bulk electrolyte where the mass transport occurs.
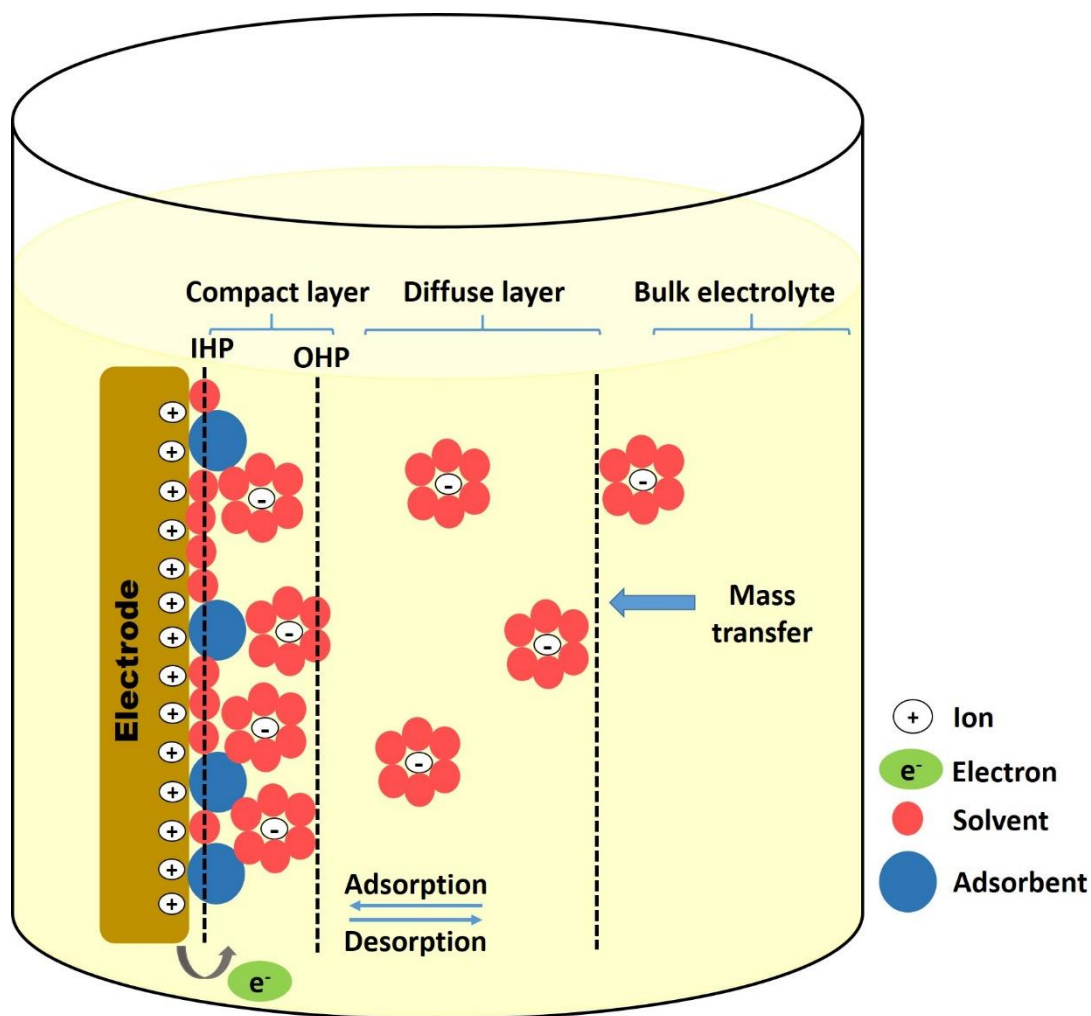
Figure 1.4: Schematic of electrical double layer in ionic solution

A schematic showing the formation of electrical double layer following the Stern model. An electrified electrode, in this case a positively charged surface electrostatically attracts anion and other solvent molecules onto the electrode surface. The charge adsorption or accumulation at the electrode-electrolyte interface generates an electrical double layer capacitance which comprises of a compact layer and a diffuse layer. The compact layer consists of inner and outer Helmholtz planes (IHP and OHP), respectively. Mass transport occurs in the bulk solution which located next to the diffuse layer.

1.5.3 Type of electrochemical transduction

In principle, the electrochemical biosensors can be categorised into amperometric, voltammetric, impedimetric and potentiometric sensors. A brief discussion of each transduction technique is presented in the following section and extensive details will be focused on the principle of cyclic voltammetry (**section 1.5.3.2**) and electrochemical impedance spectroscopy (**section 1.5.4**) which are the two main techniques employed in the development of biosensors in this study.

1.5.3.1 Amperometric biosensors

The amperometric biosensor was the first biosensor that was developed in 1962 and is still widely used worldwide. The glucose sensor (Clark and Lyons, 1962) is an enzyme-based biosensor used for monitoring blood sugar levels in diabetic patient and accounts for around 85% of the world market for biosensors (Turner, 2013). Since the invention of the glucose sensor, amperometric biosensors have undergone several improvements. Technically, amperometric biosensors measure changes in current generated by electroactive analyte species upon binding onto the bioreceptor when a constant potential is applied. The current produced by the electrochemical redox reaction is described by the Faraday's law (**Equation 1.2**). The concentration of target analyte can be quantified from the calibration curve as the measured currents are generally proportional to the concentration of analyte.

$$i \;=\; n \,.\, F \,.\, A \,.\, J$$

Equation 1.2 : Faraday's law

Where:

i is the measured current, typically in the nA-mA range,

n is the number of electrons transferred at the electrode,

F is the Faraday's constant in Coulombs (96,487 C mol^{-1}),

A is the area of the electrode (cm^2) and

J is the flux coefficient (mol cm^{-2} s^{-1}) which is the transfer of substrate or analyte to the electrode surface

The first generation of biosensors was based on detection of oxygen or hydrogen peroxide in the blood catalysed by glucose oxidase immobilised in between a semi-permeable dialysis membrane (Clark and Lyons, 1962). The glucose concentration was measured based on the differential current generated during the enzyme-catalysed reaction. However, the biosensor is constantly dependent on ambient oxygen as a co-substrate for the enzyme to function optimally. The high potential applied at the working electrodes also gave problems due to oxidation of common blood components (Wang, 2008). This led to the development of second generation biosensors based on mediated enzyme electrodes. The use of artificial redox mediators such as ferrocene and ferricyanide improved the sensor performance via rapid shuttle of electrons between the redox center of the glucose oxidase active site and the electrode surface, hence eliminating the dependence on the O_2 concentration (Ronkainen et al., 2010). Additionally, the use of mediator allowed a lower redox potential to be used thereby avoiding oxidation of other blood components. At present, the commercial glucose sensors that are available operate based on the second generation biosensor model.

The third generation of amperometric biosensors which is an improved version over the second generation design is based on direct and unmediated electron transfer between the enzyme's redox center and the working electrode surface (Ronkainen et al., 2010). This can be accomplished either via direct electrical contact between the enzyme and the electrode or via co-immobilization of both the enzyme and mediator in a conducting polymer. The conducting polymer can accelerates electron transfer from the enzyme's redox center to the electrode surface and *vice versa*. In addition, co-immobilization can prevent the mediators from leaching out of the biosensor film which makes it ideal for repeated measurements, thereby reducing the cost per measurement (Ronkainen et al., 2010).

It is important to highlight that the basis of amperometric biosensors measurement is dependent on redox reaction of electroactive analyte species. This limits the range of analytes that can be detected and most are common metabolites such as glucose, lactate and cholesterol. Apart from these, amperometric biosensors are also susceptible to interferences such as ascorbate, urate and paracetamol that are potentially oxidised or reduced at the working potential, and results in false positive measurements (Geise et al., 1991). Studies involved in the development of amperometric biosensors have used biorecognition elements not limited to enzyme, but also including antibodies, DNA and

aptamers (Belluzo et al., 2008). However, the fabrication of these biosensors must include probes containing redox species to enable amperometric measurement to take place.

1.5.3.2 Voltammetric biosensors

The principle of voltammetric biosensors are similar to amperometric biosensors. The only difference is voltammetric biosensors measure changes in current generated by electroactive analyte species when variation of potentials are applied to a working electrode relative to a reference electrode. There are several types of voltammetric techniques that commonly used in the biosensor application which differ in terms of how the potential is applied and when the current is measured. These include linear sweep voltammetry, cyclic voltammetry, differential pulse voltammetry and square wave voltammetry (Grieshaber et al., 2008). Since cyclic voltammetry (CV) is one of the key techniques used in this study, greatest detail will be focused on this technique using ferricyanide $[Fe(CN)_6]^{3-}$ and ferrocyanide $[Fe(CN)_6]^{4-}$ as redox mediators.

CV is similar to linear sweep voltammetry in which the potential is swept linearly over time at a fixed scan rate. Linear sweep voltammetry scans the potential in one direction which only yields either an oxidation or reduction peak, whereas CV undergoes a reversible scan which yields both oxidation and reduction peaks at each scan cycle. When the forward scan is swept towards the positive potential, $[Fe(CN)_6]^{4-}$ undergoes oxidation at the electrode and current begins to flow. At this stage, the current increases gradually as the potential increased until $[Fe(CN)_6]^{4-}$ is completely oxidised at the electrode surface. This is reflected in the anodic peak potential (E_{pa}) in the voltammogram (**Figure 1.5**). Depletion of $[Fe(CN)_6]^{4-}$ at the electrode surface leads to mass transport diffusion of the species from bulk solution. However, this process is impeded by the diffusion layer generated during the oxidation process that results in a decrease in the anodic current (i_{pa}) as the scan continues. When a reverse scan is applied at the switching potential towards negative direction, the oxidation product $[Fe(CN)_6]^{3-}$ at the electrode surface is reduced until its reached the maximum reduction at the cathodic peak potential (E_{pc}). The electrons consumed during this process lead to the increasing negative current (i_{pc}). Subsequently, the same diffusion phenomenon reoccur when $[Fe(CN)_6]^{3-}$ is depleted at the electrode surface. The i_{pc} then gradually decreases until the reverse scan is complete.

Since CV is a surface sensitive technique which provides qualitative information about electrochemical reactions, it has been widely employed as a tool to characterise the

electrochemical properties of modified electrodes (Zhang et al., 2016, Vusa et al., 2017). The oxidation and reduction patterns in the voltammogram are useful to determine electrochemical properties such as anodic or cathodic net charge of a nanocomposite (Gao et al., 2015). In biosensor applications, CV is frequently utilised for electrodeposition of polymer. The real-time detection enables observation of the polymer growth and its conductivity behaviour. In addition, sequential steps in biosensor construction can easily be evaluated by analysing the voltammogram profile. Apart from these, cyclic voltammograms also produce quantitative analysis such as determination of redox potential and electrochemical reaction rates of analyte solution as well as quantification of analyte concentration (Grieshaber et al., 2008).
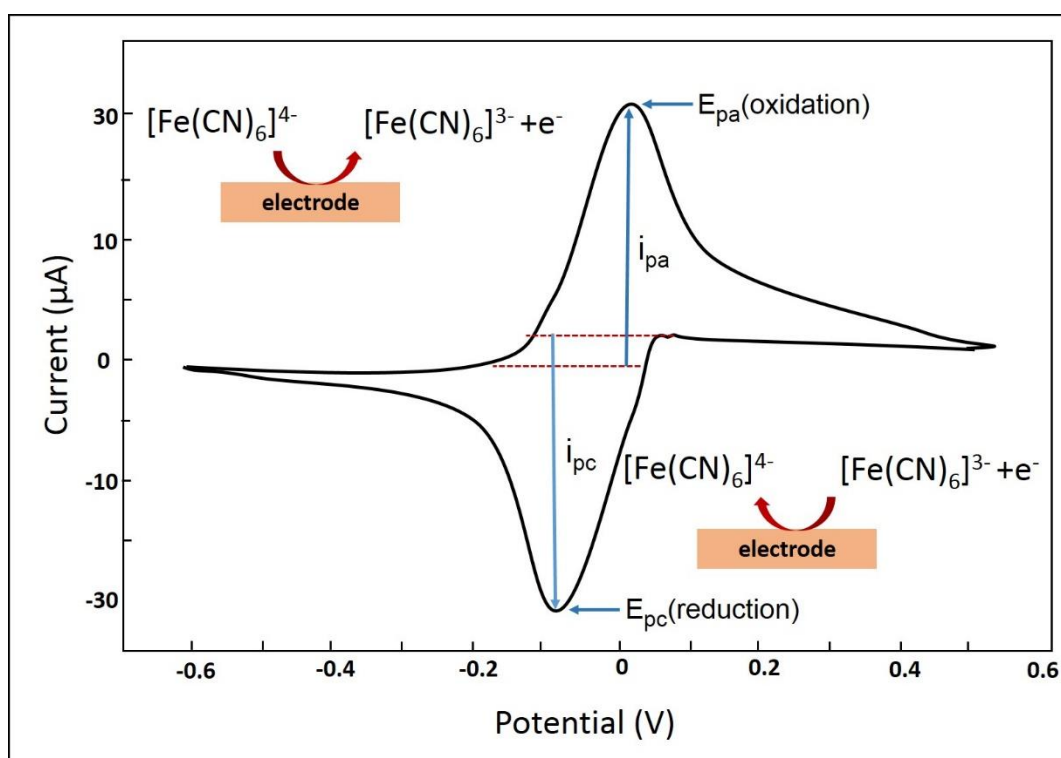
Figure 1.5: Cyclic voltammogram in faradaic biosensor

Simulated data showing cyclic voltammogram of a single electrochemical reactant when the potential is swept from -0.6 V to $+0.55$ V and cycled back to the initial potential point at a constant scan rate. E_{pa} (anodic potential) and E_{pc} (cathodic potential) denote the peaks where the oxidation and reduction processes respectively occur at a maximum. The currents measured at maximum oxidation and reduction are termed as i_{pa} (anodic current) and i_{pc} (cathodic current). Insets show the process of oxidation and reduction occurring on the electrode surface.

1.5.3.3 Potentiometric biosensors

In a sense, potentiometric biosensors operate in the opposite way to amperometric and voltammetric biosensors whereby changes in potential which are proportional to the analyte concentration are measured when zero current flows in the electrochemical cell. Potentiometric biosensor normally measure specific ion concentrations as a result of reaction involving the analyte. The relationship between ion concentrations and potential is governed by the Nernst equation as shown in **Equation 1.3**.

$$E_{cell} = \frac{E° - RT}{nF} \log \frac{[A_{OX}]}{[A_{RED}]}$$

Equation 1.3: Nernst equation

Where:

E_{cell} is the measured cell potential at zero current,

$E°$ is the constant potential for the redox reaction,

R is the gas constant (8.314 J K^{-1}mol^{-1}),

T is the temperature in degree Kelvin (298 K),

n is the number of electrons transferred in the redox reaction,

F is the Faraday constant in Coulombs (96,487 C mol^{-1}),

A_{OX} is the activities of the oxidised species and

A_{RED} is the activities of the reduced species.

Unlike other electrochemical biosensors which often employ a three-electrode system, potentiometric biosensors are normally based on a two-electrode system consists of a working electrode or also known as indicator electrode and a reference electrode with known potential. Potentiometric biosensing only involves a half-cell electrochemical reaction under static conditions and the potential is measured when the sensor reaches thermodynamic equilibrium on the working electrode. Meanwhile the remaining half-cell

electrochemical reaction occurs on the reference electrode whereby the potential is constant and unaffected by the electrochemical reaction in the cell.

There are several types of electrode that are frequently used including glass, metallic and membrane based electrodes. Amongst these, specific functional membranes are widely used and confer ion-selective, ion-permeable or ion-exchange properties that can prevent ionic interference that derives from complex samples containing more than one ionic species which can contribute to the measured potential. Biosensors based upon ion-selective electrodes (ISE) or ion-sensitive field effect transistors (ISFET) generate an output signal from the accumulation of ions, as a result of an enzyme catalysed reaction, at the interface of the ion-selective membrane on the electrode surface (Rahman et al., 2010).

Potentiometric biosensors are easily miniaturised and portable. They enable continuous measurements which are beneficial for medical and environmental applications. Recent advances in nanomaterial technology has shown that incorporation of nanoparticles into ISEs results in highly sensitive detection (Yin and Qin, 2013). However, the application of potentiometric biosensors is still limited to biocatalytic interactions and they are not suitable for bioaffinity interactions. Most research investigating detection of target analyte based on a bioaffinity interaction requires incorporation of a labelled enzyme to catalyse the reaction. Label-free detections are highly prone to non-specific interaction with components within the complex sample matrix (Koncki, 2007, Yin and Qin, 2013).

Several reports have shown the possibility of potentiometric biosensors in medical applications such as detection of single-nucleotide polymorphisms (SNPs) (Kaisti, 2017), determination of glucose based on monitoring the pH drop in the glucose oxidase reaction (Pisoschi, 2012) and in detection of cancer biomarkers (Tothill, 2009, Li et al., 2012). Although potentiometric biosensors offer excellent selectivity and non-destructive technique the majority of them are still low sensitivity and have slow response times (Rushworth et al., 2013b).

1.5.3.4 Impedimetric biosensors

Impedimetric biosensors that measure the impedance, comprise resistive and capacitive components within the electrochemical cell when a small amplitude sinusoidal AC voltage is applied as a function of frequency. The main technique in impedance biosensors is electrochemical impedance spectroscopy (EIS). This is a surface sensitive technique that probes electrochemical phenomena on the electrode surface as well as changes in the bulk solution. Initially, EIS was widely used in material science, such passivity and corrosion analysis and monitoring the function of batteries and fuel cells (Lisdat and Schäfer, 2008, Cañas et al., 2013, Macdonald, 2006). However, advances in the development of biosensors have shown that EIS can be utilised as a tool to characterise the electrochemical properties of modified surfaces such as the electrodeposition of a polymer layer on electrodes (Randviir and Banks, 2013, Rushworth et al., 2014). In addition, due to the sensitivity of this technique, EIS has been shown to be useful in determining the dielectric properties of the transducer layer, evaluating the electrochemical and electrical properties of ionic materials and investigation of electrodes porosity and passive surfaces (Macdonald, 2006, Kokkinos et al., 2016).

According to a recent review by Randviir and Banks (2013), the majority of EIS nowadays is for biological applications, including biomedical diagnostics, environmental and food industries. Studies have shown the implementation of capacitive and impedimetric biosensors in evaluating binding events on the transducer surface and determination of analyte concentration (Prodromidis, 2010, Kokkinos et al., 2016, Hammond et al., 2016). Apart from these applications, EIS also been used in monitoring the immobilisation of bioreceptors onto the transducer surface.

1.5.4 Principle of electrochemical impedance spectroscopy (EIS)

The impedance (Z) is a complex parameter but similar to the resistance (R) component in a DC circuit which follows Ohm's law (**Equation 1.4**) and share the same measured unit that is Ohm (Ω). The difference between impedance and resistance is the measurement of impedance is performed over a range of AC frequencies which leads to a shift in phase angle (Φ) and magnitude (|Z|) as illustrated in **Figure 1.6 (A)**. In contrast, the resistance measured in a DC circuit is frequency-independent which is technically equivalent to the impedance with zero phase angle (Randviir and Banks, 2013). Hence, the principle of impedance (Z) is analogous to the Ohm's law which is defined as ratio of

31

the voltage-time function and current-time function and taking into accounts the phase shift and the magnitude ($|Z|$) between the input voltage and output current when a small amplitude of AC voltage is applied at a particular frequency as described below in the **Equation 1.5**.

$$R = \frac{V}{I}$$

Equation 1.4 : Ohm's law

$$Z = \frac{V(t)}{I(t)} = \frac{V_m \sin(\omega t)}{I_m \sin(\omega t + \Phi)}$$

Equation 1.5 : Impedance

Where:

R is resistance,

Z is impedance,

V_m and I_m are the maximum input voltage and output measured current,

t is the time,

ω is the applied angular frequency which equal to $2\pi f$,

f is the frequency in Hz, and

Φ is the phase shift between the voltage-time and current-time function.
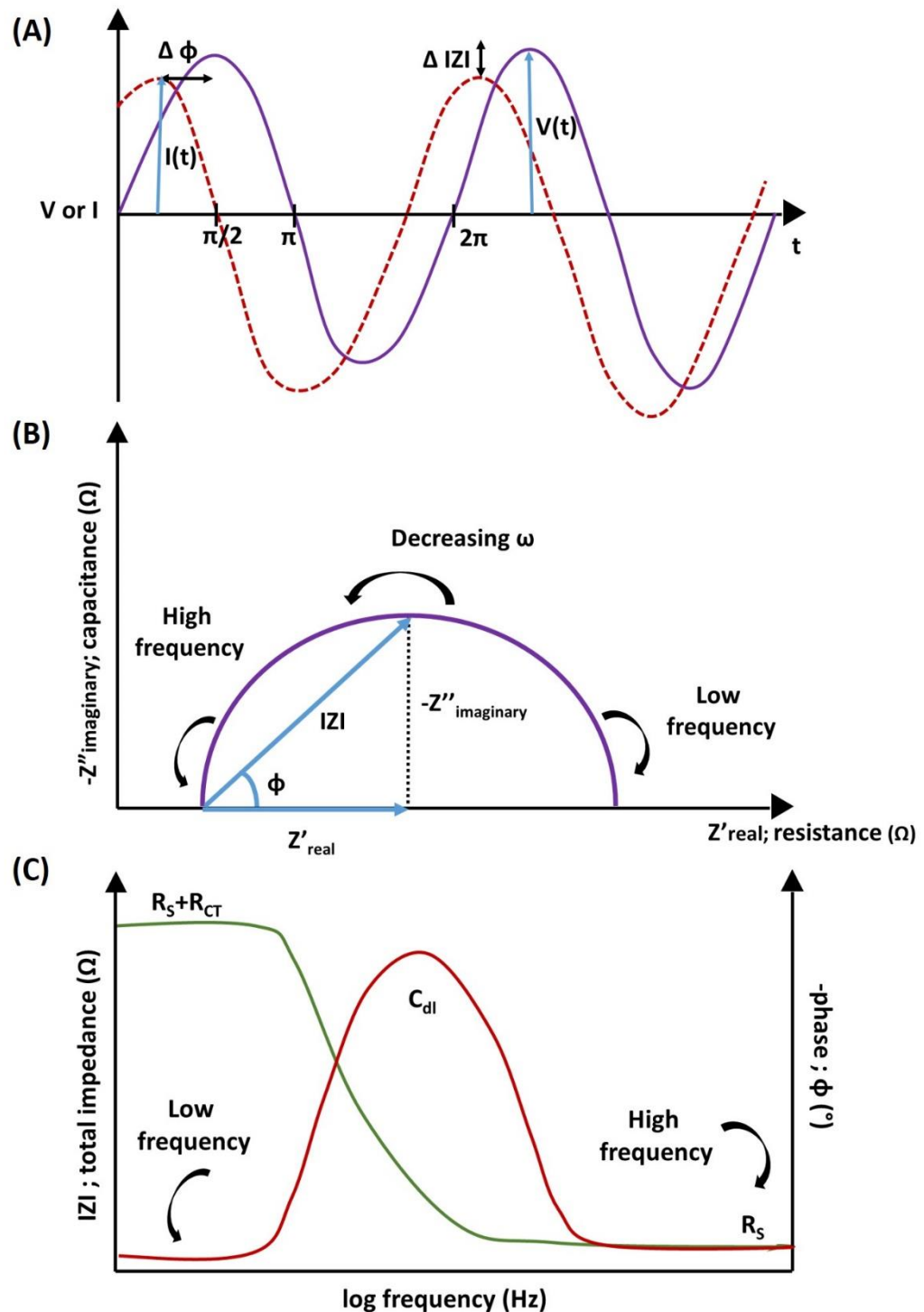
Figure 1.6: Phasor diagram and complex impedance plot

(A) Phasor diagram showing the shift in phase angle (Φ) and magnitude (|Z|) upon analyte binding onto the transducer surface when a small perturbation of AC voltage is applied (typically 10 mV or less). The impedance value can be expressed in two ways: either as; the real part (Z') and the imaginary part (Z'') of impedance as plotted in (B) a Nyquist plot or described as the magnitude (|Z|) and phase angle (Φ) against log frequency (Hz) as plotted in (C) a Bode plot. These diagrams are adapted from (Lvovich, 2012). See section 1.5.4.1 for a discussion of how useful variables like R_{CT} and C_{dl} are derived.

33

The purpose of using a small amplitude of applied AC voltage (typically 10 mV or less) during the impedance measurement is to prevent damage or disturb the bioreceptor-antigen binding interaction on the transducer surface (Daniels, 2010, Randviir and Banks, 2013, Bahadir and Sezginturk, 2014). This is additional advantage of EIS compared to voltammetry or amperometry where normally much larger voltages are frequently applied.

As described earlier in this section, impedance not only measures the resistance of electrical current flow in a circuit (the real part of the impedance, Z'), but it also measures the ability of a circuit to store electrical energy when no current flows. This is referred to the capacitance or imaginary part of impedance (Z''). A complex impedance plot comprised of real and imaginary parts of impedance is presented in **Figure 1.6 (B)** and is known as a Nyquist plot. The phase angle (Φ) is derived from the ratio of the imaginary and real impedance components at a particular angular frequency (ω) as shown in **Equation 1.6**. Meanwhile, the magnitude (|Z|) or absolute impedance is derived from **Equation 1.7**.

$$\tan \Phi \quad = \quad \frac{Z''}{Z'}$$

Equation 1.6 : Calculation of phase angle

$$(|Z|) = \sqrt{(Z')^2 + (Z'')^2}$$

Equation 1.7 : Calculation of magnitude of Z

The data of impedance measurement can be presented in different ways including the Bode plot and Nyquist plot. When the magnitude (|Z|) and phase angle (Φ) are plotted as a function of frequency, this is called a Bode plot (**Figure 1.6 C**). Alternatively, the Nyquist plot is generated when the imaginary part of impedance (Z'') is plotted against the real part of impedance (Z'). The selection of data to plot and its analysis is closely related to the experimental setup which depends if the impedance measurements are conducted in the presence of a redox probe, termed as Faradaic EIS, or in the absence of redox probe, known as non-Faradaic EIS. The Bode plot is useful when analysing the capacitive component of the electrochemical cell and frequently utilised in evaluating capacitive biosensors (Randviir and Banks, 2013). The electrode surface in capacitive

biosensors are normally covered with a dielectric layer that is pinhole free and which behaves like a capacitor (Daniels, 2010, Zhurauski et al., 2018).

In contrast, Nyquist plots are employed when analysing the resistive parameter of impedimetric biosensor under faradaic condition. The electrode surface of this type of biosensors can be modified in variety of ways. These include using a non-insulating layer or one partially covered with an insulating layer which usually contains pinholes that permits a charge transfer from the redox probe to the electrode interface (Prodromidis, 2010, Rushworth et al., 2014, Goode et al., 2016). An extensive discussion in the following **section 1.5.4.1** will focus on the details of the Nyquist plots and the electrical equivalent circuit which are the key techniques in analysing the EIS data of this thesis. The faradaic impedimetric biosensors offer advantages over the capacitive biosensors including simpler fabrication which does not require post insulation steps and flexibility in terms of physicochemical properties of the transducer layer (e.g., porosity of the electrode, surface roughness and selection of conducting or non-conducting polymer layers) (Kokkinos et al., 2016). Additionally, faradaic impedimetric biosensors exhibit higher sensitivity than capacitive biosensors and were reported to be more suitable in the quantification of target analytes instead of merely detecting their presence (Chang and Park, 2010, Kokkinos et al., 2016).

1.5.4.1   Electrical equivalent circuit and EIS data presentation

In practise, EIS experimental data is presented as a Nyquist plot and commonly simulated by a Randle's electrical equivalent circuit which facilitates interpretation and analysis of the observed response (Randles, 1947, Macdonald, 2006). As discussed earlier in **section 1.5.4**, the impedance measurement can be conducted in the presence (Faradaic) or absence (non-Faradaic) of a redox probe. The Randle's equivalent circuit of Faradaic EIS (**Figure 1.7 D**) consists of electrolyte resistance (R_S) and double-layer capacitance (C_{dl}) that in parallel with the charge-transfer resistance (R_{CT}), and Warburg impedance (Z_W) which all can be extracted from the Nyquist plot (**Figure 1.7 C**). Meanwhile, in non-Faradaic EIS (**Figure 1.7 A**), R_S is in series with the C_{dl} and in parallel with the polarisation resistance (R_P) as shown in **Figure 1.7 B**. R_P is normally used in non-Faradaic EIS electrical circuit instead of R_{CT}.
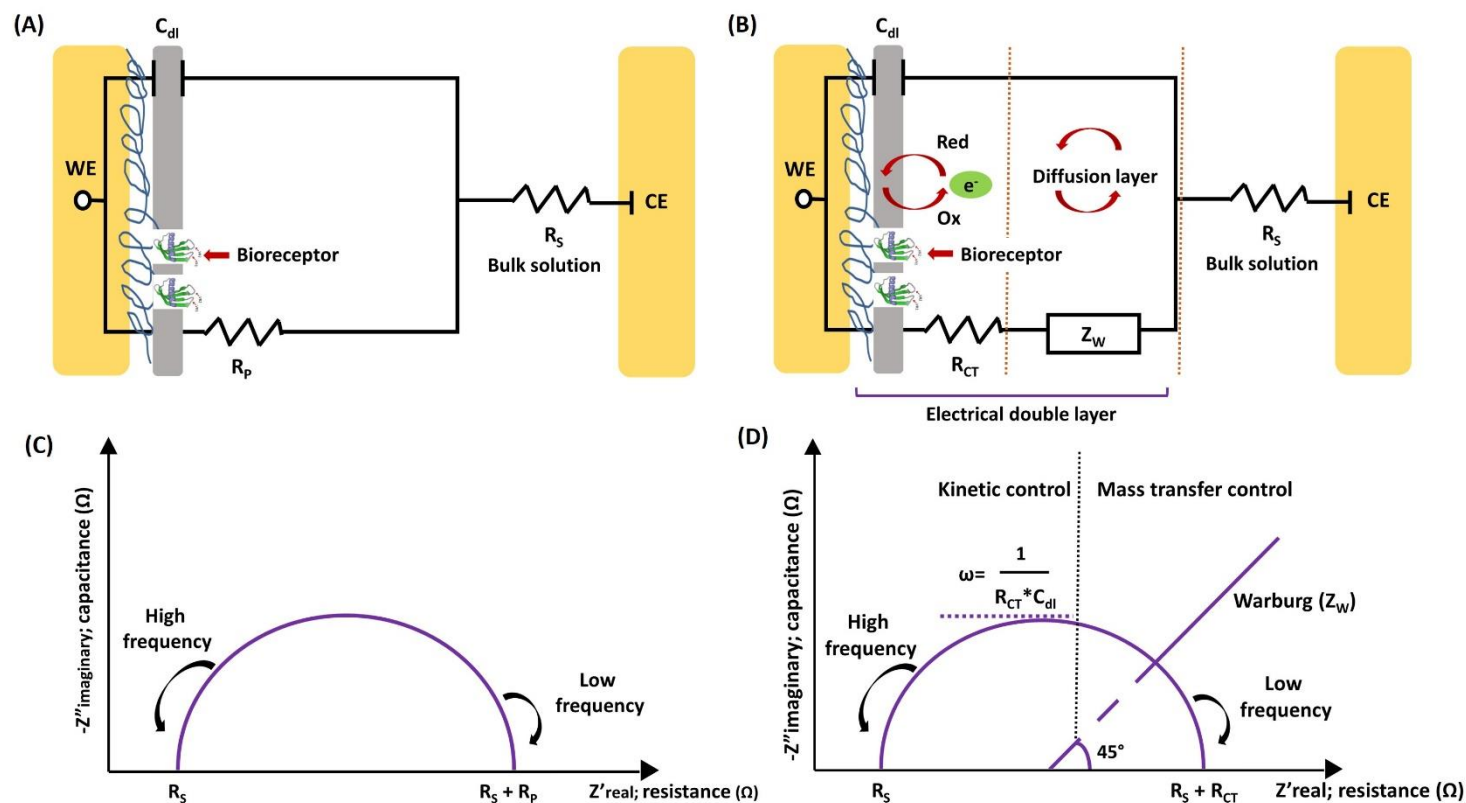
Figure 1.7: Nyquist plots and Randle's equivalent electrical circuits

Schematic of Randle's electrical equivalent circuits in the (A) non-Faradaic EIS and the (B) Faradaic EIS along with the corresponding Nyquist plots (C and D). The Nyquist plot shows the different components present in each circuit. The Randle's equivalent electrical circuit is drawn comprising immobilised bioreceptor and the origin of each circuit element in solution-electrode interface. R_S, solution resistance; R_P, polarisation resistance; R_{CT}, charge transfer resistance; C_{dl}, double layer capacitance; Z_W, Warburg impedance; WE, working electrode and CE, counter electrode. The schematics are not drawn to scale and adapted from Kokkinos et al. (2016).

The solution resistance (R_S) which commonly observed at high frequency where the phase angle is 0° in the Nyquist plot (**Figure 1.7 A and C)**, is derived from the drift of ions in bulk solution as a result of applied voltage on the transducer layer. This resistance is determined by the solution conductivity and the geometry of the reaction cell (Bahadir and Sezginturk, 2014), and is not involved in target binding. Whilst R_S measures the bulk solution resistance, R_{CT} measures the resistance to electron transfer mediated by the redox probe (e.g., $[Fe(CN)_6]^{3-/4-}$) in the electrolyte solution across the electrode interface. This charge transfer process only occurs in Faradaic impedimetric biosensors and takes place close to the electrode surface in the electrical double layer region (**Figure 1.7 D**). R_{CT} can be observed in the kinetically controlled region at low frequencies (typically 0.1 to 1.0 Hz) in the Nyquist plot (Prodromidis, 2010, Lvovich, 2012). Deposition of polymer layer onto the electrode surface or bioreceptor-analyte interaction will increase the kinetic barrier and impedes electron movement. This leads to increase in the R_{CT} value which is a common parameter used for quantification of analyte concentration in impedimetric biosensors or characterisation of electrochemical properties of the modified transducer layer.

An electrical double layer generated on the electrode-electrolyte interface is known as double layer capacitance (C_{dl}) which behaves electrically like a double plate capacitor. The C_{dl} stores electrical charge generated from the electrostatic ions accumulation or adsorption on the electrified electrode and the current flows without charge transfer across the electrode-electrolyte interface. The C_{dl} can be estimated from the highest point in a Nyquist plot circle. In practise, C_{dl} is commonly modelled as a constant phase element (CPE) in EIS measurements. The use of CPE is more realistic than a pure capacitor because the impedance of solid electrodes often deviates from pure capacitor characteristics and the observed capacitance is frequency dependent (Abouzari et al., 2009, Córdoba-Torres et al., 2015). Additionally, there are several parameters that support the rationale of using a CPE instead of a pure capacitor including electrode inhomogeneity and surface roughness, inconsistency in thickness and conductivity of surface coating, electrode porosity and varying distribution of potential and current at the surface (Lvovich, 2012, Córdoba-Torres et al., 2015).

The CPE commonly dominates the overall measured impedance under non-Faradaic conditions which is primarily used in capacitive biosensor measurements. In this type of biosensor, the interaction of bioreceptor-analyte binding on the electrode surface

can be evaluated via parameters such as the change in dielectric properties or thickness of the dielectric layer at the electrode-electrolyte interfaces (Prodromidis, 2010, Kokkinos et al., 2016). Meanwhile, the change in R_{CT} plays a major role in the total measured impedance in Faradaic impedimetric biosensors upon analyte binding. In this case, CPE only plays minor role as the signal which predominantly arises from the electroadsorption of ions in the electrolyte solution.

The Warburg impedance (Z_w) only exists under Faradaic impedimetric biosensor conditions. It is determined by diffusion of redox probe species in the diffuse layer to the electrode interface. This phenomenon is controlled by mass transfer when the concentration of electroactive species nearby the electrode surface is depleted and consequently a concentration gradient between the bulk solution and the electrode interface is generated. The Z_w can be observed as a 45° shift in phase angle at the lowest frequency range of impedance in the Nyquist plot (Lisdat and Schäfer, 2008).

The use of Randle's electrical equivalent circuit to analyse the impedance data must be used with caution as over simplification can occur. In addition, the fitting data may not represent the real experimental data as the fitted data can be modified according to the electrical equivalent circuit. Thus, a proper control is required to eliminate these possibilities.

In general, a change in impedance is typically proportional to an increase in the analyte-bioreceptor binding. Hence, the quantification of target analyte concentration can be obtained by plotting a calibration curve of the change in R_{CT} (or CPE) against a series of analyte concentrations. Impedance can also decrease if the nanostructure of the sensor surface or nature of chemical alters upon analyte binding onto the bioreceptor (Rushworth et al., 2014, Goode et al., 2016). The works in this thesis use Faradaic impedimetric biosensors and CEA detection was evaluated by looking at the change in R_{CT} (described in details in **Chapter 4 and 5**). Although data were analysed with respect to changes in C_{dl} and phase angle (**section 4.3.3.1**).

Impedance biosensors offer greater potential than amperometric and potentiometric biosensors as they can measure a wide range of analytes which are not limited to electroactive species but can also detect whole bacterial cells (Ahmed et al., 2013), virus particles (Caygill et al., 2012), nucleic acids (Gupta et al., 2013), proteins (Li et al., 2017, Rushworth et al., 2014) and even small molecules (Pilehvar et al., 2014).

Similarly, a range of bioreceptor can be used including affinity molecules such as antibodies (Sharma et al., 2018), non-immunoglobulin binding proteins (Sharma et al., 2016a) and aptamers (Arya et al., 2018). The main drawback in the impedance biosensors is non-specific background binding from complex sample that can affect the measured impedance.

1.6 Bioreceptors

As described in **Section 1.5**, biosensors can be categorised according to the type of biorecognition element or type of transducer (Rushworth et al., 2013b). The interaction between biorecognition element and target analyte is the main determinant factor that generates the signal on the working electrode. This subsequently translates into electrochemical or non-electrochemical transduction depending on the type of transducer used. There are a wide variety of biorecognition element available at present, but the most frequently utilised is the fabrication of biosensors for cancer diagnosis are outlined below.

1.6.1 Oligonucleotides

Nucleic acid aptamers comprised of single stranded DNA or RNA oligonucleotides have gained considerable attention for bioanalytical applications. They have been a popular choice as biorecognition elements in affinity based detection devices apart from the conventional antibody and enzyme. Since their invention, nucleic acid aptamers offer advantages over the traditional bioreceptors including strong affinity and high specificity towards their target. They are easily synthesized for large scale production as well as having high stability and reusability. In most of the bioanalytical and biochemical assays, specific orientation is essential to obtain high performance binding. This can easily be achieved via incorporation of a range of reactive groups e.g. $-NH_2$ and -SH, in synthesis.

Selection of nucleic acid aptamers is based on *in vitro* screening of combinatorial oligonucleotide libraries using a systematic evolution of ligands by exponential enrichment (SELEX) technology (Ni et al., 2011, Santosh and Yadava, 2014). Selection of aptamers with high affinity binding normally involves several rounds of positive and negative selection on the immobilised target. Generally, the process is comprised of screening of aptamer against the target molecule, followed by separation of the bound aptamer and its amplification using polymerase chain reaction (PCR). Aptamers possess

some advantage over antibodies whereby binding is not limited to nucleic acid target molecules but can also include small molecules such as metal ions (Bala and Górski, 2018) protein (Ilkhani et al., 2015) and even whole cells (Park, 2018). With regards to their self-annealing properties, aptamers can bind to this targets by folding into a unique secondary or tertiary structures (Chambers et al., 2008, Park, 2018). The unique characteristic of aptamers over other bioreceptors is that they can differentiate small differences in their target molecules. Based on these promising features, several studies have showed the potential of aptamers as biorecognition elements in developing biosensors for cancer diagnostics including detection of CEA (Shekari et al., 2017, Huang et al., 2018, Taghdisi et al., 2018), HER2 (Qureshi et al., 2015) and VEGF(Amouzadeh Tabrizi et al., 2015, Fu et al., 2016).

1.6.2 Proteins

1.6.2.1 Antibodies and their derivatives

Immunoglobulins (Ig) are extensively used as diagnostic tools and binding reagents in the biomedical and bioanalytical applications. Immunoglobulins are secreted by B cells in the blood in response to foreign molecules and pathogens. There are five isotypes of immunoglobulin which are classified as IgG, IgE, IgD (monomer), IgA (monomer and dimer) and IgM (pentamer) and two types of light chain known as κ and λ (Harlow et al., 1999, Sharma et al., 2016c). IgG is the most abundant isotype and predominantly secreted in the human serum. An IgG is made of four polypeptides forming a Y-shape molecule consisting of two identical copies of a ~55 KDa heavy chain and a ~25 KDa light chain which interconnected by disulphide bonds. Both heavy and light chains contain variable regions (Fv) located at the amino-terminus and constant regions (Fc) located towards the carboxy-terminus. The variable regions consist of six hypervariable regions also known as complementarity-determining regions (CDRs) which serve as antigen binding sites, whilst the constant regions mediates the immunological effector functions.

In a research setting, conventional antibodies (Ab) can be produced as polyclonal (pAbs) or monoclonal (mAb) forms. The generation of monoclonal and polyclonal antibodies involve immunising an animal (e.g., rabbit, goat, mouse and others) with a specific target analyte. Polyclonal Abs are normally isolated from serum which contains a pool of antibodies that bind to different epitopes on the same antigen which are derived

from multiple clones of immune cells. In contrast, mAbs are produced using hybridoma technology which involves fusion of a single B cell clone isolated from the immunised animal with myeloma cells yielding a hybridoma cell. Each hybridoma cell produces identical antibodies that are monoclonal normally secreted into the supernatant of tissue culture or ascites fluid from mice injected with hybridoma cells (Council, 1999). Hence, a mAb is more specific than a pAb as it binds exclusively to a single epitope. Owing to the high specificity mAbs, they are widely utilised as biotherapeutic agents in targeted therapy (Scott et al., 2012), whilst pAbs are most often used as research reagents in applications such as immunochemical assays, ELISA, western blotting and flow cytometry (O'Kennedy et al., 2017). Researchers soon discovered a number of limitations when antibodies became popular as biorecognition molecule. In biotherapeutic applications, the large molecular size of antibodies limits their tissue penetration and their complex architecture make them difficult to genetically or chemically modify, especially when incorporating them into biomaterials. Additionally, pAbs are expensive and labour intensive for mass production, lack thermal stability and have a short shelf-life, hampering their use in bioanalytical devices. These shortcomings triggered invention of recombinant antibody technology to produce antibody fragments which are smaller and are monoclonal. They have better tissue penetration, higher specificity and can also be produced via bacterial expression systems (Ban and Blake, 2012). They can also be genetically reengineered to contain specific attachment points (e.g. cysteine to provide – SH) for oriented immobilisation in bioanalytical platform (Yu et al., 2017).

To date, there are plethora of recombinant antibodies that have been engineered including single chain Fv (scFv, ~25 kDa), single chain antibody (scAb), diabody (Db, ~50 kDa), antigen-binding fragment (Fab, ~50 kDa) (Romer et al., 2011, Sharma et al., 2016b) and nanobodies, a single variable domain derived from naturally occurring heavy-chain antibodies from camelids (Steeland et al., 2016, Arbabi-Ghahroudi, 2017). **Figure 1.8** is a schematic showing antibody structure and its derivatives. A summary of anti-CEA recombinant antibodies that have been investigated in diverse applications is given in **Table 1.1**. For instances, some of these studies have shown application of anti-CEA nanobodies as molecular probes for *in vitro* and *in vivo* imaging in the detection of colorectal cancer (Vaneycken et al., 2010) and non-small cell lung cancer (Wang et al., 2017a). Pavoni et al. (2006) demonstrated the use of affinity matured scFv (MA39-E8) antibody as binding reagent in immunochemical staining of CEA in colon, breast, lung and metastatic melanoma in cells and tissue. Meanwhile, anti-CEA/anti-DOTA bispecific

antibody has been used as a biotherapeutic agent in a preclinical study for targeted therapy of colorectal cancer (Yazaki et al., 2012). Another study demonstrated the use of anti-CEA×anti-CD3 diabody antibodies as immunotherapy in CEA-expressing tumour cells (Molgaard et al., 2017).
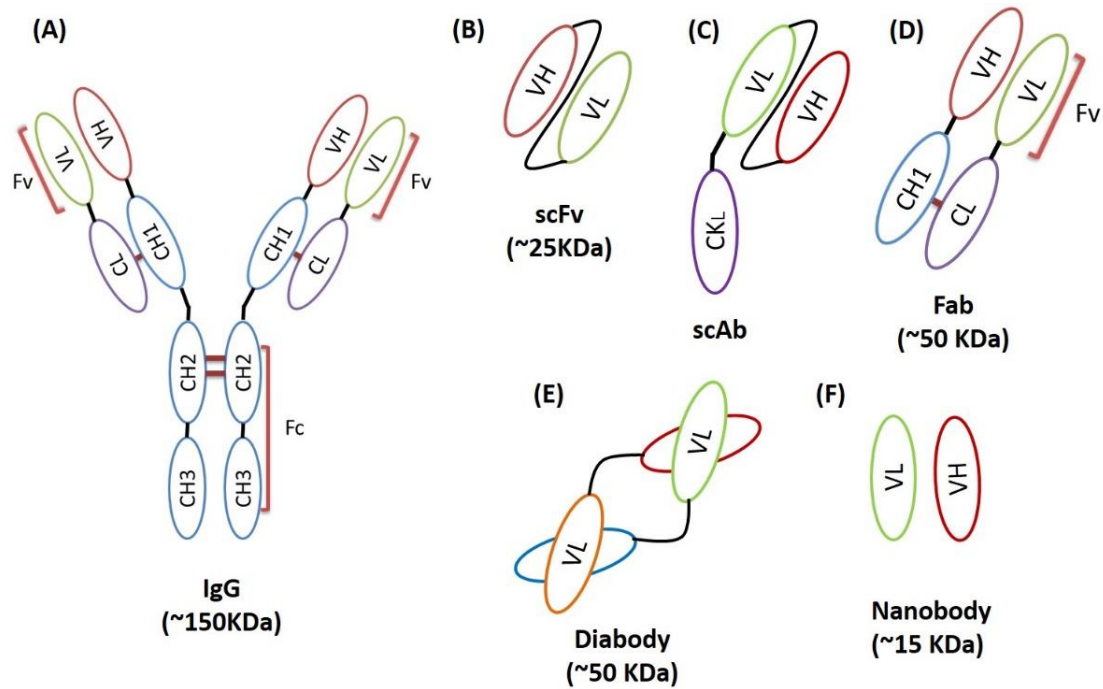
Figure 1.8: Antibody and its derivatives

Schematic showing a comparison of IgG structure and its derivatives. (A), IgG consists of two heavy and two light chains; (B), single chain Fv consists of a variable heavy (V_H) and variable light (V_L) domain connected by a peptide linker; (C), single chain antibody (scAb) is similar to scFv with extra constant light chain (CK_L); (D), Fab fragment consists of VH and VL domains within both constant heavy and light chains; (E), Diabody is a fusion of two scFv and antigen-binding fragment (Fab) comprise of V_H and V_L domains joining by a disulphide bond at the constant domains (CH1 and CL); (F), nanobody contains a single antibody domain (V_{HH} or V_L).

Table 1.1: List of some anti-CEA antibodies

Immunoglobulin scaffolds					
Scaffold	Parental protein/ Origin of species	Structure	MW (kDa)	Application	Reference (s)
scFv	scFv yeast display library / murine	Single-chain variable antibody fragment	27	Selection of improved humanized MFE-23 scFv antibody that bind to CEA with longer dissociation half-time (4 day) and better stability at 37°C	(Graff et al., 2004)
	Synthethic ETH-2 antibody phage library / human	Single-chain variable antibody fragment	26	Immunochemical staining of CEA expressed colon, breast, lung and metastatic melanoma cells and tissue using an improved affinity matured scFv (MA39-E8) antibody	(Pavoni et al., 2006)
Diabody	scFv	Derivatised MFE-23 scFv antibody fragment	~66	In vitro study of immunotherapeutic strategy using two-chain anti-CD3 × anti-CEA diabody mediating T-cell activation and cytotoxicity against carcinoembryonic antigen-positive tumor cells	(Molgaard et al., 2017)
Nanobody	Nanobody / camelid	Variable region of heavy chain antibody (V_HH)	15	Radio labelling of nanobody coupled to Technetium (^{99m}Tc) for *in vitro* and *in vivo* imaging of colorectal and non-small cell lung cancers	(Vaneycken et al., 2010, Wang et al., 2017a)
Bispecific antibody (BsAb)	Humanized M5A IgG1 monoclonal antibody/ mouse	Fusion of anti-DOTA C8.2.5 scFv antibody to anti-CEA humanized hT84.66-M5A IgG1 mAb	210	Development of radiolabeled tetravalent BsAb for pre-targeted radioimmunotherapy of colorectal cancer against CEA in animal xenograft model	(Yazaki et al., 2012)
	scFV	Bispecific antibodies	~26-60	Comparison between scFv and diabodies of anti-CD3x anti-CEA bispecific antibodies in gene immunotherapy	(Compte et al., 2014)

Although recombinant antibody technology has enabled production of smaller antibody fragments that can be generated *in vitro*, most of them still require animal immunisation with a specific antigen to generate the antibody libraries. This has limited the range of antigens that can be immunised and toxic compounds or non-immunogenic molecules are difficult to tackle, although it is still possible to biopan naïve libraries for potential binders. In addition, not all antibody fragments are compatible with bacterial expression. Since the presence of intradomain disulphide bonds in the protein structure that are crucial for stability, results in improper protein folding inside the bacterial cells and which affects the functionality of the engineered antibodies (Ban and Blake, 2012). Recombinant V_H or V_L domains also tend to produce less soluble proteins and are prone to aggregation when engineered as a single domain because these domains contain hydrophobic amino acid residue on the surface (Deffar et al., 2009, Helma et al., 2015). All of these drawbacks have limited the usage of antibodies and some of its derivatives in biomedical and diagnostic applications and have driven researchers to discover alternative binding protein from non-immunoglobulin protein scaffolds.

1.6.2.2 Non-immunoglobulin binding protein

In order to substitute alternative binding proteins for conventional antibodies and their derivatives as bioreceptors, they should have high affinity and specific binding against the target analyte. Ideally, the protein scaffold should be made of a small single domain with compact and structurally rigid core which serves as a backbone to the affinity molecule, and devoid of disulphide bonds. Modification around the binding region either via deletions, insertions or substitutions of amino acid sequences at the primary structural level through DNA mutagenesis should not interrupt the folding properties of the protein scaffold and its overall stability (Nygren and Skerra, 2004, Yu et al., 2017). The most important features of excellent alternative binding proteins are functional and soluble expression of the engineered protein in inexpensive prokaryotic systems, resistance to harsh chemical environment and protease activity, thermal stability at higher temperature and ease of modification for downstream applications (Löfblom et al., 2011). These features enable long-term storage at ambient temperature which is vital for most of bioanalytical devices and administration of the novel affinity proteins in a reducing environment, notably in biotherapeutic and biotechnological applications. Additionally, large library sizes and ability to produce the engineered protein *in vitro* provide advantages which enable screening for binders against small ligands and non-immunogenic antigens that are difficult to achieve from antibody libraries or by conventional antibody production, i.e., immunization.

The production of alternative binding proteins involves three general processes that begin with designing a combinatorial library on a selected protein scaffolds via site-directed mutagenesis or random mutagenesis to introduce diversification. This is followed by selection of variants using a display technique comprising of cell-surface display (e.g., phage, yeast, bacterial, insect and mammalian cells) or cell-free display (e.g., ribosome and mRNA displays) (Hamzeh-Mivehroud et al., 2013). Ultimately, enrichment of variants to increase the affinity of binding and specificity or further genetic or chemical modifications are tailored according to the specific application.

To date, there are approximately more than 20 novel non-antibody protein scaffolds which can be divided into two categories (Skerra, 2007, Weidle et al., 2013). The first is based on scaffold mediated binding via amino acids on surface-exposed side chains of secondary structural elements. This type of protein scaffold normally binds conformationally to the non-contiguous epitope of the target antigen. Meanwhile, the

second category is based on scaffold mediated binding via amino acids in one or several exposed loops on a rigid protein structure which imitate the antibody paratope and are most suitable for concave-shape epitope. Affibodies, Designed Ankyrin Repeat Proteins (DARPins), Affilin and Centyrin are examples of the first category. Meanwhile, Monobodies, Anticalins, Kunitz domain, peptide aptamer, Atrimer, Avimer, Fynomer and Affimer are examples of the second category. A selection of non-antibody binding proteins from each category is shown in **Figure 1.9**. Although there are plethora of non-antibody binding proteins that have been invented, only a small proportion of them have shown applicability in biomedical and biotechnological areas. Therefore, the rest of this section will be focused on those that widely used in cancer diagnostics application.
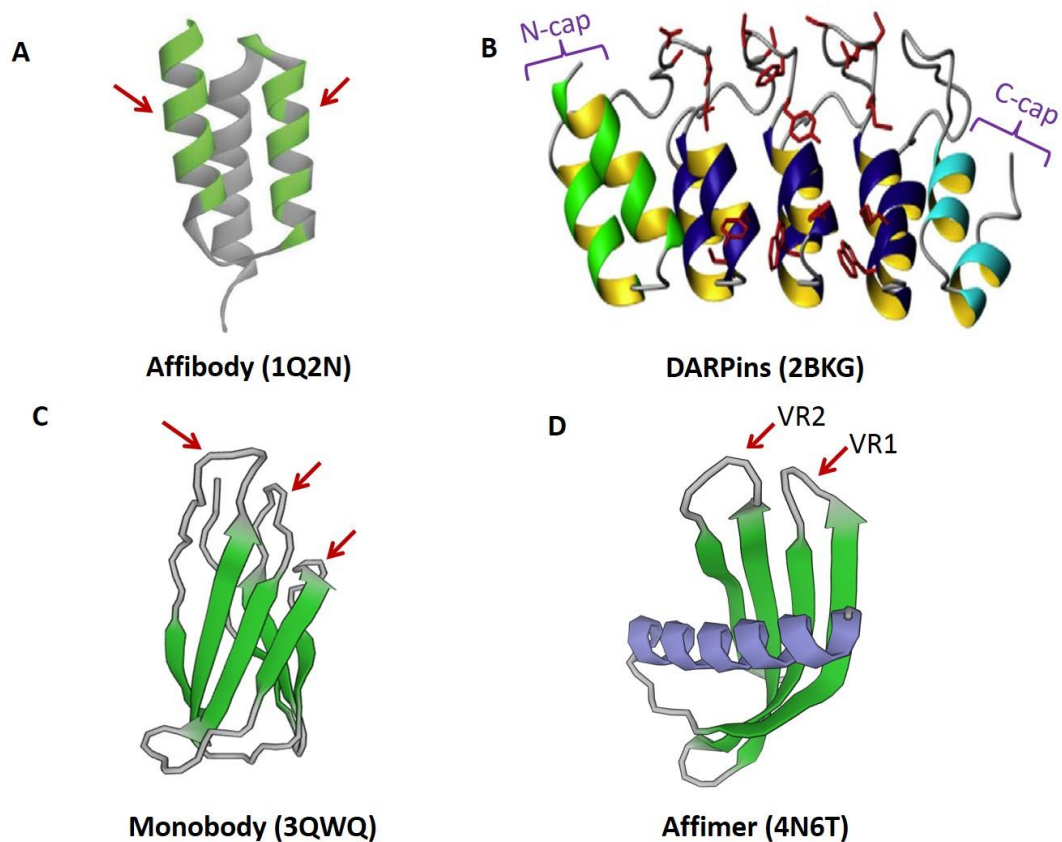
Figure 1.9 Examples of non-antibody binding proteins.

Ribbon representation of (A), Affibodies consist of three α-helices with randomization of 13 surface-exposed amino acids located in helices 1 and 2 of the Z domain coloured in green (red arrow) (pdb ID: 1Q2N); (B), DARPins consist of an N-capping repeat (green ribbon), internal repeat (blue ribbon) with randomized residues in red color and a C-capping repeat (cyan ribbon) (pdb ID: 2BKG); (C), Monobody consists of seven β-sheets and three CDR-like loops which serve as the binding sites indicated by red arrows. (pdb ID: 3QWQ); (D), Affimer consists of an alpha helix and four anti-parallel β-strands. The variable regions are indicated as VR1 and VR2 as shown by red arrows (pdb ID: 4N6T).

47

1.6.2.2.1 Affibodies

The Affibody is one of the earliest alternative binding protein invented 20 years ago which demonstrated broad functions across diverse applications. The protein scaffold was originally derived from the Z-domain of staphylococcal protein A which is an IgG-binding domain (Nord et al., 1995). This protein family is among the smallest single domain protein scaffold. Affibodies are structurally based on a non-cysteine containing three-helix bundle domains of 58 amino acid residues (6.5 KDa) (**Figure 1.9 A**). Diversification of the binding regions are generated by combinatorial randomisation of 13 surface-exposed amino acids that are solvent accessible and located in helices 1 and 2 of the Z domain. In a recent review, the innovators of the Affibody reported that the applications of Affibody are predominantly focussed on biotechnological and medical applications such as molecular imaging, receptor signal blocking and delivery of toxic payloads, notably in neurodegenerative, inflammation disorder and cancer studies (Stahl et al., 2017).

Meanwhile, their application to the field of biosensors is still rare. Most of the published work reported that the majority of Affibody biosensor techniques are optical based. These optical techniques are primarily focused on kinetic binding analysis using SPR for the detection of human papilloma virus 16 (HPV16 E7) (Xue et al., 2016) and vascular endothelial growth factor receptor 2 (VEGFR2) (Fleetwood et al., 2014). Interestingly, some research groups also investigated the potential of using bispecific Affibodies which simultaneously bind to human epidermal growth factor receptor 2 (HER2) and epidermal growth factor receptor (EGFR) (Friedman et al., 2009) or HER2 plus HER3 (Magdalena et al., 2014). Apart from SPR-based technique, Renberg and co-workers demonstrated the utilisation of Affibodies in protein microarrays to evaluate the specificity towards various proteins such as IgA, IgG, IgE TNFα, insulin and *Taq* DNA polymerase (Renberg et al., 2005, Renberg et al., 2007). Lofblom et al. (2010) reported the use of Affibodies as polymerase inhibitor in the polymerase chain reaction assay whilst, other studies demonstrated the use Affibodies as biosensors in Förster resonance energy transfer (FRET)-based detection (Renberg et al., 2004, Engfeldt et al., 2005).

By contrast, electrochemical based biosensors are less popular technique in the study of Affibodies as biorecognition element. Labelled detection using a sandwich assay format on magnetic beads has been investigated for the detection of HER2 (Ilkhani et al., 2016) and TNFα (Baydemir et al., 2016). Both of these studies measured the analyte

binding using direct pulse voltammetry (DPV). A label-free biosensor which detected HER2 on gold nanostructured screen printed graphite electrode used impedimetric interrogation (Ravalli et al., 2015).

1.6.2.2.2 DARPins

Designed ankyrin repeat proteins (DARPins) are artificial scaffolds derived from the human ankyrin repeat domain made up of a 33 amino acid consensus ankyrin repeat that stacks together to build a folded domain (Binz et al., 2003). Each repeat consists of a β-turn followed by two antiparallel α-helices and is flanked by the first (N-cap) and last repeat (C-cap) as shown in **Figure 1.9 B** (Tamaskovic et al., 2012). Both caps are essential for DARPins to efficiently fold in the *E.coli* and prevent them from aggregation (Interlandi et al., 2008). The presence of the caps also creates a hydrophilic structure on the outside of the domain and protects the hydrophobic core (Pluckthun, 2015).

DARPins consist of a fixed region which represents the conserved framework residues and a variable region which interacts with the target molecule. The introduction of six randomised surface-exposed amino acid residues (any combination of the 20 amino acid residues except cysteine, glycine and proline) per repeat module usually takes place in the variable region (Tamaskovic et al., 2012). This modification generates a rigid and concave binding surface that conformationally binds towards the target molecule. However, DARPin recognition has been shown to be limited and Schilling et al. (2014) have tried to improve the original DARPin library by designing "loop-based DARPins". The design of LoopDARPins library are inspired by the long CDR-H3 region in antibodies. A 19 amino acid loop consensus sequences is engineered into the existing DARPin scaffold located at the original β-turn position to generate a continuous convex paratope. The improved library produces higher affinity binders ranging from mid pM to low nM affinities (Schilling et al., 2014).

DARPins have been broadly applied to diverse applications including as a monoclonal reagent for breast cancer diagnostics (Theurillat et al., 2010), or crystallization chaperones (Batyuk et al., 2016), in targeted tumour therapy (Jost et al., 2013), as adapters in viral retargeting (Dreier et al., 2013) and clinically, for the treatment of diabetic macular edema and age-related macular degeneration (Pluckthun, 2015).

Based on systematic reviews of DARPins in biosensors application, published works showed that their use has largely been limited to optical techniques. Kummer et al.

(2013) developed an intracellular fluorescent biosensor for real-time detection of phosphorylated extracellular signal-regulated kinase (pERK) based on conformational changes. Reagentless fluorescent biosensors based on DARPins coupled to solvatochromic fluorophore were investigated for the detection of maltose binding protein (Brient-Litzler et al., 2010, Miranda et al., 2011, de Picciotto et al., 2016). Meanwhile, a versatile optical biosensor based on green fluorescence protein (GFP)-binding DARPins fused to fluorogen activators showed potential for *in situ* detection of a target protein and for studying protein–protein interactions (Schütz et al., 2016).

1.6.2.2.3 Monobodies

Monobodies also known as bioengineered Adnectins, are protein scaffolds based on the tenth fibronectin type III (FN3) domain derived from human fibronectin (Koide et al., 1998). The structure of the FN3 domain is homologous to the immunoglobulin domain and consists of seven β-sheets and three CDR-like loops (**Figure 1.9 C**). This protein scaffold is small in size with 94 amino acids, exists in a monomeric form and presents a flat or convex paratope shape. Genetic randomization takes place at the CDR-like loops and retrieving protein binders involves several types of display libraries including phage, mRNA and yeast display. Owing to its stable framework structure in the absence of any intramolecular disulphide bridge, many publications have reported the implementation of Monobodies in protein-protein interaction studies. These include Monobodies directed against Ab1 SH2 domain, maltose-binding protein and ySUMO-binding Monobody 1 and 9 (Koide et al., 2012) and as an inhibitor for SARS virus replication (Liao et al., 2009). Interestingly, Lipovsek (2011) reported that Monobodies have been used as anti-VEGFR-2 targeted therapy in phase II clinical trials of glioblastoma multiforme, non-small cell lung cancer and metastatic colorectal cancer.

1.6.2.2.4 Affimers

Affimers are engineered protein scaffolds originally derived from a cystatin consensus sequence (Tiede et al., 2014). Cystatins are a family of cysteine protease inhibitors and are small proteins (~100 amino acids). Originally, Affimers were invented by the BioScreening Technology group (BSTG) from the University of Leeds and named "Adhiron" (Tiede et al., 2014). Later on, they were commercialised by Avacta Life Sciences Ltd and known as Affimer type II. Apart from this, there is also another type of Affimer, known as Affimer type I which is based on human Stefin A proten scaffold

(Stadler et al., 2011). Both of these Affimers are related in structure and consist of a single alpha helix and four anti-parallel β-strands (**Figure 1.9 D**). The variable regions (VR), which resemble the CDR loops of antibodies, consist of two loops containing nine randomised amino acids (excluding cysteine) in each loop located between the first and second β strands (VR1) and between the third and fourth β strands (VR2). The molecular recognition event occurs at the variable regions. Work carried out in this thesis is based on Affimer type II which will just be referred to as Affimer in the remainder of this thesis. The Affimer library quite diverse with $\sim 3 \times 10^{10}$ independent clones. Apart from designing a double VR-based Affimer library, Tiede et al. (2014) successfully generated single VR (Tiede et al., 2017) and triple VR-based (Raina et al., 2015) libraries as well. The variety of Affimer libraries enable screening of diverse range of target molecules including small organic compound (e.g., 2,4,6-trinitrotoluene and methylene blue) (Koutsoumpeli et al., 2017), whole cells (Tiede et al., 2017), viruses (Jackson, 2017) and antibodies (Raina et al., 2015).

Although Affimers are still fairly new as alternative binding protein, their features such as monomeric structure and high solubility, absence of disulphide bonds, small size (12-13 KDa), no glycosylation sites and high thermostability have attracted attention for various applications. This can be seen in recent studies whereby Affimers have shown excellent potential in the modulation of protein function and protein–protein interaction (Michel et al., 2017, Hughes et al., 2017, Robinson et al., 2018, Kyle et al., 2015), as monoclonal reagent in biochemical assays (Xie et al., 2017, Tiede et al., 2014), affinity-fluorescent probes for labelling F-actin in live and fixed cells (Lopata et al., 2018), for *in vivo* imaging and super resolution microscopy (Tiede et al., 2017), as reagents for MRI imaging (Fisher et al., 2015) and as a tool for controlling material synthesis on a magnetic nanoparticle (Rawlings et al., 2015).

In addition to biotechnological and medical applications, Affimers are also increasingly used as biorecognition elements in biosensors. The absence of cysteine residues in the scaffold itself allows one to be introduced at the C- terminus and thereby assists oriented immobilization. Electrochemical biosensors are the main technique where Affimers have been used as alternative bioreceptors. Capacitive biosensors were developed for the detection of an anti-myc tag antibody (Raina et al., 2015), human interleukin-8 (Sharma et al., 2016a), human epidermal growth factor receptor 4 (Zhurauski et al., 2018) and cyclin-dependent kinase 2 (Estrela et al., 2010) with limit of

detection at 6.7 pM, 90 fg/ml, 1 pM and 100 fM, respectively. Meanwhile, Johnson et al. (2012) developed an impedimetric biosensor for the detection of C-reactive protein, a biomarker for a range of conditions including cardiovascular disease.

Diverse range of optical biosensors based on Affimers have also been investigated. Affimers conjugated to quantam dot were employed to develop ratiometric biosensors (Wang et al., 2017b). Interestingly, Affimers are also being studied for the development of high throughput biosensor using chiral plasmonic nanostructures (Tullius, 2017) and the development of nanoparticle size-shift assay coupling with dynamic light scattering (Mahatnirunkul, 2017). Apart from these, there are also studies that employed mechanical biosensors based on Affimers, particularly the quartz crystal microbalance with dissipation monitoring (QCM-D) technique. This technique was used to determine the kinetic binding analysis (Weckman et al., 2016, Koutsoumpeli et al., 2017).

1.7 Application of biosensors for CEA detection

To date research in biosensors has expanded tremendously since the innovation of the amperometric glucose biosensor in 1962 (Clark and Lyons, 1962). Emerging techniques in analytical chemistry, molecular biology and nanotechnology have resulted in many new technologies being developed for biosensor applications. The range of biosensors application has become wider and not limited to enzymatic based detection, but expanded to affinity based detection. In addition, incorporation of nanomaterials during the fabrication of biosensors has been used to produce better sensitivity and enable miniaturisation of the sensor devices.

Extensive research in genomic and proteomic biomarkers in cancer diagnosis have paved a new avenue for cancer diagnostics. For the past thirty years, research in the development of biosensors for cancer biomarkers detection have increased significantly. Previous work reported that human chorionic gonadotropin (hCG) (Aizawa et al., 1979), prostate-specific antigen (PSA) (O'Neill et al., 1995), α-fetoprotein (Kato et al., 1997), tumour suppressor *p53* gene (Wang et al., 1997), cancer antigen (CA-125) (Dai et al., 2003) and CEA (Dai et al., 2004) are among the earliest cancer biomarkers that have been investigated to develop biosensors for prostate, ovarian and colorectal cancers, respectively. Interestingly, most of these biosensors are based on amperometric and optical based sensing.

When analysing publications related to biosensors for CEA detection from 1988 to 2018 listed by the ISI Web of Science (**Figure 1.10**), data show that electrochemical biosensing is the most abundant approach compared to the other categories. It can be clearly seen that amperometric biosensors are the most prominent technique used followed by optical and voltammetric based techniques. Meanwhile, within the electrochemical category, impedimetric, capacitive and potentiometric measurements have been less frequently used. It is not a surprise that the amperometric approach is the leading technique used as this technique is the most developed for biosensor platforms.

Table 1.2 outlines a summary of published work involved in developing CEA biosensors with the primary focus on electrochemical techniques. It is important to note that the examples given are not exhaustive but representative of each category. Data within **Table 1.2** showed that the vast majority of electrochemical biosensors being developed primarily used antibodies as the bioreceptor. DNA aptamer and molecular

imprinted polymers are widely employed as biorecognition elements in the fabrication of voltammetric and potentiometric biosensors, respectively, for CEA detection apart from antibodies.
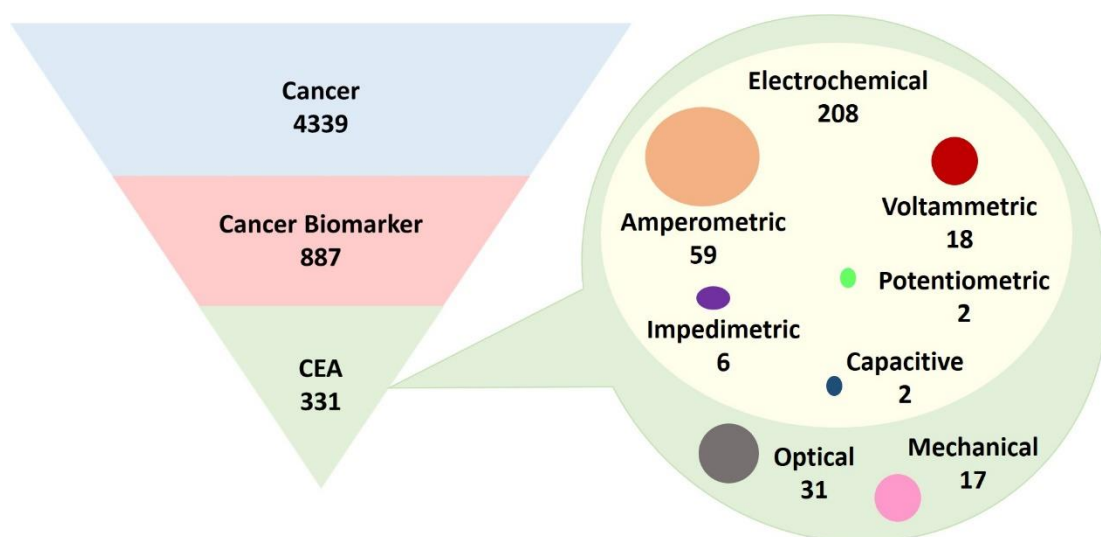
Figure 1.10: Publications in biosensors for cancer detection in general and type of biosensors in CEA detection from 1988 to 2018

Published data were retrieved from the ISI Web of Science by including the search terms 'biosensor' and 'cancer' between the periods of 1988 to 2018. The pyramid showing distribution of published articles in cancer detections in general followed by cancer biomarkers and narrow down to biosensors for CEA detection. The pointed circle showing different techniques used for the detection of CEA. The size of circle shows the proportion of publications associated with corresponding technique of biosensors.

Table 1.2 : Electrochemical biosensors for CEA detection

Random orientation						
Detection	**Biosensor**	**Transducer**	**Immobilization technique**	**Bioreceptor**	**LOD**	**Reference (s)**
Label-free	Impedimetric	Gold	Electro-copolymerization of *o*-aminophenol with CEA-Ab-glutathione monolayer modified AuNP	Antibody	0.1 ng/ml (500 fM)	(Tang et al., 2007)
	Impedimetric	Glassy carbon electrode (GCE)	Physisorption of anti-CEA antibody onto GCE modified with AuNP/ polymeric self-assembled nanoparticles (poly (ɤ-glutamic acid)-dopamine-chitosan	Antibody	10 fg/ml (50 aM)	(Xu et al., 2017)
	Impedimetric	Glassy carbon electrode (GCE)	Covalent immobilisation of amine-modified CEA aptamer on GA-AuNP/AMCM-GCE	DNA Aptamer	0.98 pg/ml (4.9 fM)	(Shekari et al., 2017)
	Impedimetric	Conducting Whatman paper	Covalent immobilization of anti-CEA antibody onto amine-functionalised surface coated with conducting poly (3,4ethylenedioxythiophene):poly(4-styrene sulfonate) on paper electrode	Antibody	2.68 ng/ml (13.4 pM)	(Kumar et al., 2016)
	Impedimetric	Graphite-based screen-printed electrode	Covalent immobilization of anti-CEA antibody onto poly-(pyrrole-3-carboxylic acid)-modified electrode	Antibody	33.33 pg/ml (166.65 fM)	(Iordănescu et al., 2018)
	Amperometric	Gold electrode	Physisorption of BSA-anti-CEA-AuNPs-poly(2-aminothiophenol)-gold electrode	Antibody	0.015 fg/ml (0.08 aM)	(Liu and Ma, 2013)
	Amperometric	Glassy carbon electrode (GCE)	Physisorption of anti-CEA/AgNPs/thionine/infinite coordination polymer/GCE	Antibody	0.5 fg/ml (2.5 aM)	(Lu et al., 2014)
	Voltammetric	Glassy carbon electrode (GCE)	Covalent binding of anti-CEA antibody to electropolymerized PANI nanowires grown on PEDOT/ionic liquid (IL) conducting polymer	Antibody	0.7 pg/ml (3.5 fM)	(Sun et al., 2017)
	Voltammetric	Graphene nanocomposite	Physisorption of anti-CEA/AuNPs/PEDOT/graphene	Antibody	0.1 pg/ml (500 aM)	(Gao et al., 2015)
	Voltammetric	Glassy carbon electrode (GCE)	Anti-CEA antibody covalently linked to GCE modified with redox membrane made from chitosan and thionine, then coated with nafion/AgNP/polyethyleneimine and glutaraldehyde	Antibody	1 fg/ml (5 aM)	(Wang et al., 2013)

Table 1.2 (continued)						
	Capacitive	Interdigitated gold electrode (IDE)	Covalent immobilization of anti-CEA antibody onto AuNP-SAM modified IDE	Antibody	5 pg/ml (25 fM) in buffer 20 pg/ml (100 fM) in serum	(Altintas et al., 2014)
Labelled	Impedimetric	Indium tin oxide (ITO) electrode on a glass slide	Covalent immobilization of anti-CEA antibody onto aldehyde-functionalised ITO electrode and sandwich with magnetic beads coated with secondary antibody for signal enhancement	Antibody	1 ng/ml (5 pM)	(Yeh et al., 2016)
	Impedimetric	Glassy carbon electrode (GCE)	Covalent immobilization of anti-CEA antibody onto AuNP-modified GCE and sandwich with HRP conjugated to secondary antibody functionalised with graphene oxide nanosheets and coupled with enzymatic biocatalytic precipitation of 4-chloro-1-naphthol	Antibody	0.64 pg/ml (3.2 fM)	(Hou et al., 2013)
	Capacitive	Interdigitated gold electrode (IDE)	Covalent immobilization of anti-CEA antibody onto SAM-modified IDE and sandwich with magnetic beads coated with secondary antibody for signal enhancement	Antibody	5 pg/ml (25 fM) in buffer 20 pg/ml (100 fM) in serum	(Altintas et al., 2012)
	Voltammetric	Glassy carbon electrode (GCE)	Anti-CEA antibody immobilised onto GCE modified with chitosan/ O-phenylenediamine/nano gold composite and sandwich with magnetic DNA-tagged nanoprobes	Antibody	5 pg/ml (25 fM)	(Gan et al., 2011)
	Voltammetric	Glassy carbon electrode (GCE)	Hairpin DNA containing CEA-specific aptamers and DNAzyme chains. The DNAzyme sequence hybridised with methylene blue labelled substrate chain that bind onto the surface of graphene quantum dot-ionic liquid-nafion (GQDs-IL-NF) composite film coated the GCE	DNA Aptamer	0.34 fg/ml (1.7 aM)	(Huang et al., 2018)

Table 1.2 (continued)						
	Voltammetric	Glassy carbon electrode (GCE)	Hairpin-shaped oligonucleotide-functionalized gold nanorods conjugated to HRP binds to preimmobilised streptavidins on chitosan/graphene/GCE modified electrode via interaction with biotin	DNA Aptamer	1.5 pg/ml (7.5 fM)	(Wen et al., 2016)
Site-directed orientation						
	Voltammetric	Indium tin oxide (ITO)	Covalent binding of anti-CEA antibody to ITO electrode grafted with hyperbranched polyester.	Antibody	2.36 pg/ml (11.8 fM)	(Miao et al., 2014)
	Potentiometric	Gold coated silicon chip	Molecular imprinting of CEA with hydroxyl functionalized alkanethiol molecules self-assembled on a gold-coated silicon chip	Molecular imprinted CEA	8 ng/ml (40 pM)	(Wang et al., 2010)
Label-free	Potentiometric	Gold electrode	Molecular imprinted CEA on SAM-modified gold electrode	Molecular imprinted CEA	0.5 ng/ml (2.5 pM)	(Yu et al., 2016)
	Voltammetric	Screen printed gold electrode (SPGE)	Chemisorption of thiolated CEA-Aptamer onto SPGE	DNA aptamer	0.9 pg/ml (4.5 fM)	(Taghdisi et al., 2018)
Labelled	Amperometric	Glassy carbon electrode (GCE)	Covalent immobilization of anti-CEA antibody onto GCE coated with Au NPs functionalized polydopamine and sandwich with labelled secondary antibody containing cubic Au-Pt dendritic nanomaterials functionalized nitrogen-doped graphene loaded with copper ion	Antibody	0.167 pg/ml (835 aM)	(Lv et al., 2018)

Abbreviations: AuNP, gold nanoparticle; AgNP, silver nanoparticle; Au-Pt, gold-platinum; CEA, carcinoembryonic antigen; SAM, self-assembled monolayer; DNA, deoxyribonucleic acid; HRP, horseradish peroxidase; GA, glutaraldehyde; PEDOT, poly (3,4ethylenedioxythiophene); PANI, polyaniline and AMCM, amino-functionalized MCM–41.

Another factor that plays a crucial roles in developing effective biosensor performance is the choice of electrode material used as the transducer layer. There are mostly two types of electrodes that have been used in developing CEA biosensors which can be categorised as carbon based using glassy carbon or graphite-based screen printed electrodes, and gold based, including atomically flat gold, interdigitated gold electrodes and screen printed gold electrodes. Interestingly, one study reported the use of a conducting polymer coated on a paper electrode (Kumar et al., 2016) whilst several other studies utilised an indium tin oxide electrode for direct immobilisation of the bioreceptor (Miao et al., 2014) and in a sandwich immunoassay (Yeh et al., 2016).

It can be clearly seen that in the majority of label-free detection procedures the biorecognition element is randomly immobilised via amine-coupling (Sun et al., 2017, Altintas et al., 2012, Iordănescu et al., 2018). Meanwhile, site-directed immobilisation is commonly achieved using coupling to thiols (Taghdisi et al., 2018) or carboxylic acids (Lv et al., 2018). Most CEA biosensors are based on a label-free detection technique. However, emerging technologies in nanomaterial science have driven researchers to investigate its application to biosensors notably in labelled detection techniques such as sandwich immunoassays. Incorporation of nanomaterials (e.g., gold nanoparticles, silver nanoparticles and gold nanorods) in the sensor construct enhanced the sensitivity and selectivity of detection (Xu et al., 2017, Lu et al., 2014, Wang et al., 2013). These improvements were also observed in the biosensors developed using small bioreceptors such as DNA aptamers (Shekari et al., 2017, Huang et al., 2018, Wen et al., 2016) which for some target analytes work better than traditional antibody based biosensors. Based on these observations, the high sensitivity obtained from using nanomaterials and small bioreceptors are probably due to the availability of ample binding sites for analyte interaction. Although labelled detection showed better sensor performance, the overall fabrication of these biosensors was usually complex and time-consuming which deviates from the objective of a POC application. Therefore, they are normally studied as prototypes but unlikely to reach a commercialise market.

When analysing published data from **Table 1.2** it emerges that the utilisation of molecular imprinted polymers as biorecognition element for CEA detection can only be found in potentiometric biosensors. In addition, the use of potentiometric biosensors to detect CEA is limited compared to other electrochemical techniques. With regard to limit of detection, potentiometric measurement was less sensitive (pM limit of detection)

compared to impedimetric and amperometric measurements (approximately aM to fM limit of detections).

1.8 Aims of the project

The main objective of this project was to develop a label-free electrochemical impedimetric biosensors on a commercial screen printed gold electrode using a novel antibody mimetic binding protein, the Affimer, as an alternative bioreceptor, for rapid detection and quantitation of CEA in colorectal cancer (CRC). Late detection in diagnosing CRC is associated with high morbidity and mortality rates. Although early detection is ideal and favourable, validated biomarkers for early screening of CRC are still arguable. Therefore, CEA was selected as a target analyte in this study because CEA is the only clinically validated prognostic and surveillance biomarker that is currently utilised in diagnosing CRC. Conventional diagnostics to determine the CEA level in the blood are ELISAs which require a centralised laboratory and are time-consuming. The impact from the development of this biosensor device could possibly revolutionise the current diagnostic strategy and accelerate the CRC diagnosis, and possibly population screening.

In particular, this study was designed to focus on two main topics. The first part is to investigate the potential of anti-CEA Affimers a*s* alternative affinity-bioreceptors. It was postulated that the Affimers would have comparable selectivity and binding capacity towards CEA similar to, or better than, conventional antibodies. The CEA binders were initially selected from an Affimer phage display library and several characterisation procedures were carried out to confirm the specificity and selectivity against CEA. Ultimately the aim is to fabricate and optimise impedimetric biosensors and use them as biorecognition element for CEA detection in buffer and diluted normal serum solutions. CEA immunosensors that represent the traditional antibody based biosensor were developed in parallel to enable comparison to the Affimer-based biosensors system. The possibility to develop single receptor or multi-receptor Affimer-based biosensors were also evaluated to mimic monoclonal vs polyclonal antibody based systems.

The second principle aim is to ascertain the possibility of using polyoctopamine as novel non-conducting polymer base layer that could be utilised as an alternative amine-bearing surface for the fabrication of impedimetric biosensors. This study will aid the understanding of processes at the biosensor interface coated with POct and its versatility to immobilise large or small bioreceptors such as antibodies and Affimers, respectively.

Chapter Two

Materials and Methods

Chapter 2 : Material and Methods

2.1 Materials

All materials used in the production and characterization of Affimer binders against CEA analytes and development of biosensors are described here in details.

2.1.1 Chemicals

Trimethylamine, 10x casein blocking buffer, glycerol, sodium meta-periodate, NaH_2PO_4, $K_3Fe(CN)_6$ and $K_4Fe(CN)_6.3H_2O$, biotin-N-hydroxysuccinimide ester (biotin-NHS), biotin-maleimide, octopamine hydrochloride, dimethyl sulfoxide (DMSO) and ethylenediaminetetraacetic acid (EDTA) were purchased from Sigma Aldrich (UK). Sulfosuccinimidyl 4-(N-maleimidomethyl) cyclohexane-1-carboxylate (sulfo-SMCC), EZ-Link® NHS-SS-Biotin, high sensitivity streptavidin-HRP, Halt protease inhibitor cocktail (100X) and SYBR™ Safe DNA gel stain were purchased from Thermo Scientific. NaCl was purchased from Fisher Scientific (UK). SeramunBlau® fast TMB/substrate solution was purchased from Seramun. Streptavidin beads (Dynabeads® MyOne™ Streptavidin T1, 10 mg/ml) was purchased from Invitrogen. 2-Log DNA Ladder (0.1-10 kb) and 100 bp ladder were purchased from New England BioLabs Inc.

2.1.2 Antibodies

Antibodies used in the project were purchased from the suppliers as outlined below.

Table 2.1 : List of antibodies used in immunoblotting, immunofluorescence staining and biosensors construction

Antibody	Origin	Source
Anti-CEA	Mouse monoclonal IgG	Thermo Scientific
	Rabbit polyclonal IgG	Genscript Ltd.
Anti-mouse-HRP	Goat polyclonal IgG	Abcam Plc.
Anti-mouse-Alexa Fluor® 488 conjugate	Goat polyclonal IgG	Invitrogen
Anti-6X His tag-HRP	Rabbit polyclonal IgG	Abcam Plc.
Anti-Digoxin	Sheep polyclonal IgG	Therapeutic Antibodies UK Ltd.
Anti-Sheep-HRP	Rabbit polyclonal IgG	Sigma Aldrich

2.1.3   Production of Affimers against CEA protein

Purified native CEA protein (Ab742) was purchased from Abcam Plc and used for screening of Affimers. ER2738 *E.coli* cells obtained from the BioScreening Technology Group (BSTG), University of Leeds, UK were used for amplification of the phagemid subclones during the biopanning process. XL1-Blue supercompetent cells were purchased from Agilent Technologies for plasmid amplification and BL21 Star™ (DE3) chemically competent *E.coli* cells were purchased from Life Technologies for protein expression. Phagemid vector *pBSTG1*, a cloning vector, and M13K07 helper phage were used during screening of the phage display library containing the Affimer coding sequences whilst *pET11(a)* vector was used for protein expression. Both vectors were obtained from the BSTG group and contained of *Nhe*1 and *Not*1 restriction sites. *Nhe* I-HF, *Not* I-HF and *Dpn* I restriction enzymes were purchased from New England BioLabs Inc. and were used as per the manufacturer's instructions. High fidelity (HF) enzymes were used to prevent star activity which resulted in cleavage of similar to the defined restriction site sequences by the restriction enzymes.

2TY and Luria-Burtani (LB) media containing 100 μg/ml of carbenicillin were used to culture the bacteria whilst LB agar was used for inoculating transformed cultures. Details of media composition can be found in **Appendix I**. 100 µg/ml of carbenicillin was used in the majority of the bacterial cultures either using LB or 2TY media. For culturing ER2738 *E.coli* cells, 12 μg/ml of tetracycline and 50 μg/ml of kanamycin were used.

For subcloning of selected Affimer coding regions into the *pET11(a)* vector, PCR amplification were performed using primers listed in **Table 2.2** following the experimental condition summarized in **Table 2.3**.

Table 2.2 : Primers used in PCR amplification

Forward primer	5'-ATGGCTAGCAACTCCCTGGAAATCGAAG
Reverse primer	5'-TTACTAATGCGGCCGCACAAGCGTCACCAACCGGTTTG

Table 2.3 : Cycling conditions of PCR amplification

Cycle step	Temperature	Time	Cycles
Initial Denaturation	98°C	30 seconds	1
Denaturation	98°C	20 seconds	
Annealing	54°C	20 seconds	30
Extension	72°C	20 seconds	
Final extension	72°C	10 minutes	1
Hold	4°C	Hold	

2.1.3.1 Affimer protein extraction and purification

All buffers used for protein extraction are summarized in **Appendix I**. Ni^{2+}-NTA affinity resin was purchased from Expedeon. Pierce 5 ml capacity centrifuge columns were purchased from Thermo Scientific. Dialysis was carried out when necessary using a Pur-A-Lyzer™ midi dialysis kit purchased from Sigma Aldrich.

2.1.4 SDS-PAGE

Mini-PROTEAN® TGX™ 4-15% precast gels, 2x Laemmli sample buffer, 2-mercaptoethanol and 10x Tris-Glycine SDS-PAGE running buffer were purchased from Bio-Rad whilst Coomassie Instant Blue staining solution was purchased from Generon. Spectra™ multicolor broad range protein ladder was purchased from Thermo Scientific.

2.1.5 Immunoassays

PVDF membrane and 10x Tris-Glycine transfer buffer were purchased from Bio-Rad and used for western blotting. SuperBlock T20 (TBS) blocking buffer, pH7.4 and Pierce™ ECL western blotting substrate were purchased from Thermo Scientific. ProLong® gold antifade reagent with DAPI was purchased from Molecular Probes (Life Technologies) for immunofluorescence staining.

2.1.6 CEA protein production

All reagents and consumables used for cell culture work were obtained from Gibco® (Life Technologies) unless otherwise specified. Fetal bovine serum was purchased from Sigma-Aldrich. CEA protein was extracted using mammalian cell PE LB™ lysis buffer and Mammalian ProteaseArrest™ inhibitor cocktail. These reagents were purchased from G-Biosciences. Bicinchoninic acid (BCA) protein assay kit was purchased from Sigma-Aldrich for protein quantification.

2.1.7 Deglycosylation assay

Deglycosylation of CEA protein was carried out using a PNGase F deglycosylation kit purchased from the New England BioLabs Inc. RNase B, which is used as PNGase F positive control protein was also purchased from the same company.

2.1.8 Electrodes

Screen printed gold electrodes (CX2223AT) were purchased from DropSens (Asturias, Spain). This electrode is made of two round gold working electrodes with 1.6 mm diameter, a gold counter electrode and a Ag/AgCl reference electrode fired onto a ceramic base. Four silver connectors at the bottom of the chip connect all electrodes to the potentiostat via a DropSens connector. Working electrode 1 (WE1, left) and 2 (WE2, right) were used to immobilise the non-specific and specific bioreceptors, respectively. The picture of the electrode is depicted in **Figure 2.1**.
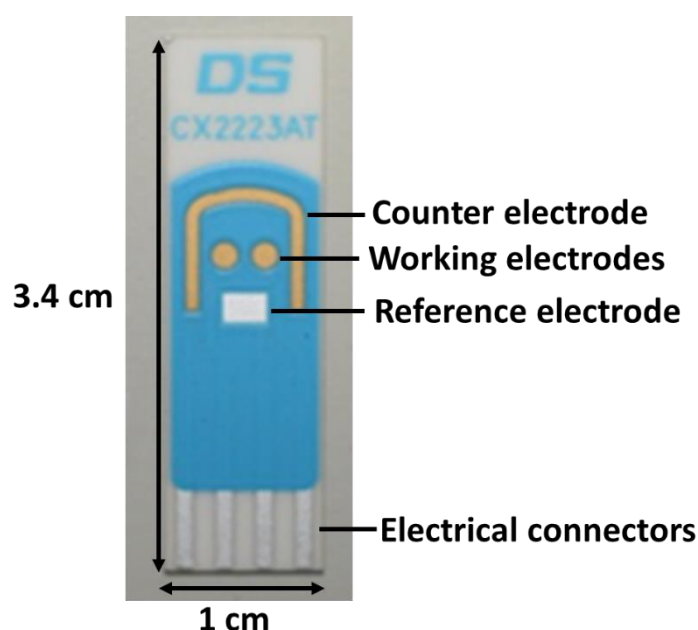
Figure 2.1 : Picture of DropSens screen printed gold electrode.

The dimensions of the electrode is 3.4 cm length x 1.0 cm width x 0.05 cm height coated with a ceramic base. Two round gold working electrodes, a gold counter electrode and a silver reference electrode are connected to four silver strips at the bottom which connect to a potentionstat via a DropSens connector.

2.2 Methods

2.2.1 Phage display for Affimer screening

2.2.1.1 Biotinylation of CEA

One hundred µl of 1 mg/ml CEA protein solution and yeast SUMO (ySUMO), which was used as a positive control, were mixed individually with 0.53 µl of 5 mg/ml EZ-Link® NHS-SS-Biotin. The mixtures were incubated for 1 h at RT and desalted to remove any excess biotin using Zeba spin desalting columns as per manufacturer's protocol. The success of biotinylation was validated via ELISA. Fifty microliters of PBS were aliquoted into each well and mixed with biotinylated proteins that were prepared earlier. Overnight incubation at 4°C was carried out followed by washing three times with 300 µl of PBST per well, and re-incubated for 1 h at RT on a vibrating platform shaker with 50 µl of diluted high sensitivity Streptavidin-HRP at a concentration of 1:1000 in 2× blocking buffer. The wells were repeatedly washed six times prior to developing in TMB/substrate solution. Absorbance was measured at 620 nm using an Ascent™ microplate reader (Thermo Scientific).

2.2.1.2 Biopanning of phage display library

Three phage display panning rounds of one standard and two consecutive competitive binding pannings were carried out for screening for Affimers against the CEA target binders. Throughout the whole panning rounds, CEA or ySUMO were used as target molecules and positive control, respectively. For the first panning round, biotinylated CEA or ySUMO were bound to the streptavidin coated (HBC) 8-well strips for 1.5 h at RT on a vibrating platform shaker. The pre-panned phage library was added into each biotinylated sample and incubated for another 2 h. Panning wells were then washed 27 times with 300 µl of PBST using a plate washer and the bound phages were eluted with 100 µl of 0.2 M Glycine, pH 2.2 for 10 min and the eluent was neutralized with 15 µl of 1 M Tris-HCl, pH 9.1. The eluted phage were rapidly transferred into 8 ml of fresh culture containing ER2738 cells in 2TY media plus 12 µg/ml of tetracycline followed by second elution in 100 µl of 0.1 M triethylamine for 6 min with neutralization with 50 µl of 1 M Tris-HCl, pH 7. The eluted phage were transferred again to the same culture to infect ER2738 cells by incubating for 1 h without shaking at 37°C. This was followed by plating onto LB agar plates containing 100 µg/ml carbenicillin and growth

overnight at 37°C. Colonies were scraped into 7 ml of 2TY media containing 100 µg/ml carbenicillin. The cells were then diluted to a new 8 ml culture and re-incubated for 1 h at 37°C while shaking at 230 rpm. After incubation, the cells were infected with 1 µl of 1:3 dilution of M13K07 helper phage (titre ca. 10^{14}/ml) and further incubated for 30 min at 37 °C and 90 rpm after which they were incubated overnight with 50 µg/ml of kanamycin at 25°C and 170 rpm. Later, the phage-infected cultures were centrifuged at $3,500 \times$ g for 10 min and the supernatant was transferred to a new 15 ml Falcon tube. An aliquot of 125 µl of phage-containing supernatant was used for the second panning round, whilst the remaining phage were precipitated with 4% (w/v) PEG 8000, 0.3 M NaCl and incubation overnight at 4°C. The phage were centrifuged at $4,816 \times g$ for 30 min and pellets were re-suspended in 320 µl of TE followed by another centrifugation at $16,000 \times g$ for 10 min. The supernatant containing phage was diluted with 40% (v/v) glycerol and stored at -80°C.

A second round of selection was performed via competitive panning by mixing an aliquot of 125 µl of phage-containing supernatant from the first panning with an equal volume of 2× blocking buffer and 25 µl of pre-blocked streptavidin magnetic beads. This mixture was incubated for 1 h at RT on the rotator. Simultaneously, 15 µl of biotinylated CEA or ySUMO were added separately to 200 µl of 2x blocking buffer and 50 µl of the pre-blocked streptavidin beads followed by incubation for 1 h at RT on a rotator. The CEA or ySUMO labelled beads were washed 3 times with 500 µl of 2x blocking buffer and subsequently incubated with pre-panned phage for 1 h then washed again 4 times using a KingFisher Flex robotic platform (Thermo Fisher). The beads were released into 100 µl of PBS and mixed with 60 µl of both 10x blocking buffer and 80% (v/v) glycerol, 3 µl of Halt protease inhibitor cocktail (100x), 2.5 µg of each non-biotinylated CEA and ySUMO, respectively, then the total volume was adjusted to 300 µl in PBS. The mixture was incubated overnight at RT on the rotator and washed 6 times with 500 µl of 2x blocking buffer. The phage were eluted and amplified as described in the first panning round.

The second competitive binding was performed in the third panning round using a Neutravidin high binding capacity (HBC) coated 8-well strip. The pre-panning steps were carried out following the same procedures as the first panning round whereby 200 µl of phage-containing supernatant from the second panning were used in pre-panning the phage. In the meantime, 10 µl of biotinylated CEA and ySUMO were mixed with 100

µl of 2× blocking buffer and incubated for 1 h at RT on a vibrating platform shaker. These wells were used for panning against CEA and ySUMO, whilst, the negative wells were prepared without any biotinylated protein. These wells were then washed 3 times with 300 µl of PBST and incubated with 100 µl of pre-panned phage for another 45 min. Once the incubation was complete, the wells were washed again for 27 times using a plate washer prior to the addition of 80 µl of 2x blocking buffer, 20 µl of 80% (v/v) glycerol, 1 µl of Halt protease inhibitor cocktail (100 x) and 2.5 µg of each non-biotinylated CEA and ySUMO into respective wells and incubated for overnight at RT on a vibrating platform shaker. The phage were eluted and amplified as described for the first panning round.

2.2.1.3   Phage ELISA

Phage ELISA was performed to select for positive clones. Forty eight individual ER2738 colonies from the third panning round were randomly picked and grown overnight at 37°C and constantly agitated at 1050 rpm in 200 µl of 2TY media containing 100 µg/ml of carbenicillin in a 96-well V-bottom deep well plate. An aliquot of 25 µl of the overnight culture was transferred to 200 µl of fresh 2TY media containing 100 µg/ml of carbenicillin and further grown for 1 h. Subsequently, 10 µl of ca. 1×10^{11}/ml M13K07 helper phage were added to the fresh cultures and incubated for another 30 min, 450 rpm at RT. Following this, an aliquot of 10 µl of 50 µg/ml kanamycin solution was added to the phage infected cultures and incubated overnight at RT with constant agitation at 750 rpm. Streptavidin-coated 96-well plates were blocked with 200 µl of 2× blocking buffer per well overnight at 37°C without agitation followed by washing once with 300 µl of PBST. The plates were then incubated with 50 µl of biotinylated CEA and ySUMO, respectively for 1 h at RT on shaker. Aliquots of 50 µl of 2× blocking buffer per well were added to the negative control wells in each plate. Later, the plates were washed once with 300 µl per well of PBST and 10 µl per well of 10× blocking buffer was added. Once incubation was complete, the phage-infected cultures were centrifuged at 3,500 $\times g$ for 10 min and 40 µl of the supernatant was aliquoted into each well including the negative control wells. The plates were further incubated for 1 h at RT with shaking, followed by a single wash with 300 µl of PBST and incubated with 50 µl of diluted anti-Fd-bacteriophage-HRP at a concentration of 1:1000 for another 1 h at RT. Final washes were done in 10 times of 300 µl PBST and developed in 50 µl of TMB/substrate solution prior to measuring the absorbance at 620 nm.

2.2.1.4   Subcloning of Affimer coding regions into *pET11(a)*

Positive clones from phage ELISA were sent for sequencing and the selected Affimer coding regions were amplified by PCR amplification using primers listed in **Table 2.2**. Nucleotides coding for a single cysteine residue was inserted in the reverse primer to generate protein with a C-terminal cysteine. Both DNA amplified-Affimer coding sequences and *pET11a* vector were digested with *Nhe*I-HF and *Not*I-HF restriction digestion enzymes at 37°C for 2 h. Digested *pET11(a)* was dephosphorylated by incubation at 65°C for 5 min with 5 U/µl of Antartic phosphatase to prevent re-ligation of linearized plasmid DNA. The digested vector was separated by running through 0.7% (w/v) gel agarose electrophoresis at 90 V for 75 min followed by extraction according to the manufacturer's protocol using NucleoSpin® Gel and PCR Clean-up kit. Meanwhile, digested DNA insert was treated with 10 U/ml of *Dpn*I at 37°C for 1 h to remove the *dam* methylated DNA prior to purification using the same kit as mentioned above. Then, 30 fmol of digested *pET11(a)* vector were ligated with 90 fmol of insert DNA in the presence of 200 U/µl of T4 DNA Ligase and 0.5 µl of 10X T4 DNA ligase buffer by overnight incubation at 16°C.

2.2.1.5   Transformation of *E.coli* cells using heat shock treatment

XL1-Blue supercompetent cells were used to transform the ligation product whilst BL21 (DE3) *E.coli* cells were used to express the Affimer proteins. In general, *E.coli* cells were gently thawed on ice and aliquoted 10 µl prior to mix with 1 µl of ligation mixture, or 1 µl of plasmid obtained after a miniprep and incubated on ice for 30 min. The mixture was heat shocked at 42°C for 45 sec and immediately incubated on ice for 2 min. Then, 180 µl of SOC medium were added and continue incubation at 37°C for 1 hour with shaking at 230 rpm. Finally, 100 µl of the transformation mixture were plated onto LB/ carbinicillin (100 µg/ml) plates and grown overnight at 37°C.

2.2.1.6   Affimer expression and purification

Starter culture was prepared by inoculating single colony from the transformation plate into 2ml 2TY media containing 100 µg/ml of carbinicillin plus 1 % (w/v) glucose and grown overnight at 37°C with shaking at 230 rpm. Following these, 1 ml of the overnight culture was transferred into 50 ml LB media containing 100 µg/ml of carbinicillin and growth continued for another 2 h using the same incubation condition.

Once OD_{600} reached about 0.8, the culture was induced for 6 h with 0.1 mM IPTG and incubated at 25°C with shaking at 150 rpm. The cells were harvested and lysed for 20 min at RT on rotator in 1 ml of lysis buffer (**Appendix I**) supplemented with 10 µl of each Triton-X-100, 10 mg/ml lysozyme and 100X halt protease inhibitor, respectively, and 10 U/ µl of benzonase nuclease. Non-specific proteins were heat denatured by incubation at 50°C for 20 min. The lysate was mixed with 300 µl of washed Ni-NTA slurry for 2 h at RT on rotator and washed thoroughly with wash buffer and eluted in 1 ml elution buffer as listed in **Appendix I**.

2.2.1.7 Biotinylation of Affimers

Purified Affimers were biotinylated via the cysteine residue at the C-terminus using biotin-maleimide. First, 150 µl of 40 µM Affimer in elution solution was mixed with an equal volume of washed immobilized TCEP disulphide reducing gel for 1 h at RT on a rotator. The solution was centrifuged at 1000×g for 1 min. Supernatant containing freshly reduced Affimer was immediately mixed with 27 µl of 2 mM biotin-maleimide and incubation continued for 2 h at RT. Excess biotin was removed by using Zeba spin desalting column (7 MWCO) following the manufacturer's protocol.

2.2.1.8 Pull-down assay

Purified Affimer (20 µg) was dialysed in 1x PBS prior to incubation with 40 µl of washed Ni^{2+}-NTA slurry for 90 min at 4 °C on rotator. Affimer loaded resins were washed once with 1X PBS and mixed with purified CEA from Abcam, cell lysates of LoVo, CEA secreted into the medium or deglycosylated CEA after treatment with PNGase F. These mixtures were incubated overnight at 4 °C on a rotator. The resins were washed three times with 1X PBS and proceed with SDS-PAGE analysis and western blotting to determine the success of the pull-down assay.

2.2.1.9 Analysis of binding kinetics via SPR

Kinetic binding analysis was conducted using a BIACore 3000 instrument (GE Healthcare, Sweden). The instrument temperature was set at 25°C throughout the experiments. The instrument was cleaned by priming with running buffer (1×PBS + 0.1% Triton-X-100) before and after docking a new streptavidin (SA) sensor chip. Prior to immobilization of biotinylated Affimers, the SA chip was preconditioned by injecting 1 M NaCl and 50 mM NaOH at a flow rate of 40 µl/min. Three flow cells (cells 2 to 4)

were used for immobilization of 10 nM of biotinylated Affimer-CEA-I, II & III, respectively and flow cell 1 was used as a reference cell. Biotinylated Affimers and CEA were diluted in the same running buffer prior to use to minimize loss of the bioreceptors or analyte due to absorption to the tubing and the fluidics channel of the instrument. A low density surface (~270 RU) was generated by immobilizing the biotinylated Affimers at a flow rate of 5 µl/min. CEA analyte was prepared by 2-fold serial dilutions from 7.81 nM to 1 µM. A running buffer was flowed over to equilibrate the flow cells prior to successive injections of CEA analyte. CEA was injected using the KINJECT command in increasing concentrations at a flow rate of 50 µl/min for 3 min. The dissociation rate of the CEA/Affimer complex was then monitored for 5 min followed by surface regeneration via injecting 1×PBS containing 1 M NaCl for 4 min before injecting the subsequent CEA concentration. After the final injection of CEA, a running buffer was flowed over again to monitor the stability of the baseline. Experiments were done in triplicate. Double referencing was performed to subtract drift and noise derived from the blank injection and systematic artefacts from the reference surface by using BIAevaluation software version 3.2. Global fitting was performed to extract the kinetic binding parameters which will be described in details in **section 2.2.9**.

2.2.2 CEA protein production

2.2.2.1 Cell culture

LoVo cell line (ATCC® CCL229™), a cell line that positively expressed CEA, was grown in F-12 Nutrient Mixture containing GlutaMax™_I supplemented with 10% (v/v) heat-inactivated fetal bovine serum, 50 U/ml of penicillin and 50 µg/ml of streptomycin at 37˚C under 5% CO_2 humidified conditions. Culture medium was aspirated every 3 days and collected for CEA protein isolation, whilst the cells continued to grow as monolayer until reaching confluency at day 7 in a 150 cm^2 flask. Meanwhile, HEK 293 cells (ATCC® CRL-1573™), a cell line that did not express CEA, was grown in DMEM containing GlutaMax™-I supplemented with 10% (v/v) heat-inactivated fetal bovine serum. At the time of confluence, cells were counted manually with a hemocytometer using the Trypan Blue exclusion test to determine the percentage of viable cells as well as the average amount of cells that released CEA protein during the protein isolation procedure.

2.2.2.2 CEA protein isolation

The collected medium was centrifuged at $3220 \times g$ for 5 min at $4°C$ to remove cell debris. The supernatant was then concentrated using an Amicon® Ultra Centrifugal Filter (15 ml, 50 KDa device, Millipore) for another 10 min at $5000 \times g$ and $4°C$ prior to protein extraction. Once cells reached confluency, media was discarded and cells were washed once with $1\times$ ice-cold Dulbecco's PBS. Protein was extracted from LoVo and HEK 293 cells by lysis in 1ml of Mammalian cell PE LB™ lysis buffer containing 10 µl of $100\times$ Mammalian ProteaseArrest™ inhibitor cocktail and incubated for 10 min at $4°C$. Protease inhibitor was included to prevent proteolytic degradation. Cell lysates and the CEA secreted into the medium were then centrifuged at $16,000 \times g$ for 30 min at $4°C$ and stored at -20 $°C$ until further use.

2.2.3 Affinity-fluorescence staining

To evaluate the potential of Affimers as monoclonal reagent in affinity-fluorescence staining in fixed cells, indirect Affimer based staining was carried out on LoVo and HEK 293 cells. The cells were seeded at 3×10^5 cells / well for 3 days incubation on cover slips in 6-well plates and cultured in the same condition as described in **section 2.2.2.1**. When the cells reached about 70% confluency, the medium in the 6-well plate was discarded, followed by washing three times with PBS (pH7.4) buffer and incubated for 5 min at RT for each washing step. Washed cells were fixed in 4% (w/v) paraformaldehyde solution for 10 min at RT. Fixative solution was discarded and fixed cells were washed three times with PBS buffer and blocked in SuperBlock T20 (TBS) blocking buffer, pH7.4 and incubated for 30 min at RT. Then, 10µg/ml of biotinylated Affimers in blocking buffer were applied and incubated overnight at 4 $°C$. Mouse anti-human IgG CEA (1µg/ml) was used as a primary antibody and included as a positive control on separate coverslips. After overnight incubation, the coverslips were washed again three times with PBS and incubated with detection reagent. Goat anti-mouse IgG secondary antibody conjugated with Alexa Fluor® 488 was used on the positive control coverslip whilst, Streptavidin DyLight 488 conjugate was applied on cells probed with biotinylated Affimers. A dilution of 1:1000 of secondary reagent from 1 mg/ml stock was prepared and incubations were carried out for 1 h at RT in the dark. Coverslips were washed $3\times$ with PBS and mounted with ProLong® gold antifade reagent with DAPI. Primary antibody or biotinylated Affimers were omitted in the negative controls. CEA

protein localization was visualized using an AxioObserver Z.1 microscope equipped with an ApoTome system of structured illumination (Zeiss, Germany).

2.2.4 Deglycosylation of CEA protein using PNGase F treatment

Deglycosylation of CEA protein using PNGase F treatment was done under denaturing conditions. RNase B protein was used as the positive control for PNGase F treatment. Purified CEA or RNase B (20 µg) were heat denatured at 100°C for 10 min in 1X glycoprotein denaturing buffer (0.5% (w/v) SDS, 40 mM DTT). Samples were subsequently treated with 500 U/µl of PNGase F in 1x GlycoBuffer 2 and 1% NP-40 and incubated for 1 h at 37°C. The extent of deglycosylation assay was visualized via SDS-PAGE gels and subsequently used for pull-down assay to determine the binding capacity of Affimer against deglycosylated CEA.

2.2.5 SDS-PAGE

SDS-PAGE analyses with Coomassie staining were performed to analyze the purity of purified Affimers, homogenates of LoVo cell lysates and in pull-down assays. In general, 10 µg of total protein sample was mixed with an equal volume of 2× Laemmli sample buffer and heated at 95°C for 5 min prior to electrophoretically separated via SDS-PAGE using a pre-casted 4-20% (w/v) gradient polyacrylamide gel for 70 min at 100 V in SDS running buffer (**Appendix I**). Prestained molecular weight marker proteins (10 to 260 KDa) were also loaded. After electrophoresis, gels were stained with Generon quick Coomassie stain for 30 min followed by destaining several times in deionised water before visualizing using a Syngene G-Box imager.

2.2.6 Western blotting and dot blotting

For western blotting, protein samples were separated following the same procedure as for SDS-PAGE analysis. Once electrophoresis was complete, the proteins were transferred via wet electroblotting onto 0.2 µm PVDF membranes by applying a constant voltage of 100 V for 90 min with cooling. Dot blotting was conducted by spotting nitrocellulose membranes with 2 µl of each 1 µM CEA or BSA which is used as negative control analyte and allowed to air dry completely. Following this, both techniques shared the same procedure began with blocking the membranes with SuperBlock T20 (TBS) blocking solution for 30 minutes on a rocking platform. Membranes were washed 3× after with 0.1 % (v/v) TBST for 5 min each time and subsequently probed with appropriate

primary antibody diluted 1:1000 in blocking solution and incubated for 1 h at RT with gentle rocking. Membranes were washed 3× after each incubation and incubated with appropriate secondary antibody HRP conjugated (1:2000) for 1 h at RT. Final washes (3×) were carried out in 0.1% TBST followed by three washes in 1xTBS before adding ECL substrate and imaging using a Syngene G-Box imager.

2.2.7 Preparation of electrode

2.2.7.1 Oxidation of antibody oligosaccharide using sodium *meta*-periodate

Antibody at 2 mg/ml was mixed with an equal volume of 20 mM sodium *meta*-periodate in Glycolink coupling buffer pH 5.5. The oxidation reaction was carried out in the dark at RT for 30 min using constant rotations of the reaction tube. Excess of sodium *meta*-periodate was removed using Zeba spin desalting column (7 MWCO) following the manufacturer's protocol. The concentration of oxidized antibodies was measured using a Nanodrop 2000 spectrophotometer (Thermo Scientific).

2.2.7.2 Biofunctionalization of transducer surfaces for IgG based sensors

Monomer solution was prepared by dissolving 5 mM octopamine in 100 mM phosphate buffer pH 7.5 and 20% (v/v) DMSO. Electrochemical polymerization was conducted via cyclic voltammetry (CV) in the prepared solution with potential scanning between +0 V to +1.6 V and back at a scan speed of 100 mV/s for 2 cycles. Electrodes were washed thoroughly with 100 mM PBS pH 7.1 to remove excess octopamine monomer and incubated for 5 min in PBS. Freshly oxidized antibodies containing reactive aldehyde groups were diluted to 0.1 mg/ml in 100 mM phosphate buffer pH 7.1 and covalently bound to the functionalized aminated group on the working electrodes surface for 1 h at RT in a moist chamber. The modified electrodes were washed extensively with PBS to remove unbound antibodies and equilibrated for 30 min in PBS to obtain baseline signal stability. These fully constructed immunosensors were ready for electrochemical interrogation and testing for analyte binding. Monoclonal or polyclonal anti-CEA antibodies were used as specific receptors whilst anti-digoxin polyclonal antibody was used as a non-specific receptor. Both non-specific and specific receptors were immobilised separately onto working electrodes 1 and 2, respectively, in a single chip.

2.2.7.3 Electrochemical biofunctionalization of transducers for Affimer-based sensors

Fabrication of Affimer-based sensors comprised a step-wise process. Initially, 20 mM octopamine solution was mixed with an equal volume of 26 mM sulfo-SMCC and allowed to react for 1 h at RT on a rotator. Both reagents were prepared in 100 mM phosphate buffer pH 7.5 and 20% (v/v) DMSO. Then, 0.2 mg/ml of freshly reduced Affimer containing free sulfhyldryl groups were mixed with an equal volume of octopamide-SMCC conjugate and further incubated for another 1 h at RT on a rotator. Affimers were reduced using immobilized TCEP reducing gel and diluted from stock in 100 mM phosphate buffer pH 7.1 prior adding to the octopamide-SMCC conjugate. Electrochemical deposition of octopamide-SMCC-Affimer conjugates was effected via CV using the same protocol as described above. These fully functionalized sensor surfaces, either with or without blocking, were ready for electrochemical investigation and testing of analyte binding.

2.2.7.4 Analyte addition

Fully functionalized sensors either using antibodies or Affimers as bioreceptors were tested against a range of analyte concentrations by sequential addition beginning with the lowest concentration. Purified CEA purchased from Abcam Plc. was used for sensor interrogation. CEA was diluted in 1X PBS pH 7.4 prior to incubating on working electrodes for 20 min in a moist chamber at RT. Electrodes were rinsed in 100 mM PBS pH 7.1 to remove any unbound analytes followed by electrochemical measurements. Copious rinsing with the same washing buffer was carried out after the measurements were taken prior to incubation with subsequent samples. The optimised sensors were then tested for sensor performance in a range of diluted normal human sera which were commercially purchased from the Thermo Fisher Scientific. The sera were serially diluted in 1X PBS and subsequently spiked with varying concentrations of CEA.

2.2.7.5 Electrochemical measurements

Electrochemical measurements were conducted in a standard three cell system using a µAutolab type III electrochemical workstation fitted with frequency response analyser 2 (FRA2) module (Metrohm Autolab B.V., The Netherland) . Electrochemical impedance spectroscopy (EIS) analysis was used to investigate the electrochemical

characteristics of fabricated sensors and monitor the analyte recognition. EIS measurements were carried out in an electrolyte solution containing 1:1 ratio of 10 mM $K_3[Fe(CN)_6]$/ $K_4[Fe(CN)_6]$ in 100 mM PBS pH 7.1. The impedance data were recorded over the frequency range from 2.5 KHz to 0.25 Hz with a modulation voltage of 10 mV at 0 V applied potential relative to the reference electrode. Autolab NOVA software was used to process and analysed the collected data. Experiments were replicated ($n \geq 3$) on independent sensor surfaces. Change in charge transfer resistance (R_{CT}) was used to analyse the analyte binding activity on sensor surface as it has been reported to be the most sensitive technique and widely used in impedimetric analysis of biosensors (Goode et. al 2016, Johnson et al., 2012). To minimize the batch-to-batch variability of the electrodes, the R_{CT} value of each concentration was normalized to the R_{CT} measured from the initial baseline of a fully constructed sensor in the absence of analyte using the following equation:

$$\text{Change in } R_{CT} (\%) = \frac{R_{CT \, (CEA)} - R_{CT \, (\text{blank analyte})}}{R_{CT \, (\text{blank analyte})}} \times 100$$

Equation 2.1: Equation for the normalisation of change in R_{CT}

2.2.8 Midland blotting

Midland blotting was employed according to the established protocol (Rushworth et al., 2013a) to characterize the presence of functional group created after polymerization, the presence of bioreceptors after immobilization and to validate the binding of target analytes on fully constructed sensors. For determination of surface amine or sulfhydryl moiety after polymerisation of octopamine or octopamide-SMCC conjugate, modified electrodes were incubated in the presence or absence of biotin-NHS or biotin-maleimide (2 µg/ml), respectively for 1 h at RT in moist chamber. The electrodes were washed once in 0.1% PBST and incubated for another 1 h in 1 µg/ml of streptavidin-HRP. These were followed by three washes in 0.1% PBST and four washes in 1×PBS prior to incubation in ECL reagent and immediately imaged using a Syngene G-Box imager. To evaluate the presence of bioreceptors after immobilization or bound analytes, appropriate primary antibodies and secondary antibodies conjugated to HRP were employed as listed in **Table 2.1**. The same washing steps and incubation with ECL reagent were performed. Images taken were further processed using ImageJ software. Original images captured were chemiluminescence (white light on a black background)

but processed images were pseudo-green colour superimposed on chemiluminescence images for ease of analysis.

2.2.9 Data analysis

Statistical analyses were performed using either Origin Pro or GraphPad Prism 7 software to analyse the electrochemical experiments. Kinetic binding analysis was carried out using BIAevaluation software version 3.2 using a simple 1:1 Langmuir binding interaction model (**Equation 2.2**) to determine the association and dissociation rate constants (k_a and k_b, respectively) and equilibrium dissociation constant (K_D). These analyses are based on combination of numerical integration as shown in the **Equation 2.3** below and non-linear least-squares global curve fitting.

$$\text{A+B} \underset{k_b}{\overset{k_a}{\rightleftharpoons}} \text{AB}$$
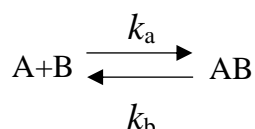
Equation 2.2: 1:1 Langmuir binding interaction model

$$
\begin{aligned}
d[\text{A}]/dt &= 0 \\
d[\text{B}]/dt &= -k_a\,[\text{A}][\text{B}] + k_d\,[\text{AB}] \\
d[\text{AB}]/dt &= k_a\,[\text{A}][\text{B}] - k_d\,[\text{AB}] \\
R &= [\text{AB}] + RI
\end{aligned}
$$

Equation 2.3: Numerical integration

The concentration of CEA in the bulk flow is denoted as [A] in the model and is assumed to be constant during the association phase. Meanwhile, [B] denotes the immobilized anti-CEA-Affimers on the surface, [AB] is the CEA/Affimer complex formed during the reaction, R denotes the SPR response and RI denotes the reponse generated from the bulk refractive index effect and all expressed in response units (RU). The modelled data were subsequently fitted to the experimental data using the non-linear least-squares global curve fitting to obtain the kinetic rate constants. The equilibrium dissociation constant (K_D) is derived from the ratio of the kinetic rate constants as shown in **Equation 2.4** below:

$$K_D\,(\text{M}) = \frac{k_a\,(\text{M}^{-1}\,\text{s}^{-1})}{k_b\,(\text{s}^{-1})}$$

Equation 2.4: Equilibrium dissociation constant

Chapter Three

Screening and characterization of CEA binding Affimers

Chapter 3 : Screening and characterization of CEA binding Affimers

3.1 Introduction

This chapter focuses on screening and characterization of CEA binding Affimers that will be used as biorecognition element to develop an electrochemical biosensor for detection of the colorectal cancer biomarker, CEA. The screening involves a biopanning process using a phage display of Affimer library. In brief, two types of cloning vectors were used, *pBSTG1* phagemid and *pET11a*. The *pBSTG1* phagemid vector (**Figure 3.1 A**) is derived from *pHEN* (Hoogenboom et al., 1991) vector with *pBR322* origin of plasmid replication and ampicillin resistant marker for selection of transformants. It also contained a DsbA signal sequence for translocation of the fusion gene into the periplasm of the bacterial cell wall, C-terminus of truncated pIII coat gene derived from M13 phage for displaying the fusion protein on the surface of the phage and a TAG amber stop codon for continuity of protein translation from Affimer coding sequence to pIII gene. Apart from these, the Affimer coding sequence was flanked by *Nhe 1* and *Not 1* restriction sites that can be used for subcloning purpose.

Based on these features, the phagemid vector was only suitable for amplification of the DNA insert in bacterial cell but not optimized for expression of recombinant protein. Thus, engineered *pET11a* vector was used for expression of recombinant protein (**Figure 3.1 B**). *pET11a* consists of the same origin of plasmid replication with insertion of *Not 1* restriction site to facilitate subcloning of Affimer coding sequence from phagemid to *pET11a* vector. In addition, this vector possesses a T7 promoter and terminator flanking the Affimer coding sequence which plays important roles in transcription and translation of the recombinant protein. The expression of recombinant protein was controlled by induction of IPTG at exponential growth phase which releases the *lac* repressor from binding to *lac* operator.

Characterization on the specificity of CEA binding Affimers was investigated via affinity-fluorescence staining on LoVo cells, a highly expressing CEA cell line from an aggressive metastatic colorectal cancer, and affinity-precipitation assay against the homogenates of LoVo cells and CEA released into the media. Further evaluation was also conducted to determine whether the anti-CEA Affimer binders recognized the glycan or protein domain as CEA is a highly N-linked glycosylated protein. Analysis of kinetic

binding parameters via surface plasmon resonance (SPR) was performed to evaluate the association and dissociation rate constants and to obtain the equilibrium dissociation constant (K_D). The outputs retrieved from these characterization are essential in optimizing and developing Affimer-based impedimetric biosensors and will be discussed in detail in **Chapter 5**.
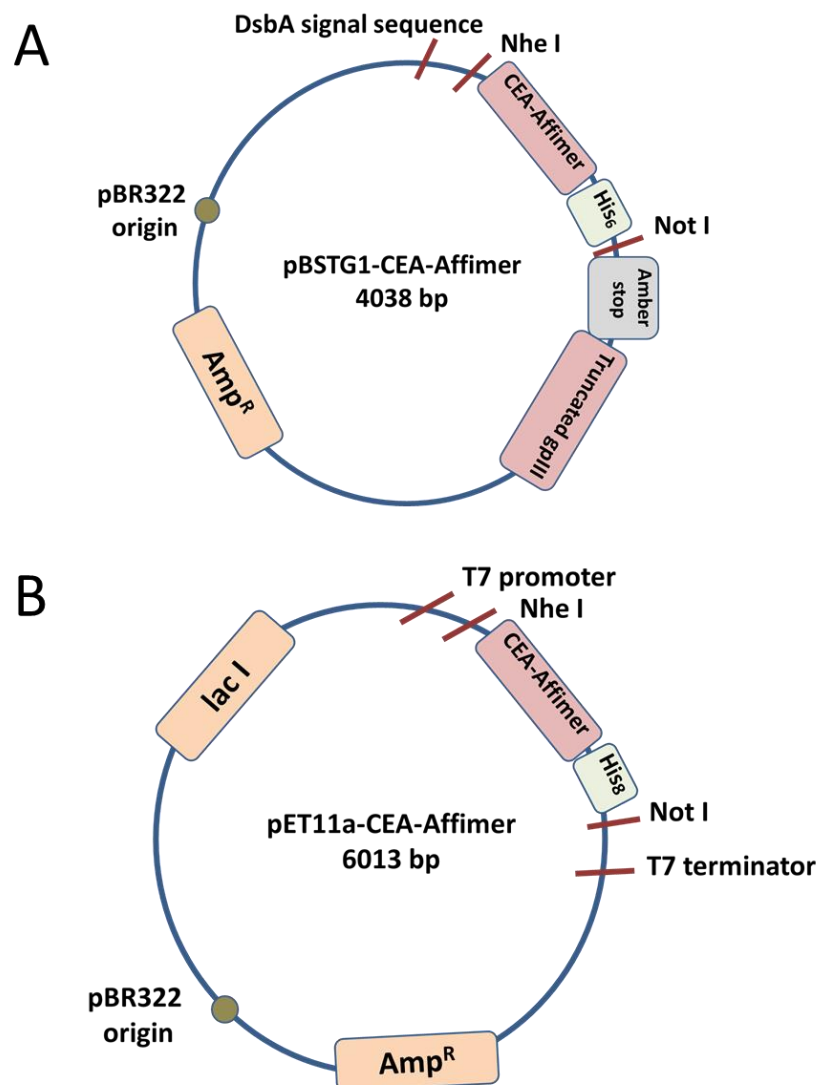
Figure 3.1 : Schematic of *pBSTG1* phagemid vector and engineered *pET11a* expression vector.

(A)The *pBSTG1* is a cloning vector consisting of a Dsb A signal sequence which targets translocation of the fusion gene to the periplasm, a coding sequence for the Affimer flanked by *Nhe*1 and *Not*1 restriction sites followed by a His$_6$ tags. An amber codon is incorporated in between of His$_6$ tag and truncated pIII gene to allow continuous translation of Affimer protein and pIII coat protein and assists in incorporating the fusion protein into the phage coat protein III. (B) Engineered *pET11a* was used as an expression vector comprising of the same ampicillin resistant gene for selection with the addition of a T7 promoter and terminator flanking the restriction sites and coding sequence of the Affimer. Both vectors contain the same origin of replication as the *pBR322* plasmid. Image is adapted from Raina (2013).

3.2 Screening of Affimers against CEA via phage display

CEA protein was initially biotinylated as a target analyte together with a positive control protein, ySUMO, and they were used to screen for Affimers during the biopanning process. The success of biotinylation was validated via ELISA and results **Figure 3.2** showed that biotinylation of both protein CEA (**Figure 3.2**, wells A - C) and ySUMO (**Figure 3.2**, wells E - G) were confirmed by colour change from colourless in the negative control wells (**Figure 3.2,** wells D and H) omitted the biotinylated protein to a blue colour as shown in the positive wells. Increases in A_{620} paralleled with increasing concentration of biotinylated proteins (**Figure 3.2 B**). These biotinylated proteins were subsequently immobilized onto streptavidin coated surfaces and screened against phage display library obtained from the BioScreening Technology Group (BSTG - University of Leeds, UK) to isolate the binding Affimers. Forty eight randomly picked positive Affimer clones from the third panning round were investigated for their ability to bind to CEA (**Figure 3.3 A and C**) and ySUMO (**Figure 3.3 B and D**) via phage ELISA. No binding was observed in the negative control wells (well A7 to H12) which contained the corresponding clones as in the positive wells, but omitted their biotinylated targets which were replaced by the blocking solution. These indicated that all of Affimer clones against CEA were specific and coincided with the ySUMO positive control results. All clones were sent for sequencing and data revealed that the positive clones represented only 3 unique binders with two variable regions. There were termed as CEA-Affimers I, II and III (**Table 3.1**). Both CEA-Affimer-I and II consisted of 9 distinct amino acid residues in each variable region. Interestingly, there are 10 amino acid residues presented in the variable regions 2 of CEA-Affimer-III.

Table 3.1 : CEA binding Affimers and the amino acid sequences of the variable regions are presented

Affimer	Variable region 1	Variable region 2	Protein pI[a]
CEA-Affimer-I	W V S G H M Q V D	N P W G D Q Y P R	7.17
CEA-Affimer-II	W I V G W R Q P D	N W I K N N M E L	7.14
CEA-Affimer-III	D Y Q K D N I K H	W F H L I S P I M F	7.20

[a]protein pI was calculated based in the full-length sequence of Affimer using the ProtParam software
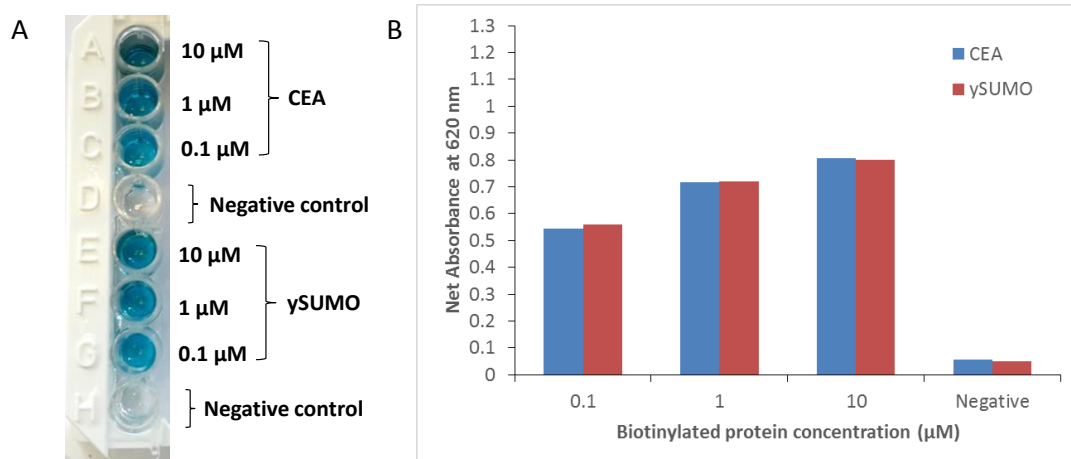
Figure 3.2: ELISA of biotinylated CEA and ySUMO proteins

(A) Well A to C and E to G contained biotinylated CEA and ySUMO proteins, respectively, in decreasing concentration from 10 to 0.1 µM. Well D and H represent negative controls for each sample in which the biotinylated protein was omitted (B) Comparison between biotinylated CEA (blue bar) and ySUMO (red bar) at each analyte concentration are shown. Data is A_{620} using TMB as substrate.
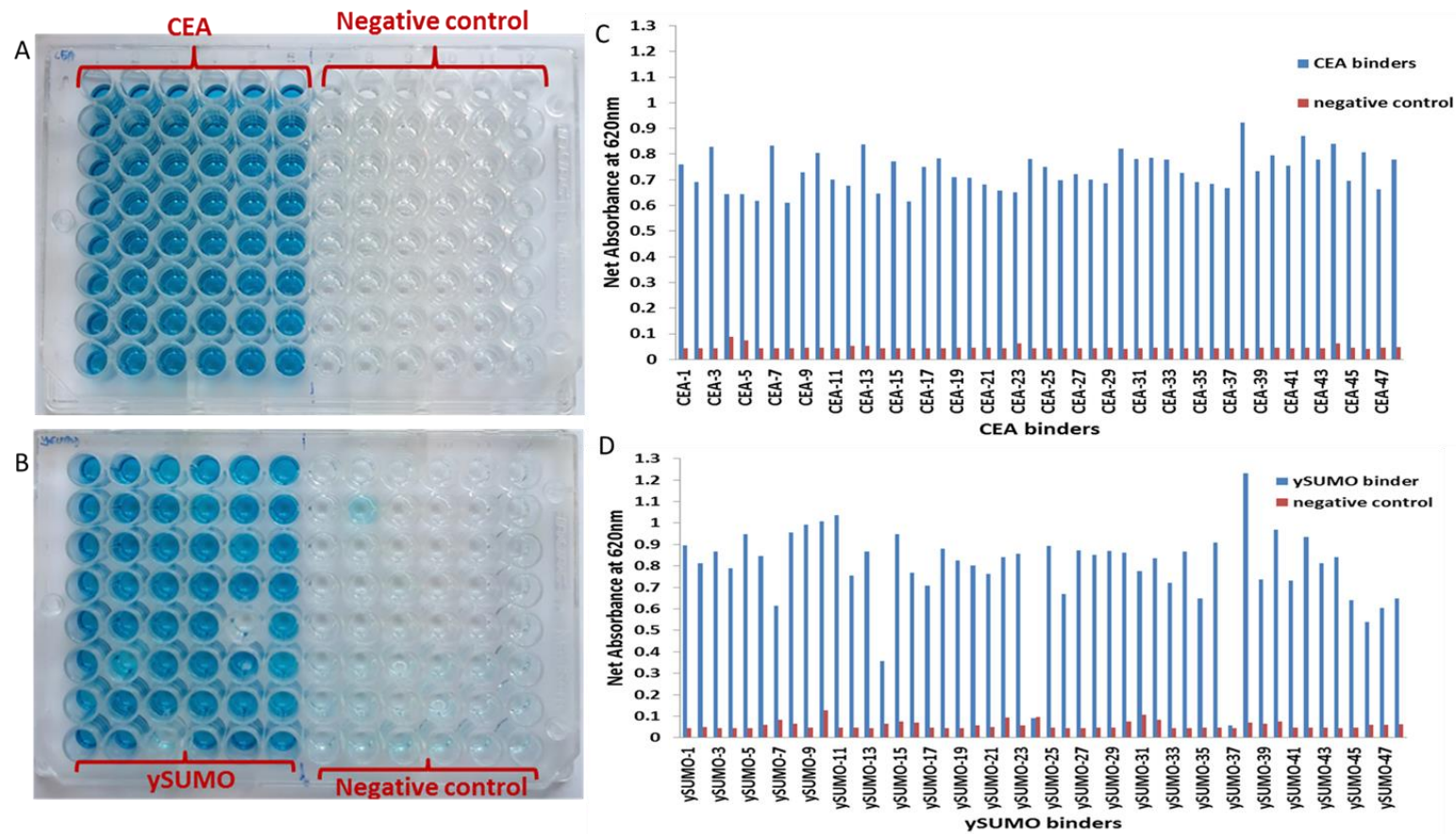
Figure 3.3 : Phage ELISA of Affimers from 48 positive clones

Forty eight positive clones were incubated in wells containing biotinylated (A) CEA and (B) ySUMO targets. Biotinylated targets were omitted in the negative control wells. The histogram in (C) and (D) show the A_{620} from each well after the addition of TMB substrate, (■), CEA or ySUMO; (■), negative control.

3.2.1 Subcloning Affimer coding sequence into the *pET11a* expression vector

The three unique clones of CEA binding Affimers in phagemid vector were re-cultured and plasmids were extracted and purified using a miniprep kit. The quality of purified phagemids was investigated by running through 0.8% (w/v) gel agarose electrophoresis and quantified for yield and purity using nanospectrophotometry. The 260/280 nm absorbance ratio was around 1.8 indicating that all samples were pure. Samples were loaded at the same volume onto a 0.8% (w/v) agarose gel and data showed that DNA yields of CEA-Affimer-1 was less concentrated than the other CEA binders. Two distinct bands were observed across all CEA binders which most likely correspond to the linearized (6 kb) and supercoiled DNA form (~3 kb) as shown in **Figure 3.4 A**. An open circular form was also observed in CEA binder 2 and CEA binder 3 which is indicated by a band above the linearized form. These observations are in accordance with the normal features of uncut plasmid DNA.

To express the protein of anti-CEA Affimers, subcloning of Affimers' coding sequence from phagemid vector to expression vector needed to be done. In this study, engineered *pET11a* vector was used as an expression vector contained the *Nhe* 1 and *Not* 1 restriction sites. The purity of uncut purified *pET11a* vector was analyzed and data showed 2 bands that corresponded to supercoiled (4 kb) and open circular form of DNA (~10 kb) as shown in **Figure 3.4 A**. The coding sequence of each Affimer was amplified via PCR prior to digestion with *Nhe* 1 and *Not* 1 restriction enzymes. The PCR products were examined via electrophoresis on a 1.5% (w/v) gel agarose and a single band was observed at approximately 300 bp which is coincided with the theoretical size of the Affimer of around 326 bp (**Figure 3.4 B**). The *Nhe* 1 restriction site sequence was incorporated in the forward primer whilst a cysteine codon, *Not* 1 restriction site sequence and part of an 8 histidine tag were incorporated in the reverse primer.

Subcloning of Affimer's coding sequence into *pET11a* was performed after double digestion with restriction enzymes on both DNA. Ligation was carried out using T4 DNA ligase alongside with negative controls comprising digested *pET11a* without DNA insert in the presence and absence of T4 DNA ligase. Transformants containing the positive subclones were randomly picked and mini-prepped and the success of ligation was determined via PCR amplification using the same primers as before. Gel electrophoresis of the PCR products showed that all subclones possessed the DNA insert

as shown in **Figure 3.5**. Subclones were subsequently sent for DNA sequencing to further confirm that they did contained the correct sequence. The DNA sequences were translated into protein sequences and aligned using a BioEdit software as shown in **Figure 3.6**.
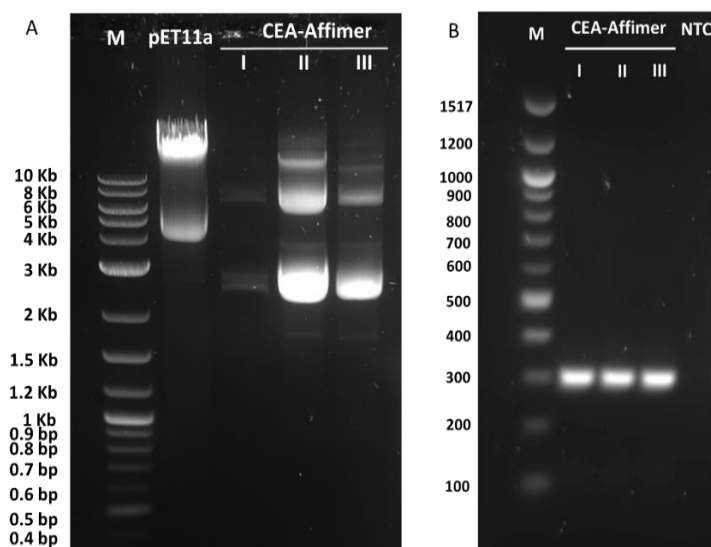
Figure 3.4: Gel electrophoresis of purified CEA binding Affimers in phagemid vector, *pET11a* expression vector and PCR amplified DNA Affimer insert

(A)The purified Affimers (lane 2-4) and *pET11a* (lane 1) vector were electrophoresed in 0.8% (w/v) agarose gel prestained with SYBR™ Safe in 1X TAE buffer. (B) The amplified coding sequences of Affimers (lane 1-3) were electrophoresed in 1.5% (w/v) agarose gel. No template control (NTC) was included as a negative control in the PCR amplification. A 2-Log DNA ladder (0.1-10 kb) and 100 bp ladder were used as markers (M) in gel A and B, respectively.
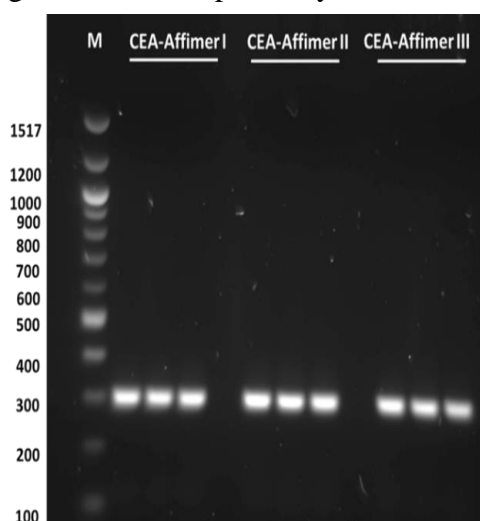
Figure 3.5: PCR amplification of Affimer subclones in *pET11a* expression vector

PCR products of CEA binding Affimer subclones in *pET11a* vector were electrophoresed in 1.5% (w/v) agarose gel prestained with SYBR™ Safe in 1X TAE buffer. Three random subclones were selected for each of the CEA binder. The marker lane (M) consists of 100 bp ladder.
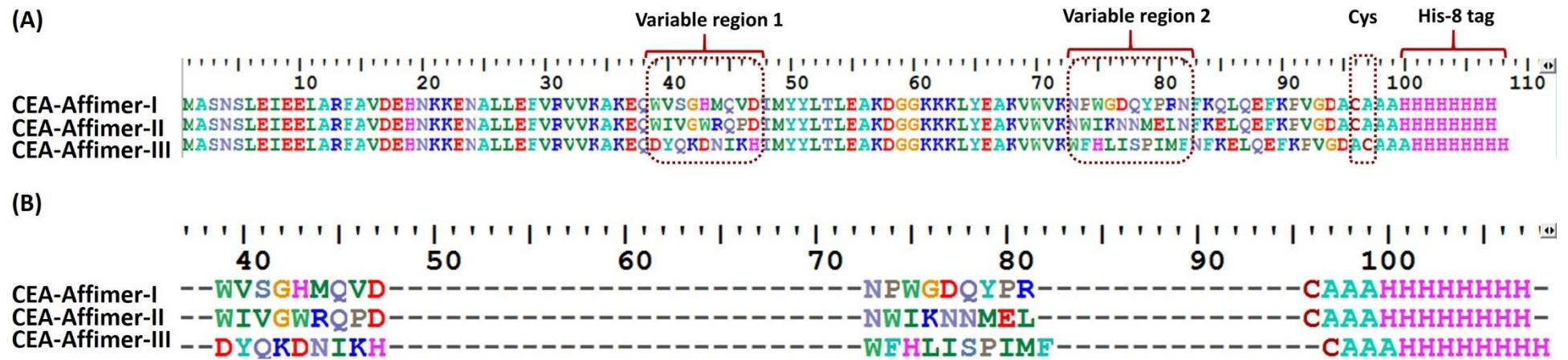
Figure 3.6: Protein sequences of CEA binding Affimer subclones

(A) All CEA binders were successfully subcloned into *pET11a* with the correct orientation of variable regions and incorporation of single

cysteine residue at the C-terminal; (B) The magnified version of variable regions 1 and 2.

3.2.2 Protein expression and purification of CEA binding Affimers

Validated subclones of anti-CEA Affimers were subsequently expressed in BL21 (DE3) *E.coli* cells and affinity purified using Ni^{2+}-NTA column chromatography through the His_8 tag region as described in **section 2.2.1.6**. These protocols had been optimized by the BSTG group (Tiede et al., 2017). The unbound fractions collected after anti-CEA Affimers bound to the Ni^{2+}-NTA resin confirmed that Affimers had fully saturated the resin as there were remnants of Affimer proteins that can be seen between 10 and 15 KDa (**Figure 3.7**). A distinct single band was observed at 10-15 KDa from the first and second elution fractions indicated that the washing steps were sufficient and the Affimer monomers were successfully purified. Based on A_{280} measurements and the intensity of the bands observed from the reducing SDS-PAGE gel, results showed that CEA-Affimer-II and III were highly expressed as compared to CEA-Affimer-I. From 50 ml culture, 0.24, 8.3 and 6.27 mg of CEA-Affimer-I, II and III were expressed, respectively. SDS-PAGE analysis only gave the estimated molecular weight of protein relative to the protein marker. Thus, purified proteins was sent for mass spectrometry analysis to determine the real molecular masses of Affimers proteins. **Figure 3.8** showed that the molecular masses of CEA-Affimer-I, II and III were 12,676, 12, 499 and 12,612 Da, respectively. These findings were similar to the theoretical mass of protein derived from the ProtParam software. A prominent population of dimer forms was observed from CEA-Affimer-I and III resulting from the formation of a disulphide bond between thiol groups located at the C-terminus. In addition, ProtParam analysis also provided theoretical isoelectric point (pI) of Affimers based on the protein sequence. The theoretical pI of CEA-Affimer I, II and III are 7.17, 7.14 and 7.2, respectively, as summarized in **Table 3.1**.
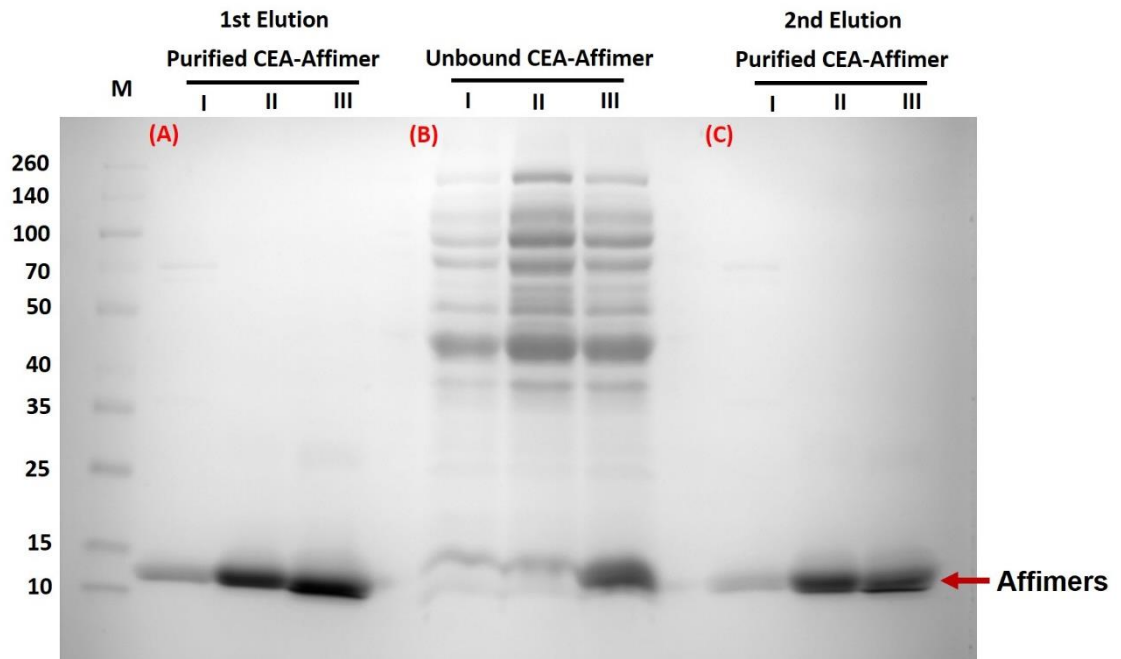
Figure 3.7: Protein purification of CEA binding Affimers

SDS-PAGE analysis of protein purification running in 4-20% (w/v) gradient gel under reducing condition. Panels A and C show purified protein of each CEA binder from the 1st and 2nd elution, respectively. Samples in the panel B are unbound fractions collected after Ni^{2+}-NTA resin had been loaded with crude CEA binders. 10 µl of sample was loaded into each well. M denotes the protein markers in KDa.
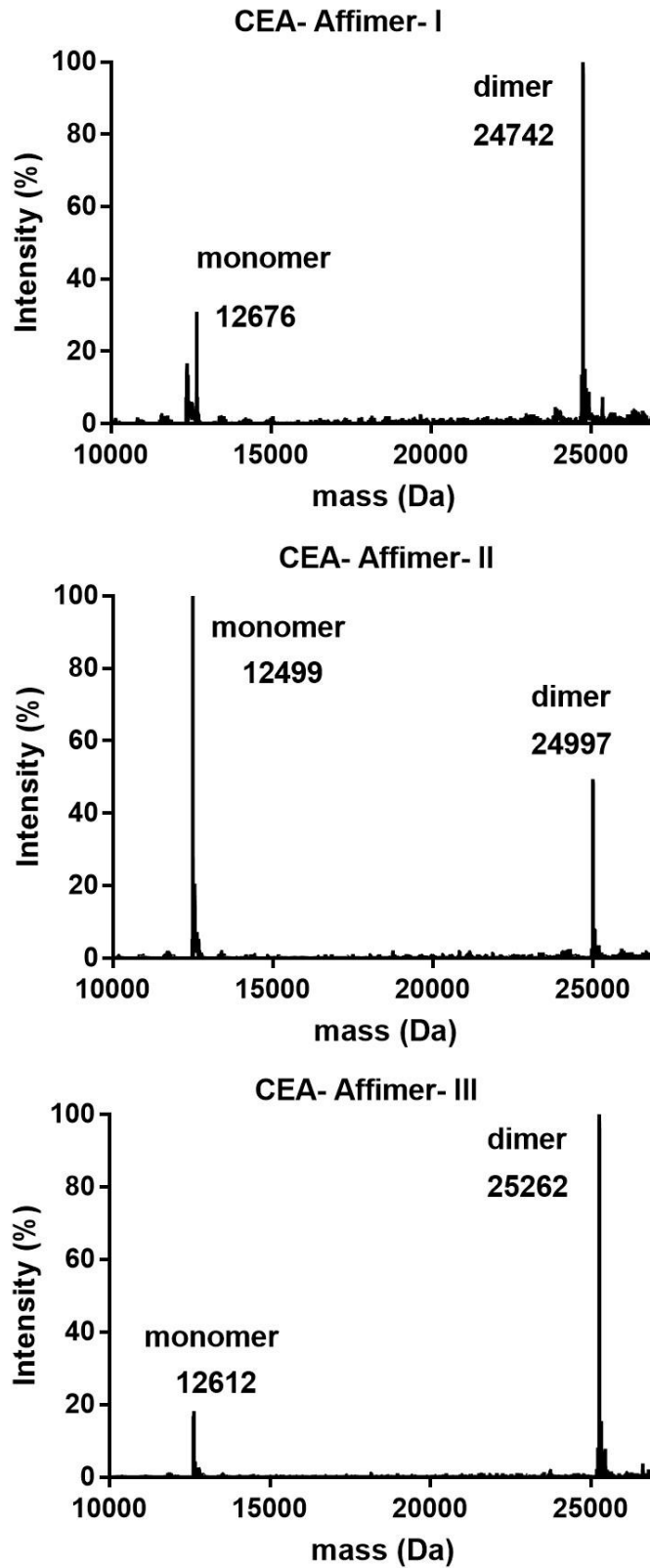
Figure 3.8: Mass spectra of purified CEA binding Affimers protein

Peaks showing the monomer (~12.5 KDa) and dimer (~25 KDa) forms of Affimers protein of each binder.

3.3 Characterization of CEA binding Affimers

3.3.1 Validation of CEA expression in LoVo cells and its secretion

CEA protein expression and localization on LoVo cells was investigated via immunofluorescence staining prior to characterizing the specificity of CEA binding Affimers. Cells were fixed with 4 % (v/v) paraformaldehyde solution after growth for 24 h and 7 d. CEA protein was observed on the surface of the cell membrane which coincides with CEA being a membrane–anchored glycoprotein (**Figure 3.9 A and B**). This pattern of localization was seen for both incubation times. No expression of CEA protein was found in the HEK 293 cells which were used as a negative control (**Figure 3.9 C and D**). The specificity of the anti-CEA antibody was confirmed by the absence of CEA staining in slides of Lovo cells in which the primary antibody was omitted (**Figure 3.9 E and F**).

To determine the capability of Affimers bind specifically to CEA in a complex protein matrix, LoVo cells and culture medium collected after 3 days of incubation were lysed and extracted for CEA protein as described in **section 2.2.2.2**. SDS-PAGE analysis showed multiple protein bands from both sources which is a normal features of unpurified homogenates (**Figure 3.10 A**). The presence of CEA in these samples was further confirmed by immunoblotting using monoclonal anti-CEA antibody (**Figure 3.10 B**). Results showed that CEA protein released in the media mainly contained a protein band of around 160 KDa which represents the soluble form of CEA circulating in the blood. In contrast, the membrane bound CEA protein showed bands of 120 and 200 KDa.
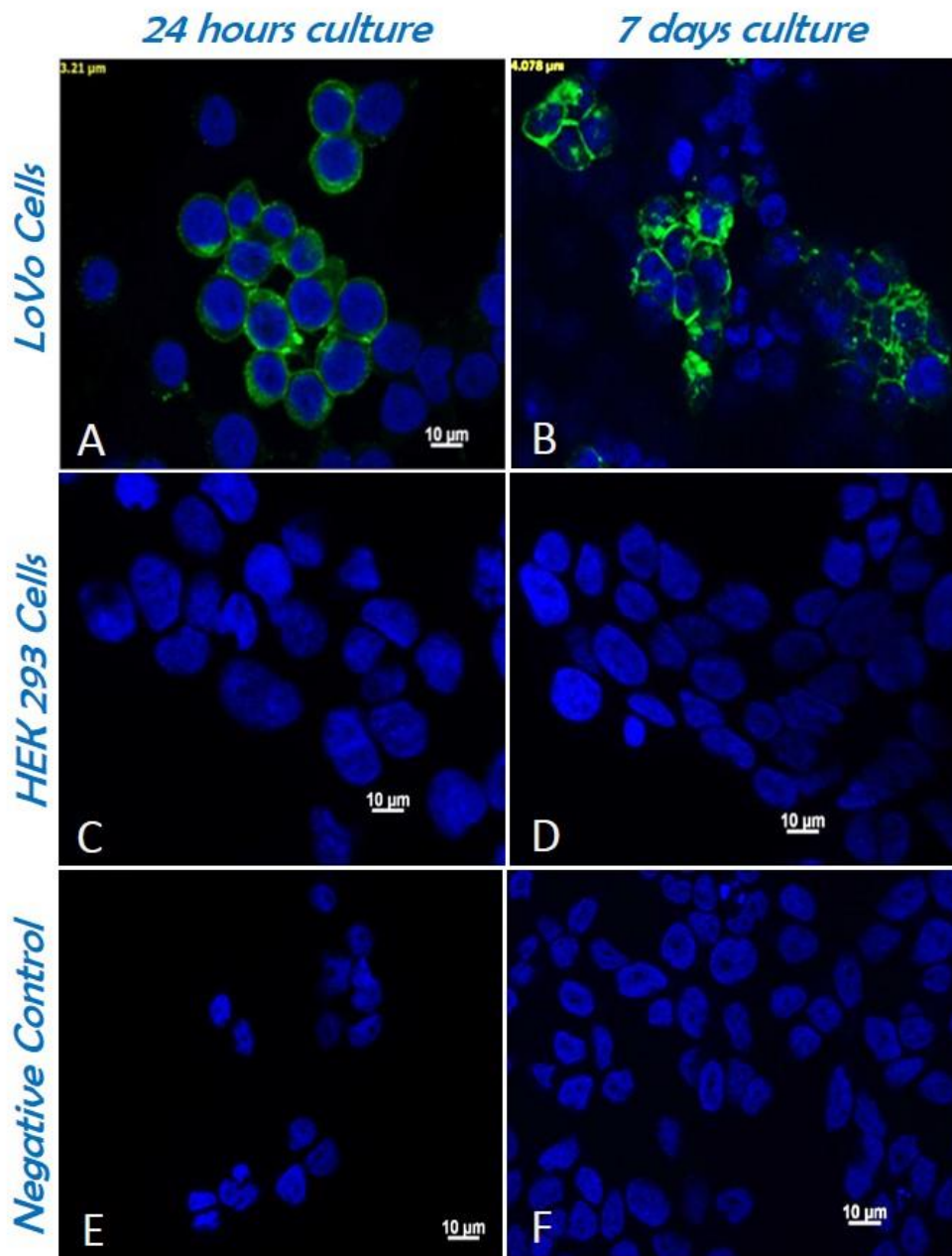
Figure 3.9: Immunofluorescence staining of CEA protein on LoVo cells

Cells were fixed with 4% (v/v) paraformaldehyde solution after culture for 24 h (A, C and E) and 7 d (B, D and F). HEK 293 cells were used as negative control. Primary antibody was omitted in the negative control slides of LoVo cells (E and F). Green fluorescent staining shows positive staining by anti-CEA antibody whilst nuclei were stained blue with DAPI. Scale bars are 10µm.
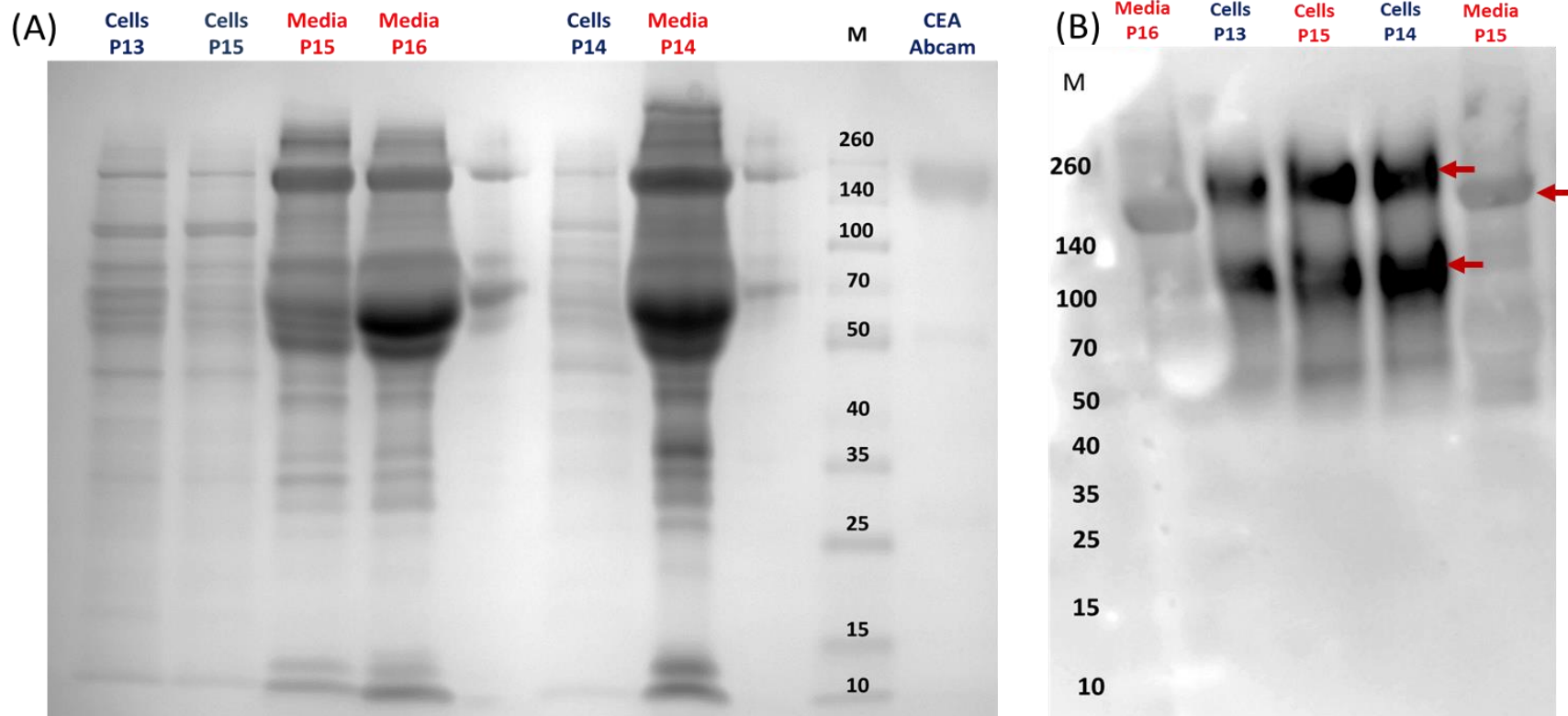
Figure 3.10: SDS-PAGE and immunoblotting analyses of CEA protein isolated from the culture medium and LoVo cells

(A) Homogenates of LoVo cells from different passages (P13 to P16) and proteins present in the culture medium after 3 d of incubation were separated using 4-20% (w/v) reducing SDS-PAGE and stained with Coomassie Blue. (B) Identical samples were transferred onto 0.2 µm PVDF membrane and immunoblotted for the detection of CEA. Red arrow shows glycosylated CEA probed with mouse anti-human IgG CEA. P13-16 indicates the number of passage. M denotes molecular weight markers in KDa.

3.3.2 Affimer-fluorescence microscopy of LoVo cells

Immunofluorescence staining using monoclonal anti-CEA antibody confirmed the localization of CEA protein on the surface of LoVo cells membranes as shown earlier. Thus, anti-CEA Affimers were biotinylated using biotin-maleimide conjugation to the cysteine residue at the C-terminus as described in **section 2.2.1.7** to determine the specificity of anti-CEA Affimers. Streptavidin conjugated DyLight 488 was used as a detection reagent instead of secondary antibody. A schematic comparison between affinity- and immunofluorescence stainings is shown in **Figure 3.11 I and J**. Data showed that all Affimers bound specifically to CEA on the cell membrane of LoVo cells (**Figure 3.11 A-C**) with the same staining pattern as the antibody (**Figure 3.11 D**). Interestingly, the Affimers demonstrated a higher intensity of staining with a broader distribution compared to the antibody. No expression of CEA protein was found in the HEK 293 cells which were used as a negative control (**Fig. 3.11 E-H**). These findings demonstrated that CEA binding Affimers have better sensitivity than antibody. This could be due to their small size that allows for better penetration into fixed cells and greater binding sites on the CEA protein.
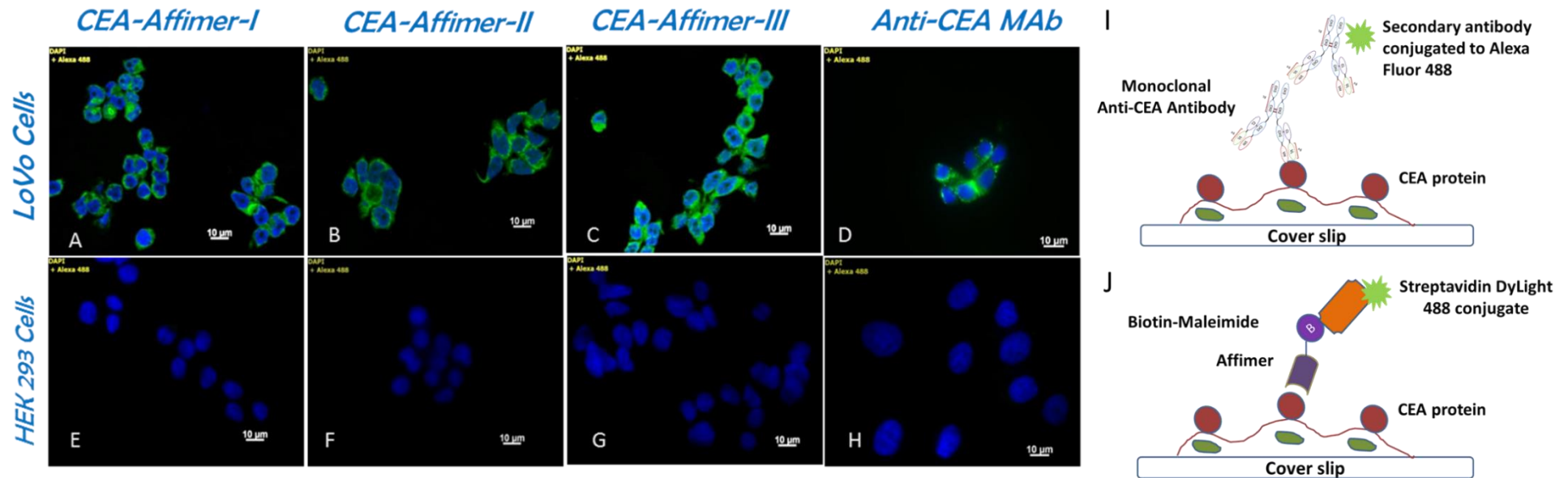
Figure 3.11: Anti-CEA Affimer staining of cells in culture

Figure 3.11 A to C show staining by CEA binding Affimer I,II and III on LoVo cells (A-C) compared to immunofluorescence staining using anti-CEA monoclonal antibody (D). No binding is present on HEK 293 negative control cells (E to H). I and J, schematics comparing between Affimer and immunofluorescent staining. (I) Immmunofluorescent staining used monoclonal anti-CEA as primary antibody and Alexa Fluor 488 conjugated secondary antibody as detection reagent. (J) Affimer staining used biotinylated Affimer as primary reagent and streptavidin conjugated DyLight 488 as detection reagent.

3.3.3 Affinity-precipitation of CEA binding Affimers against native CEA

Identical samples of cell lysates from LoVo cells and the culture media were used in pull-down assays to determine the ability of Affimers to specifically bind to CEA in complex protein mixture. The affinity-precipitation assay was performed as described in **section 2.2.1.8** by immobilizing the purified Affimer onto Ni^{2+}-NTA resin which was subsequently used to pull-down the CEA from protein mixtures as illustrated in **Figure 3.12**. Results from SDS-PAGE analysis showed that all anti-CEA Affimers successfully pulled-down fully-glycosylated CEA from both the cell lysates and CEA secreted into the media as shown by a band detected at around 200 KDa (**Figure 3.12 A-C**). The same size of band was also observed in the positive control sample whereby CEA binding Affimers bound specifically to the reference CEA that was commercially obtained from Abcam and loaded onto the same gel. No band at this position was detected in the cell lysates of HEK 293 cells which were used as a negative control analyte. Similarly, no high molecular weight protein was seen on anti-yeast SUMO-10 Affimer which used as ligand (**Figure 3.12 D**). However it was difficult to see the 200 KDa CEA band from the pull-downs complex of LoVo's cell lysates in all set of experiments when using anti-CEA Affimers as ligand. This could be due to the amount of pulled-down CEA from LoVo cell lysates being too small and below the limit of detection (< 20 ng of protein) when stained with Coomassie blue staining (Kang et al., 2002, Dyballa and Metzger, 2009).

Thus, immublotting of the corresponding pull-down complex were performed to further confirm that the protein bands detected represent the actual CEA and Affimer proteins. The western blot probed with anti-CEA antibody confirmed that the band detected at 200 KDa in SDS-PAGE gel was specific to CEA (**Figure 3.13 A**). Immunoblotting is known to be more specific and sensitive than Coomassie blue staining and the missing CEA band from LoVo cell lysates samples was now seen. No bands were observed from the pull-downs of HEK 293 cell lysates or by the yeast SUMO-10 Affimer. In contrast, the western blot probed with an anti-His tag antibody confirmed that protein band detected at 13 KDa did represent the corresponding Affimer (**Figure 3.13 B**). Taken together, these findings demonstrated that CEA binding Affimers were able to specifically bind CEA protein from the protein complex.
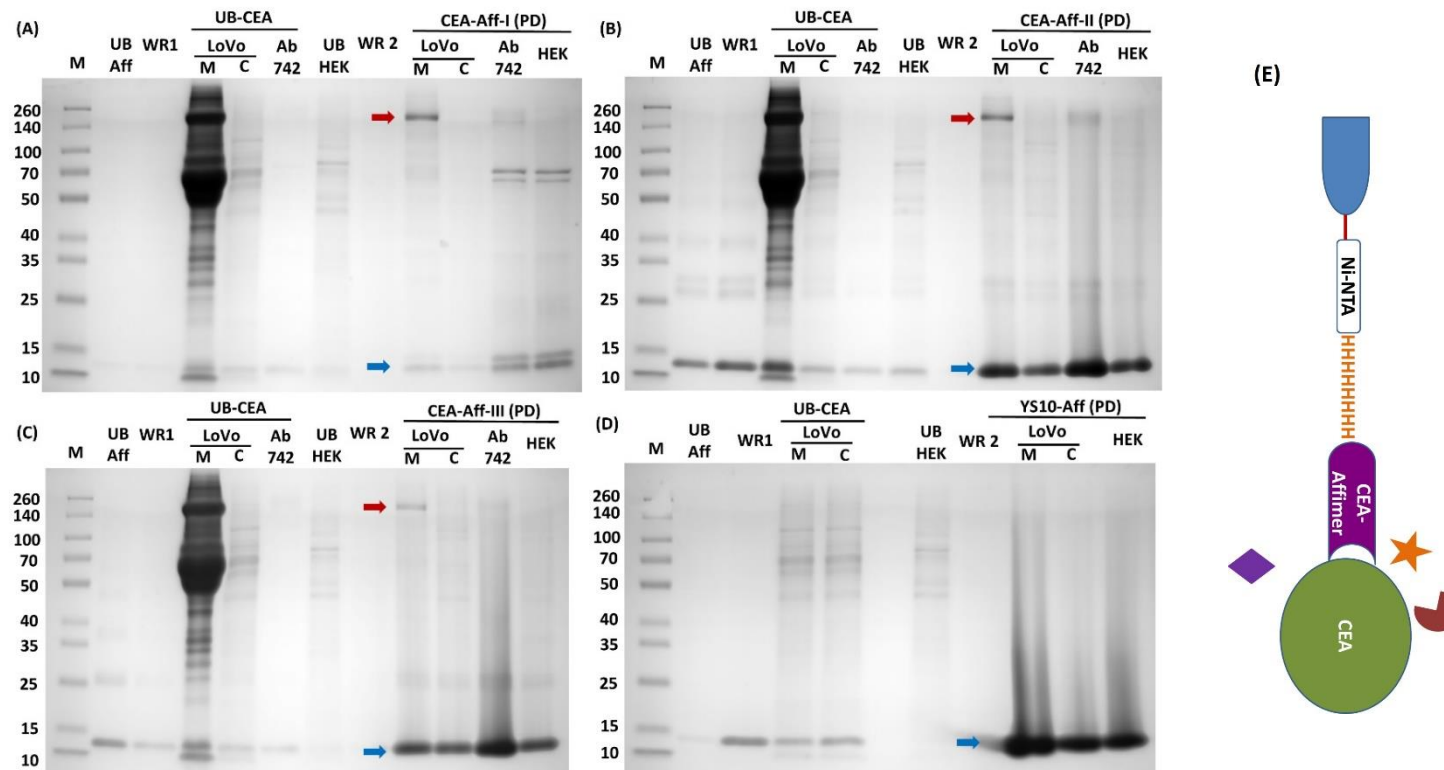
Figure 3.12: Anti-CEA Affimers specifically pull-down CEA protein

Gels showing the fractions collected during the pull-down assay using CEA binding Affimer-I to III (A-C) as ligand to capture the CEA protein from Lovo cell lysates (LoVo C) and from media (LoVo M). (D) Yeast SUMO-10 binding Affimer was used as a control, cell lysates of HEK 293 were used as negative control analyte and pure native CEA from Abcam (Ab742) was used as positive control of CEA. WR 1 and 2 indicate collected wash solution fractions, PD was the pulled-down mixture and M shows protein markers. UB Aff, UB-CEA and UB-HEK indicate the unbound fraction of Affimer, CEA and HEK 293, respectively. Red arrow showing the pulled-down CEA, whilst blue arrow showing the Affimers band. (E) Schematic depicts the arrangement of components in the pull-down assay.
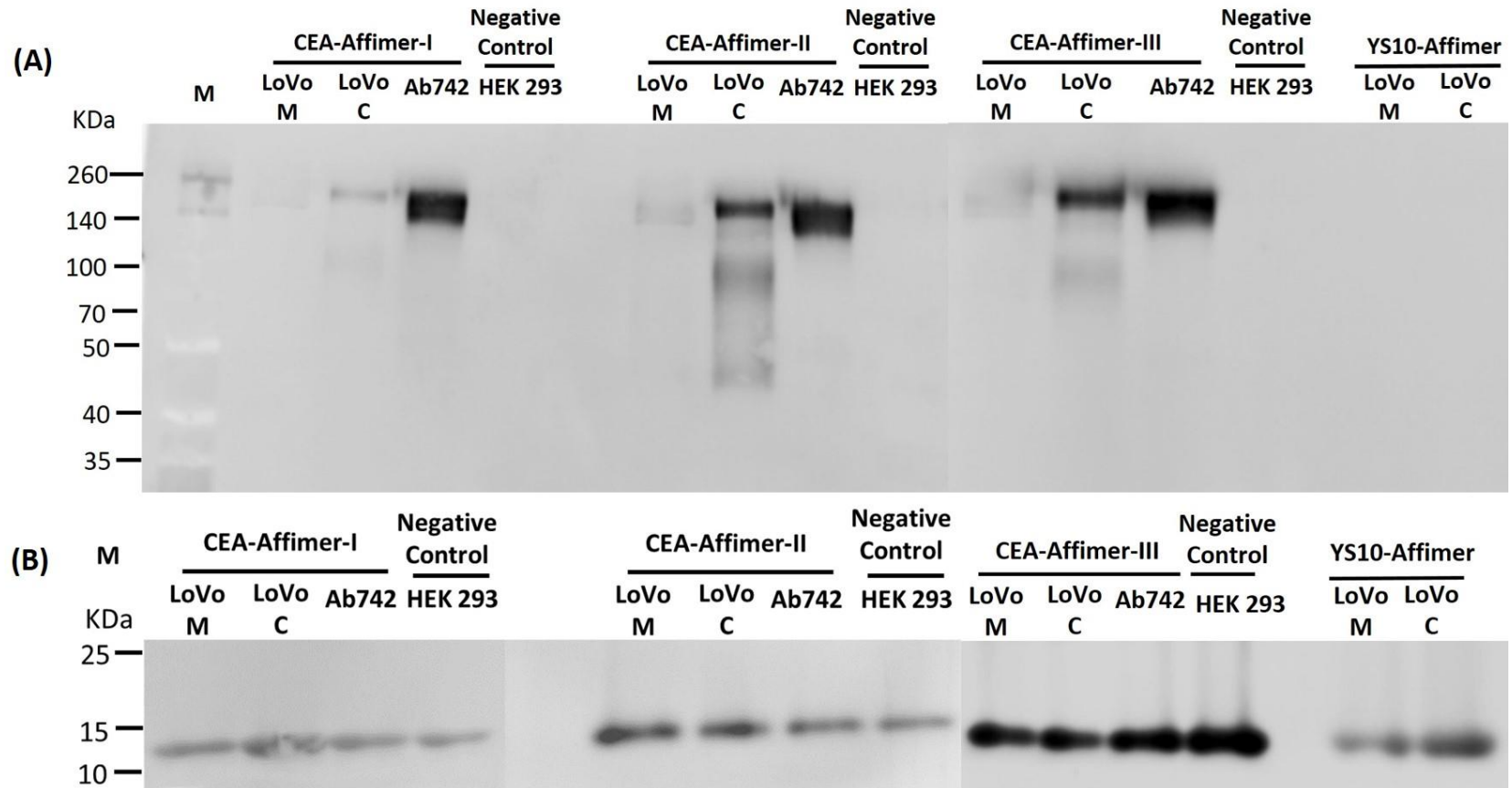
Figure 3.13: Immunoblotting of Affimer precipitated CEA

Monoclonal anti-CEA and anti-His tag antibodies were used to probe (A) the CEA protein and (B) Affimers, respectively from the pull-down complex. Yeast SUMO-10 binder was used as a control Affimer. Commercial CEA from Abcam was used as positive control and cell lysates from HEK 293 as negative control.

3.3.4 Affimer precipitation of CEA using deglycosylated CEA

CEA protein is comprised of 60% of oligosaccharides derived from N-glycosylation during post-translational modification. To distinguish whether CEA binding Affimers react to sugar or protein epitopes, deglycosylation of CEA protein via PNGase F treatment was performed. Pure native CEA from Abcam, together with RNase B protein which is a positive control for the PNGase F treatment, were investigated in parallel. The success of PNGase F cleavage was analysed by separating the digested proteins on a reducing SDS-PAGE gel. Data showed that the molecular weight of deglycosylated CEA was reduced to around 100 KDa compared to 200KDa when in fully-glycosylated form (**Figure 3.14**). The efficiency of PNGase F cleavage was confirmed by complete removal of single N-linked glycan of RNase B protein which led to the size reduction from 17 KDa to 15 KDa.

Following these experiments, affinity-precipitation using CEA binding Affimers was repeated using deglycosylated CEA. Western blotting was performed to determine the outcome of the pull-down assay. Data from immunoblotting using monoclonal anti-CEA antibody showed that all CEA binding Affimers reacted specifically to the deglycosylated form of CEA (**Figure 3.15 A**). No binding was observed from the non-specific analyte samples, digested RNase B, or using control Affimer, the yeast SUMO-10 Affimer. Additionally, an immunoblot probed using anti-His tag antibody confirmed the presence of Affimers in the pull-down complex as shown in the **Figure 3.15 B**. Based on these findings, the data demonstrated that CEA binding Affimers recognize the protein epitope of CEA.
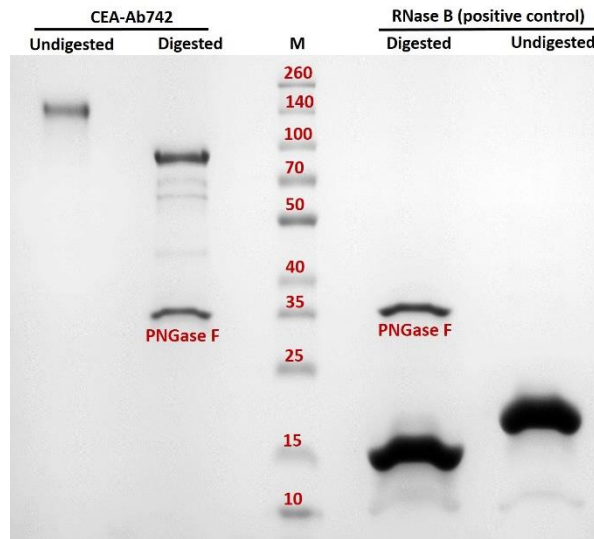
Figure 3.14: SDS-PAGE analysis of deglycosylated CEA

Deglycosylation assay using PNGase F treatment to remove the N-glycan from CEA protein. RNase B was used as a positive control for PNGase F treatment and pure native CEA (Ab742) was commercially obtained from Abcam. M shows the protein markers in KDa.
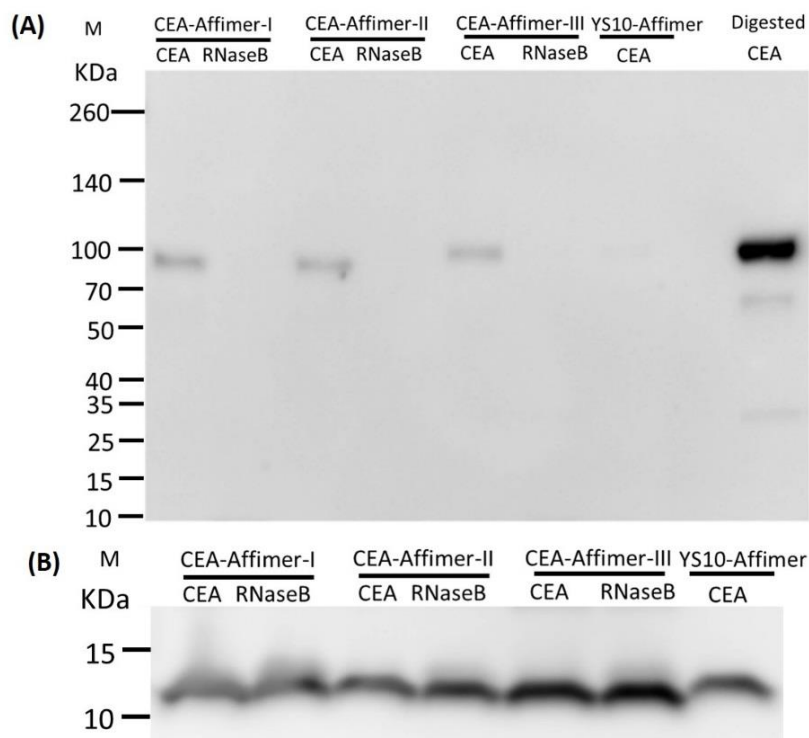
Figure 3.15: Immunoblotting of Affimer precipitated deglycosylated CEA

Immunoblotting of affinity-precipitation using CEA binding Affimers as ligand to pull-down deglycosylated CEA (n=2). Monoclonal anti-CEA and anti-His tag antibodies were used to probe the pulled-down (A) deglycosylated CEA and (B) Affimers, respectively. Yeast SUMO-10 binder was used as a control Affimer and RNase B was used as non-specific analyte. Digested CEA was used as a reference to the pulled-down CEA in blotting.

3.3.5 Kinetic binding analysis of anti-CEA Affimers using SPR

3.3.5.1 Immobilization of Affimers on streptavidin coated chip

A low density surface was generated as described in **section 2.2.1.9** by immobilizing 10 nM of biotinylated anti-CEA Affimers as bioreceptors. Sensograms in **Figure 3.16** depict the normalized response signals of respective anti CEA-Affimers against the unmodified reference surface. The SPR signals are proportional to a change in mass at the solution-surface interface. Results showed that 270 RU of biotinylated anti-CEA-Affimer-I and II were successfully immobilized whilst a slightly lower amount of anti-CEA-Affimer-III (230 RU) was seen. The amount of immobilized anti-CEA-Affimers are in agreement with standard SPR protocols which suggest that the low density surface (<500 RU) should be used to eliminate the mass transport limiting factor (Katsamba et al., 2006). Stable signals observed during the washing step after the immobilization (~200-300 secs) indicated that the Affimers were bound tightly to the surface and stable. The derivatised flow cells were then used to determine kinetic binding of CEA analyte.
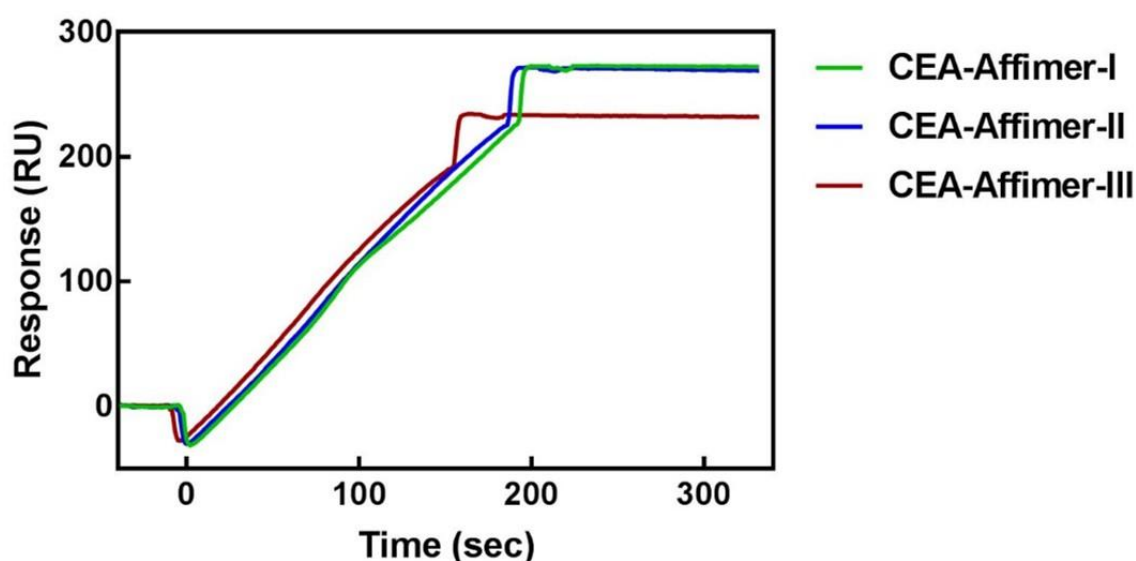
Figure 3.16: Immobilization of biotinylated CEA binding Affimers on streptavidin coated SPR chip

Sensograms show immobilization of biotinylated anti-CEA Affimers onto streptavidin coated surface at low density (~230-270 RU). The corrected response signals were obtained by subtracting the response from an unmodified reference surface.

3.3.5.2 Kinetic analysis of CEA/Affimer interaction

One of the main issues in kinetic studies which can cause deviation from real binding interactions are mass transport effects. In order to minimize these effects, a high flow-rate (e.g. 50 µl/min) and low density surface were used throughout. **Figure 3.17 A to C** shows the overlays of binding interactions between CEA and immobilized anti-CEA-Affimer-I, II and III. CEA was injected in increasing concentrations from 7.8 nM to 1 µM for 3 min and dissociation was monitored for 5 min. Raw data were processed and corrected using a double referencing technique which begins with subtracting data from the receptor surface to the reference surface followed by subsequent subtraction of each CEA concentration trace against the buffer blank injection.

Kinetic binding analysis was evaluated by global fitting the experimental data using a 1:1 Langmuir interaction model as shown in **Figure 3.18**. The kinetic parameters were extracted by global fitting and are summarized in **Table 3.2**. Small χ^2 values from 0.066 to 1.94 indicated a very close-fit between the fitted curves (red lines) and the experimental curves (black lines) which can be seen by excellent overlay between both curves. CEA-Affimer-I and II have similar association rate constants (k_a) that are (2.00 $\pm$ 0.84) $\times 10^6$ $M^{-1}s^{-1}$ and (1.14 $\pm$ 0.84) $\times 10^6$ $M^{-1}s^{-1}$, respectively. Likewise, the dissociation rate constant (k_d) of CEA-Affimer-I and II also within the same range, (1.29 $\pm$ 0.13) $\times 10^{-2}$ s^{-1} and (1.75 $\pm$ 1.08) $\times 10^{-2}$ s^{-1}, respectively. In contrast, CEA-Affimer-III has slower association and dissociation rate constants, (6.78 $\pm$ 1.86) $\times 10^4$ $M^{-1}s^{-1}$ and (2.33 $\pm$ 0.26) $\times 10^{-3}$ s^{-1}, respectively. Interestingly, the R_{max} value of immobilized anti-CEA-Affimer-II was half that (27.11 RU) compared to anti-CEA-Affimer-I and III (86.66 and 113.79 RU) even though the same density surfaces were immobilized. This may be due to steric hindrance due to the position of the CEA epitope recognised by CEA-Affimer-II. Equilibrium dissociation constants were calculated from the ratio of the association and dissociation rates as described in **section 2.2.9**. CEA-Affimer-I has the highest affinity at K_D = 6.46 $\pm$ 1.38 nM, whilst CEA-Affimer-II and III show moderate affinities with K_D = 15.3 $\pm$ 0.37 nM and 34.4 $\pm$ 16 nM, respectively.
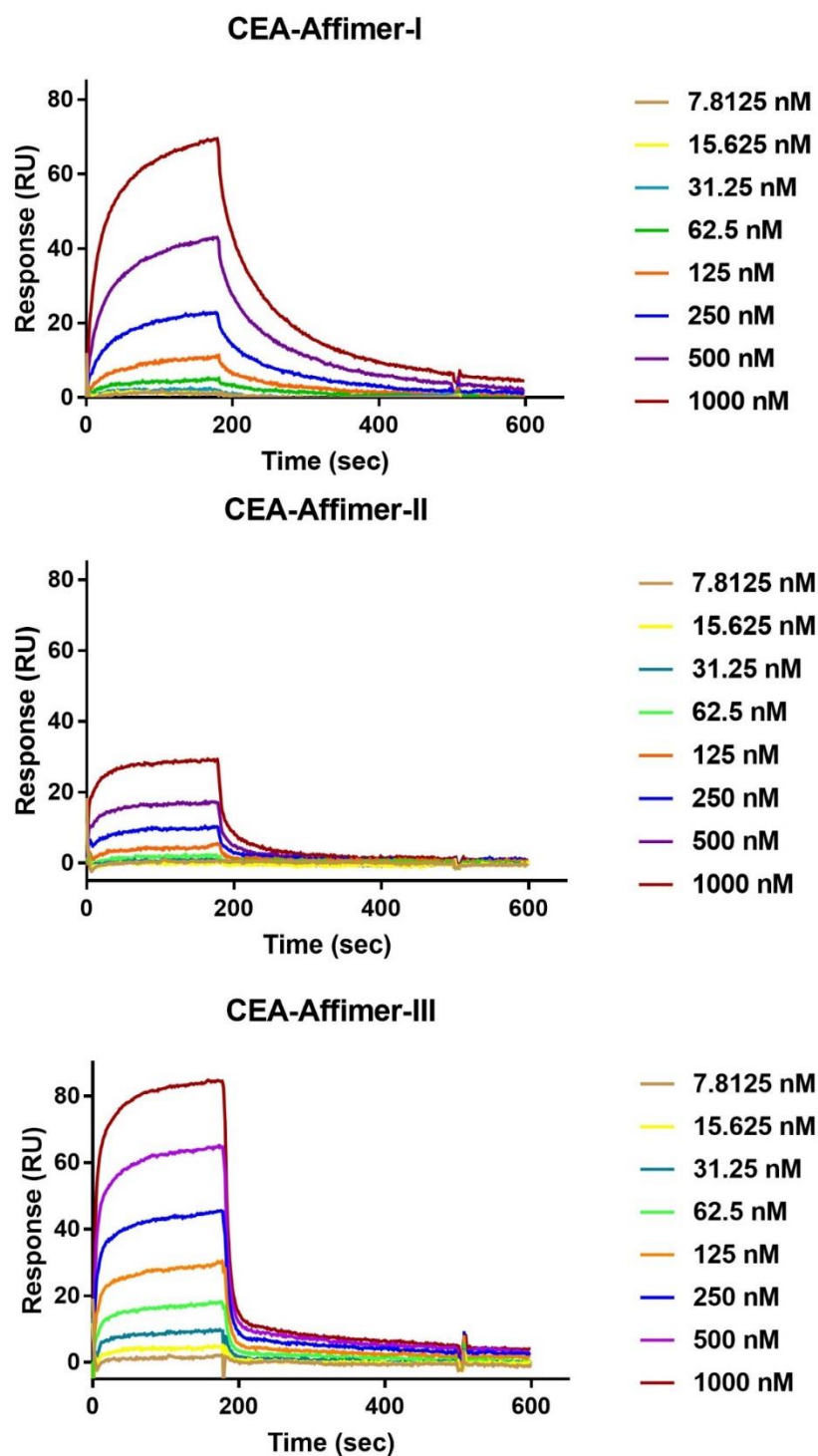
Figure 3.17: Sensograms show overlay of the normalized responses generated from the association and dissociation phase of CEA protein and anti-CEA Affimer interaction

Binding of CEA protein was tested at concentrations of 7.8 nM-1 µM using 2-fold dilutions on immobilized Affimer. (A) CEA-Affimer-I; (B) CEA-Affimer-II and (C) CEA-Affimer-III. Data were normalized using a double-referencing methods by subtracting the responses from an unmodified reference cell and blank injection using running buffer only.
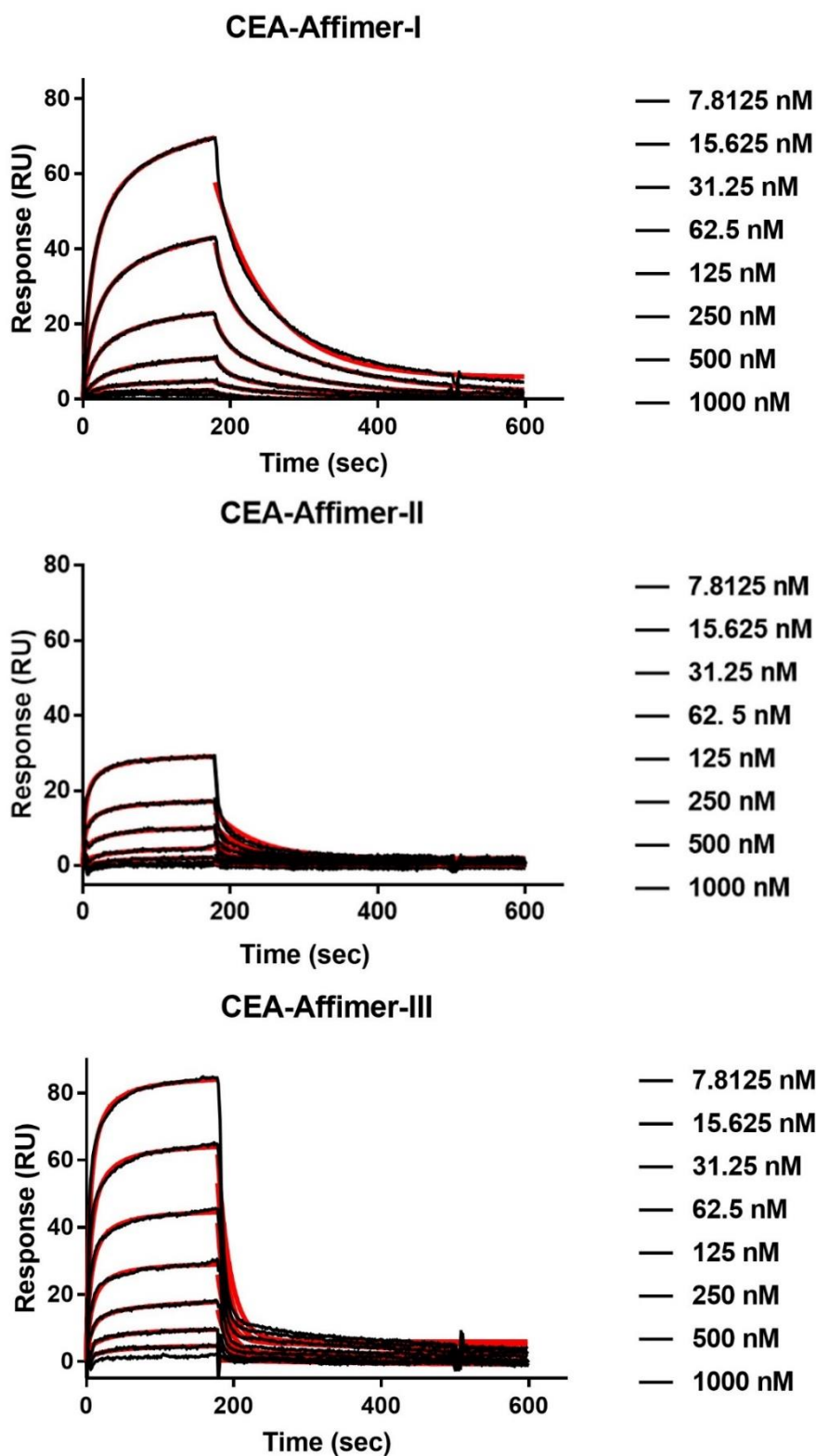
Figure 3.18: Global fit analysis of the CEA/Affimer binding data using a simple 1:1 Langmuir binding interaction model

The experimental SPR trace (black lines) from Figure 3.17 and theoretical fit (red lines) are overlaid. Binding of CEA protein was tested in 2-fold dilutions from 7.8 nM to 1 µM on immobilized Affimer. (A) CEA-Affimer-I; (B) CEA-Affimer-II and (C) CEA-Affimer-III.

Table 3.2: Kinetic parameters of CEA-Affimer interactions

Receptor	$k_a \pm$ SE (M^{-1}s^{-1})	$k_d \pm$ SE (s^{-1})	$K_D \pm$ SE (nM)	χ^2
CEA-Affimer-I	$(2.00 \pm 0.84) \times 10^6$	$(1.29 \pm 0.13) \times 10^{-2}$	6.46 ± 1.38	0.066
CEA-Affimer-II	$(1.14 \pm 0.84) \times 10^6$	$(1.75 \pm 1.08) \times 10^{-2}$	15.3 ± 0.37	0.049
CEA-Affimer-III	$(6.78 \pm 1.86) \times 10^4$	$(2.33 \pm 0.26) \times 10^{-3}$	34.4 ± 16	1.94

3.4 Discussion

The main aim of this study was to use Affimers as novel alternative binding reagents for detection of the colorectal cancer biomarker, CEA. Based on screening for CEA binding Affimer from an Affimer phage display library, three unique binders were identified from the 48 positive clones that were selected. Interestingly, there are three repetitive domains present on the protein structure of CEA (Hatakeyama et al., 2013). However, CEA protein is comprised of 60 % glycan which suggested that there was possibility that CEA binding Affimers might recognise the sugar epitopes. Extensive studies on epitope mapping of CEA protein using 25 distinct monoclonal antibodies tested against recombinant CEA protein that has been expressed in Chinese hamster ovarian cells (CHO) concluded that there were two types of epitope present on CEA, protein and sugar epitopes (Shoichi et al., 1992, Kuroki et al., 1992). The functional protein epitopes comprised of four domains that are N, I (A1-B1), II (A2-B2) and III (A3-B3) as discussed in **Chapter 1**. Domains I to III are known as repetitive domains. Findings in this study showed that the CEA binding Affimers selected recognise the protein epitopes of CEA. However, further evaluation would be needed to be conducted to elucidate which protein domain the anti-CEA Affimers recognise.

Several studies have investigated the relationship between specificity and affinity in antibody/protein interactions. They concluded that the antibody paratopes are substantially enriched in amino acid residues containing aromatic side chains (tyrosine, tryptophan and phenylalanine) and these are surrounded by short-chain hydrophilic side chains (aspartate, asparagine, serine, threonine, and glycine) which plays an important role in attaining the conformation that enables high affinity binding (Koide and Sidhu, 2009, Peng et al., 2014). Interestingly, these amino acid residues present in each variable region of all anti CEA-Affimers with approximately 44% frequency. Selection of CEA-Affimers confer high affinity constants within the nanomolar range from 6.46 nM to 34.4 nM is also in agreement with this notion. Accordingly, Sha et al. (2017) postulated that

this phenomenon occurred in the majority of synthetic binding proteins including the Nanobody and Monobodies whereby these residues confer favourable interaction to the epitope surface during the short period of phage display screening under strong selection pressure. Apart from the chemical properties of epitopes that contribute to the protein-protein interaction, shape complementary also plays a major role in this interaction. The protruding variable loops of the Affimers produce a convex shape which normally has a strong preference toward concave surface of an antigen. This suggests that the epitope surface of CEA could be concave in shape. However further evaluation on the structure of the CEA-Affimer complex needs to be investigated to confirm this notion which is beyond the aim of this study.

Since anti-CEA Affimers will be used as bioreceptors in developing a biosensor, extensive characterization is crucial, particularly in regard to specificity of the Affimers against CEA. There are several analyses that can be conducted and one approach is to investigate the specificity of anti-CEA Affimers on protein expressed on the cells or tissue. For the preliminary analysis, cell line investigation is a better option due to cellular homogeneity prior to further evaluation in tissues which display cellular heterogeneity. Based on these grounds, Lovo cells, an established metastatic colorectal adenocarcinoma cancer cell line, was chosen since it has been well studied and frequently used for the study of CEA (Tiernan et al., 2015). The earliest study of CEA using LoVo cells was done in 1980 and it was reported that CEA protein was highly expressed after 7 to 11 days of culture (Drewinko and Yang, 1980). Meanwhile, preliminary results in this study showed that Lovo cells secreted CEA protein as early as 24 hours incubation after seeding and up to 7 days of culture (**Figure 3.9 A and B**). Accordingly, results from Affimer-fluorescence analysis demonstrated that all three anti-CEA Affimers were highly specific to CEA secreted on the cell surface and no binding observed in negative control cells. This is in accordance with CEA being membrane–anchored glycoprotein. In addition, these findings are comparable to the gold standard immunofluorescence staining. It is important to highlight that fluorescent staining using anti-CEA Affimer as a monoclonal reagent offers additional advantages and cost effectiveness as it does not require secondary antibody for detection which sometimes can cross reacts and introduces false positive staining. Inclusion of single cysteine residue at the C-terminus of the Affimer can facilitate oriented immobilization of the bioreceptor during the fabrication of biosensors. Additionally, data from the kinetic binding analysis such as k_a and k_d are also

important determinants in the optimization and development of Affimer-based impedimetric biosensors. These will be discussed in details in **Chapter 5**.

Finally, anti-CEA Affimers showed the capability to specifically bind to CEA in complex protein matrices from homogenates. They recognise multiple forms of functional CEA including the fully glycosylated native form as well as incompletely glycosylated and deglycosylated forms. One of the main constraint when this study began was to obtain pure native CEA protein to be used as target analyte in biosensor interrogation. However, when available, it is very expensive and having specific and cheap anti-CEA Affimer potentially provides a route for CEA purification.

Chapter Four

Fabrication and optimization of immunosensors for CEA detection

Chapter 4 : Fabrication and optimization of immunosensors for CEA detection

4.1 Introduction

The ultimate aim of this study was to develop a point-of-care device for CEA detection. To achieve this, the transducer price needs to be affordable but should not compromise the performance of the biosensor. The fabrication of the biosensor should be simple and at the same time produce a highly sensitive and specific detection device. Based on these grounds, a commercial screen printed gold electrode (SPGE) as described in **section 2.1.8** was selected as the electrode to develop the impedimetric biosensors for CEA detection. Screen printing of gold electrodes normally generates a rough and uneven surface. Previous studies in our group have investigated several strategies for biosensor construction using these electrodes including self-assembled monolayers (SAMs) and mixed SAMs (mSAMs) (Ahmed, 2015), and conducting polyaniline copolymerized with 2-aminobenzylamine (2-ABA) (Goode, 2015). However, several drawbacks were identified during these studies including the fabrication of mSAM based biosensor for bacterial detection was not feasible on SPGE due to surface roughness and disruption of the SAM layer upon binding of analyte with multiple binding sites (e.g., oligosaccharides, bacteria and viruses) (Shahidan, 2012, Ahmed, 2015). Additionally, it was difficult to control the oxidation state of polyaniline/2-ABA copolymer when deposited on SPGE that led to impedance instability (Ahmed, 2015, Goode, 2015). Based on these limitations, they have concluded that electrodeposition of non-conducting polytyramine (PTyr) produced the best transducer base layer on the SPGE with abundant surface amines. It is suitable for anchoring the bioreceptor via covalent immobilization either binding to carboxyl or aldehyde groups produced via periodate oxidation of oligosaccharides on IgG moieties.

Polytyramine, a type of phenolamine, is widely known as a non-conducting polymer used in biosensor application. It shares a similar chemical structure to its biological by-product octopamine which has extra one hydroxyl group on its amine side chain (**Figure 4.1**). To the best our knowledge, there are no reports on the use of octopamine as a polymer layer to immobilize bioreceptors on the electrode. Most studies were focused on the development of biosensors for the detection of octopamine in food and beverages to trace the presence of biogenic amines (Zhang et al., 2016) and detection

of octopamine as a neurotransmitter in invertebrates (Cooper and Venton, 2009). Thus, the present study was aimed to investigate the potential of octopamine as a novel non-conducting transducer polymer base layer. The electrochemical characterization of polyoctopamine (POct) was conducted using cyclic voltammetry (CV) and electrochemical impedance spectroscopy (EIS). Midland blotting (Rushworth et al., 2013a) was performed and used on-sensor chemiluminescence to determine the presence of surface amines generated from the electrodeposited POct film and to further confirm the binding of CEA on the sensor surface. Several immobilization techniques including random and specific orientation were evaluated to determine the optimum fabrication protocol for immunosensors for CEA detection which were later used as a comparison to the Affimer-based biosensors. The ability of optimized immunosensors to detect CEA was monitored both in PBS and medically relevant matrix, i.e normal human serum.
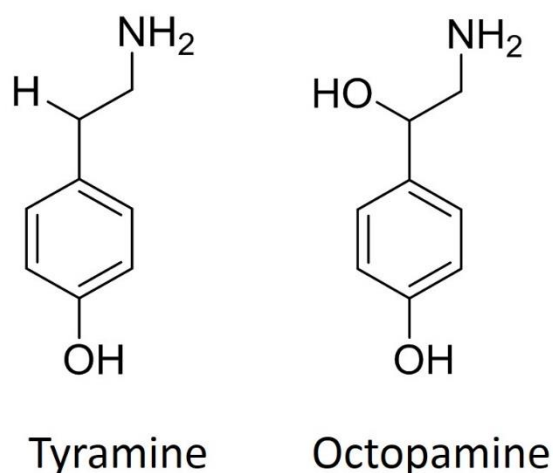
Figure 4.1: Chemical structures of tyramine and octopamine

Tyramine and octopamine are types of phenolamines that comprised of phenol ring and amine moiety on the side chain in both chemical structures. They only differ in the extra hydroxyl group on the side chain of octopamine.

4.2 Characterization of octopamine as non-conducting polymer layer

4.2.1 Effect of various deposition cycles on CV mediated octopamine and tyramine electropolymerisation

To determine the electrochemical behaviour of polyoctopamine (POct) as a new transducer base layer, electrodeposition of a monomer solution containing 5 mM octopamine dissolved in 100 mM phosphate buffer, at pH 7.5, was prepared and polymerised using cyclic voltammetry. The voltage was swept from 0 to +1.6 V and back at a scan rate of 100 mV/s. Electrodeposition using several scan cycles were investigated using 2, 4 and 6 cycles alongside the electrodeposition of polytyramine (PTyr) for 2 cycles only as a comparison. Overlay of CV curves from different deposition cycles are shown in **Figure 4.2 A**. The cyclic voltammogram from all cycles showed that the electrochemical reaction of polyoctopamine on bare DS gold electrode was irreversible as indicated by the presence of single anodic peak potential observed at around +0.52 V in the first scan cycle. Additionally, a sudden decrease of the anodic peak current was observed from the second scan cycle onwards. The anodic peak current of 2, 4 and 6 cycles of POct deposition were 10, 4 and 12 times higher in the first cycle compared to those in the second scan cycle. The same trend was observed from the CV curves of PTyr deposition except that the anodic peak potential shifted towards more negative values which was +0.45 V and the anodic peak current reduced dramatically from 10.3 µA to 962 nA. **Figure 4.2 B** shows an enlarged image of **Figure 4.2 A** from 0.2 to 0.7 V potential to provide a better view of the anodic peak current from each cycle. The presence of a sole anodic peak potential also suggested that the polymer underwent a single oxidation reaction that left the pendant amine free. Midland blotting was subsequently performed as on-sensor analysis to validate this hypothesis which will be described in the following sections.

The effect of varying the deposition cycles on impedance properties were further evaluated using electrochemical impedance spectroscopy. Data collected from the impedance spectra are presented as Nyquist plots and overlays of the impedance data derived from the corresponding modified electrodes are shown in **Figure 4.2C**.
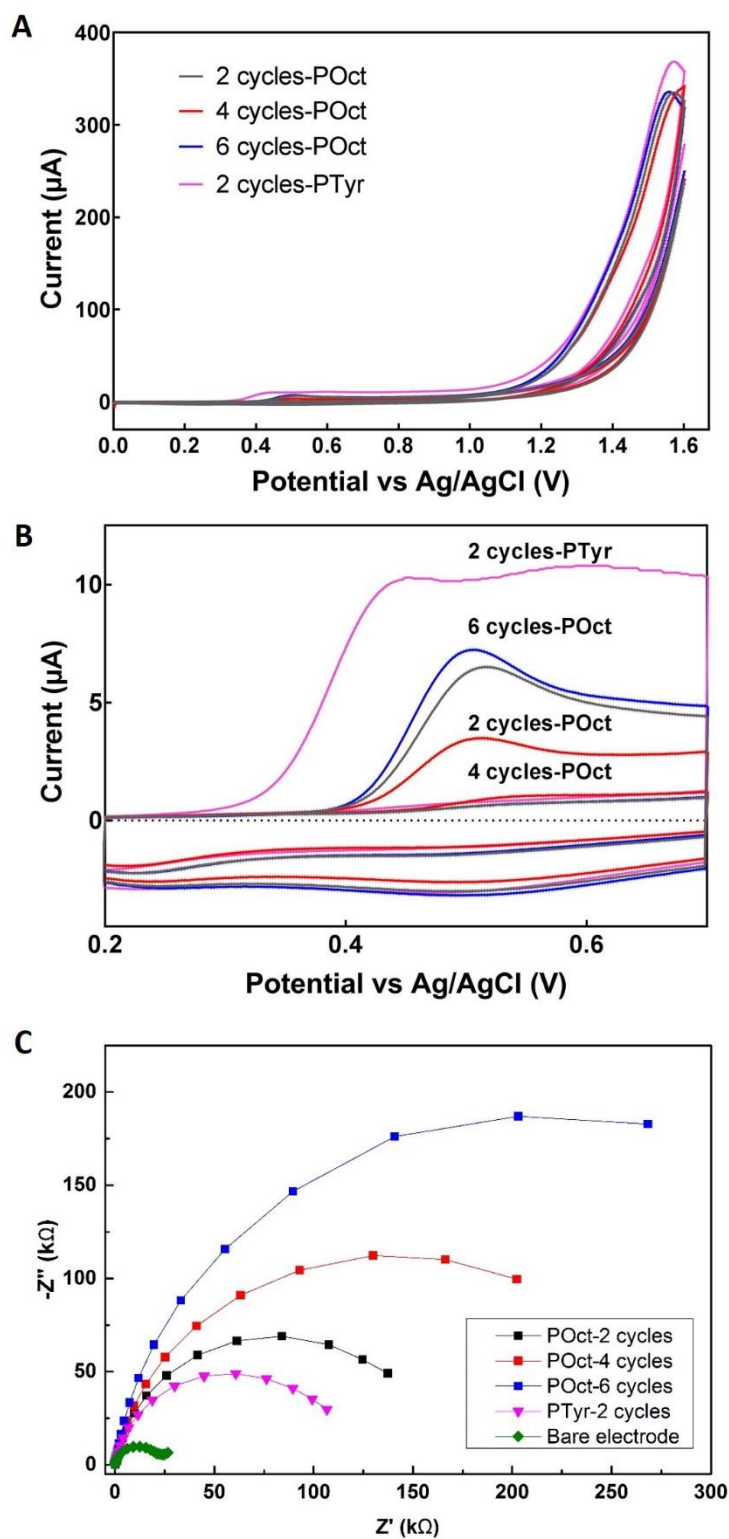
Figure 4.2: Electrochemical characterization of POct and PTyr deposition on different scan cycles

(A) CV of POct deposition from different scan cycles; 2 (—), 4(—) and 6 (—) at scan rate 100 mV/s from 0 to +1.6 V and back. PTyr was deposited for 2 cycles using the same scan rate and potential range as a comparison model; (B) The enlarged CV curves of figure A; (C) Corresponding impedance data of the deposited polymers recorded in 1:1 ratio of 10 mM [Fe(CN)6]3-/4- in 100 mM PBS pH 7.1

Results showed that the deposition of polyoctopamine with two cycles generated a semi-circular shape of Nyquist plot with low R_{CT} value (137.5 kΩ) but slightly higher than the polytyramine sensor (106.7 kΩ) and significantly greater than the bare DS gold electrode (26.6 kΩ). Interestingly, when the deposition of polyoctopamine exceeding two scan cycles, the sensors became highly capacitive and resistive. The Nyquist plots also tended to lose the semi-circular shape. Together these results indicate that the polymer growth was self-limiting and a very thin polymer film with low resistance was successfully deposited on the electrode surface. Thus from these findings, further optimization was carried out to evaluate the effect of different scan rates employed during deposition by keeping the two cycles constant.

4.2.2 Effect of CV scan rate on electropolymerisation of octopamine and tyramine

Preliminary experiments on different numbers of scan cycles demonstrated that electrodeposition of POct at 100 mV/s scan rate for 2 scan cycles successfully passivated the electrode surface with a thin layer of polymer. To determine the optimum scan rate for polymerizing octopamine onto the electrode surface, further investigation was conducted by applying scan rates from 100 to 400 mV/s with the deposition cycle kept constant for 2 cycles. Electrodeposition of PTyr at 100 and 200 mV/s were included for comparison since these scan rates were found optimum in polymerizing PTyr film onto DS SPGE as indicated by previous work in the Millner group (Ahmed et al., 2013, Goode et al., 2016). **Figure 4.3 A and C** show the CVs of POct and PTyr at different scan rates as described earlier and the graphs were rescaled and magnified from 0.2 to 0.7 V potential range (**Figure 4.3 B and D**) for clarity of anodic peak current at each scan rate. It was apparent from the linear plot that the anodic peak current increased proportionally as the scan rate increased with a good R^2 value of 0.996 (**Figure 4.3 E**). On the contrary, the Nyquist plot showed an inverse linear relationship (**Figure 4.4 A**) whereby increased in the scan rate resulted in decreased impedance (**Figure 4.4 B**). The same trends were also observed from the deposition of PTyr. A semi-circular shape of the Nyquist plot was maintained in all scan rates indicating that the POct film did not overly insulate the electrode surface, making it permeable for redox mediator accessibility.
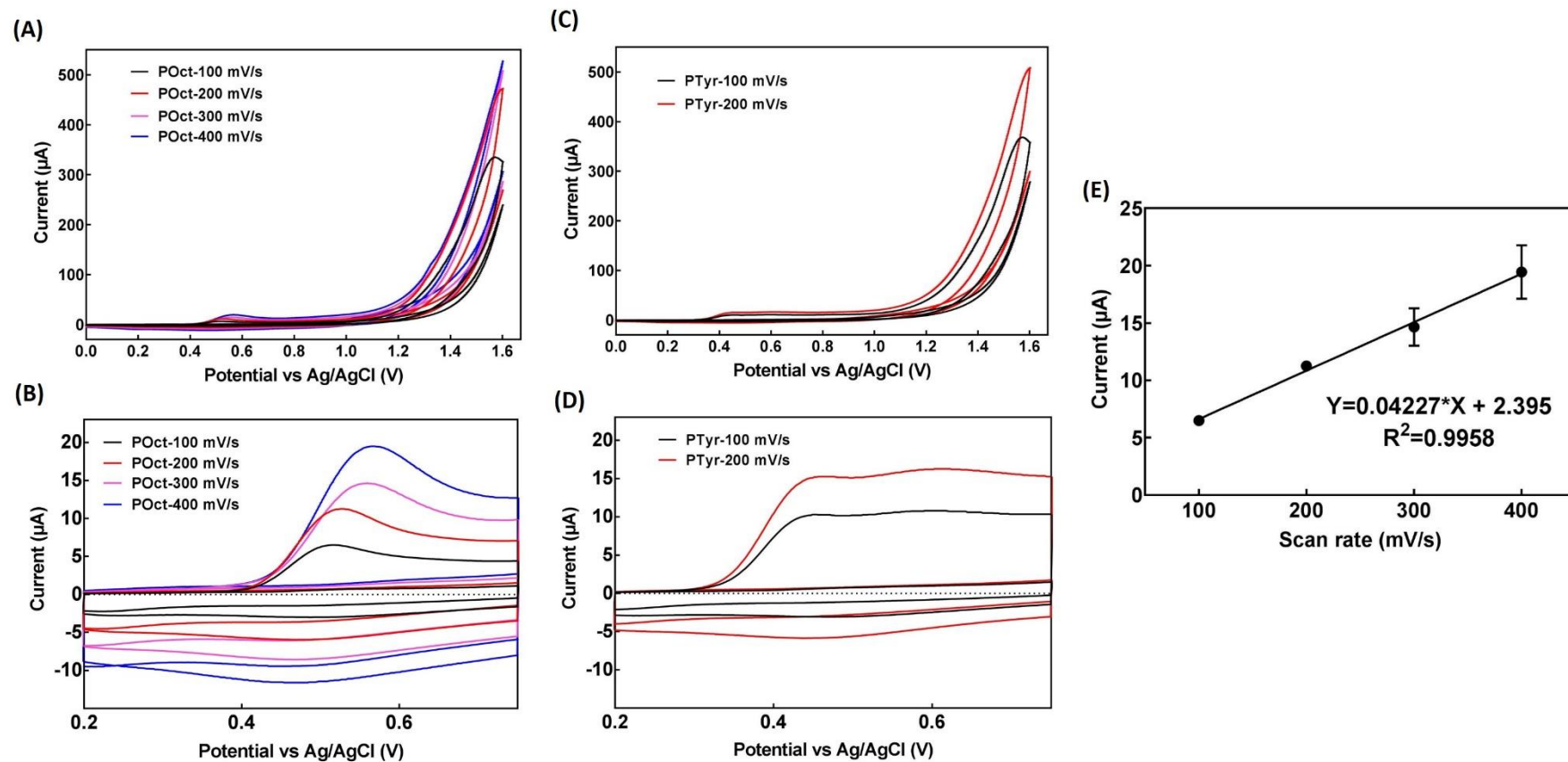
Figure 4.3: Effect of scan rate on POct deposition

(A) CVs of different scan rates mediated POct deposition (100-400 mV/s) and (B) the magnification of panel A from 0.2 to 0.7 V potential range; (C) CVs of different scan rates mediated PTyr deposition (100 and 200 mV/s) and (D) the corresponding enlarged CV curves of panel C; (E) The linear relationship between anodic peak current and scan rate of POct deposition. All polymers were deposited for 2 cycles from 0 to +1.6 V and back in 100 mM phosphate buffer pH 7.5.
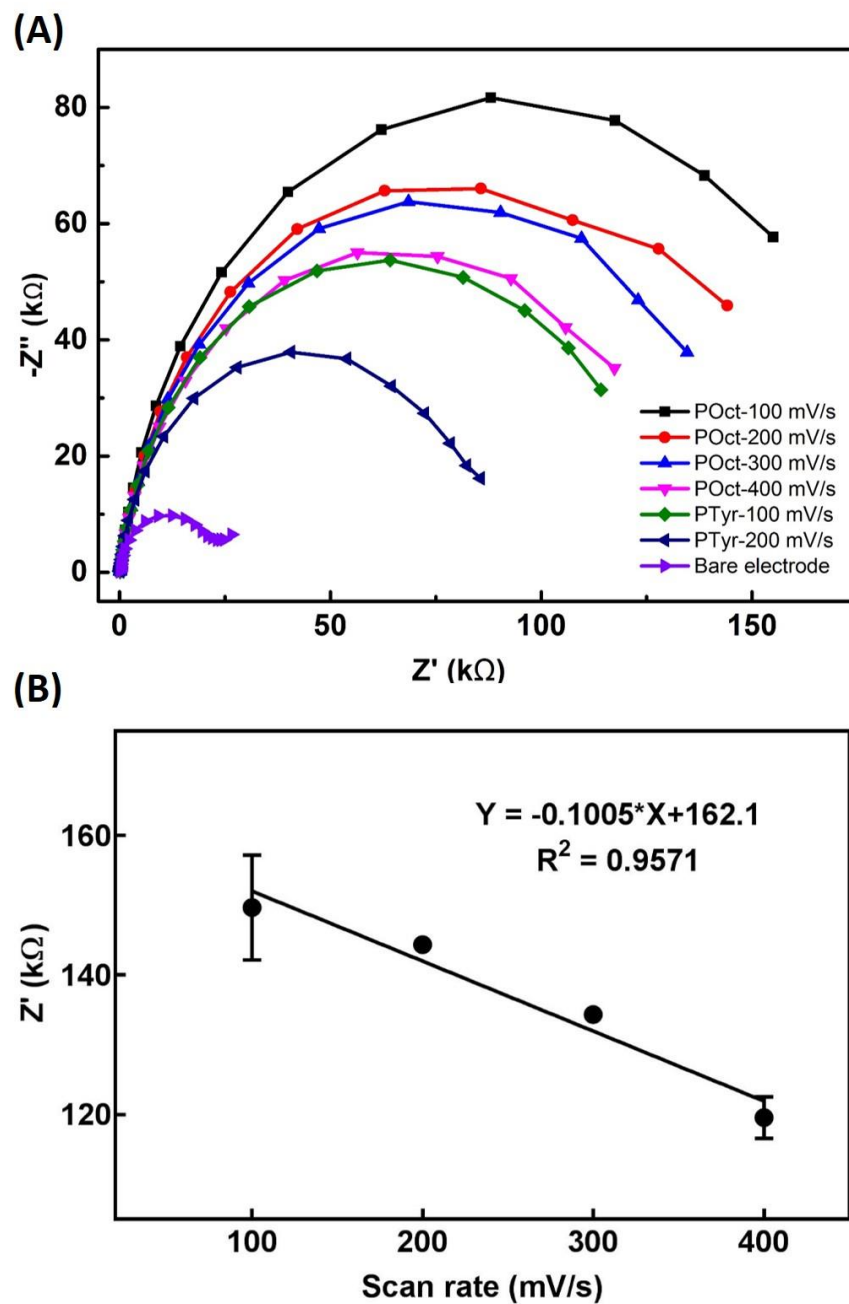
Figure 4.4: The impedance behaviour of different scan rates employed during POct deposition

(A) Nyquist plots of different scan rates employed during electrodeposition of POct (100-400 mV/s) and PTyr (100 and 200 mV/s); (B) The inverse linear relationship between impedance and scan rate of POct deposition. EIS measurement were recorded in redox mediator solution containing 1:1 molar ratio of 10 mM $[Fe(CN)_6]^{3-/4-}$ in 100 mM PBS, pH 7.1.

4.2.3 Determination of available surface amines generated by electrodeposition of POct

The electrochemical characterization of polyoctopamine films using CV and EIS have shown that the electrode surface was successfully passivated by a thin layer of polymer film. However, this does not guarantee that the polymer generated sufficient surface amines, with correct orientation for bioreceptor conjugation. On-sensor blotting , Midland blotting (Rushworth et al., 2013a), was performed after polymer deposition to determine the availability of surface amine following an established protocol. Two scan rates were evaluated, 100 mV/s and 200 mV/s, for electrodeposition of POct and PTyr scanned over 2 cycles. The working electrodes were incubated with and without biotin-NHS after polymer deposition, followed by streptavidin HRP and ECL substrate prior to imaging. A bare gold screen printed electrode was included as an additional control. The Midland blot data showed that both scan rates provided abundant surface amines for both polymers (**Figure 4.5**) based on significant signals observed from the positive electrodes incubated with biotin-NHS and streptavidin-HRP. On the contrary, a negligible ECL was observed from the bare gold electrodes and the electrodes where biotin-NHS incubation was omitted, which could be due to non-specific adsorption of streptavidin-HRP onto the sensor surface. Considering these data together with previous optimization, electrodeposition of POct using cyclic voltammetry for 2 cycles at 100 mV/s scan rate was used to construct the biosensors throughout this study.
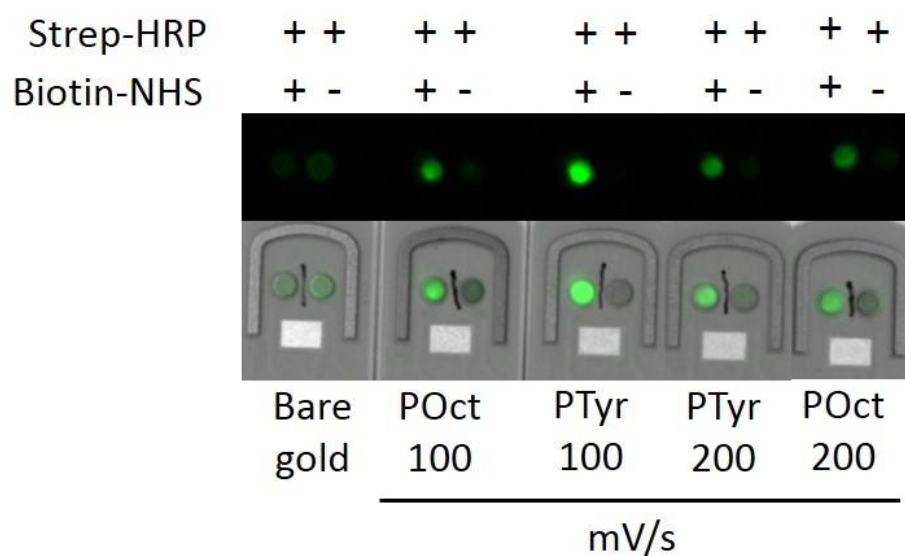
Figure 4.5: Midland blotting of available surface amines after polymer deposition

Electrodes were electropolymerised with POct and PTyr at scan rate of 100 mV/s and 200 mV/s for 2 scan cycles. After polymer deposition, the working electrodes (WE) were incubated with (left WE) and without (right WE) biotin-NHS followed by streptavidin HRP. The ECL substrate was subsequently added and the electrodes were imaged simultaneously in the imager. Bare gold screen printed electrodes were included as control. The top panels show pseudo-green colour of the captured images, and the bottom panels are superimposed image of the electrodes and pseudo-green colour illumination.

4.2.4 Assessment of POct stability after consecutive impedance scan

To evaluate the stability of the polyoctopamine film, consecutive impedance measurements were performed in redox mediator solutions containing 10 mM $[Fe(CN)_6]^{3-/4-}$ in 100 mM PBS pH 7.1 without any intermediate washing step. Data from five impedance scans (**Figure 4.6**) showed that the polymer film was stable, with first to third scans overlapping each other. Minimal increase was observed on the fourth and fifth scans. It is important to note that the semi-circular shape of the Nyquist plot was retained throughout the scanning which indicated that the polymer maintained its conformation and stability and the electrolyte (e.g. salt presents in the buffer solution) did not contribute to the shift in impedance signal due to common electrostatic interaction.
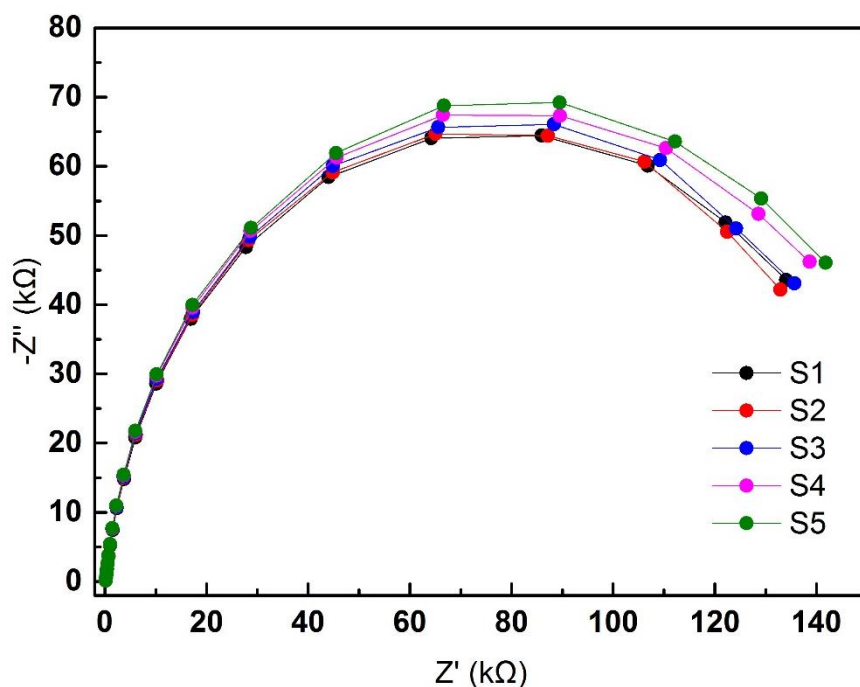
Figure 4.6: Nyquist plots of consecutive impedance scanning on POct film in redox mediator

Five consecutive impedance measurements were performed on a single working electrode after electrodeposition of POct film. The measurement was taken in presence of redox mediator solution (1:1 molar ratio 10 mM $[Fe(CN)_6]^{3-/4-}$ in 100 mM PBS pH 7.1). Experiments were done on six independent working electrode and the result is representative of a single electrode.

4.3 Optimization of antibody immobilisation onto sensor surface

Antibodies have been widely used as biorecognition elements in the development of biosensors due to their high specificity and affinity binding towards their target analytes. One of the main key elements impacting on the performance of a biosensor is the immobilisation strategy used to place antibody on the sensor surface. These strategies can be divided into random and oriented immobilisation. The simplest technique is through non-covalent immobilisation either via physisorption, chemisorption or entrapment and covalent coupling through amines, all of which could lead to random orientation. Specific orientation via covalent coupling to (e.g. thiol and oligosaccharides) and affinity based interaction to the Fc region of antibody (eg. avidin-biotin and intermediate protein A/G) have gained increasing interest due to better performance of the biosensor's detection capability. Thus, in this study, both random and specific orientation of antibodies were tested to determine which immobilisation technique produced the best biosensor.

4.3.1 Validation of antibodies specificity via dot blots

To ensure signals derived from the impedance scanning represent specific binding between antibody and analyte, dot blotting was performed as described in **Section 2.2.6**. A positive signal was visible in the CEA spot only and its absence in the negative control indicated that the polyclonal anti-CEA antibody was binding specifically to CEA (**Figure 4.7**). In addition, no discernible signal was seen in the absence of primary antibody confirming that positive signal observed represents true binding by the bound antibody. Similarly, no detectable signal appeared on the membrane incubated with polyclonal anti-digoxin antibody suggesting that this antibody is suitable to be used as negative control bioreceptor for sensor construction. Throughout the immunosensor development in this study, polyclonal anti-CEA and anti-digoxin antibodies were used as specific and non-specific receptors, respectively.

| Secondary | Goat-anti-rabbit-HRP | | Anti-sheep-HRP |
| Primary | Anti-CEA | No | Sheep-anti-Digoxin |

CEA

Negative Control

(A)   (B)   (C)
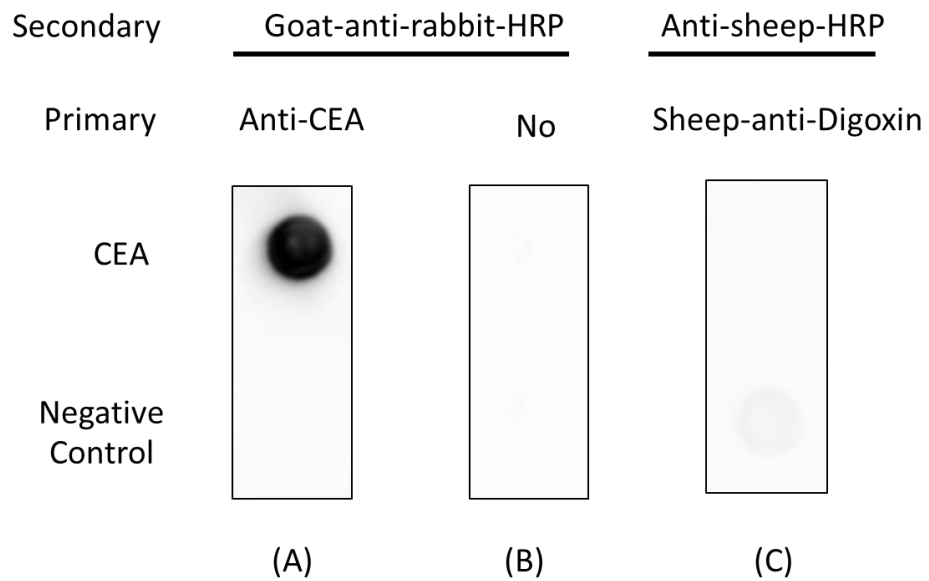
Figure 4.7: Dot blot characterization of antibodies specificity

One µM of CEA protein and BSA as negative control were spotted onto each membrane. Rabbit polyclonal anti-CEA (1:1000) was incubated on membrane (A) as primary antibody but omitted on membrane (B) followed by incubation in goat anti-rabbit HRP as secondary. Sheep polyclonal anti-digoxin was incubated on membrane (C) followed by incubation in anti-sheep HRP as secondary which serves as control for non-specific antibody.

4.3.2 Random orientation of antibody

4.3.2.1 Antibody entrapment via electropolymerisation of octopamine and MS (PEG)$_4$ conjugate

Preliminary investigation on electrochemical characterization of POct deposition onto SPGE demonstrated that the polymer generated an abundance of positively charge surface amine. This allowed for both direct and indirect tethering of bioreceptors via amine coupling. Positively charged surfaces are commonly prone bio-fouling as the majority of proteins exist as negatively charged ions leading to non-specific electrostatic interaction. To overcome this effect, the biosensors were initially constructed based on the conjugation of octopamine and MS (PEG)$_4$-NHS in an equimolar ratio of 5 mM each for 1 h , followed by electropolymerisation of the conjugate with 0.1 mg/ml of anti-CEA polyclonal antibody. Control sensors were fabricated following the same technique using an anti-digoxin polyclonal antibody. The hypothesis behind this sensor construct was to prevent bio-fouling by incorporating the PEG in the conjugate whilst the presence of methyl terminus would generate a neutral charged biosensor surface. Since there was no reactive group available for conjugating the antibody to the conjugate, the antibody was physically trapped via cyclic voltammetry into the electrogenerated polymers which should result in random orientation. The optimisation of antibody density on DropSens SPGE has been extensively investigated by Dr. Timothy Gibson from ELISHA Systems Ltd. and 0.1 mg/ml antibody concentration was found to be the optimum concentration to produce an effective immunosensor response (personal communication). Thus, this concentration was used in the fabrication of all immunosensors in this chapter.

The CV of electropolymerisation of the conjugates with antibodies showed an irreversible oxidation reaction that was similar to the electropolymerisation of POct alone (**Figure 4.8 A**). However, a marked increase in the anodic peak current (52.9 µA) and more positive anodic peak potential (+0.95V) were observed compared to the CV of POct alone that are 6.5 µA and +0.52 V, respectively. The positive increment seen in both anodic peak current and potential may be derived from the MS (PEG)$_4$ component.
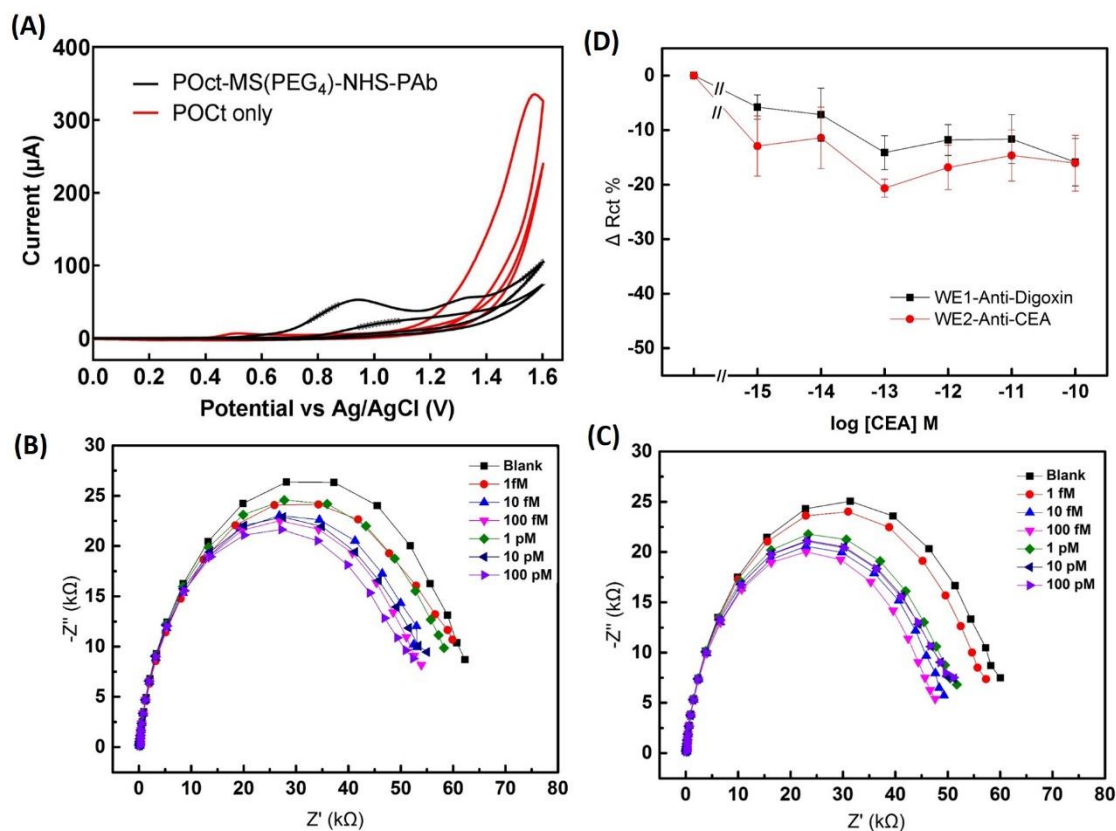
Figure 4.8: Electrochemical characterization of POct-MS(PEG)$_4$ based immunosensor

(A) Comparison of CVs from the electropolymerisation of antibodies with octopamine and MS(PEG)$_4$ conjugates and electropolymerisation of octopamine alone; Corresponding Nyquist plots of (B) anti-digoxin and (C) anti-CEA immunosensors for CEA detection with increasing concentration; 1 fM (●), 10 fM (▲), 100 fM (▼), 1 pM (♦), 10 pM (◄), 100 pM (►) and blank analyte (■). (D) Calibration curve of CEA immunosensor using anti-CEA IgG as specific (●) and anti-digoxin IgG as non-specific (■) receptors, normalised data showing percentage change in R$_{CT}$ (n= 4± SEM) and no significance difference (p<0.05) observed between both sensors.

To investigate the binding ability of fabricated biosensors to CEA, the same sensors were subsequently incubated for 20 min with increasing concentration of CEA from 1 fM to 100 pM as described in **Section 2.2.7.4**. After each incubation, the sensor was washed thoroughly and the impedance measurement was recorded in $[\text{Fe (CN)}_6]^{3-/4-}$ redox mediator solution. Observation from the Nyquist plot of anti-digoxin and anti-CEA sensors supported the initial hypothesis that the construct could prevent the non-specific binding (**Figure 4.8 C and D**). However, when the R_{CT} value of each analyte concentration was normalised to the blank sensor to obtain the percentage change, no significant difference was observed between anti-CEA and anti-digoxin sensors after coplotted against increasing concentration of CEA (**Figure 4.8 B**).

To further evaluate the possibility that CEA binding did occur but could not be detected by impedance scanning, Midland blotting was conducted on sensors incubated with a single concentration of CEA at the highest level (100 pM). After impedance measurements were taken, the sensors were washed and incubated for 1 h in anti-CEA monoclonal antibody, followed by secondary antibody conjugated to HRP. Then, several washes were given prior to ECL reagent exposure and images were captured. **Figure 4.9** from the Midland blot corroborated the impedance data that CEA binding had not taken place. A possible explanation for this phenomenon that in agreement with previous review (Cosnier, 2005) would be the antigenic binding sites might be hindered during the electropolymerisation which prevent the analyte from binding.
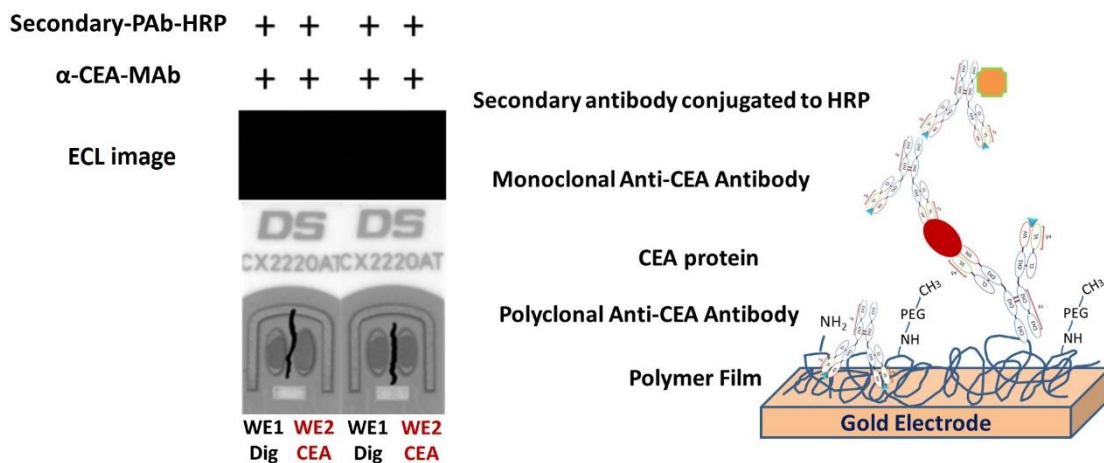
Figure 4.9: Midland blot to investigate CEA binding on sensor surface

Anti-digoxin (WE1) and anti-CEA (WE2) antibodies were electropolymerised with octopamine and MS(PEG)$_4$ conjugates on respective working electrodes (WE). After 100 pM of CEA bound to the sensors and impedance reading was measured, the working electrodes were incubated with anti-CEA monoclonal antibody followed by secondary antibody conjugated to HRP. A chemiluminescent image was captured after exposure to ECL reagents. The upper panels show no illumination of the captured images indicating no binding occurred whilst, the lower panels are superimposed image of the electrodes and the captured images of above panel. Experiments were run on duplicate electrodes. The schematic diagram on the right shows the corresponding detection principle.

4.3.2.2 Electropolymerisation of periodate oxidised IgG conjugated to octopamine

Initial optimisation on antibody immobilisation using random orientation based on physical entrapment of antibody during electropolymerisation of octopamine and MS (PEG)$_4$ showed that the sensor was not successful in producing appreciable signal upon CEA binding. Another common technique for immobilising antibody onto aminated functionalised surface is via direct covalent linkage to oxidised oligosaccharide in the Fc region. It is well known that IgG contains two carbohydrate sites located on the heavy chain in the Fc region. According to previous report (Wolfe and Hage, 1995), oxidation of the carbohydrate moiety using 10 mM periodate at pH 5-6 for 30 min is a controllable process and should generate an average of two labelling sites per IgG antibody. Based on this technique, antibody was initially oxidised using sodium *meta*-periodate as described in **Section 2.2.7.1** to produce a reactive aldehyde group and covalently bound to octopamine monomer in solution for 1 h. Random orientation was evaluated by electropolymerising the oxidised antibodies pre-conjugated to octopamine using the cyclic voltammetry technique as described earlier.

The CV of electrodeposition of oxidised antibody conjugated to octopamine showed a similar trend as electropolymerisation of POct alone with slightly reduced anodic peak potential and anodic peak current (0.51 V and 5.63 µA, respectively, **Figure 4.10 A and B**). The modified sensors were subsequently incubated with increasing concentration of CEA from 1 fM to 100 nM for 20 min to determine the binding performance against CEA. The impedance spectra from the Nyquist plot of anti-CEA immunosensor showed a decrease in resistance when increasing concentrations of CEA were applied to the sensor surface (**Figure 4.11 B**). Unfortunately, the same decreasing pattern was also observed in the anti-digoxin immunosensor (**Figure 4.11 A**). Unlike the octopamine and MS (PEG)$_4$ based sensor which showed 13% and 6% R_{CT} changed on anti-CEA and anti-digoxin sensors, respectively, when 1 fM CEA was applied (**Figure 4.8 B**), approximately 50% change in R_{CT} was observed in the present anti-CEA sensor (**Figure 4.11 C**). However, a shifting in the R_{CT} of the same magnitude was also observed in the anti-digoxin sensor (54%). This finding demonstrated that the current immunosensors construct showed some improvement in terms of binding to CEA but experiencing a non-specific binding problem at the same time.
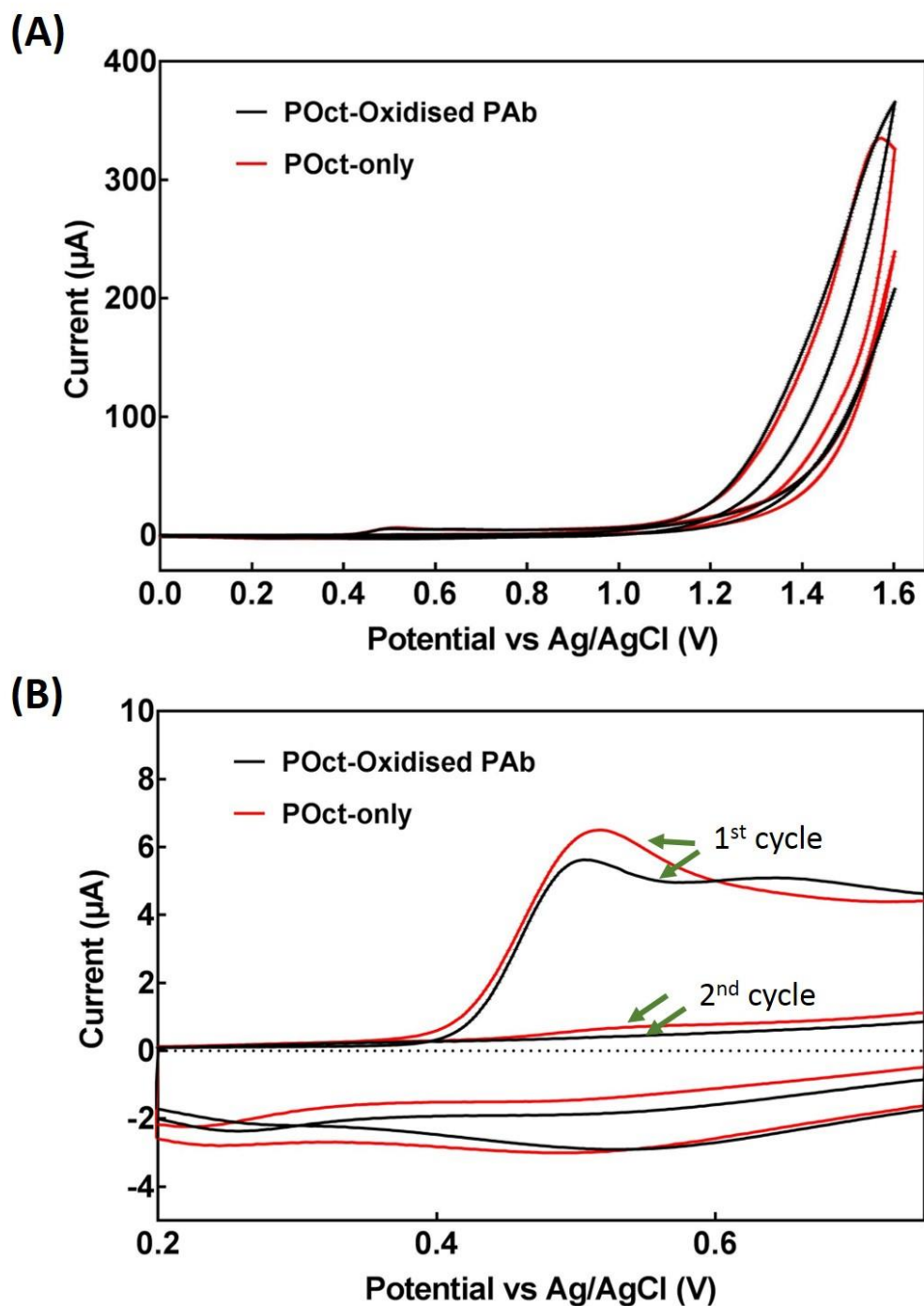
Figure 4.10: Electropolymerisation of oxidised antibody covalently conjugated to octopamine

(A) CV from the electropolymerisation of oxidised polyclonal antibody conjugated to octopamine compared to POct alone; (B) the magnified CV curves of (A) from 0.2 to 0.7 V potential range. All polymers were deposited for 2 cycles from 0 to +1.6 V and back in 100 mM phosphate buffer pH 7.5.
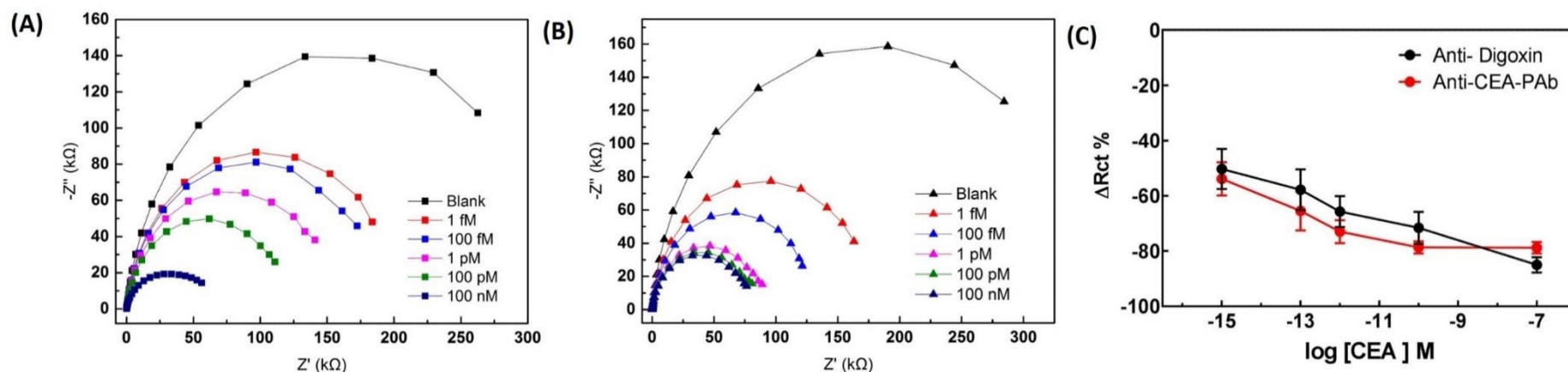
Figure 4.11: EIS data of immunosensors fabricated based on electrodeposition of oxidised antibodies conjugated to POct

Nyquist plots showing increasing concentration of CEA (from 1 fM to 100 nM) that cumulatively incubated onto fully constructed (A) anti-digoxin and (B) anti-CEA polyclonal antibodies sensors; (C) Calibration curve of corresponding immunosensors plotted as normalised data showing the percentage change in R_{CT} (n= 4± SEM). EIS was recorded in 10 mM $[Fe(CN)_6]^{3-/4-}$ in 100 mM PBS pH 7.1. The mean differences between anti-CEA and anti-digoxin sensors in each concentration was not statistically significant by independent t-test (p<0.05).

4.3.3 Specific orientation

4.3.3.1 Site-directed immobilisation of oxidised IgG-oligosaccharide onto amine-functionalised POct film

Immunosensors constructed based on a simple one step electropolymerisation of oxidised antibody pre-conjugated to octopamine showed better binding interaction of CEA on sensor surface compared to the former sensor construct but non-specific binding was also observed. Thus, site-directed immobilisation onto amine-functionalised POct film via covalent linkage of oxidised oligosaccharide located in the Fc region of antibody was evaluated. Sensor chips were fabricated by directly functionalising the oxidised antibody onto a POct film for 1 h as described in **Section 2.2.7.2** prior to CEA interrogation. Since the immobilisation of antibody was performed after polymerisation of the POct film, this fabrication should provide a favourable access to antigen interaction and could eliminated the non-specific fouling binding. In the development of this biosensor, both monoclonal and polyclonal antibodies have been used as a biorecognition elements. Hence, fabrication of both sensors using both the monoclonal and polyclonal antibodies reagents was evaluated using the site-directed immobilisation as depicted in the schematic diagram (**Figure 4.12 A**).

Data from the polyclonal antibody based sensor showed a gradual decrease in the impedance signal as observed from the Nyquist plot of anti-CEA sensor when increasing concentration of CEA were interrogated (**Figure 4.12 C**) whilst, the impedance remained static in the control sensor (**Figure 4.12 B**). It was apparent from the calibration curve (**Figure 4.12 D**) that a significance decrease in the percentage change of R_{CT} was observed when compared between the anti-CEA and control sensors over the CEA concentration range. The sensor generated a highly sensitive and specific CEA detection with a limit of detection of 1 fM and broad dynamic range from 1 fM to 100 nM. There was no shift in the R_{CT} values detected from the control sensor which indicated that the impedance signal observed from the anti-CEA sensor represented specific binding.

The same declining trend was observed in the monoclonal anti-CEA antibody based sensor as presented in **Figure 4.13 B and C**. It can be clearly seen from the calibration curve that a significance change in the percentage of R_{CT} was also observed when compared between the anti-CEA and control sensors under the same concentration setting (**Figure 4.13 C**). Interestingly, the sensitivity was reduced by 100-fold less

compared to the polyclonal antibody based sensor and had a narrower dynamic range from 100 fM to 1 nM. At the highest analyte concentration, the mean difference of R_{CT} change between anti-CEA and control sensor was significant but the magnitude of change in R_{CT} started to level off. No significant changes were observed from the control sensor when plotted against CEA concentration and the trend showed almost a flat line. This indicated that non-specific binding did not occur, in a similar way to the polyclonal antibody based sensor.
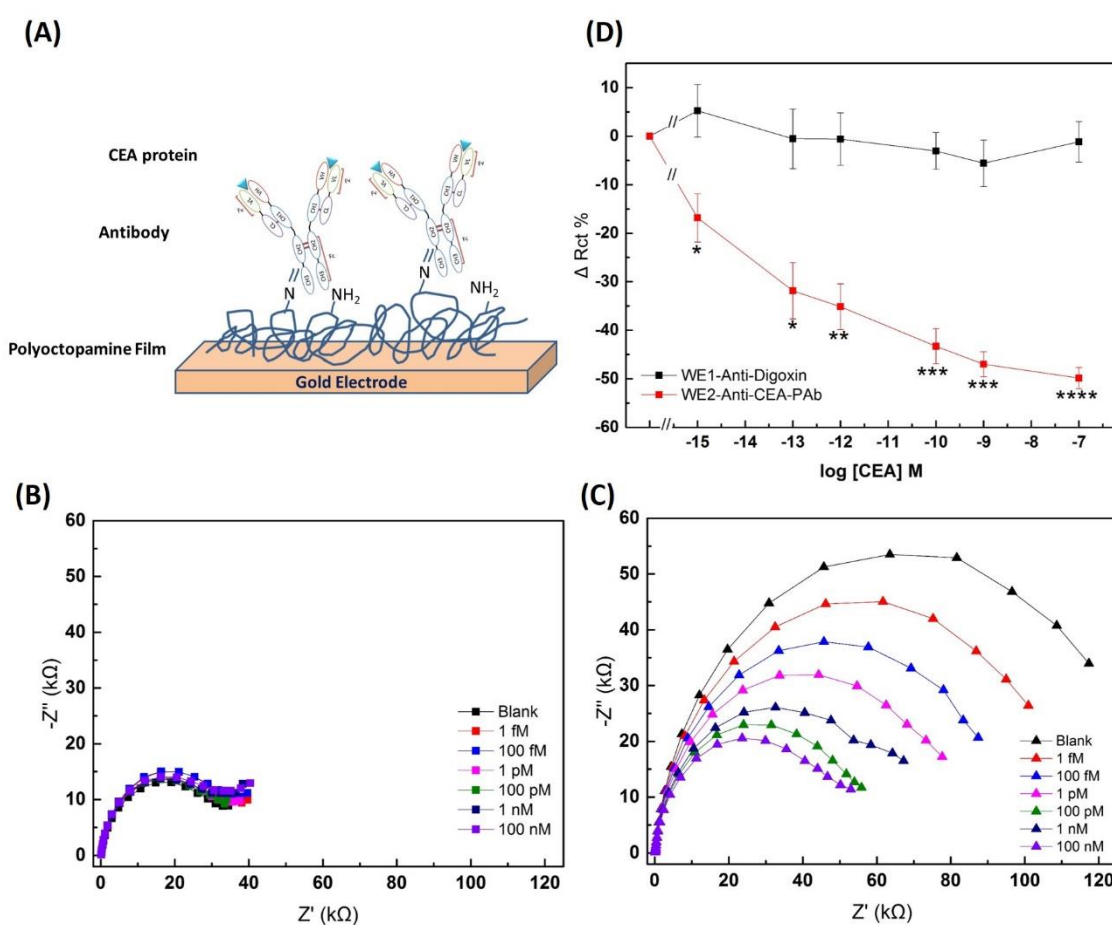
Figure 4.12: Impedance behaviour of oriented immobilisation of anti-CEA polyclonal antibody based sensor

Immunosensors were fabricated by post-functionalisation of the oxidised polyclonal antibody onto POct film via covalent binding as shown by the schematic diagram (A). Nyquist plots showing impedance signals when increasing concentration of CEA (from 1 fM to 100 nM) cumulatively incubated onto fully constructed (B) anti-digoxin and (C) anti-CEA polyclonal antibodies sensors; (D) Calibration curve of normalised data from the corresponding immunosensors showing the percentage change in R_{CT} (n= 4± SEM). Mean differences between anti-CEA and anti-digoxin sensors tested under the same CEA concentration were statistically significant by independent t-test (*, **, *** and **** denote significance with p-value <0.03, 0.002, 0.0002 and 0.0001, respectively).
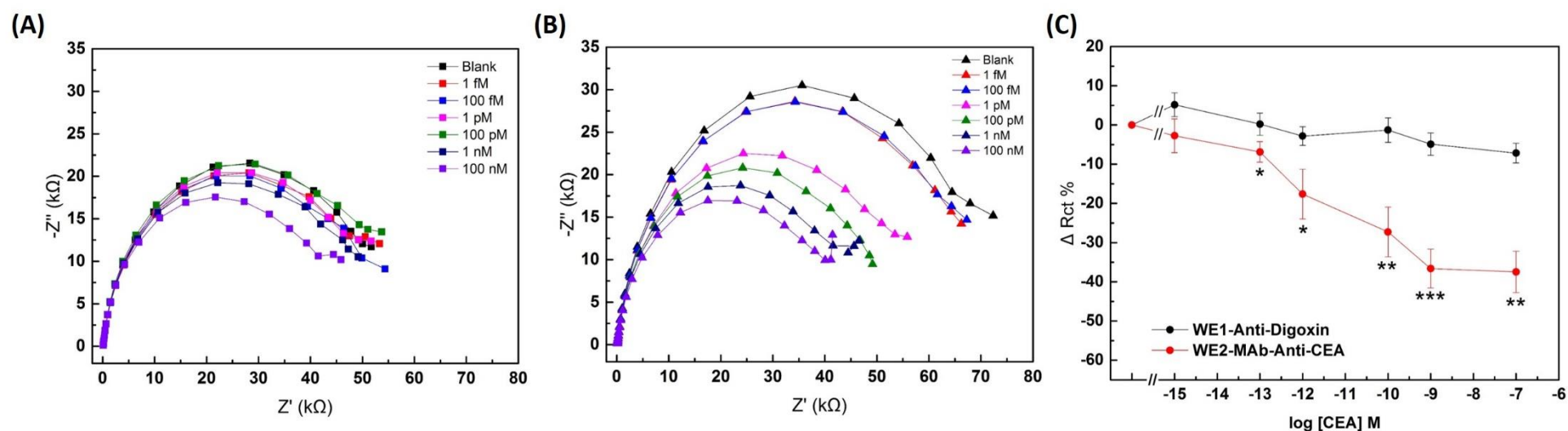
Figure 4.13: Impedance profile of oriented immobilisation of anti-CEA monoclonal antibody based sensor

Immunosensors were constructed based on covalent immobilisation of oxidised Fc region of the antibodies onto electropolymerised POct transducer base layer. Increasing concentration of CEA (from 1 fM to 100 nM) were successively incubated onto (A), anti-digoxin polyclonal antibody and (B), anti-CEA monoclonal antibody as shown by the Nyquist plots; (C), calibration curve of normalised data from the corresponding immunosensors showing the percentage change in R_{CT} (n= 4± SEM). Mean differences between anti-CEA and anti-digoxin sensors tested under the same CEA concentration were statistically significant by independent t-test (*, ** and *** denote significance with p-value <0.03, 0.002 and 0.0002, respectively)

As described in **section 1.5.4**, impedance measurements are comprised of complex parameters including resistive and capacitive components. Although the resistive component (R_{CT}) plays a major role in the total measured impedance in Faradaic impedimetric biosensors, it is also worth analysing other parameters that are present in the Randle's electrical equivalent circuit which was used for curve-fitting of the measured EIS data. This including capacitance (CPE), phase angle and total impedance (|Z|). Data from the polyclonal antibody based sensors were used to evaluate these parameters. All data from each circuit element were normalised to the blank sensor to obtain the percentage change at each analyte concentration.

In contrast to the R_{CT} data, decrease in the percentage change of capacitance (~10-12%) was observed from the calibration curve of control sensor instead of the anti-CEA sensor (**Figure 4.14**). However, no significant difference was observed in both sensors when analysing increasing concentration of CEA.
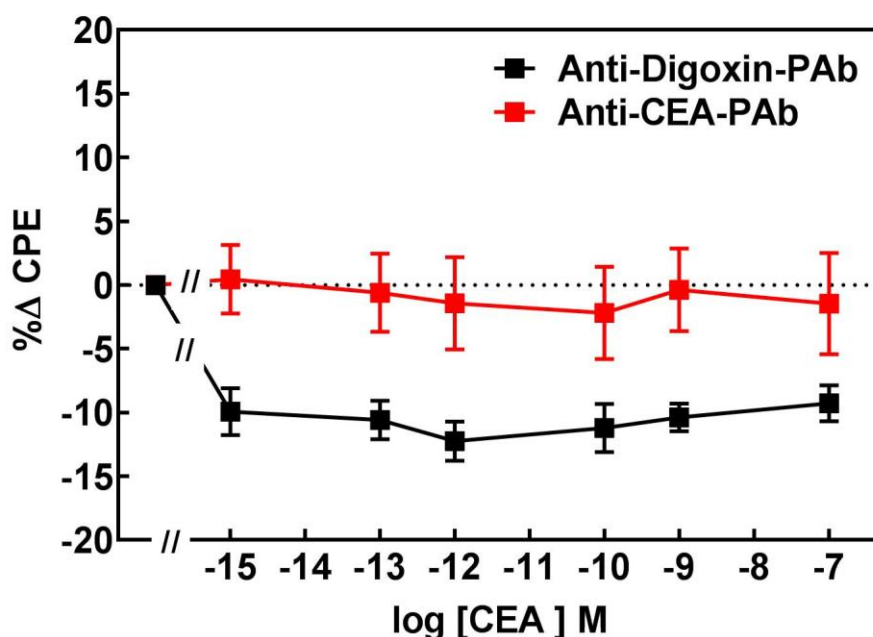
Figure 4.14 : Change in capacitance of polyclonal antibody based sensors

Calibration curve of normalised data from the anti-CEA (■) and anti-digoxin (—■—) polyclonal antibody sensors showing the percentage change in capacitance. Capacitance data are from the CPE values generated during the electrochemical impedance measurement. Data presented are means, (n = 4) ±SEM.

Apart from the CPE circuit element, shift in the phase angle is routinely used when analysing the capacitive effect of biosensors notably in non-Faradaic EIS. Although impedance was measured under Faradaic conditions in this study, non-Faradaic current can also occur in the electrical double layer region due to electroadsorption of ions from the electrolyte solution. To evaluate the effect of analyte binding on the capacitive component, values at 53.86 Hz were selected from the phase angle curves of anti-CEA (**Figure 4.15 A**) and control sensors (**Figure 4.15 B**), where the maximum phase angle was observed. These values corresponding to the maximum capacitive effect measured by the sensor. It is clear from the calibration curve of normalised data that the difference in percentage change of phase angle was very limited (less than 2%) between the anti-CEA and control sensors when increasing concentrations of CEA were interrogated. Both CPE and phase angle results suggested that the effect of capacitance upon analyte binding was minor. In addition, these results also proved that the fully fabricated immunosensors displayed mostly resistive features.

It is also interesting to evaluate the effect of $|Z|$ during analyte binding on the immunosensors interface. When analysing the $|Z|$ curves plotted against log frequency, a striking difference over CEA concentrations was observed at the lowest frequency, 0.25 Hz (**Figure 4.16 A**) in the anti-CEA sensor. In contrast, the curves remained constant in the control sensor (**Figure 4.16 B**). Thus, this frequency was selected to further analyse the change in $|Z|$. Data from the calibration curve (**Figure 4.16 C**) showed the same changing trend as in the R_{CT} analysis (**Figure 4.12 D**). Similarly, a significant decrease in the percentage change of $|Z|$ was observed in the anti-CEA sensor compared to the control sensor with increasing CEA concentrations. However, the overall magnitude of change in R_{CT} was higher compared to $|Z|$. Taking into consideration all analysed data, analysis of impedance will focus on the R_{CT} parameter throughout this study.
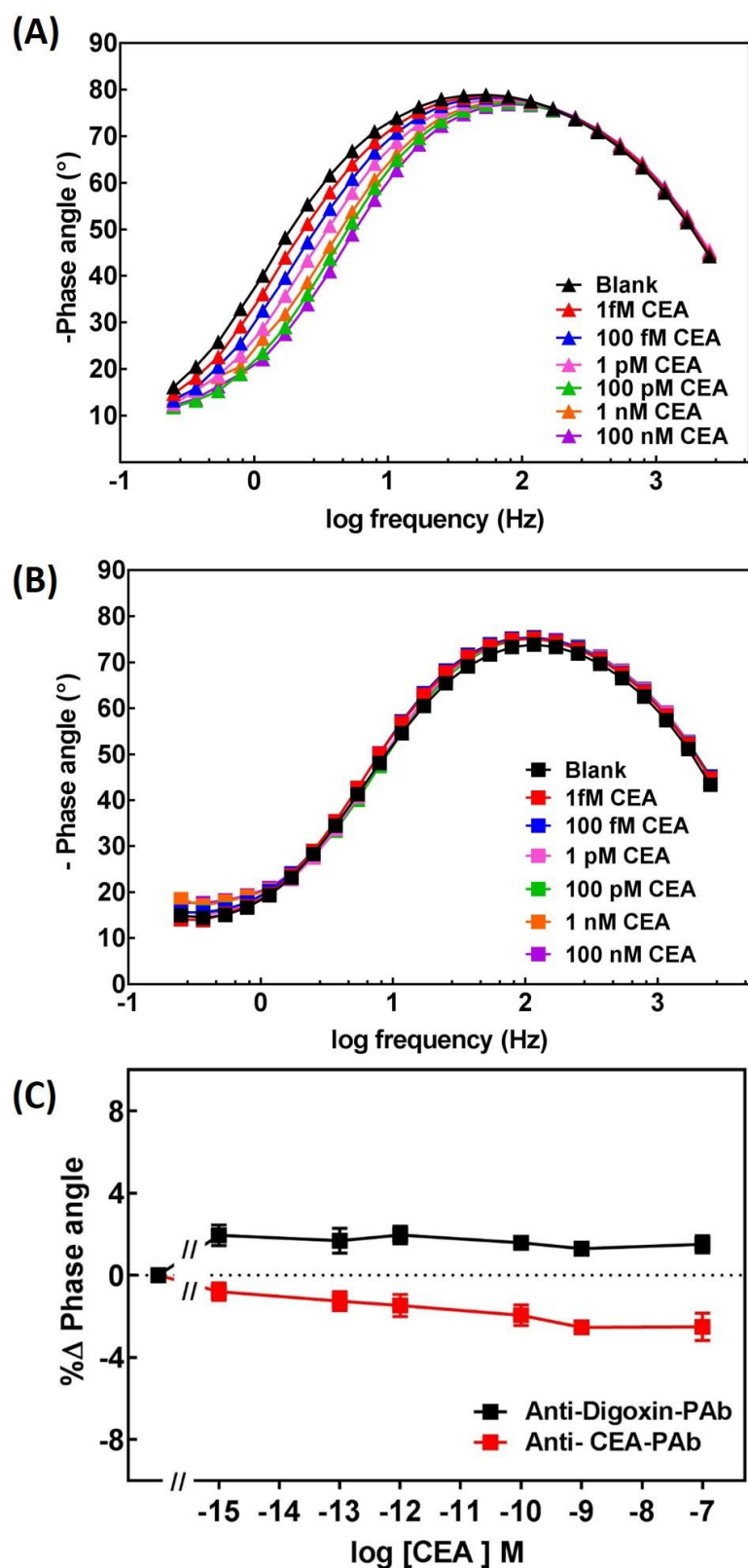
Figure 4.15 : Shift in phase angle analysis of polyclonal antibody based sensors

EIS phase angle data for interaction between (A) anti-CEA and (B) anti-digoxin polyclonal antibodies sensors with CEA concentrations in PBS scanned from 2.5 KHz to 250 mHz. (C) Calibration curve of normalised data from the corresponding immunosensors showing the percentage change in phase angle at 53.86 Hz. Data are means (n= 4)±SEM.
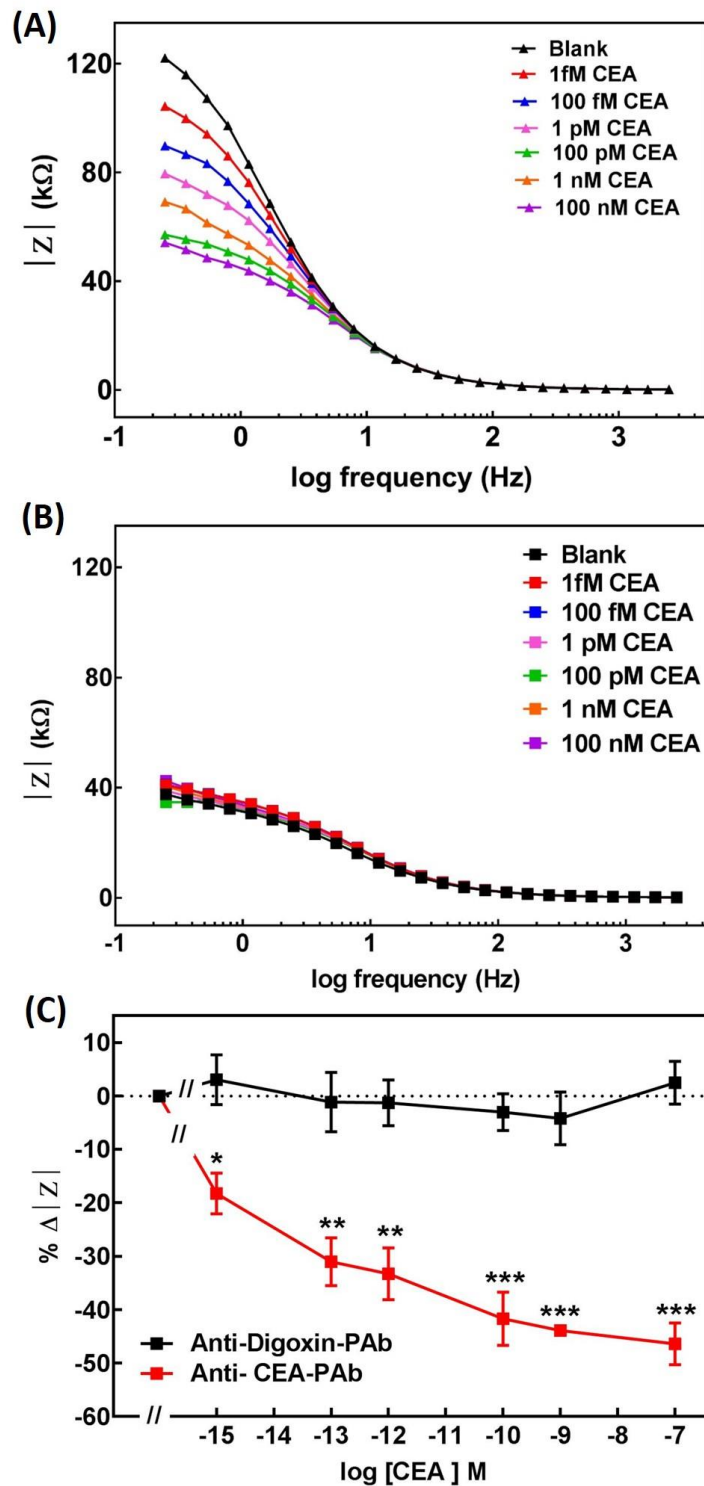
Figure 4.16 : Total impedance analysis of polyclonal antibody based sensors

Total impedance ($|Z|$) data for interaction between (A) anti-CEA and (B) anti-digoxin polyclonal antibodies sensors with CEA concentrations in PBS scanned from 2.5 KHz to 250 mHz. (C) Calibration curve of normalised data from the corresponding immunosensors showing the percentage change in $|Z|$ at 0.25 Hz. Data are means, (n=4)±SEM. Mean differences between anti-CEA and anti-digoxin sensors tested under the same CEA concentration were statistically significant by independent t-test (*, **, *** and **** denote significance with p-value <0.03, 0.002, 0.0002 and 0.0001, respectively).

4.3.4   Sensor performance in normal human serum

4.3.4.1   Evaluation of sensor performance in normal human serum

After demonstrating proof of concept in an optimised buffered system, the immunosensors were tested in the presence of normal human serum. The presence of CEA in serum is routinely used to monitor the recurrence of CRC after tumor removal. The serum used as diluent in this work was commercially purchased from Thermo Fisher Scientific. To determine the optimum concentration of serum diluent that did not cause substantial non-specific binding, fully fabricated polyclonal based immunosensors were incubated in undiluted, 10 % (v/v) and 1% (v/v) diluted sera in 10 mM PBS, pH 7.4 for 20 min in the absence of target analyte. The change in impedance was calculated by subtracting the impedance measured in PBS from impedance recorded in diluted serum and normalised to percentage change. Normalised data from the impedance spectra demonstrated that the undiluted sera produced the highest non-specific signal on both polyclonal anti-CEA (10%) and control sensors (23%) (**Figure 4.17**). On the contrary, the signals were minimal (~2%) in control sensor when tested in 1% and 10% sera but slightly higher in the anti-CEA sensor at both dilutions (~10%). Based on this finding, the following immunosensors were evaluated for CEA detection by spiking in either 1% or 10 % serum diluents.
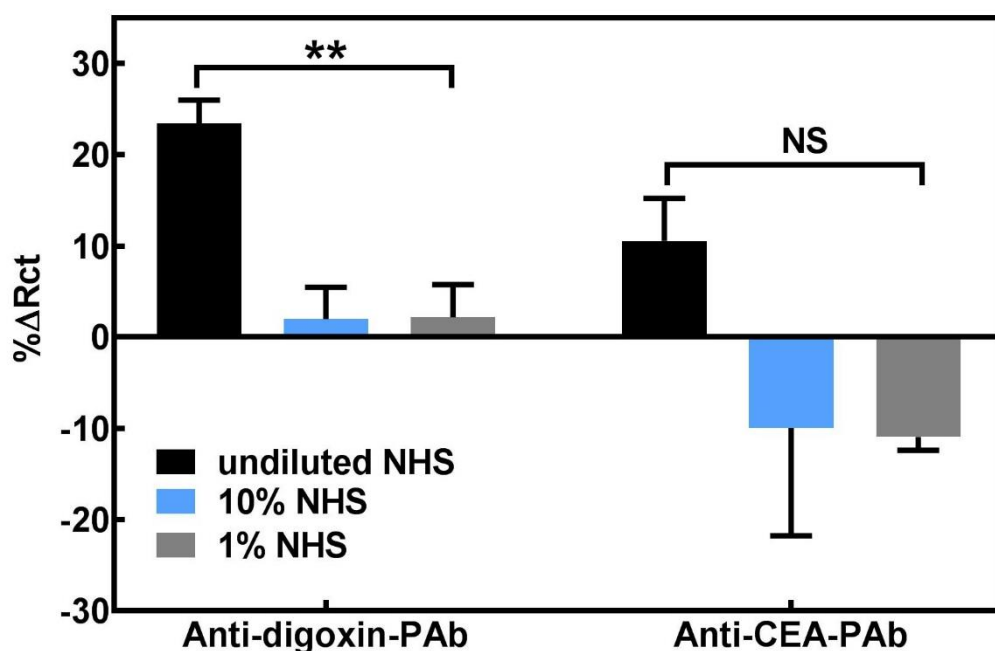
Figure 4.17: Evaluation of fully constructed polyclonal based immunosensors in a range of normal human serum diluent only

Each set of immunosensors were tested against undiluted, 10 % (v/v) and 1% (v/v) normal human serum (NHS) diluted in 10 mM PBS, pH 7.4 in absence of target analyte. In all cases, polyclonal anti-CEA IgG was used as positive sensor whilst polyclonal anti-digoxin IgG served as negative control. The change in impedance was calculated by subtracting the impedance measured in PBS from impedance recorded in diluted serum and normalised to percentage change. Data are mean ± SEM (n=4). The mean differences between 1% and 10 % diluted serum compared to undiluted NHS in anti-digoxin sensor were statistically significant by independent t-test (p-value < 0.002) and not significant in anti-CEA sensor.

4.3.4.2   Testing of optimised immunosensors using CEA spiked into 1% (v/v) and 10 % (v/v) human serum

The preliminary screening of normal human serum on fully constructed immunosensors demonstrated that 10% (v/v) and 1% (v/v) diluted sera in 10 mM PBS, pH 7.4 yielded minimal non-specific binding signal in the absence of target analyte. To evaluate the performance of immunosensors in the biological media, EIS measurements were repeated under previous parameters using the same set of CEA concentrations (1fM - 100 nM) tested in the buffered solution, but this time they were spiked with serum at 10% or 1% (v/v). Both dilutions of serum were tested on polyclonal anti-CEA immunosensors alongside the control sensor, a polyclonal anti-digoxin immunosensor. Meanwhile, the monoclonal anti-CEA immnunosensor was interrogated using CEA spiked with 1% serum. The corresponding R_{CT} data are shown in **Figure 4.18**.

It can be clearly seen that a significant change in R_{CT} was observed in the 1% (v/v) serum samples from the polyclonal anti-CEA immunosensor compared to the control sensor with the same magnitude as those previously seen in the buffered solution (**Figure 4.18 A**) but this time the trend was for relative increase in R_{CT} (**Figure 4.18 B**). The lowest level of detection remained at 1 fM though a linear calibration as in the buffered solution was difficult to retain. In contrast, the change in R_{CT} was generally reduced by half when interrogated in 10 % (v/v) serum and the same trend was seen with the monoclonal based anti-CEA sensor when tested in 1% (v/v) serum. Non-specific binding was not observed from the control sensor which confirmed the specificity of the anti-CEA immunosensor.
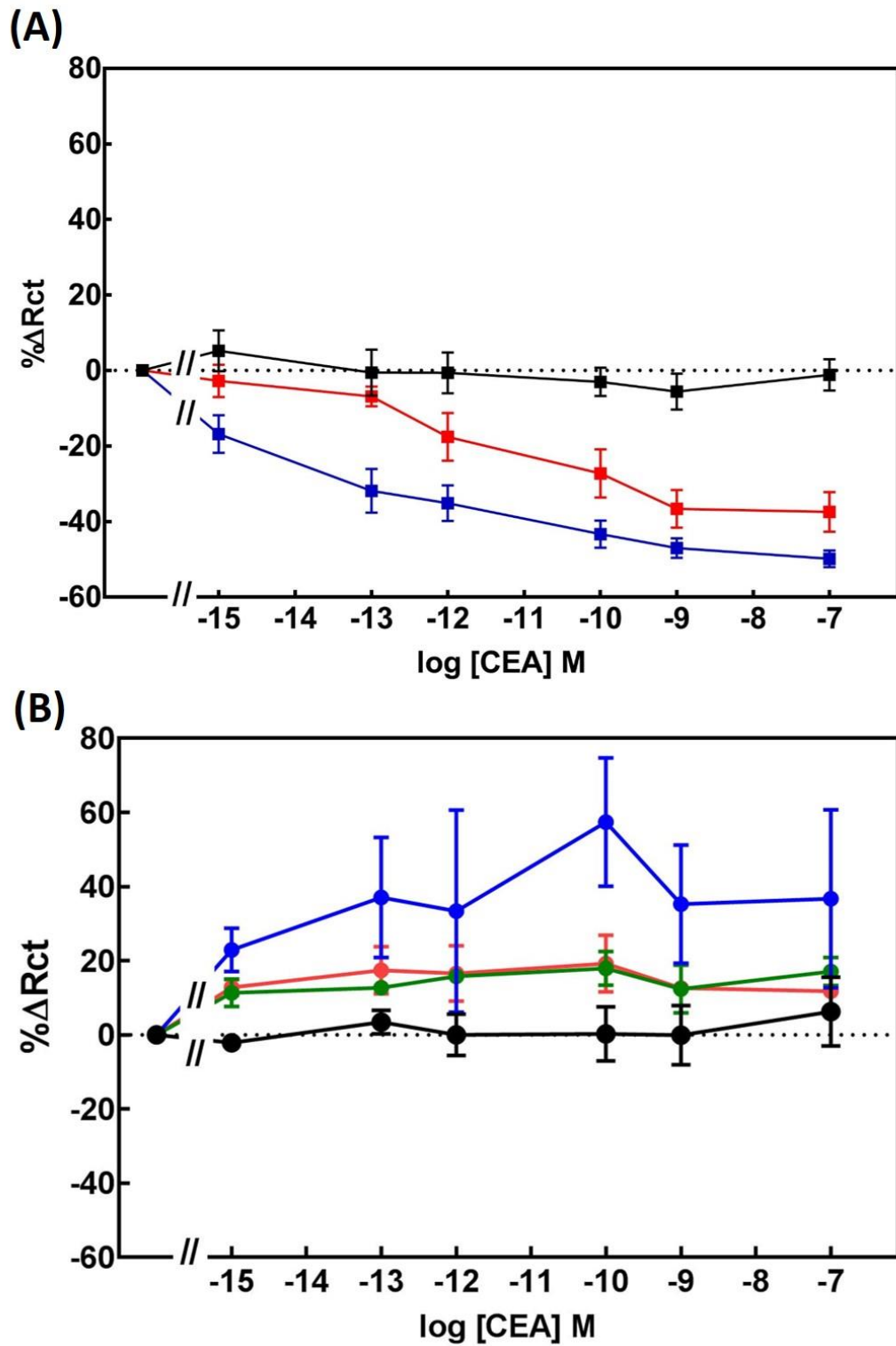
Figure 4.18: Comparison of sensor performance in buffer and diluted sera

(A) Impedance measurement of monoclonal (■) and polyclonal (■) anti-CEA antibodies in optimised buffer system compared to control sensor, polyclonal anti-digoxin antibody (─■─); (B) Sensors performance were tested in diluted sera; CEA spiked in 1% (v/v) (●) and 10% (v/v) (●) diluted sera on polyclonal anti-CEA antibody based sensors, CEA spiked in 1% (v/v) (●) diluted sera on monoclonal anti-CEA antibody based sensor and control sensor (●). (n= 4± SEM)

4.4   Comparison of commercial CEA ELISA assay kit with CEA immunosensors

To validate the performance of CEA impedimetric immunosensors, a commercial human CEA ELISA assay kit purchased from Cusabio Technology LLC (Houston, USA) and evaluated in parallel. Calibration curves of monoclonal-based and polyclonal-based anti-CEA immunosensors tested in buffer (**Figure 4.18 A**) were replotted again with calibration curve generated by ELISA as shown in **Figure 4.19**. Interestingly, the sensitivity and range of detection of both CEA immunosensors were superior to the commercial kit. The sensitivity of CEA detection produced from the kit was 2 ng/ml (i.e. ~10 pM) with a standard curve range from 5 ng/ml – 120 ng/ml that is equal to 25-600 pM. In contrast, current work showed a highly sensitive and specific polyclonal-based CEA immunosensor with a limit of detection at 1 fM and wider detection range from 1 fM-100 nM. Similarly, the monoclonal based CEA immunosensor showed better sensitivity than the commercial kit although it was slightly less sensitive than the polyclonal sensor. The lowest detection limit that the sensor able to detect was reduced to 100 fM with dynamic range from 100 fM-1 nM.
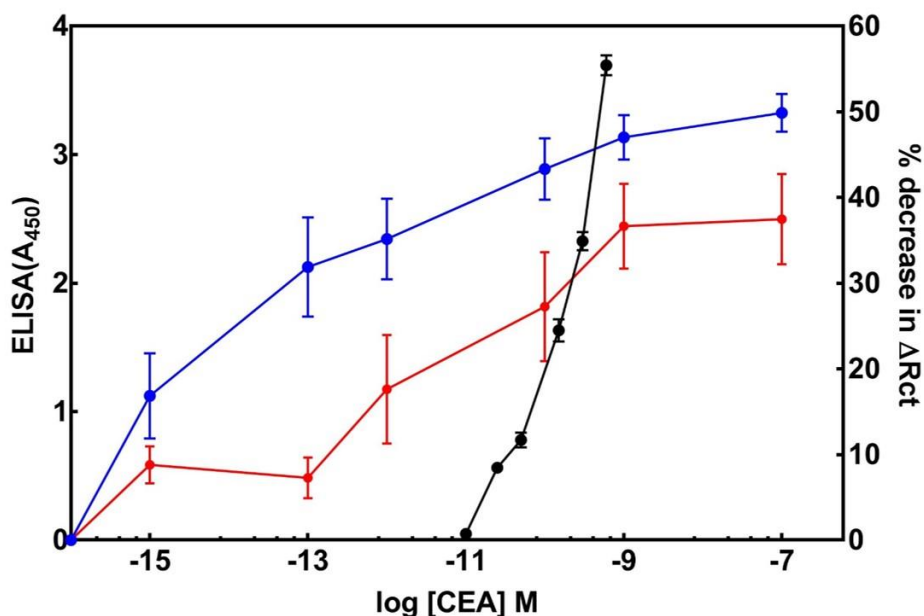
Figure 4.19: Comparison of ELISA kit and CEA immunosensors detection range

The graph plots showing differences of calibration curves generated by ELISA (⬝), compared to polyclonal (⬝) and monoclonal (⬝) anti-CEA based immunosensors. Data points are mean±SEM for n=4. The ELISA output was measured at A_{450} while the immunosensors showing percentage change in R_{CT}.

4.5 Discussion

The electrochemical characterisation of POct film using cyclic voltammetry and electrochemical impedance spectroscopy together with the on-sensor Midland blotting analysis showed that POct formed a novel non-conducting polymer film similar to its precursor tyramine. Finding in this study indicated that electropolymerisation of octopamine monomer in 100 mM phosphate buffer pH 7.5 for 2 cycles generated a thin layer of polymer film and this passivated the screen printed gold electrode surface but provided abundant of surface amines suitable for anchoring bioreceptors such as IgG. Interestingly, the polymer features of POct film developed from a low concentration of octopamine monomer (5 mM) was similar to previous study in which a polytyramine film was prepared at higher concentrations (25 mM) dissolved in 0.3 M NaOH basic medium (Ahmed, 2015). The formation of polymer was controllable as the polymer growth was limited after the second cycle of deposition. The polymer was shown to be stable even after several consecutive impedance scans and showed excellent electron transfer resistance on EIS. Taking into account all of these data, POct could be used as alternative non-conducting base polymer layer for functionalisation via amine-coupling.

To determine the functionality of the POct film in tethering the IgGs, impedimetric immunosensors for CEA detection were fabricated using this polymer as a base layer. Dot blotting was initially performed to confirm the specific binding interaction between CEA and anti-CEA antibodies and selection of appropriate negative control receptor, anti-digoxin antibody. Several immobilisation techniques for the antibodies were then evaluated including random orientation and site-directed immobilisation. Random orientation via antibody entrapment into an electropolymerised POct film most likely hindered the majority of the antigen binding sites as the orientation of the antibody was uncontrollable. However, incorporation of MS (PEG)$_4$ in the polymer conjugate provided the best option for the fabrication of a biosensor with a neutral charge surface that could eliminate the non-specific fouling. The POct-MS (PEG)$_4$ based immunosensor might produce a better specific binding signal if oriented immobilisation of antibody could be achieved. Meanwhile, immobilisation of oxidised antibody pre-conjugated to octopamine monomer and subsequently electropolymerised together, generated a mixed orientation where some antigen binding sites might protrude on the sensor surface. This would favour antigen binding. The major limitation of this immunosensor fabrication

strategy was it was prone to non-specific binding due to abundance of unoccupied amines which might require extra blocking steps prior to analyte interrogation.

Site-directed immobilisation of oxidised antibody post-functionalised onto POct film showed the best immunosensor performance. The fabrication of this sensor was simple and stable and surprisingly, post-functionalisation of the antibodies generated an anti-fouling effect. Hence, no blocking step was required as non-specific binding was not detected during CEA interrogation in the buffered solution as well in buffer spiked with normal human serum. A possible explanation for this phenomenon is that the antibody bound to most of the available surface amine and that unoccupied amines were sterically blocked by the immobilised IgG. It should also be noted that the immobilization of the antibody was performed near the neutral pH without additional chemical reactions that might alter the binding of the antibody. Pertaining to analyte interrogation in the buffered solution, close proximity of the immune complex antibody-antigen interaction to the transducer surface markedly enhanced the sensitivity of CEA detection with a limit of detection of 1 fM and broad dynamic range detection (1 fM - 100 nM) from the polyclonal antibody based sensor. In contrast, the monoclonal antibody based sensor showed 100-fold less sensitivity than the polyclonal antibody based sensor and shorter dynamic range (100 fM - 1 nM). This coincided with the biochemical features of the monoclonal antibody that recognised a single epitope leading to a narrow detection range. Saturated signal observed at the highest analyte concentration most probably was due to the limited availability of free antibodies for binding.

Previous studies on impedimetric immunosensors developed using polytyramine as a transducer base layer on screen printed gold electrode reported that increased in resistance was proportional to increase in analyte binding (Hirst, 2014, Ahmed, 2015). However, the opposite trend was observed in the current study whereby decrease in resistance was recorded with increasing concentrations of CEA. This is most likely due to the antibody being closely packed on the sensor surface and directly bound to the polymer interface without any linker compared to the aforementioned sensors that immobilised the biotinylated antibody through an avidin-biotin interaction. Here, the antibody would extending out from the electrode surface. Thus upon analyte binding, it was postulated that the polymer became distorted which led to pinholes and allowed for rapid charge transfer to the electrode interface (**Figure 4.20 A**). In contrast, this pinhole effect was not observed in the previous reported work probably due to the flexibility of

avidin-biotin crosslinker used to conjugate the biotinylated antibody onto the fabricated sensors. The polymer was not disrupted during analyte binding, therefore increasing the kinetic barrier and slowing down the charge transfer across the electrode surface leading to an increase in resistance. This notion is in agreement with (Goode et al., 2016) findings in which different length of spacer arms used to immobilise the nanobody onto polytyramine transducer base layer influenced the signal generated upon analyte binding.

As a proof of concept, the optimised CEA immunosensors were evaluated in diluted normal human serum. Overall, the promising results in buffer showed reproducible results from the polyclonal CEA immunosensor when analyte interrogation performed in 1% (v/v) serum but did not translate well in the monoclonal based sensor. The sensor performance was also reduced when a higher concentration of serum was used. This was expected as the presence of a high level of serum proteins might block the binding sites and thus limit the signals generation. Interestingly, in all of the experiments, when analyte interrogations were conducted in diluted serum, an increase in resistance was observed. This further supports the earlier theory observed in the buffered system. However this time, the presence of serum components occupied the empty spaces in between the immobilised antibody. Therefore, upon analyte binding stretching of the polymer was restricted the normal kinetic barrier that led to increase in resistance was retained (**Figure 4.20 B**). The CEA immunosensors were prove to be highly sensitive and specific and superior to the traditional ELISA detection. Additionally, the fabrication of CEA immunosensors in this study was simple with LOD and dynamic range of detection were comparable or, to some extent, better than the published works as summarised in **Table 4.1**.

Taken together, findings in this Chapter has demonstrated for the first time the potential of a polyoctopamine film to be utilize as an alternative transducer base layer for amine-functionalisation in electrochemical biosensor applications. Additionally label-free CEA immunosensors with highly sensitive and specific detection, rapid response time (5 min) and the usage of small sample volumes (10 µl) have successfully been developed in this study. Based on the success of these sensors construct, another impedimetric biosensor using a novel non-immunoglobulin bioreceptor, CEA-Affimer prepared in **Chapter 3**, was investigated which will be discussed in the following **Chapter 5**.
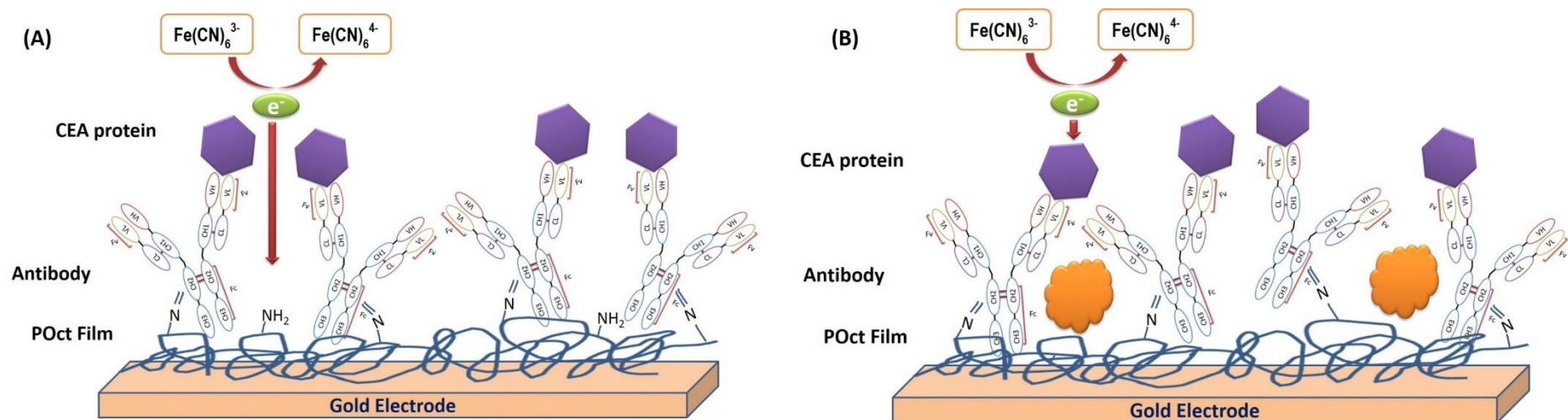
Figure 4.20: Hypothesis of kinetic barrier mechanism upon analyte binding on CEA immunosensor

Schematic diagrams showing (A) Distortion of polymer upon analyte binding leads to rapid charge transfer to the transducer surface that reduces the resistance, R_{CT}; (B) Presence of serum components in the analyte diluent restricts the polymer shift during analyte binding, thus increases the resistance on the transducer surface.

Table 4.1: Comparison of CEA immunosensors developed in this study with published works

Detection	Biosensor	Transducer	Immobilization technique	Bioreceptor	LOD	Reference (s)
Random orientation						
Label-free	Impedimetric	Gold	Electro-copolymerization of o-aminophenol with CEA-Ab-glutathione monolayer modified AuNP	Antibody	0.2 ng/ml (500 fM)	(Tang et al., 2007)
	Impedimetric	Glassy carbon electrode (GCE)	Physisorption of anti-CEA antibody onto GCE modified with AuNP/ polymeric self-assembled nanoparticles (poly (γ-glutamic acid)-dopamine-chitosan	Antibody	10 fg/ml (50 aM)	(Xu et al., 2017)
	Impedimetric	Glassy carbon electrode (GCE)	Covalent immobilisation of amine-modified CEA aptamer on GA-AuNP/AMCM-GCE	DNA Aptamer	0.98 pg/ml (4.9 fM)	(Shekari et al., 2017)
	Impedimetric	Conducting Whatman paper	Covalent immobilization of anti-CEA antibody onto amine-functionalised surface coated with conducting poly (3,4ethylenedioxythiophene):poly(4-styrene sulfonate) on paper electrode	Antibody	2.68 ng/ml (13.4 pM)	(Kumar et al., 2016)
	Impedimetric	Graphite-based screen-printed electrode	Covalent immobilization of anti-CEA antibody onto poly-(pyrrole-3-carboxylic acid)-modified electrode	Antibody	33.33 pg/ml (166.65 fM)	(Iordănescu et al., 2018)
Labelled	Impedimetric	Indium tin oxide (ITO) electrode on a glass slide	Covalent immobilization of anti-CEA antibody onto aldehyde-functionalised ITO electrode and sandwich with magnetic beads coated with secondary antibody for signal enhancement	Antibody	1 ng/ml (5 pM)	(Yeh et al., 2016)
	Impedimetric	Glassy carbon electrode (GCE)	Covalent immobilization of anti-CEA antibody onto AuNP-modified GCE and sandwich with HRP conjugated to secondary antibody functionalised with graphene oxide nanosheets and coupled with enzymatic biocatalytic precipitation of 4-chloro-1-naphthol	Antibody	0.64 pg/ml (3.2 fM)	(Hou et al., 2013)
Site-directed orientation						
Label-free	Impedimetric	Screen printed gold electrode (SPGE)	Covalent immobilization of anti-CEA antibodies onto electropolymerised polyoctopamine coated SPGE	Monoclonal antibody Polyclonal antibody	20 pg/ml (100 fM) 0.3 pg/ml (1 fM)	**Current work***

Chapter Five

Fabrication and optimization of CEA-Affimer based biosensors

Chapter 5 : Fabrication and optimization of CEA-Affimer based biosensors

5.1 Introduction

Development of CEA immunosensors using polyoctopamine (POct) as a transducer base layer to immobilize the antibodies have shown promising results. As described in **Chapter 1**, antibodies have inherent several limitations that restrict their application in the point-of-care device applications, particularly due to stability, storage and production issues. To address these problems, the potential of a non-immunoglobulin based electrochemical biosensor using an anti-CEA Affimer as a novel biorecognition element was investigated. Data in **Chapter 3** have shown the specificity of anti-CEA Affimers in recognizing the CEA on cells and in complex matrices and their potential to be used as biorecognition elements in fluorescence imaging, affinity precipitation, and as a ligand in SPR analysis.

Work in this chapter began with optimizing the immobilization of CEA-Affimer using the same transducer base layer, the POct film, onto the DropSens commercial screen printed gold electrode identical to the one used in previous **Chapter 4**. Since the Affimer contain a single cysteine residue at the C-terminus site-directed orientation was performed by conjugating the Affimer to octopamine via a sulfo-SMCC cross-linker and then electrodeposition onto the gold electrode as shown in the schematic in **Figure 5.1**. Biosensors using all three CEA-Affimer clones were fabricated individually to determine the best monovalent Affimer-based sensor. Throughout this chapter, anti-calprotectin Affimers were included as a negative control. These Affimers were kindly provided by Dr. Jack Goode, (School of Biomedical Sciences, University of Leeds) who used them to detect calprotectin, a biomarker for inflammatory bowel disease. The inclusion of anti-calprotectin Affimer will pave the way for the development of future dual biosensors, to distinguish between inflammatory bowel disease and colorectal cancer. However development of dual biosensors was beyond the scope of this study. Apart from this, non-specific binding was experienced at the beginning of the study and several blocking conditions were evaluated to troubleshoot the issue.

Multi-receptor based Affimer sensors were also constructed and investigated to simulate the polyclonal antibody based system. The proportion of Affimers mixture were

prepared according to the mathematical binding model generated using their equilibrium dissociation constants (K_D) obtained from the kinetic binding analysis as described in **Section 3.3.5**. To enhance the understanding of kinetic barriers on the fully constructed sensor upon analyte binding, the effect of bioreceptor distance from the transducer surface in generating the impedance signal was evaluated. After showing proof of concept in the clean buffered system, the monovalent anti-CEA Affimer-II sensor was identified as the best sensor as compared to the rest in terms of sensitivity and detection range. This sensor was subsequently tested for the reproducibility of CEA detection in the presence of diluted normal human serum.
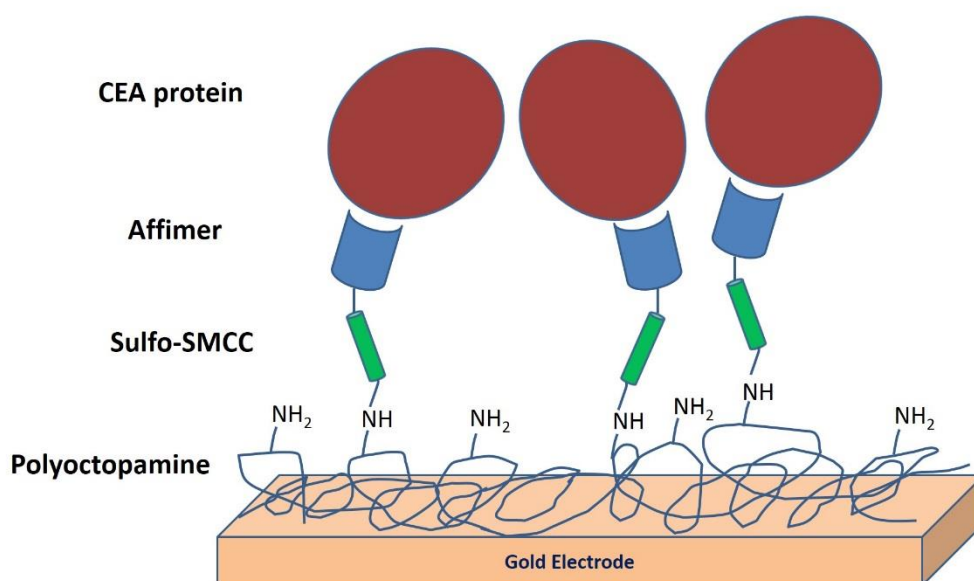
Figure 5.1: Schematic of Affimer-based impedimetric biosensor construction

Schematic showing site-directed immobilisation of Affimer conjugated to polyoctopamine (POct) via sulfo-SMCC linker on DS screen printed gold electrode. The drawing is not to scale.

5.2 Optimization

5.2.1 Effect of polymerisation technique

As indicated in **Chapter 4**, POct polymer layer provides abundant surface amines which are suitable for anchoring the bioreceptors. During the subcloning of anti-CEA Affimers from the phagemid vector into the *pET11a* expression vector, a single cysteine residue was incorporated at the C-terminus (**Section 3.2.1**). Hence, site-directed immobilisation was feasible by conjugating the Affimer to octopamine using sulfo-SMCC linker as described in **Section 2.2.7.3**. Unlike the CEA immunosensor where the oxidised antibodies were immobilised onto POct coated electrode surface, the Affimer was prepared in a step-wise format prior to immobilisation onto the electrode. Initially, the octopamine monomer was conjugated via its amine to sulfo-SMCC in an equal ratio, followed by coupling to freshly reduced Affimer via its -SH and subsequently the octopamine-Affimer complex was electrodeposited onto the electrodes using the same parameters as previously (**Section 4.2.1**).

To determine the optimum immobilisation conditions, different electrodeposition methods were evaluated by electropolymerising the Affimer conjugates simultaneously onto different working electrodes and this was compared to when they were electropolymerised separately. CEA-Affimer-II was immobilised on both electrodes to reduce the variable. Electrodes polymerised with POct alone and POct coupled to sulfo-SMCC without Affimer were included as controls to evaluate the differences in electrochemical signal. The cyclic voltammogram in **Figure 5.2 A and B** showed that the anodic peak current (I_{pa}) of electrodes polymerised simultaneously (PT) were twice that of the one electropolymerised separately (PS) (8.63 µA vs 4.64 µA, respectively). However, the anodic peak potential (E_{pa}) appeared at the same potential (0.63 V) and was located in between the E_{pa} of POct alone (0.52 V) and the E_{pa} of POct conjugated to sulfo-SMCC (0.73 V).

An inverse trend was observed when the impedance was subsequently measured. The R_{CT} of working electrodes (WE) polymerised simultaneously were half (WE1-237.2 kΩ and WE2-210.76 kΩ, respectively) that of the separately polymerised sensor (PS-WE1 and PS-WE2). This same trend was also observed during the polymerisation of the POct layer tested at various scan speeds which showed increased in I_{pa} led to decreased in R_{CT} when the scan rate was increased (**section 4.2.2**). It is interesting to note the striking

difference between the R_{CT} of PS-WE1 (137.53 kΩ) and PS-WE2 (307.64 kΩ) when polymerising the anti-CEA Affimer-II separately onto the respective working electrodes.

Midland blotting was subsequently performed to determine the success of Affimer immobilisation and the effect of different polymerisation technique. After electrodeposition of Affimer conjugates and recording of impedance, the corresponding modified electrodes were washed with PBS and incubated with anti-HisTag-HRP antibody for 1 h at RT prior to exposure with ECL reagent and image capture. Results from **Figure 5.2 D** showed that both polymerisation techniques successfully immobilised the Affimers on the working electrode surfaces. There was no ECL signal from the bare gold electrode polymerised with POct layer only and POct-conjugated to sulfo-SMCC conjugate alone which further confirmed the positive signal derived from the electrode consisted of functionalised Affimer. Based on these data, electropolymerisation of Affimer simultaneously on different working electrodes was selected as the optimum immobilisation technique used throughout this study.
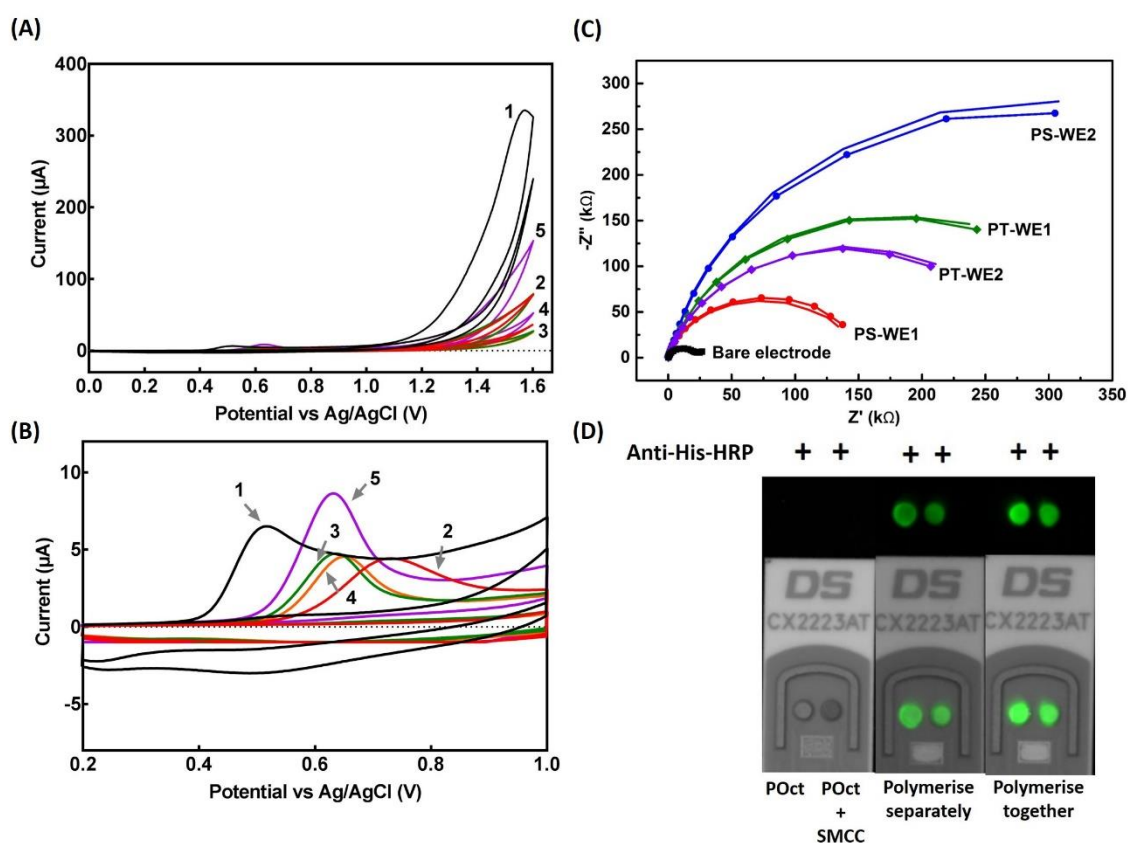
Figure 5.2: Effect of different immobilisation technique

(A) Cyclic voltammogram showing electropolymerisation of POct (1, ▬), POct conjugated to sulfo-SMCC linker only (2, ▬), and POct conjugated to Affimer via sulfo-SMCC linker and electropolymerised simultaneously (5, ▬) and separately PS-WE1(3, ▬) and PS-WE2 (4, ▬); (B) Magnification of the corresponding CV curves in Figure A; (C) Impedance data of electrodeposition of Affimer conjugates simultaneously (PT-WE1 and PT-WE2) and separately (PS-WE1 and PS-WE2) compared to the bare gold electrode. WE1 and WE2 denote working electrodes 1 and 2 that immobilised using the same CEA-Affimer-II; (D) Midland blotting probed with anti-HisTag-HRP confirming the immobilisation of CEA-Affimer on sensor surfaces after electrodeposition with octopamine conjugates both separately and simultaneously.

151

5.2.2 Optimisation of CEA-Affimer concentration on sensor surface

In developing a successful biosensor platform, the optimum amount of immobilised bioreceptor is equally important apart from the immobilisation technique in generating an effective signal on target analyte binding. Preliminary optimisation of Affimer loading onto the sensor surface was investigated at three different concentrations. The starting concentration of Affimer loading was selected at 7.92 μM which is similar to the optimum amount of immobilised antibodies. In parallel, the effect of sensor performance in detecting the binding of increasing concentrations of CEA when the Affimer density was twice (15.84 μM) or half (3.96 μM) this loading were also evaluated. Anti-CEA Affimer-II and anti-calprotectin Affimer were used in this optimisation as positive and control sensors.

In general, prominent non-specific binding was observed across all sensors constructed in both anti-CEA Affimer and control sensors when co-plotted against a series of CEA concentrations ranging from 1 fM to 1 μM (**Figure 5.3**). At the highest concentration of CEA interrogation in the control sensor, a 36% shift in R_{CT} was observed from sensor immobilised with 7.92 μM of anti-calprotectin Affimer (**Figure 5.3 B**) which was the least non-specific binding signal generated compared to those with 3.96 μM and 15.84 μM Affimer immobilised that showed an increase in R_{CT} change to 49% (**Figure 5.3 A and C**, respectively).

The same decreasing pattern was consistent in the anti-CEA Affimer-based sensors but the reduction in R_{CT} was double in magnitude in all set of sensors construct. Sensor immobilised with the least amount of anti-CEA Affimer (3.96 μM) showed the highest percentage change in R_{CT} (80%) compared to those with 7.92 μM immobilised (68%) and 15.84 μM (74%). Taken all data in this section together, immobilisation of both specific and non-specific Affimer at 7.92 μM showed minimum non-specific binding signal compared to the rest. Thus, this concentration was selected as the optimum concentration of Affimer to immobilise on sensor surfaces and was taken forward for further optimisation. It was also obvious that current sensors constructs were prone to

non-specific binding. Hence, eliminating this factor to obtain a specific CEA detection was crucial and is addressed in the following **section 5.2.3**.
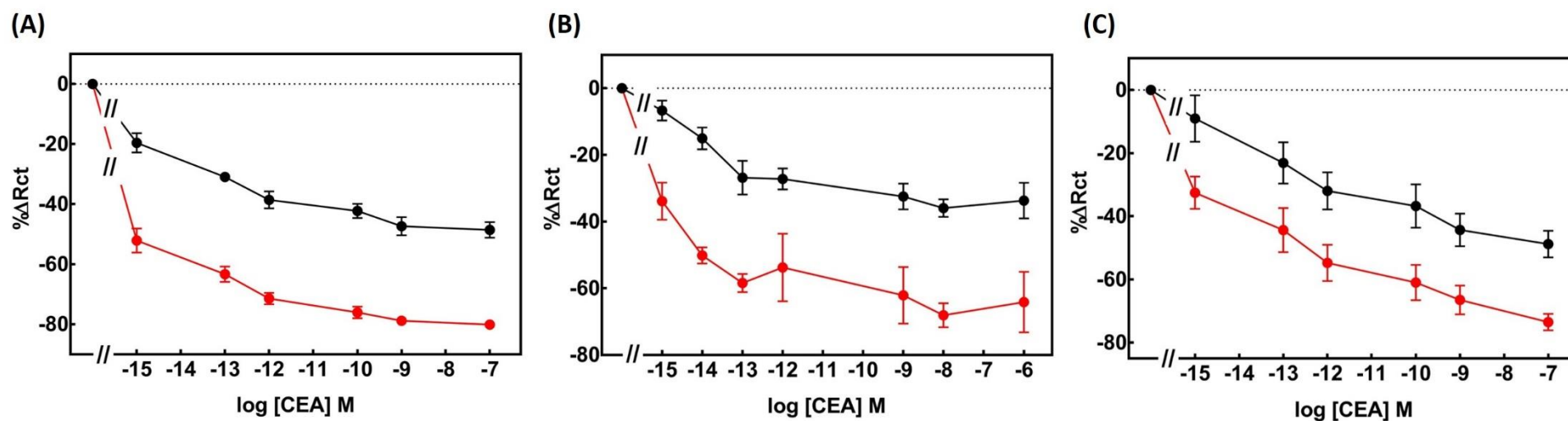
Figure 5.3: Optimisation of anti-CEA Affimer-II concentration on sensor surface

The normalised impedance data showing percentage change in R_{CT} when different concentration of anti-CEA Affimer-II ( ) immobilised on sensor surface; (A) 3.96 µM; (B) 7.92 µM and (C) 15.84 µM alongside with the control sensor, anti-calprotectin-Affimer ( ). All biosensors construct showing non-specific binding on both positive and control sensors. CEA binding was interrogated in cumulative fashion from 1 fM to 1 µM (n = 5± SEM).

5.2.3 Effect of different blocking conditions

As reported in **Chapter 4**, POct provides abundant surface amines. Therefore, the transducer base layer was prone to non-specific binding notably from common electrostatic interaction since at neutral pH the amines would be present as $-NH_3^+$. The isoelectric point (pI) of CEA protein is 4.7. Thus, CEA normally exists as an anion in the buffered solution at pH 7.4 which also potentially contributes to the common electrostatic interaction as seen in earlier sections. Based on this possibility, several blocking strategies were evaluated.

Initially, fully fabricated Affimer-based sensors were blocked with the most common blocking solution used in immunoassays, i.e., 1% (w/v) bovine serum albumin (BSA) solution. Calibration curves were generated by plotting the change in impedance against increasing concentration of CEA from 1 fM to 1 nM. It can be clearly seen from **Figure 5.4 A** that the blocking suppressed the binding signal generated from the specific interaction on the anti-CEA Affimer sensor whilst a low level of non-specific binding signal was observed from the control sensor (~15% of R_{CT} change at the highest CEA concentration). A possible explanation for this scenario would be steric hindrance caused by the BSA blocking as Affimers are small (12.5 KDa) compared to serum albumin (~66.5 KDa). In addition, the Affimers were in very close proximity to the transducer base layer. Hence, the BSA blocking might have limited the binding interaction between Affimer and CEA.

Since the first blocking attempt was unsuccessful, a second optimisation attempt was made out by creating a negatively charged sensor surface. This blocking technique might resolved the non-specific binding derived from electrostatic interactions. To test this hypothesis, pyromellitic dianhydride (PMDA) was selected because it contains a double carboxylic acid anhydride. Typically, the reaction between one anhydride and an amino yields a peptide bond and a free carboxyl group. Meanwhile, the second anhydride group becomes hydrolysed, leading to two further free carboxy groups. Overall, this results in conversion of one $-NH_3^+$ to three $-COO^-$ groups. Several concentrations of PMDA were evaluated including 1 mM, 5 mM and 10 mM. Blocking with 1 mM PMDA exacerbated the non-specific binding effect on control and positive sensors whereby a 50% increase in R_{CT} was observed (**Figure 5.4 B**). In contrast, when the concentration of PMDA was increased to 5 mM, non-specific binding was significantly reduced to the baseline level in the control sensor whilst a 15% change in R_{CT} which indicated the

specific interaction was observed on the anti-CEA Affimer-based sensor (**Figure 5.4 C**). However, the magnitude of change in R_{CT} remained the same even when increasing concentrations of CEA were applied. Interestingly, non-specific signal began to increase in the control sensor from 10 pM of CEA incubation and beyond. The best blocking effect was observed when sensors were blocked with 10 mM PMDA (**Figure 5.4 D**). The non-specific signal was significantly reduced to the baseline level and remained stable across all CEA concentrations whilst a linear calibration was observed covering three concentrations of CEA detection from 1 fM up to 100 fM before the change in R_{CT} started to level off.
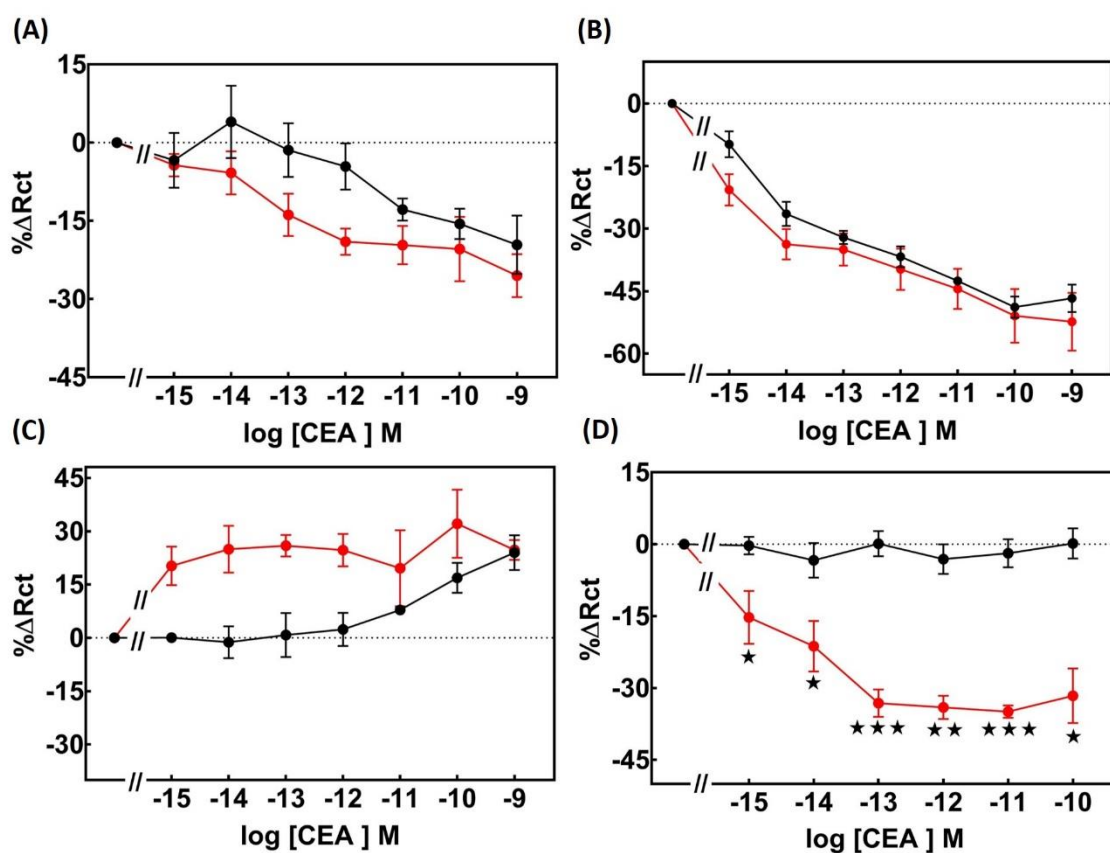
Figure 5.4 : Effect of different blocking conditions

Fully fabricated anti-CEA Affimer sensor (●—) and anti-calprotectin-Affimer (●) as control sensor were blocked with (A) 1% (w/v) BSA and PMDA blocking at (B) 1 mM; (C) 5 mM and (D) 10 mM concentrations to block non-specific binding on sensor surface during CEA interrogation. Mean differences between anti-CEA Affimer and anti-calprotectin Affimer sensors tested under the same CEA concentration were statistically significant by independent t-test (*, ** and *** denote significance with p-value <0.03, 0.002 and 0.0002, respectively) (n= 5± SEM).

5.2.4 Effect of CEA binding before and after 10 mM PMDA blocking

To determine the difference of CEA binding on fully constructed Affimer sensor without blocking and after blocking with 10 mM PMDA, a parallel comparison was performed. Data from **Figure 5.3 B and 5.4 D** were selected and replotted again in **Figure 5.5 and 5.6** to compare the Nyquist plots and calibration curves of CEA binding between a non-blocked sensor surface and after blocking with 10 mM PMDA. It can be clearly seen that the non-specific binding observed from the non-blocking sensor surface was most likely due to electrostatic interaction. Blocking the sensor surface with 10 mM PMDA prior to CEA interrogation that should produce a negatively charge sensor surface strongly support this hypothesis. A significant decreased with 4-fold change in impedance were observed in anti-CEA Affimer (**Figure 5.5 C**) and control sensors (**Figure 5.5 D**) after blocking with 10 mM PMDA upon analyte binding compared to the corresponding non-blocked sensor surface (**Figure 5.5 A and B**). The normalised impedance data (**Figure 5.6**) showed that the blocking successfully eliminated the non-specific interaction while retaining the specific binding on the anti-CEA Affimer-based sensor. The 34% R_{CT} change (**Figure 5.6 A**) consisted of a mixture of specific and non-specific signal observed at the initial concentration of CEA incubation from the non-blocking of CEA-Affimer sensor was significantly reduced to 15% after it was blocked (**Figure 5.6 B**). In addition, the non-specific signal (~15-35%) from the control sensor also decreased to the baseline level across the series of CEA concentrations.

Midland blotting was conducted again but this time to confirm the success of 10 mM PMDA blocking in eliminating the non-specific binding problem. After the impedance measurements were taken at 1 pM CEA, the non-blocked electrode and electrode blocked with 10 mM PMDA were washed with PBS, incubated for 1 h at RT with monoclonal anti-CEA antibody and followed by secondary antibody conjugated to HRP. After exposure to ECL reagent and the image was recorded. Results from **Figure 5.6 C** further supported the impedance data and confirm that the specific interaction seen on blocked sensor surface did represent true CEA binding as pseudo-green colour illumination only appeared on the anti-CEA Affimer sensor (WE2-CEA, right panel) but was absent from the control sensor (WE1-CP, right panel). This indicated that the PMDA modification on the transducer base layer did not affect the antigen binding site on the anti-CEA Affimer. In contrast, a false positive signal was observed from the non-blocked electrode of the control sensor. Taking into consideration of all optimised data, fabrication

of Affimer sensor throughout this study was set constant by immobilising the specific and control Affimers simultaneously on a single chip at 7.92 µM and blocking with 10 mM PMDA prior to CEA interrogation.
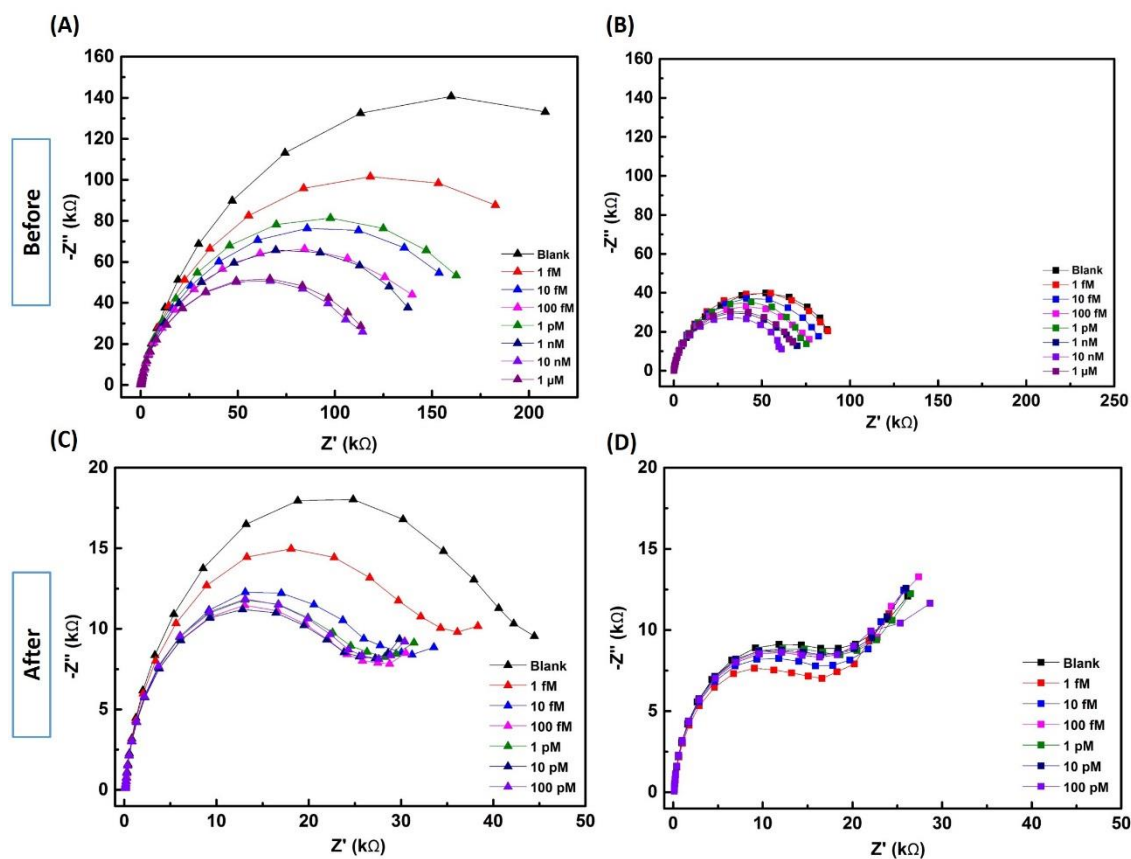
Figure 5.5 : Nyquist plots of before and after 10 mM PMDA blocking

Nyquist plots showing the effect of CEA binding on fully fabricated sensors before (A and B) and after (C and D) 10 mM PMDA blocking technique. The specific and non-specific sensors were constructed using anti-CEA Affimer-II (▲) and anti-calprotectin Affimer (■), respectively. Increasing concentration of CEA (from 1 fM to 1µM) were successively incubated onto respective sensors.
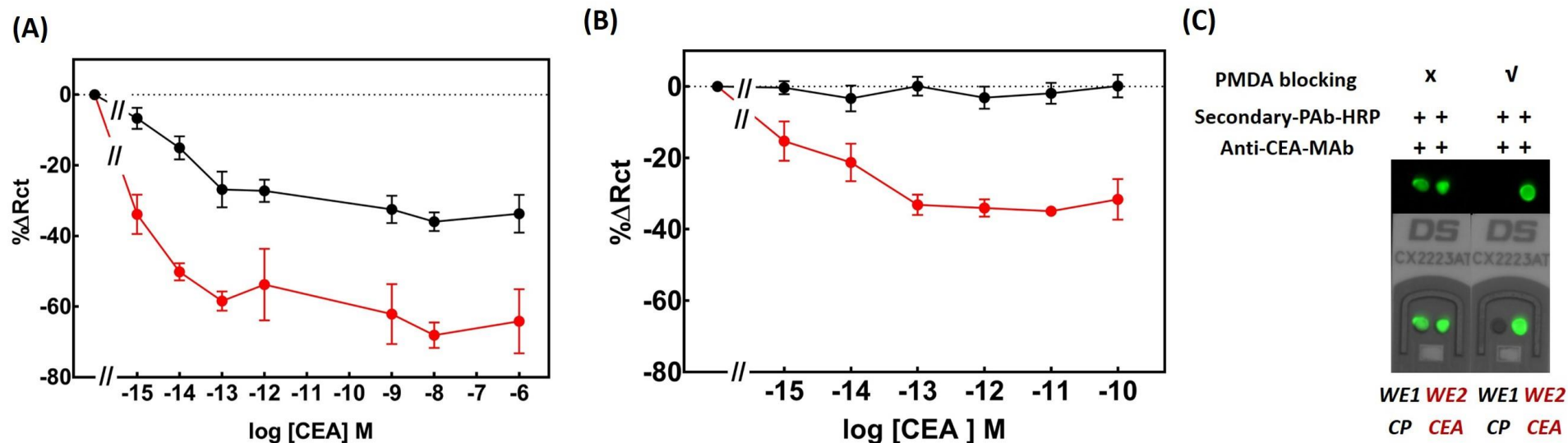
Figure 5.6: Effect of CEA binding before and after 10 mM PMDA blocking

Comparison of CEA binding on fully constructed sensor (A) without blocking and (B) after blocking with 10 mM PMDA solution. The specific and non-specific sensors were constructed using CEA-Affimer (●–) and Calprotectin-Affimer (●–), respectively. (C) Midland blotting after 1pM of CEA interrogation showing sensors blocked with 10 mM PMDA (right panel) successfully eliminate the non-specific signal from the control sensor (WE1-CP). The pseudo-green colour illumination on specific sensor (WE2-CEA, right panel) represents true specific CEA binding whilst those observed from the non-blocking sensors on the left represents the non-specific interaction of CEA on sensor surface. The top panels show pseudo-green colour of the captured images, and the bottom panels are superimposed image of the electrodes and pseudo-green colour illumination.

160

5.2.5 Monovalent based CEA-Affimer biosensors

Three unique anti-CEA Affimer clones were identified and characterised in **Chapter 3**. Each of them had a different equilibrium dissociation constant (K_D) value and was expressed to different levels. To compare them with a monoclonal antibody-based system, single anti-CEA Affimer-based sensors were fabricated using the optimised parameters as described in **section 5.2.4**. Each of the anti-CEA Affimer clones was immobilised individually at the optimum concentration (7.92 µM) and then blocked with 10 mM PMDA prior to evaluation of CEA binding in a cumulative fashion, from 1 fM to 1 nM. Anti-calprotectin Affimer-based sensor was included as negative control in each set of experiments. Normalised data comprising mean percentage change in R_{CT} were then plotted against the CEA concentrations.

Although anti-CEA Affimer-I showed had the highest affinity value (6.46 nM) from kinetic binding analysis, its performance in detecting CEA binding on impedimetric biosensors was poor. A linear calibration curve upon CEA binding was impossible to plot due to fluctuation in the change of impedance when increasing concentrations of CEA were tested (**Figure 5.7 A**). Interestingly, the CEA-Affimer-II sensor demonstrated the best sensor performance in detecting CEA binding compared to the other two sensors although it possessed moderate affinity K_D (15.3 nM). A linear calibration curve was observed spanning from 1 fM to 100 fM before the change in R_{CT} started to level off (**Figure 5.7 B**). This sensor showed highly sensitive detection compared to the monoclonal anti-CEA antibody biosensor (**Figure 4.13 C**) with limit of detection at 1 fM.

The last clone, anti-CEA Affimer-III showed better sensor performance than anti-CEA-Affimer-I. The changes in impedance upon increased binding of CEA were statistically significant when compared between specific and control sensor. However, the magnitude of change across the CEA concentrations was minimal between CEA additions. After analysing these data, it was concluded that the second clone, anti-CEA Affimer-II was the best clone for fabricating a monovalent Affimer-based impedimetric biosensor for CEA detection. Thus, the anti-CEA Affimer-I and III clones were discounted as bioreceptors candidate for a monovalent-bioreceptor electrochemical biosensor platform.
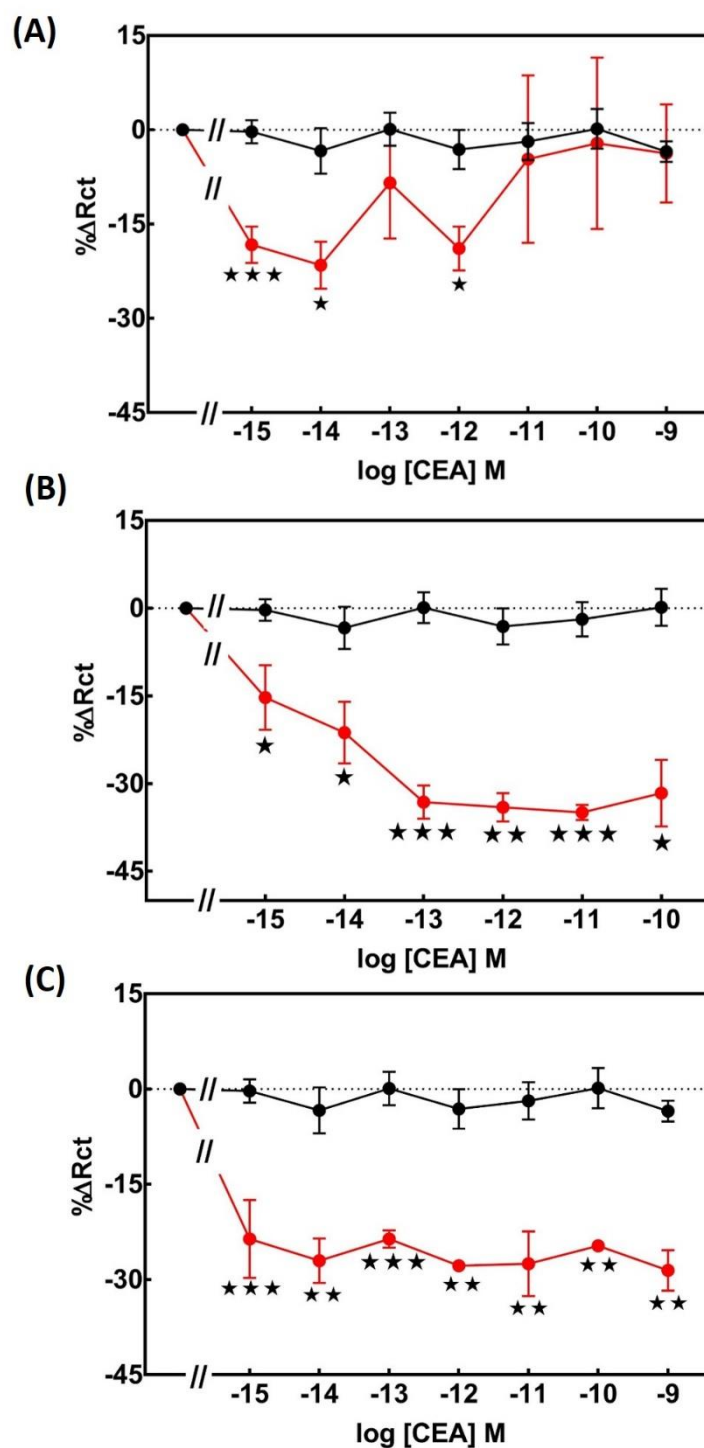
Figure 5.7: Comparison of monovalent-bioreceptor based CEA-Affimers and control biosensors

Calibration of CEA biosensors was carried out with 1 fM to 1 nM CEA. Sensors were fabricated with anti-CEA Affimers, (●) or with control anti-calprotectin Affimer (●). Sensors all used the same anti-calprotectin (control) Affimer and (A), anti-CEA Affimer-I; (B), anti-CEA Affimer-II or (C), anti-CEA Affimer-III. The mean differences between anti-CEA and anti-calprotectin based Affimer sensors were statistically significant at $p < 0.03$, (*); $p < 0.002$ (**) and $p < 0.0002$ (***) respectively. (n= 4± SEM).

5.2.6 Development of multi-receptor based CEA-Affimer biosensors

5.2.6.1 Mathematical binding model for CEA-Affimer biosensors

There is no established protocol on how to fabricate a multi-receptor based biosensor using Affimers as bioreceptors. Therefore, optimisation began with generating simulated data based on the binding isotherm model to assist in the experimental design. The binding equation was built using the established simple ligand binding equation as written below:

$$\text{Bound analtye-Affimer complex} = \frac{B_{max} * [CEA]}{K_D + [CEA]}$$

Equation 5.1: The ligand binding equation for single Affimer based sensor

B_{max} is the maximum analyte bound to ligand, which the ligand in this case was CEA and K_D is the equilibrium dissociation constant from the kinetic binding analysis data (**section 3.3.5.2**). This equation represented the simulated data for a single anti-CEA Affimer based sensor.

Meanwhile, binding curves modelling the two Affimers based sensors were generated based on the **Equation 5.1** with slight modification to it. **Equation 5.2** was formulated as below:

$$\text{Bound analtye-Affimer complex} = 0.5 * \frac{Bmax1 * [CEA]}{K_D1 + [CEA]} + 0.5 * \frac{Bmax2 * [CEA]}{K_D2 + [CEA]} + C$$

Equation 5.2 : The ligand binding equation for two Affimers based sensor

In **Equation 5.2,** the bound analyte-Affimer complex was derived from an equal molar ratio of each anti-CEA Affimer clones. The same formula was applied for the three receptors based model except that the equimolar ratio was derived from the combination of three anti-CEA Affimer clones as shown in **Equation 5.3**:

$$\text{Bound analtye-Affimer complex} = 0.33 * \frac{Bmax1 * [CEA]}{K_D1 + [CEA]} + 0.33 * \frac{Bmax2 * [CEA]}{K_D2 + [CEA]}$$
$$+ 0.33 * \frac{Bmax3 * [CEA]}{K_D3 + [CEA]} + C$$

Equation 5.3: The ligand binding equation for three Affimers based sensor

All simulated binding models were plotted in **Figure 5.8** and were further used for the optimisation of Affimer density on the sensor surface in fabricating the multi-receptor based sensor.
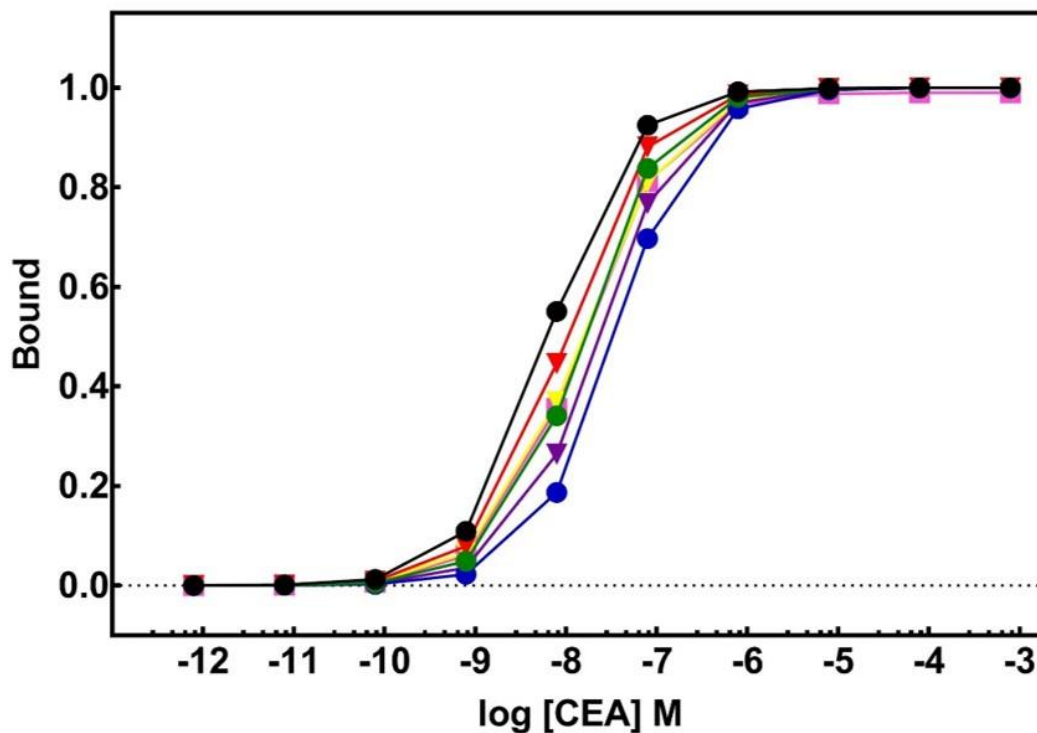
Figure 5.8 : Mathematical binding model of Affimer sensors

The mathematical binding model showing the fraction of analyte bound to Affimer complex as a function of CEA concentration. Binding curves were generated from the simulated data derived from the binding isotherm equation with anti-CEA Affimers as bioreceptors. Three types of sensor were plotted together; the single receptor based (● , ● and ● denote anti-CEA Affimer I, II, III respectively), two receptors based (▼ , anti-CEA Affimer I+II; ▼ , anti-CEA Affimer II+III; ▼ , anti-CEA Affimer I+III) and three receptors based (■).

5.2.6.2 Optimization of Affimer concentration for the fabrication of multi-receptor based biosensors

As mentioned earlier, each clone of anti-CEA Affimer has a different affinity value. From the development of monovalent Affimer based biosensors, results showed that the concentration of Affimer on sensor surface did play a major role in obtaining a meaningful binding signal. Therefore, it is important to determine the optimum combination of anti-CEA Affimers since this is the first time a multi-receptors Affimer based impedimetric biosensor being developed.

The binding isotherm model in **Figure 5.8** showed that the maximum binding of target analyte was observed when the Affimer concentration was at 7.92 µM. This was the optimum concentration of Affimer used during the fabrication of the monovalent based biosensor (**section 5.2.5**). Considering these data, three concentrations of anti-CEA Affimers were evaluated in a 10-fold dilution from 79.2 nM to 7.92 µM. Combination of all anti-CEA-Affimers were used in this optimisation. The CEA-Affimers were prepared by mixing equimolar ratio of each Affimer following the concentration derived from the **Equation 5.3** to a final concentration of 79.2 nM, 792 nM and 7.92 µM. Anti-calprotectin Affimers 4 and 19 were included as a negative control sensor. Each Affimer was prepared individually following the same parameter as in the single Affimer based sensor and was mixed prior to electrodeposition onto the electrode surface. Interrogation with CEA was performed over 1 fM to 1 nM. The impedance was recorded and the percentage change in R_{CT} was plotted against CEA concentrations as shown in **Figure 5.9**.

A significant increase in R_{CT} change was observed when the sensor with the minimum concentration of anti-CEA Affimers immobilised (79.2 nM) (**Figure 5.9 A**). In contrast, the opposite trend was observed when the maximum concentration of anti-CEA Affimers was immobilised, 7.92 µM, with decreased in R_{CT} change was seen (**Figure 5.9 C**). Additionally, sensors with 7.92 µM of anti-CEA Affimers immobilised showed better sensitivity with the lowest limit of detection at 1 fM compared to 1 pM sensitivity in the 79.2 nM of anti-CEA Affimer sensor. No significant difference was observed in the R_{CT} change between specific and control sensor when 792 nM of anti-CEA Affimers was immobilised on the sensor (**Figure 5.9 B**). The control sensors also

showed a stable signal at the baseline level throughout the CEA interrogation which indicated specific interaction was observed on the anti-CEA Affimer sensor. Based on these data, immobilisation of anti-CEA Affimers at 7.92 μM was concluded as the optimum concentration for the fabrication of a multi-receptors based sensor. This concentration was parallel to the Affimer density on single receptor sensor.
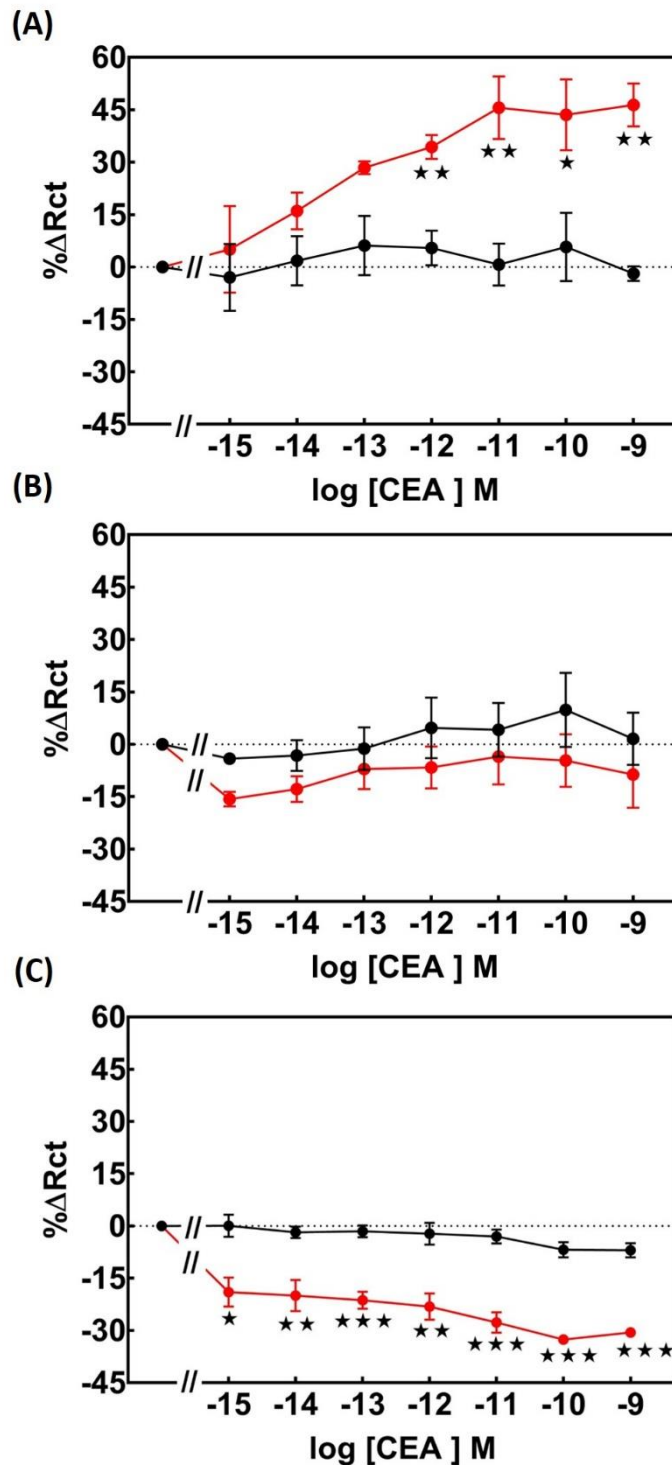
Figure 5.9 : Optimisation of Affimers concentration for the fabrication of multi-receptor based biosensors

Three different concentrations of Affimer were evaluated by mixing equimolar ratio of all three CEA-Affimer clones (—•—) derived from the binding isotherm model; (A) 79.2 nM; (B) 792 nM and (C) 7.92 µM. Anti-calprotectin-Affimers (—•—) were included as negative control receptor by mixing the clones 4 and 19 together. Mean differences between anti-CEA and anti-calprotectin Affimer sensors tested under the same CEA concentration were statistically significant by independent t-test (*, ** and *** denote significance with p-value <0.03, 0.002 and 0.0002, respectively). (n= 5± SEM).

167

5.2.6.3 Multi-receptor based anti-CEA Affimer biosensors

Once the optimum density of anti-CEA Affimer on the sensor surface to fabricate the multi-receptor based sensors was resolved, two types of biosensors were evaluated namely, bi-Affimer and tri-Affimer based biosensors. Similar to the tri-Affimer based sensor, the bi-Affimer based sensor was designed by mixing two anti-CEA Affimers in an equal ratio following the second equation (**Equation 5.2**) derived from the mathematical binding model (**Figure 5.8**).

Two sets of bi-Affimer sensors were investigated comprised of a combination of anti-CEA Affimer-I and III and a mixture of anti-CEA Affimer-II and III. Both sensors were fabricated by immobilising 7.92 µM total containing an Affimer mixture by electrodeposition onto the electrode surface using previous parameters as described in **section 4.2.3**. Again, anti-calprotectin Affimers consisting of equal proportion of Affimer 4 and 19 were included as a negative control sensor. Meanwhile, data from **Figure 5.9 C** which shows the tri-Affimers based sensor results were used and replotted again in **Figure 5.10** for a comparison between the sensors developed.

The calibration curve of bi-Affimer sensor made of a combination of anti-CEA Affimer-I and III (**Figure 5.10 A**) showed a similar binding pattern to the single anti-CEA Affimer-II sensor (**Figure 5.7 B**). This was in agreement with the simulation data from the mathematical binding model that showed overlay of each other's curves (**Figure 5.8**). The dynamic detection range of this bi-Affimer sensor also resembled the single anti-CEA Affimer-II sensor that detected CEA binding from 1 fM to 100 fM.

Meanwhile, results from the bi-Affimers sensor built from the combination of anti-CEA Affimer-II and III (**Figure 5.10 B**) also showed a similar binding pattern to the single anti-CEA Affimer-III sensor (**Figure 5.7 C**). The R_{CT} change at 1 fM CEA was exactly the same as the single anti-CEA Affimer-III sensor, whilst the change in R_{CT} at 10 fM most likely derived mainly from binding to the anti-CEA Affimer-II. These findings further support the simulation data that showed the bi-Affimer sensor would produce moderate binding which falls in-between the single anti-CEA Affimer-II and single anti-CEA -Affimer-III sensors. The anti-CEA Affimer-II was postulated to yield the best binding performance, whilst the anti-CEA Affimer-III would produce the least binding performance from the simulated data. This prediction coincided with the experimental data observed in **Figure 5.7 B and C**. The detection range of tri-Affimer

sensor (**Figure 5.10 C**) showed a similar pattern to the polyclonal anti-CEA immunosensor (**Figure 4.12 D**) except that the difference of R_{CT} change across CEA concentration was not significant.
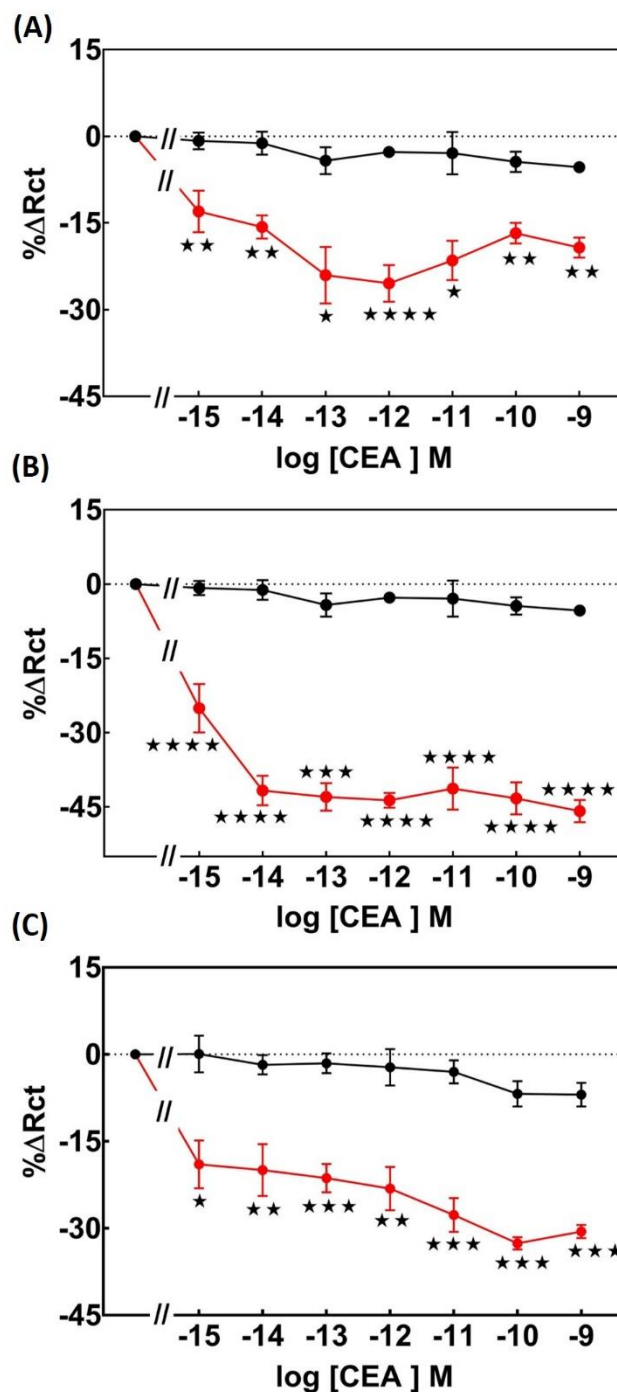
Figure 5.10 : Multi-receptor based anti-CEA Affimers and control biosensors

Comparison of bi-Affimer sensors; (A) Combination of anti-CEA Affimer-I and III, (B) Combination of anti-CEA Affimer-II and III and (C) tri-Affimer sensor; a combination of all anti-CEA Affimers (—•—). All Affimers were immobilised to a final concentration of 7.92 µM. A combination of anti-calprotectin Affimers 4 and 19 (—•—) were included as negative control biosensor and was prepared in a similar fashion as anti-CEA Affimer sensors. Calibration curve showing normalised impedance change against increasing concentrations of CEA (1 fM-1 nM). Mean differences between anti-CEA and anti-calprotectin Affimers sensors tested under the same CEA concentration were statistically significant by independent t-test (*, **, *** and **** denote significance with p-value <0.03, 0.002, 0.0002 and 0.0001, respectively). (n= 4± SEM).

170

5.2.7 Effect of bioreceptor distance from the transducer surface

To understand the electrochemical mechanism of transduction of the Affimer based sensors, different sized crosslinkers were evaluated as this allowed positioning of the Affimers at different distances from the attachment point on the transducer surface (**Figure 5.11**). Heterobifunctional linkers were used to immobilise the Affimer to the POct layer with sulfo-SMCC linker being shorter than SM (PEG$_4$) (0.83 nm vs 2.46 nm). Sulfo-SMCC has been routinely used in experiments presented in this chapter. All data with sensors using sulfo-SMCC consistently showed reduction in impedance signal with increased binding of CEA. A representative of impedance data from the single anti-CEA Affimer-II sensor and the corresponding negative control sensor using sulfo-SMCC as linker taken from **Figure 5.7 B** was replotted again in **Figure 5.11.**

A significant increase in R$_{CT}$ with the same magnitude of change was observed when using the longer SM (PEG$_4$) linker to immobilise anti-CEA Affimer-II. Additionally, the negative control remained stable at baseline level throughout the entire CEA concentrations range although the longer linker was used. These suggested that the longer linker positioned the Affimer protruding from the transducer surface and has enabled favourable interaction with CEA. Thus, the charge transfer was impeded upon analyte binding that resulted in increase in R$_{CT}$.

It can be clearly seen that sensor constructed using sulfo-SMCC as crosslinker generated better signal output as gradual decreased in R$_{CT}$ change can be observed and a linear calibration curve was possible to plot. In contrast, a striking increased in the R$_{CT}$ change of anti-CEA Affimer conjugated to SM (PEG$_4$) crosslinker occurred only from the initial concentration of CEA binding (30%). Although the mean differences between specific and control sensors were significant, the changes remained minimal (~32-42%) as increasing concentration of CEA were used. Therefore, these data demonstrated that using sulfo-SMCC as a crosslinker positioned the Affimer at the best distance from the transducer surface in producing an optimum signal during the analyte binding. Hence, sulfo-SMCC was selected as crosslinker to test the functionality of optimised sensor in biological matrix.
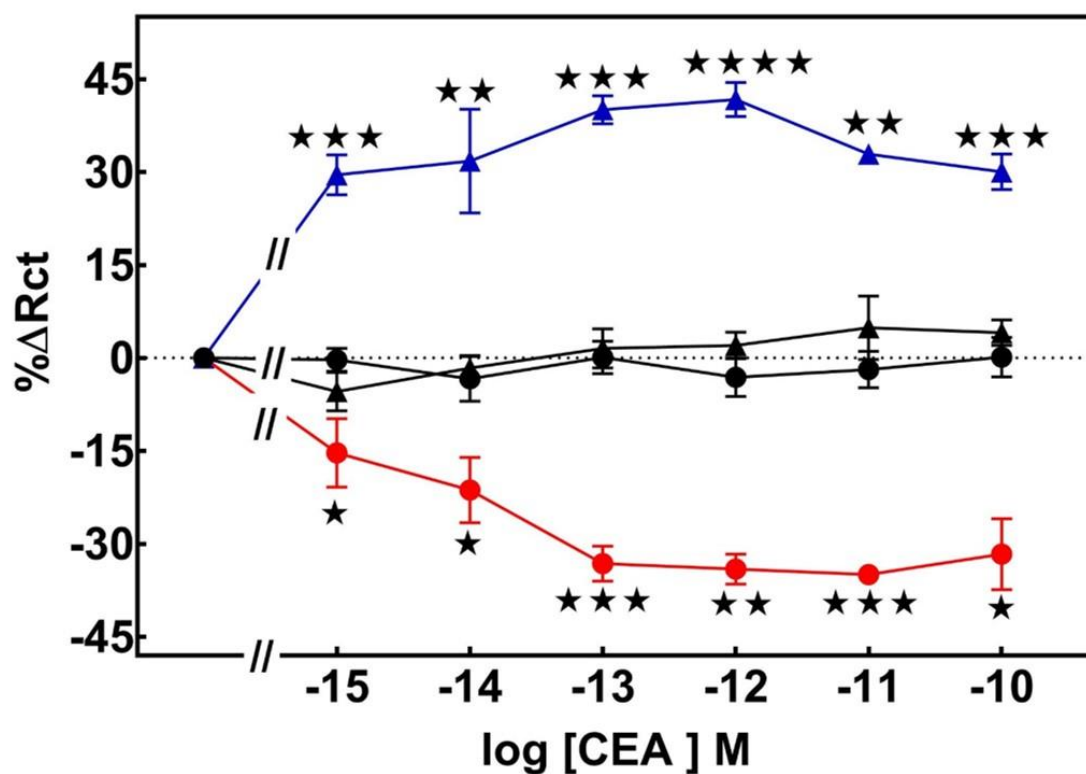
Figure 5.11 : Effect of bioreceptor distance from the transducer surface

Anti-CEA Affimer-II was linked with sulfo-SMCC (●) or SM (PEG$_4$) linkers (▲), whilst similarly the anti-calprotectin Affimer was linked with sulfo-SMCC (●) or SM (PEG$_4$) linkers (▲).The impedance data using sulfo-SMCC are replotted from Figure 5.7 B for comparison. Mean differences between anti-CEA and anti-calprotectin Affimers sensors tested under the same CEA concentration were statistically significant by independent t-test (*, **, *** and **** denote significance with p-value <0.03, 0.002, 0.0002 and 0.0001, respectively). (n= 4± SEM).

5.3 Anti-CEA Affimer sensor performance in normal human serum

5.3.1 Evaluation of sensor performance in normal human serum

After demonstrating proof of concept and optimisation in buffer, human serum was used as diluent to validate the operational capacity of the optimised Affimer biosensor in a biological matrix. As shown in **section 4.3.4.1**, the fully fabricated anti-CEA immunosensor experienced quite substantial non-specific binding even in 1% (v/v) diluted sera. Therefore, before investigating CEA detection in diluted serum, it was crucial to evaluate fully fabricated Affimer sensor performance in diluted serum with no CEA present. A series dilutions of sera was evaluated starting from 1% to 0.001 % (v/v). Impedance measurements were initially taken in PBS, followed by 20 min incubation in each dilution before rinsing in PBS and measuring the impedance again. The change in impedance was calculated by subtracting the impedance measured in PBS from impedance recorded in diluted serum and normalised to a percentage. The normalised data (**Figure 5.12**) demonstrated that the non-specific signal was at the highest in 1% serum (32% R_{CT} change). The signals then gradually reduced to ~25-27 % when serum was further diluted to 0.1% and 0.01%. However, a significant decrease was observed in the lowest dilution of serum, 0.001%, whereby the non-specific signal dropped down to 4%.
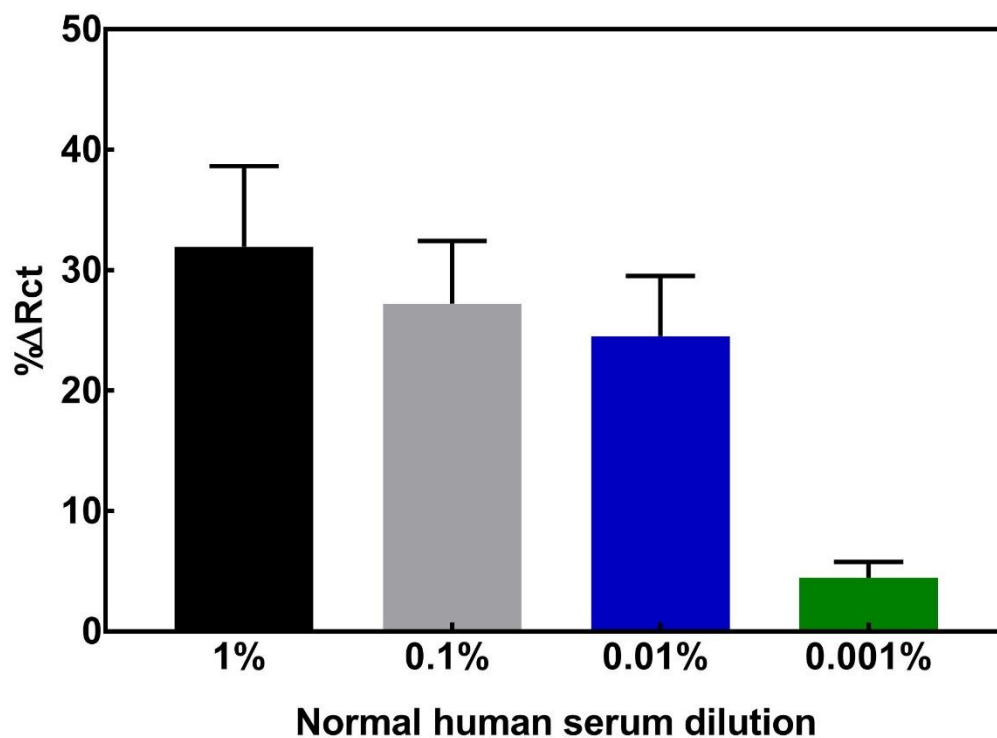
Figure 5.12 : Preliminary evaluation of optimised anti-CEA Affimer biosensor

The optimised anti-CEA Affimer-II biosensor was tested in 10-fold dilutions of normal human serum from 1, 0.1, 0.01 and 0.001% (v/v) in the absence of CEA. The serum was diluted in 10 mM PBS, pH 7.4 prior to interrogation. Normalised change in impedance data are mean ± SEM (n=4).

5.3.2 Sensor performance with CEA spiked into a range of human serum dilutions

After testing the Affimer based sensors in series of diluted serum, a range of CEA concentrations (1 fM-100 nM) were interrogated by spiking them with the diluted serum. The anti-CEA Affimer-II sensor was evaluated in 1, 0.1, 0.01 and 0.001 % (v/v) serum dilutions. In parallel, CEA spiked with 0.1% serum was interrogated on the control sensor with anti-calprotectin Affimer immobilised. Fully fabricated sensors were initially blocked with 10 mM PMDA and subsequently incubated in the blank serum for 20 min followed by a wash in PBS and measurement of the impedance. These steps were repeated with increasing concentrations of spiked CEA in each dilution of serum. R_{CT} measured in the blank serum was used as the baseline sensor. The change in impedance was calculated by subtracting R_{CT} measured in the blank serum from the R_{CT} recorded in each concentration of CEA and then normalised to a percentage change.

The normalised changes in impedance was plotted against series of CEA concentration as shown in **Figure 5.13**. From the data shown, it was observed that the 1% (v/v) serum samples produced the highest R_{CT} change (~30-34%). However, this signal predominantly represents non-specific interaction with serum components as a high degree of non-specific binding could be observed in the blank sensor (**Figure 5.12**). The signals were generally reduced by half when tested in 0.1% (v/v) and 0.01% (v/v) serum. In agreement with data from the blank sensor (**Figure 5.12**), a decrease in R_{CT} change could be due to steric hindrance caused by substantial amount of non-specific binding of serum components on the sensor surface. Interestingly, when CEA was spiked with 0.001% (v/v) serum, an increase in signal was observed resembling those previously seen in the buffered solution but this time in the opposite direction. This signal might be comprised of specific interaction between CEA and Affimer along with minimal non-specific binding. This idea was supported by minimum non-specific binding observed on the blank sensor. The lowest level of CEA detection remained at 1 fM and the maximum detection was at 100 fM which coincided with the dynamic range observed in the buffered system. Additionally, a slight increase in signal on the control sensor (~8%) was observed compared to its counterpart in the buffered system (**Figure 5.7 B**) which was not unexpected in these biological samples.
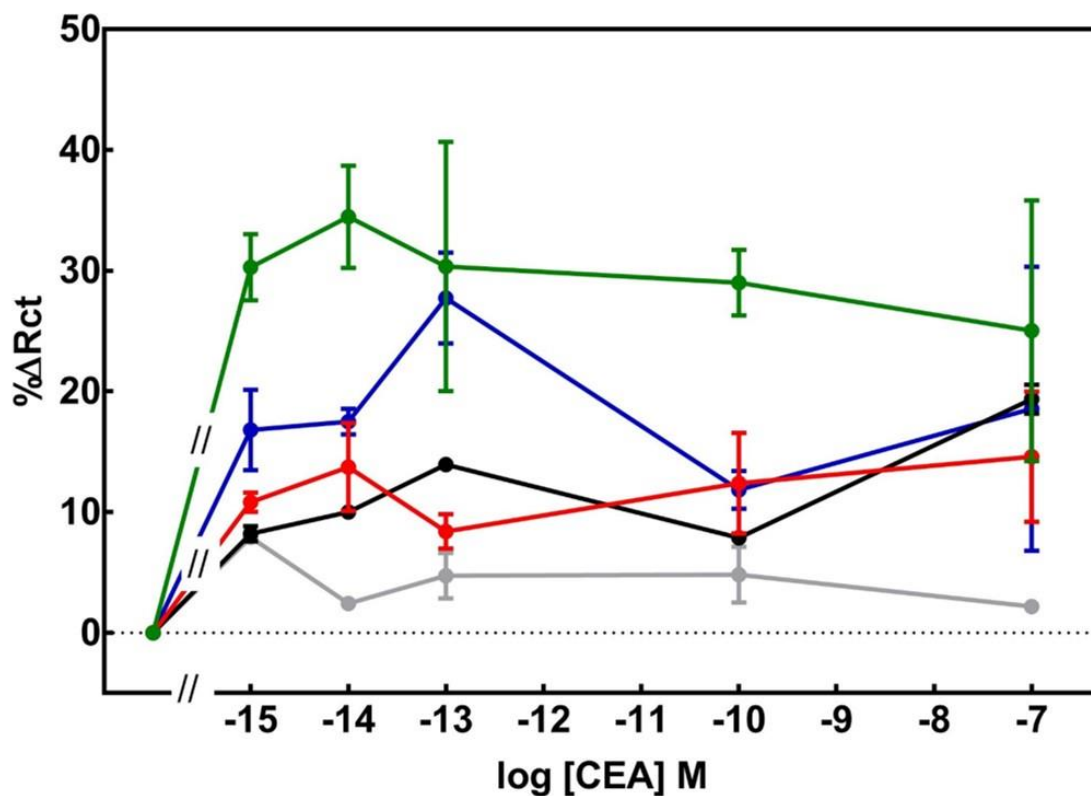
Figure 5.13 : Optimised Affimer biosensors tested on series of CEA concentrations spiked in diluted sera

The operational capacity of anti-CEA Affimer sensor for CEA in diluted serum was evaluated by spiking CEA into a range of diluted serum; CEA spiked in 1% (●), 0.1% (●), 0.01% (●) and 0.001% (●). The control sensor, using anti-calprotectin Affimer was tested in 0.1% (●) diluted serum only. Data are mean change in impedance ± SEM (n=4).

5.4 Comparison detection range of anti-CEA Affimer based biosensor with other assays

The sensitivity and detection range of optimised and fabricated anti-CEA Affimer-II based impedimetric biosensor developed in this study with the kinetic binding analysis from SPR (**section 3.3.5**), a commercial ELISA kit and anti-CEA immunosensors (**section 4.4**) were compared. Results from the sections mentioned above were replotted in **Figure 5.14** to compare between the systems. It can be clearly seen that the anti-CEA Affimer based impedimetric biosensor showed the highest sensitivity together with the anti-CEA polyclonal based impedimetric immunosensor compared to the other assays. However, the Affimer based sensor had a shorter dynamic range compared to the polyclonal based immunosensor (1 – 100 fM vs. 1 fM – 100 nM, respectively). The sensitivity in decreasing order was followed by anti-CEA monoclonal based immunosensor, ELISA and SPR. The CEA binding from the ELISA kit showed moderate sensitivity with a limit of detection at 10 pM and dynamic range from 25 to 600 pM. Meanwhile, SPR demonstrated the least sensitive detection with minimal binding was observed at 7. 8 nM and dynamic detection range from 7.8 nM to 1μM. Overall, the anti-CEA Affimer-II based impedimetric biosensor showed the best and highly sensitive detection between these assays and was comparable or even better than the published work as summarised in **Table 5.1**.
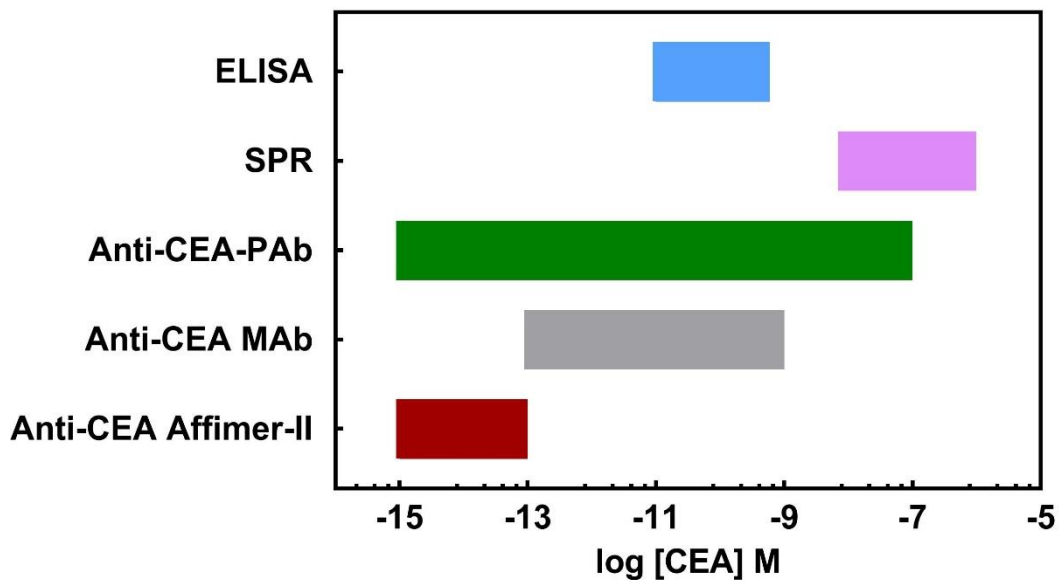
Figure 5.14: Comparison between Affimer based biosensor and other assays

Bar chart showing the dynamic detection range of anti-CEA Affimer-II biosensor (red) compared to anti-CEA immunosensors (monoclonal antibody, grey; polyclonal antibody,green), SPR (purple) and commercial ELISA kit assay (blue). The limit of detection (LOD) is calculated as limit of blank (LOB) plus 1.645 (standard deviation of the lowest sample concentration).

5.5 Discussion

The previous chapter (**Chapter 4**) showed that a POct film could be successfully used to fabricate a sensor with a large bioreceptor such as IgG. The anti-CEA immunosensors were shown to be highly sensitive with variable detection ranges. Following this, the potential to develop an impedimetric biosensor using a novel bioreceptor, the Affimer, was explored. During the optimisation of Affimer immobilisation, it was discovered that different strategies of polymerisation resulted in a large differences in the impedance behaviour. Polymerising identical Affimers separately on different working electrodes produced a highly resistive biosensor on the second working electrode (WE2) that differed greatly in impedance compared to its counterpart, WE1. Interestingly, when they were polymerised simultaneously, the difference in impedance was reduced between both working electrodes. Hence, the Affimer sensors were fabricated by immobilising the specific and control sensors simultaneously. Anti-CEA and anti-calprotectin Affimers were used as specific and control bioreceptors, respectively in developing the biosensor.

It is important to highlight that fully fabricated Affimer sensors were prone to non-specific interactions and required an additional blocking step prior to CEA interrogation. This is a common problem experienced in the majority of protein based assays in biosensors application (Berggren et al., 2001, Zhang and Heller, 2005, Seokheun and Junseok, 2010). However, the non-specific adsorption did not occur with anti-CEA immunosensors, although the same POct base polymer layer was used. A possible explanation for this is that Affimers were several times smaller in size compared to antibodies. Hence, immobilisation of an Affimer on a POct film may leave free amines which was sterically blocked by the immobilised IgG in the immunosensors. It was postulated that the non-specific signal observed was due to electrostatic interactions on the sensor surface with the $-NH_3^+$ groups. This hypothesis is supported since non-specific signals disappeared after blocking with 10 mM PMDA. The CEA protein exists as negative charge protein at pH 7.1. Thus, blocking the electrode surface with 10 mM PMDA after immobilising the Affimer would produce a negatively charge surface that minimised non-specific interaction with the mostly anionic proteins.

This hypothesis is also in agreement with Zhang and Heller (2005) findings which showed that nonspecific binding by the polycationic surface was neutralised by the

treatment with polyanions. In this particular study, they used poly(acrylic acid-*co*-maleic acid) and poly(acrylic acid) as the polyanions. This blocking technique led to a more sensitive detection of rabbit IgG from 20 pM with the non-blocked sensor surface to 40 fM after blocking. On the contrary, it was found that blocking the non-specific interaction using 1% (w/v) BSA solution was not suitable for the Affimer based biosensor construct. The results showed that the BSA is most likely creating steric hindrance to analyte binding.

A single Affimer based biosensor was developed using three different CEA-Affimers as bioreceptors to simulate the monoclonal antibody based biosensor system. Data in **section 5.2.5** showed variable success when using these Affimers as the bioreceptor. The anti-CEA Affimer-II showed the best biosensor performance (**Figure 5.7 B**) during CEA interrogation. It showed better sensitivity than the monoclonal anti-CEA immunosensor (1 fM vs 100 fM) and equivalent to a polyclonal anti-CEA immunosensor sensitivity. However, the dynamic range of anti-CEA Affimer based biosensor was shorter than the polyclonal anti-CEA immunosensor (1fM – 100 fM vs 1 fM – 1 nM). Interestingly, the detection range of anti-CEA Affimer biosensor was superior compared to its counterparts, the monoclonal anti-CEA immunosensor which showed slightly more extended detection range (100 fM -1 nM).

A mathematical binding model was generated using their equilibrium dissociation constant (K_D) values obtained from kinetic binding analysis (**Figure 5.8**) to develop multi-receptor Affimer based biosensors. It was hypothesized that the fabrication of this sensor could simulate the polyclonal anti-CEA immunosensor system. Combination of two and three different anti-CEA Affimers were investigated. The binding performance of multi-receptor Affimer based biosensors from the experimental data coincided with the binding model developed. This suggested that the mathematical binding model was reliable in predicting the experimental design of biosensor construct when using more than one bioreceptor. Additionally, this model could also be utilised to determine optimum Affimer density for loading onto the sensor surface. However, further study needs to be done to improve the multi-receptor Affimer based biosensor performance.

The effect of bioreceptor distance from the sensor surface was evaluated since distance from the sensor surface has been shown to be an important determinant of sensor response (Goode et al., 2016). The single receptor anti-CEA Affimer-II sensor was selected and immobilised with different length of crosslinker (**Figure 5.11**). Increase in

the R_{CT} change was observed when using a longer linker, SM (PEG$_4$), upon increasing concentration of CEA binding. In contrast, the opposite trend was observed when using a short linker, sulfo-SMCC. This suggested that the longer linker protruded the Affimer from the transducer surface, thus enabling favourable binding with CEA without causing any pinhole effects. Due to close proximity of Affimer when immobilised with sulfo-SMCC, the POct polymer layer became distorted during analyte binding that led to pinhole effect and therefore decreased in R_{CT} was observed. It was concluded that the optimum binding signal was successfully achieved when the Affimer was immobilised via sulfo-SMCC crosslinker.

The optimised anti-CEA Affimer-II sensor was then evaluated in a range of serum dilutions to validate the operational capacity of biosensor in a biological matrix. The anti-CEA Affimer-II was selected due to its high sensitivity and a good linear calibration curve of CEA detection in buffer. Overall, the results observed in buffer were translated well when spiking the CEA into 0.001% (v/v) serum. A similar increasing trend seen in the CEA immunosensors when tested against diluted serum (**Figure 4.15 B**) was observed again in the Affimer based sensor. The change in impedance consistently increased when interrogated with CEA in serum, whilst a decreasing change in R_{CT} was seen when the sensor was used in buffer. Although using a small bioreceptor like the anti-CEA Affimer, the trends observed further supported the kinetic barrier theory occurred in the CEA immunosensor (**section 4.5**) whereby the serum components occupied the empty spaces between the immobilised Affimer. Hence, stretching of the polymer was restricted upon analyte binding and the normal kinetic barrier that resulted in increased resistance was observed.

A substantial non-specific fouling was observed when testing out the CEA-Affimer sensors in higher dilutions of serum from 0.01% to 1% (v/v). It is important to note that the anti-CEA Affimer sensor showed better performance when evaluated in 0.001% (v/v) serum compared to the monoclonal anti-CEA immunosensor tested in 1% (v/v) serum. Although the dilution of serum seems to be high, this actually adds an extra advantages to the anti-CEA Affimer based sensor. Theoretically, when tested in a real sample patient using this sensor, the blood sample would need to be pre-diluted by 10^5 times prior to examining the CEA. The dilution factor might seem high but it is actually within the realistic range of anti-CEA Affimer based biosensor detection. The cut-off pathological value of CEA was clinically set at 5 ng/ml or higher which is equivalent to

25 pM. Hence, this concentration exceeded the detection range of the proposed sensor. However, if the sample diluted to 10^5 times, this would reduce the CEA concentration to 2.5 fM which is well within the sensor detection range. This dilution would also indirectly reduce the non-specific binding from serum components and only allow for specific signal being detected.

To the best of current knowledge, this is the first impedimetric biosensor for CEA detection based on an alternative binding protein, namely the Affimer as shown in **Table 5.1**. Findings in this study showed that the anti-CEA Affimer-II biosensor is highly sensitive, specific and confer superior detection compared to the monoclonal antibody. In addition, comparative analysis between different detection techniques (**section 5.4**) showed that the anti-CEA Affimer-II biosensor produced remarkable sensitivity and specificity. Therefore, the anti-CEA Affimer-II can be considered as the best candidate for an alternative bioreceptor to the monoclonal antibody. Apart from these, an extra advantage of POct base polymer layer was also discovered whereby it showed versatility in immobilising not only large bioreceptors (e.g., IgG) but also a small bioreceptor like the Affimer.

Table 5.1: Comparison of CEA-Affimer based biosensor developed in this study with published works

Random orientation						
Detection	**Biosensor**	**Transducer**	**Immobilization technique**	**Bioreceptor**	**LOD**	**Reference (s)**
Label-free	Impedimetric	Gold	Electro-copolymerization of *o*-aminophenol with CEA-Ab-glutathione monolayer modified AuNP	Antibody	0.4 ng/ml (500 fM)	(Tang et al., 2007)
	Impedimetric	Glassy carbon electrode (GCE)	Physisorption of anti-CEA antibody onto GCE modified with AuNP/ polymeric self-assembled nanoparticles (poly (γ-glutamic acid)-dopamine-chitosan	Antibody	10 fg/ml (50 aM)	(Xu et al., 2017)
	Impedimetric	Glassy carbon electrode (GCE)	Covalent immobilisation of amine-modified CEA aptamer on GA-AuNP/AMCM-GCE	DNA Aptamer	0.98 pg/ml (4.9 fM)	(Shekari et al., 2017)
	Impedimetric	Conducting Whatman paper	Covalent immobilization of anti-CEA antibody onto amine-functionalised surface coated with conducting poly (3,4ethylenedioxythiophene):poly(4-styrene sulfonate) on paper electrode	Antibody	2.68 ng/ml (13.4 pM)	(Kumar et al., 2016)
	Impedimetric	Graphite-based screen-printed electrode	Covalent immobilization of anti-CEA antibody onto poly-(pyrrole-3-carboxylic acid)-modified electrode	Antibody	33.33 pg/ml (166.65 fM)	(Iordănescu et al., 2018)
Labelled	Impedimetric	Indium tin oxide (ITO) electrode on a glass slide	Covalent immobilization of anti-CEA antibody onto aldehyde-functionalised ITO electrode and sandwich with magnetic beads coated with secondary antibody for signal enhancement	Antibody	1 ng/ml (5 pM)	(Yeh et al., 2016)

	Impedimetric	Glassy carbon electrode (GCE)	Covalent immobilization of anti-CEA antibody onto AuNP-modified GCE and sandwich with HRP conjugated to secondary antibody functionalised with graphene oxide nanosheets and coupled with enzymatic biocatalytic precipitation of 4-chloro-1-naphthol	Antibody	0.64 pg/ml (3.2 fM)	(Hou et al., 2013)
Site-directed orientation						
Label-free	Impedimetric	Screen printed gold electrode (SPGE)	Covalent immobilization of anti-CEA antibodies onto electropolymerised polyoctopamine coated SPGE	Monoclonal antibody Polyclonal antibody	20 pg/ml (100 fM) 0.5 pg/ml (1 fM)	**Current work*** **Chapter 4**
	Impedimetric	Screen printed gold electrode (SPGE)	Covalent immobilization of anti-CEA antibodies onto electropolymerised polyoctopamine coated SPGE	Affimer in buffer	0.2 pg/ml (1 fM)	**Current work*** **This chapter**

Abbreviations: AuNP, gold nanoparticle; CEA, carcinoembryonic antigen; SAM, self-assembled monolayer; HRP, horseradish peroxidase; GA, glutaraldehyde; and AMCM, amino-functionalized MCM–41.

Chapter Six

General Discussion

Chapter 6 : General Discussion

6.1 General discussion

Colorectal cancer (CRC) is normally diagnosed at an advanced stage due to lack of sensitivity and specificity in current diagnostic tests and time-consuming detection. Meanwhile, CEA is the only validated prognostic blood biomarker routinely used for preoperative screening of advanced CRC patients to determine the appropriate curative treatments and post-surveillance screening for tumour recurrence. Although much researches on the development of biosensors for CEA detection have been carried out, they are still far from being commercialised. Most of the biosensor systems developed at present are antibody based which is expensive for mass production and complicated in terms of fabrication. Therefore, this study initially aimed to discover the potential of anti-CEA Affimers as novel alternative bioreceptors and then, to utilise them in the development of rapid, low cost and simply fabricated impedimetric biosensors, which were highly sensitive and specific. In this chapter, detailed considerations of technical aspects, alongside the limitations that were found during the study will be covered and future recommendations are made.

6.2 Anti-CEA Affimers as novel bioreceptors

As outlined in **Chapter 1**, there are more than 20 different non-antibody binding protein scaffolds at present and the Affimer is one of the fastest emerging protein scaffolds that is being commercialised despite their recent invention (Tiede et al., 2014). To the best of our current knowledge, this is the first time CEA binders, screened against full-length native CEA protein, have been generated using a non-immunoglobulin protein scaffold, namely the Affimer. There were only two CEA binders from other protein scaffolds that have been reported at present with limited characterisation. The CEA binders were screened against recombinant CEA protein that derived from the DARPin and Affibodies protein scaffolds. The specificity of CEA-binding Affibodies selected against the A3B3 recombinant domain of CEA, was only validated by a dot blotting assay (Ahlgren, 2007). Meanwhile, the specificity of CEA-binding DARPins isolated by screening against the N-A1 recombinant domain of CEA was only characterised by immunohistochemical staining on human adenocarcinoma tissue sections (Saniz Pastor, 2008).

The evidence from our study indicated that the anti-CEA Affimers isolated showed excellent features as novel bioreceptors in several biotechnological applications including molecular imaging on CEA-expressing tumour cells, affinity precipitation assays and most importantly as bioreceptors in impedimetric biosensors. The anti-CEA Affimers showed high affinity binding towards CEA and were able to selectively recognised the multiple forms of functional CEA including the fully glycosylated native form as well incomplete and deglycosylated forms (**section 3.3.3 and 3.3.4**). The data also suggested that the anti-CEA Affimers did not recognise the substantial glycosylated region (approximately 100 KDa of 180 KDa total MW) but specifically interacted with protein epitopes of CEA even in complex protein matrices. However, further work needs to be done to distinguish which protein epitopes do the anti-CEA Affimers bind to, as there are seven protein domains within CEA. Additionally, the investigation of whether the anti-CEA Affimers from three different binders recognise the same or different epitopes would be very interesting to explore since each of them contained two unique variable loops.

It is important to highlight that several studies have been utilised the Affimer as bioreceptor in developing impedimetric biosensors, for the detection of C-reactive protein (Johnson et al., 2012), anti-myc tag antibodies (Raina et al., 2015) and interleukin-8 (Sharma et al., 2016a). However, these sensors were developed on a flat gold disc electrode using the self-assembled monolayer (SAM) format alongside an external reference and counter electrodes. Meanwhile, the Affimer-based impedimetric biosensors developed in this study were fabricated on a commercial DropSens screen printed gold electrode (SPGE) using a novel non-conducting polymer, polyoctopamine, as the transducer base layer. This commercial electrode has been widely used in point-of-care (POC) devices such as glucose biosensors due to the low cost of electrode production compared to the custom-made flat gold disc electrode. In addition, the reference and counter electrodes are printed on a single chip which is more practical for the POC approach. Dual working gold electrodes provided extra advantages because inclusion of a control sensor in parallel with the anti-CEA Affimer sensor could eliminate false positive signals and minimise the inter-batch variation measurement.

Fabrication of CEA immunosensors in this study have highlighted the importance of oriented bioreceptor immobilisation as a determinant factor in obtaining sensitive and effective biosensor operation. The incorporation of a single cysteine residue at the C-

terminus of anti-CEA Affimer has facilitated the site-directed immobilisation onto biosensor surface and significantly enhanced the sensor sensitivity for CEA detection. Moreover, the small size of anti-CEA Affimer (12 KDa) compared to the monoclonal anti-CEA antibody (150 KDa) added extra benefits by generating more binding sites for interaction with CEA and indirectly positioned the Affimer closer to the transducer surface. This in agreement with Ferrigno (2016) review which explained the ultra-sensitive detection observed from the anti-CEA Affimer-based biosensor compared to the monoclonal anti-CEA immunosensor (**section 5.4**).

6.3   Mathematical binding model for facilitating experimental design

In a conventional bioanalytical application, monoclonal and polyclonal antibodies are normally used as detection reagent due to their high affinity binding. Polyclonal antibody generally produces an extended detection range in a biosensor device compared to monoclonal antibody as shown in **section 4.3.3.1** due to avidity effects. Polyclonal antibodies interact simultaneously to multiple binding sites on a particular antigen with variety of affinities (K_D). Meanwhile, an Affimer is a monoclonal affinity reagent. To replicate the polyclonal antibody system, a mathematical binding model was developed. Observations from this study indicated that the use of such a model can facilitate optimisation of experimental design for the construction of multi-Affimer biosensors (**section 5.2.6.1**). This model will be useful if the equilibrium dissociation constant (K_D) of the bioreceptors is known prior to the fabrication of the biosensor.

Apart from this, there is a consensus in biosensor research pertaining to the importance of bioreceptor density on the sensor surface as a determinant factor of producing a successful and reproducible biosensor device. A high density of immobilised bioreceptors could cause problems with steric hindrance, whilst a low density of immobilised bioreceptors could introduce non-specific binding interaction with exposed sensor surface. Both of these effects are likely to generate less-sensitive biosensors (**section 5.2.6.2**). In this regard, the simulated data generated from the binding model assisted in determining the range of bioreceptor concentration that could potentially generate the maximum binding signal due to the bioreceptors-target analyte interaction. Additionally, it also facilitated in determining the ratio of bioreceptors in a mixture when developing a multi-Affimer based biosensor. The binding curves generated from

simulated data could also predict the binding performance of the biosensors designed and estimate the dynamic range of detection.

6.4 Polyoctopamine as a novel non-conducting polymer base layer

Another interesting findings in this study was the discovery of polyoctopamine (POct) as a novel non-conducting polymer base layer. Characterisation studies showed that the POct film has promising features of a non-conducting polymer that makes it suitable for implementation as an amine-bearing polymer layer. The synthesis of the polyoctopamine polymer film was very simple, rapid and did not require any activation process. Data showed that the formation of a very thin polymer layer was controllable as the polymerisation was self-limiting after two scan cycles. The generated polymer also showed excellent electron transfer resistance characteristic (**section 4.2**). A flat gold electrode is usually considered an ideal choice of transducer electrode in electrochemical biosensor devices. However, the cost and preparation of the electrode was not practical for commercially producible devices and is currently more suitable for laboratory based applications. The use of commercial DropSens screen printed gold electrodes seemed to be more practical but they suffered from a rough electrode surface as reported in previous study (Ahmed et al., 2013). Electrochemical characterisations via cyclic voltammetry and electrochemical impedance spectroscopy analyses in our study demonstrated that the use of POct as a transducer polymer base layer could partly resolve the roughness issue on the screen printed gold electrodes and it was feasible to develop a highly sensitive impedimetric biosensors for CEA detection based on this polymer. The POct polymer layer provides for a versatile functionalisation strategy to immobilise a variety of bioreceptors including large bioreceptors (e.g antibodies) and small bioreceptors (e.g. Affimers).

Interestingly, findings in this study showed that direct IgG immobilisation via oxidised oligosaccharide present on Fc region, via covalent immobilisation of the reactive aldehyde moiety to the POct base layer, yielded a highly sensitive and specific impedimetric CEA immunosensors (**Figure 6.1 A**). This immobilisation approach oriented the anchored antibodies in such way that favoured CEA interaction. In addition, the antigen binding sites remained active and were not affected by periodate oxidation. It was also observed that a polyclonal antibody based biosensor showed better performance

189

than the monoclonal antibody based biosensor with a limit of detection at 1 fM and 100 fM, respectively (**section 4.3.3**).

Alternatively, the POct polymer layer also provided functionalisation by the bioreceptors via the C-terminal thiol group as shown in the fabrication of anti-CEA Affimer based biosensors (**Figure 6.1 B**). Different types of heterobifunctional crosslinkers (i.e sulfo-SMCC and SM (PEG$_4$)) were tested to conjugate the Affimers to the POct polymer layer and both biosensor constructs showed the same sensitivity of detection despite differences in the length of the crosslinkers (**section 5.2.7**). It is important to note that, the fabrication of anti-CEA IgG based sensors and anti-CEA Affimer based sensor using the same POct polymer layer consistently showed a similar pattern of decreased change in impedance upon analyte binding despite disparity in the bioreceptor size. In addition, the anti-CEA Affimer-based biosensor showed the same sensitivity for detection of CEA as the polyclonal antibody based immunosensor (**section 5.2.5**). Based on the empirical observations in this study, highly sensitive detection was associated with a very thin film of POct polymer which coated the electrode surface and located the bioreceptors in close proximity to the transducer base layer. These led to effective of electron transfer to the electrode surface, hence improved the sensitivity.

Overall, the developed CEA impedimetric biosensors that were antibodies-based and Affimer-based are comparable or even better than those previously reported works as summarised in **Table 5.1**. The fabrication of CEA biosensors developed in this study was very simple and rapid and most importantly the sensors were highly sensitive to CEA over a wide dynamic range.

Figure 6.1: Amine-coupling functionalisation of polyoctopamine polymer layer for the immobilisation of anti-CEA Affimer and antibodies

(A) Immobilisation of anti-CEA Affimer onto POct polymer layer via thiol group using the crosslinkers (sulfo-SMCC and SM(PEG$_4$)) and (B) Covalent immobilisation of antibodies (monoclonal and polyclonal) to the POct polymer layer via reactive aldehyde moiety of oxidised oligosaccharide on the Fc region.

6.5 Factors contributing to the range of detection

The size of working electrode area used could be another limiting factor for the range of detection by the sensors. This notion is based on the observation that when using 1.6 mm diameter of screen printed gold working electrodes. A narrow dynamic range was observed when using a single receptor based biosensor system. The results suggested that the size of bioreceptors was not the determinant factor but the amount of available binding sites did contribute to the range of detection. A maximum of three to four concentrations of CEA binding were significantly detected from the single Affimer based sensor and monoclonal CEA immunosensor before the binding signals began to level off (**section 5.4**). However, the dynamic range of detection was expanded when employing a polyclonal antibody as bioreceptor as shown in **Figure 4.18 A**. This suggested that the multiple binding sites within polyclonal antibody mixture allowed for more analyte interaction epitopes. Observation from the tri-Affimer based biosensor (**Figure 5.9 C**) was also in agreement with this idea whereby the dynamic range of detection was similar to the polyclonal antibody based system but the changes of impedance upon increased concentrations of CEA binding were not significant. Although the tri-Affimer based sensor was comprised of a combination of different affinities CEA binders, close proximity of the Affimers to the transducer base layer probably limited the access for CEA interaction. Therefore, the tri-Affimer based biosensor performance could possibly be improved by incorporating nanomaterials (e.g. nanoparticles or multiwall carbon nanotubes) into the transducer base layer. The use of nanomaterials might provide more binding surfaces to immobilise the Affimers and hence improve the accessibility for the CEA binding, which could enhance the biosensor performance.

6.6 Minimization of non-specific binding events on sensor surface

It was observed that the biochemical properties of bioreceptor and target analyte play a vital role in the development of impedimetric biosensors notably in determining the choice of buffer used and the type of transducer surface. It is well established that the pH of the buffer used in designing the experiment determined the net charge of the protein. An anionic protein will be generated when using a buffered solution that contained pH larger than the isoelectric point (pI) of the protein and a cationic protein will be formed when using the otherwise. During the fabrication of Affimer-based biosensors, substantial non-specific signals were observed when interrogating the CEA

binding on non-blocked sensor surface. From the pI value of CEA that is 4.7, it is likely that the non-specific binding encountered was due to electrostatic interaction of the anionic CEA with NH_3^+ group on the sensor surface. The non-specific binding was eliminated when converting the sensor surface to net negative charge by modifiying with 10 mM pyromellitic dianhydride (PMDA) (**section 5.2.4**). Therefore, the empirical findings in this study suggested that the PMDA modification might be suitable to be used as a blocking strategy on positively charged sensor surfaces. However, there is a possibility that the PMDA may modify the amine moieties in the antigen binding sites of the bioreceptor which would affect its binding ability. In this regard, fabrication of neutral sensor surfaces using the MS (PEG)$_4$ with oriented immobilisation of bioreceptor might be a good option as discussed in **section 4.3.2.1**. Due to the small size of Affimers, BSA blocking was considered unsuitable as a blocking strategy in Affimer-based biosensors since it might hinder the Affimer binding sites.

6.7 Future work and opportunities

From the present available data, it seems likely that translating an anti-CEA Affimer based biosensor into a commercial platform is feasible. This is based on the basis of inexpensive and rapid production of anti-CEA Affimer that using the bacterial expression system for large scale operation, together with simple and cost-effective fabrication of the Affimer-based biosensor using a polyoctopamine polymer as the transducer base layer in a chip based sensor format. Taking this into consideration, several parameters need to be further investigated prior to commercialisation as this study is at a pilot stage and conducted at a small scale. Evaluation on batch-to-batch variation of anti-CEA Affimer for large scale production is necessary and reproducibility of fully fabricated electrodes in mass production is equally important. In addition, the reliability of sensor in detecting CEA derived from the serum of colorectal cancer (CRC) patients is crucial. This is to ensure that the sensor measurement is not affected by other interference present in the serum. Apart from testing sample in serum, it would also be interesting to test the presence of CEA from the stool samples of CRC patients. Technically, the tumour cells shed from CRC into the colon lumen and bearing CEA, would be likely to be present. This would facilitate the medical practitioner in distinguishing between CRC and inflammatory bowel disease and facilitate design of an appropriate plan of treatment. In a broader sense, this biosensor is not restricted to the detection of CEA in CRC samples only, but also applicable to any CEA-expressing solid

tumour cell such as liver, gastrointestinal tract, pancreatic, ovary and breast cancers. With the invention of the anti-CEA Affimer based biosensor, it is hope that this biosensor could be an alternative to the routinely used ELISA assay and provide a much more rapid and cheaper measurement. In addition, it could be used as a diagnostic tool for non-invasive screening of CRC and would possibly improve patient adherence.

Another avenue which merits further investigation is the incorporation of nanomaterials (eg. multiwall carbon nanotube) on the POct polymer base layer during the fabrication of Affimer-based biosensor. These could possibly enhanced the sensor sensitivity and expand the dynamic range of detection. Since the discovery of anti-CEA Affimers as novel bioreceptors have been validated in this study, their application is not limited to the impedimetric biosensor only, but they could also be used as bioreceptors in other sensor formats or as molecular probes in targeted therapy and theranostic applications.

Bibliography

ABOUZARI, M. S., BERKEMEIER, F., SCHMITZ, G. & WILMER, D. 2009. On the physical interpretation of constant phase elements. *Solid State Ionics,* 180**,** 922-927.

AHLGREN, S. 2007. *Selection of CEA and VEGFR2 Binding Affibody® Molecules Using Phage Display.* Molecular Biotechnology Programme Master thesis, Uppsala University.

AHMED, A. 2015. *Fabrication of electrochemical biosensors for detection of microorganisms.* PhD PhD, University of Leeds.

AHMED, A., RUSHWORTH, J. V., WRIGHT, J. D. & MILLNER, P. A. 2013. Novel impedimetric immunosensor for detection of pathogenic bacteria Streptococcus pyogenes in human saliva. *Anal Chem,* 85**,** 12118-25.

AIZAWA, M., MORIOKA, A., SUZUKI, S. & NAGAMURA, Y. 1979. Enzyme immunosenser: Ill. Amperometric determination of human cherienic gonadotropin by membrane-bound antibody. *Analytical Biochemistry,* 94**,** 22-28.

ALTINTAS, Z., KALLEMPUDI, S. S. & GURBUZ, Y. 2014. Gold nanoparticle modified capacitive sensor platform for multiple marker detection. *Talanta,* 118**,** 270-276.

ALTINTAS, Z., KALLEMPUDI, S. S., SEZERMAN, U. & GURBUZ, Y. 2012. A novel magnetic particle-modified electrochemical sensor for immunosensor applications. *Sensors and Actuators B: Chemical,* 174**,** 187-194.

AMOUZADEH TABRIZI, M., SHAMSIPUR, M. & FARZIN, L. 2015. A high sensitive electrochemical aptasensor for the determination of VEGF165 in serum of lung cancer patient. *Biosensors and Bioelectronics,* 74**,** 764-769.

ARBABI-GHAHROUDI, M. 2017. Camelid Single-Domain Antibodies: Historical Perspective and Future Outlook. *Frontiers in Immunology,* 8.

ARNOLD, M., SIERRA, M. S., LAVERSANNE, M., SOERJOMATARAM, I., JEMAL, A. & BRAY, F. 2017. Global patterns and trends in colorectal cancer incidence and mortality. *Gut,* 66**,** 683-691.

ARYA, S. K., ZHURAUSKI, P., JOLLY, P., BATISTUTI, M. R., MULATO, M. & ESTRELA, P. 2018. Capacitive aptasensor based on interdigitated electrode for breast cancer detection in undiluted human serum. *Biosensors and Bioelectronics,* 102**,** 106-112.

ATES, M. 2013. A review study of (bio)sensor systems based on conducting polymers. *Materials Science and Engineering: C,* 33**,** 1853-1859.

AYDEMIR, N., MALMSTRÖM, J. & TRAVAS-SEJDIC, J. 2016. Conducting polymer based electrochemical biosensors. *Physical Chemistry Chemical Physics,* 18**,** 8264-8277.

BAHADIR, E. B. & SEZGINTURK, M. K. 2014. A review on impedimetric biosensors. *Artif Cells Nanomed Biotechnol***,** 1-15.

BALA, A. & GÓRSKI, Ł. 2018. Peptide nucleic acid as a selective recognition element for electrochemical determination of Hg2+. *Bioelectrochemistry,* 119**,** 189-195.

BALLY, M., HALTER, M., VÖRÖS, J. & GRANDIN, H. M. 2006. Optical microarray biosensing techniques. *Surface and Interface Analysis: An International Journal devoted to the development and application of techniques for the analysis of surfaces, interfaces and thin films,* 38**,** 1442-1458.

BAN, B. & BLAKE, D. A. 2012. Recombinant Antibodies and Non-Antibody Scaffolds for Immunoassays. *Advances in Immunoassay Technology.* InTech.

BATYUK, A., WU, Y., HONEGGER, A., HEBERLING, M. M. & PLÜCKTHUN, A. 2016. DARPin-Based Crystallization Chaperones Exploit Molecular Geometry as a Screening Dimension in Protein Crystallography. *Journal of Molecular Biology,* 428**,** 1574-1588.

BAYDEMIR, G., BETTAZZI, F., PALCHETTI, I. & VOCCIA, D. 2016. Strategies for the development of an electrochemical bioassay for TNF-alpha detection by using a non-immunoglobulin bioreceptor. *Talanta,* 151**,** 141-147.

BEAUCHEMIN, N. & ARABZADEH, A. 2013. Carcinoembryonic antigen-related cell adhesion molecules (CEACAMs) in cancer progression and metastasis. *Cancer and Metastasis Reviews,* 32**,** 643-671.

BELLUZO, M., RIBONE, M. & LAGIER, C. 2008. Assembling Amperometric Biosensors for Clinical Diagnostics. *Sensors,* 8**,** 1366.

BERGGREN, C., BJARNASON, B. & JOHANSSON, G. 2001. Capacitive Biosensors. *Electroanalysis,* 13**,** 173-180.

BILLAH, M. M., HAYS, H. C. W., HODGES, C. S., PONNAMBALAM, S., VOHRA, R. & MILLNER, P. A. 2012. Mixed self-assembled monolayer (mSAM) based impedimetric immunosensors for cardiac troponin I (cTnI) and soluble lectin-like oxidized low-density lipoprotein receptor-1 (sLOX-1). *Sensors and Actuators B: Chemical,* 173**,** 361-366.

BILLAH, M. M., HODGES, C. S., HAYS, H. C. W. & MILLNER, P. A. 2010. Directed immobilization of reduced antibody fragments onto a novel SAM on gold for myoglobin impedance immunosensing. *Bioelectrochemistry,* 80**,** 49-54.

BINZ, H. K., STUMPP, M. T., FORRER, P., AMSTUTZ, P. & PLÜCKTHUN, A. 2003. Designing Repeat Proteins: Well-expressed, Soluble and Stable Proteins from Combinatorial Libraries of Consensus Ankyrin Repeat Proteins. *Journal of Molecular Biology,* 332**,** 489-503.

BJERNER, J., LEBEDIN, Y., BELLANGER, L., KUROKI, M., SHIVELY, J. E., VARAAS, T., NUSTAD, K., HAMMARSTRÖM, S. & BØRMER, O. P. 2002. Protein Epitopes in Carcinoembryonic Antigen. *Tumor Biology,* 23**,** 249-262.

BLUMENTHAL, R. D., HANSEN, H. J. & GOLDENBERG, D. M. 2005. Inhibition of Adhesion, Invasion, and Metastasis by Antibodies Targeting CEACAM6 (NCA-90) and CEACAM5 (Carcinoembryonic Antigen). *Cancer Research,* 65**,** 8809-8817.

BRIENT-LITZLER, E., PLÜCKTHUN, A. & BEDOUELLE, H. 2010. Knowledge-based design of reagentless fluorescent biosensors from a designed ankyrin repeat protein. *Protein Engineering, Design and Selection,* 23**,** 229-241.

CAÑAS, N. A., HIROSE, K., PASCUCCI, B., WAGNER, N., FRIEDRICH, K. A. & HIESGEN, R. 2013. Investigations of lithium–sulfur batteries using electrochemical impedance spectroscopy. *Electrochimica Acta,* 97**,** 42-51.

CASEY, B. J. & KOFINAS, P. 2008. Selective binding of carcinoembryonic antigen using imprinted polymeric hydrogels. *J Biomed Mater Res A,* 87**,** 359-63.

CAYGILL, R. L. 2012. *Developing an electrochemical assay to detect and quantify virus particles.* University of Leeds.

CAYGILL, R. L., HODGES, C. S., HOLMES, J. L., HIGSON, S. P. J., BLAIR, G. E. & MILLNER, P. A. 2012. Novel impedimetric immunosensor for the detection and quantitation of Adenovirus using reduced antibody fragments immobilized onto a conducting copolymer surface. *Biosensors and Bioelectronics,* 32**,** 104-110.

CHAMBERS, J. P., ARULANANDAM, B. P., MATTA, L. L., WEIS, A. & VALDES, J. J. 2008. Biosensor recognition elements. Texas Univ at San Antonio Dept of Biology.

CHANG, B.-Y. & PARK, S.-M. 2010. Electrochemical impedance spectroscopy. *Annual Review of Analytical Chemistry,* 3**,** 207-229.

CHEN, X., PAN, Y., LIU, H., BAI, X., WANG, N. & ZHANG, B. 2016. Label-free detection of liver cancer cells by aptamer-based microcantilever biosensor. *Biosensors and Bioelectronics,* 79**,** 353-358.

CLARK, L. C. & LYONS, C. 1962. ELECTRODE SYSTEMS FOR CONTINUOUS MONITORING IN CARDIOVASCULAR SURGERY. *Annals of the New York Academy of Sciences,* 102**,** 29-45.

COMPTE, M., ÁLVAREZ-CIENFUEGOS, A., NUÑEZ-PRADO, N., SAINZ-PASTOR, N., BLANCO-TORIBIO, A., PESCADOR, N., SANZ, L. & ÁLVAREZ-VALLINA, L. 2014. Functional comparison of single-chain and two-chain anti-CD3-based bispecific antibodies in gene immunotherapy applications. *OncoImmunology,* 3.

COOPER, S. E. & VENTON, B. J. 2009. Fast-scan cyclic voltammetry for the detection of tyramine and octopamine. *Analytical and bioanalytical chemistry,* 394**,** 329-336.

CÓRDOBA-TORRES, P., MESQUITA, T. J. & NOGUEIRA, R. P. 2015. Relationship between the Origin of Constant-Phase Element Behavior in Electrochemical Impedance Spectroscopy and Electrode Surface Structure. *The Journal of Physical Chemistry C,* 119**,** 4136-4147.

COSNIER, S. 2005. Affinity biosensors based on electropolymerized films. *Electroanalysis: An International Journal Devoted to Fundamental and Practical Aspects of Electroanalysis,* 17**,** 1701-1715.

COUNCIL, N. R. 1999. *Monoclonal antibody production*, National Academies Press.

CRIVIANU-GAITA, V., AAMER, M., POSARATNANATHAN, R. T., ROMASCHIN, A. & THOMPSON, M. 2016. Acoustic wave biosensor for the detection of the breast and prostate cancer metastasis biomarker protein PTHrP. *Biosensors and Bioelectronics,* 78**,** 92-99.

CRUK 2018. Cancer in the UK. Cancer Research UK.

DAI, Z., YAN, F., CHEN, J. & JU, H. 2003. Reagentless Amperometric Immunosensors Based on Direct Electrochemistry of Horseradish Peroxidase for Determination of Carcinoma Antigen-125. *Analytical Chemistry,* 75**,** 5429-5434.

DAI, Z., YAN, F., YU, H., HU, X. & JU, H. 2004. Novel amperometric immunosensor for rapid separation-free immunoassay of carcinoembryonic antigen. *Journal of Immunological Methods,* 287**,** 13-20.

DAMIATI, S., PEACOCK, M., MHANNA, R., SØPSTAD, S., SLEYTR, U. B. & SCHUSTER, B. 2018. Bioinspired detection sensor based on functional nanostructures of S-proteins to target the folate receptors in breast cancer cells. *Sensors and Actuators B: Chemical,* 267**,** 224-230.

DANIELS, J. S. 2010. *An integrated impedance biosensor array.* Stanford University.

DE PICCIOTTO, S., DICKSON, P. M., TRAXLMAYR, M. W., MARQUES, B. S., SOCHER, E., ZHAO, S., CHEUNG, S., KIEFER, J. D., WAND, A. J., GRIFFITH, L. G., IMPERIALI, B. & WITTRUP, K. D. 2016. Design Principles for SuCESsFul Biosensors: Specific Fluorophore/Analyte Binding and Minimization of Fluorophore/Scaffold Interactions. *Journal of Molecular Biology,* 428**,** 4228-4241.

DEFFAR, K., SHI, H., LI, L., WANG, X. & ZHU, X. 2009. Nanobodies-the new concept in antibody engineering. *African Journal of Biotechnology,* 8.

DESCHOOLMEESTER, V., BAAY, M., SPECENIER, P., LARDON, F. & VERMORKEN, J. B. 2010. A review of the most promising biomarkers in colorectal cancer: one step closer to targeted therapy. *The oncologist,* 15**,** 699-731.

DOUBENI, C. A., JENSEN, C. D., FEDEWA, S. A., QUINN, V. P., ZAUBER, A. G., SCHOTTINGER, J. E., CORLEY, D. A. & LEVIN, T. R. 2016. Fecal Immunochemical Test (FIT) for Colon Cancer Screening: Variable Performance with Ambient Temperature. *Journal of the American Board of Family Medicine : JABFM,* 29**,** 672-681.

DREIER, B., HONEGGER, A., HESS, C., NAGY-DAVIDESCU, G., MITTL, P. R. E., GRÜTTER, M. G., BELOUSOVA, N., MIKHEEVA, G., KRASNYKH, V. & PLÜCKTHUN, A. 2013. Development of a generic adenovirus delivery system based on structure-guided design of bispecific trimeric DARPin adapters. *Proceedings of the National Academy of Sciences of the United States of America,* 110**,** E869-E877.

DREWINKO, B. & YANG, L. Y. 1980. Observations on the synthesis of carcinoembryonic antigen by an established human colonic carcinoma cell line. *Oncology,* 37**,** 336-42.

DUFFY, M. J. 2001. Carcinoembryonic antigen as a marker for colorectal cancer: is it clinically useful? *Clinical chemistry,* 47**,** 624-630.

DYBALLA, N. & METZGER, S. 2009. Fast and sensitive colloidal coomassie G-250 staining for proteins in polyacrylamide gels. *Journal of visualized experiments : JoVE***,** 1431.

ENGFELDT, T., RENBERG, B., BRUMER, H., NYGREN, P. Å. & KARLSTRÖM, A. E. 2005. Chemical Synthesis of Triple-Labelled Three-Helix Bundle Binding Proteins for Specific Fluorescent Detection of Unlabelled Protein. *ChemBioChem,* 6**,** 1043-1050.

ESTRELA, P., PAUL, D., SONG, Q., STADLER, L. K. J., WANG, L., HUQ, E., DAVIS, J. J., FERRIGNO, P. K. & MIGLIORATO, P. 2010. Label-Free Sub-picomolar Protein Detection with Field-Effect Transistors. *Analytical Chemistry,* 82**,** 3531-3536.

ETAYASH, H., JIANG, K., AZMI, S., THUNDAT, T. & KAUR, K. 2015. Real-time Detection of Breast Cancer Cells Using Peptide-functionalized Microcantilever Arrays. *Scientific Reports,* 5**,** 13967.

FAKIH, M. G. & PADMANABHAN, A. 2006. CEA monitoring in colorectal cancer. *Oncology,* 20.

FERLAY, J., SOERJOMATARAM, I., DIKSHIT, R., ESER, S., MATHERS, C., REBELO, M., PARKIN, D. M., FORMAN, D. & BRAY, F. 2015. Cancer incidence and mortality worldwide: sources,

methods and major patterns in GLOBOCAN 2012. *Int J Cancer,* 136**,** E359-86.

FERRIGNO, PAUL K. 2016. Non-antibody protein-based biosensors. *Essays In Biochemistry,* 60**,** 19-25.

FISHER, M. J., WILLIAMSON, D. J., BURSLEM, G. M., PLANTE, J. P., MANFIELD, I. W., TIEDE, C., AULT, J. R., STOCKLEY, P. G., PLEIN, S., MAQBOOL, A., TOMLINSON, D. C., FOSTER, R., WARRINER, S. L. & BON, R. S. 2015. Trivalent Gd-DOTA reagents for modification of proteins. *RSC Advances,* 5**,** 96194-96200.

FLEETWOOD, F., KLINT, S., HANZE, M., GUNNERIUSSON, E., FREJD, F. Y., STÅHL, S. & LÖFBLOM, J. 2014. Simultaneous targeting of two ligand-binding sites on VEGFR2 using biparatopic Affibody molecules results in dramatically improved affinity. *Scientific Reports,* 4**,** 7518.

FRIEDMAN, M., LINDSTRÖM, S., EKERLJUNG, L., ANDERSSON-SVAHN, H., CARLSSON, J., BRISMAR, H., GEDDA, L., FREJD, F. Y. & STÅHL, S. 2009. Engineering and characterization of a bispecific HER2 $\times$ EGFR-binding affibody molecule. *Biotechnology and Applied Biochemistry,* 54**,** 121-131.

FU, X.-M., LIU, Z.-J., CAI, S.-X., ZHAO, Y.-P., WU, D.-Z., LI, C.-Y. & CHEN, J.-H. 2016. Electrochemical aptasensor for the detection of vascular endothelial growth factor (VEGF) based on DNA-templated Ag/Pt bimetallic nanoclusters. *Chinese Chemical Letters,* 27**,** 920-926.

FUNG, K. Y., TABOR, B., BUCKLEY, M. J., PRIEBE, I. K., PURINS, L., POMPEIA, C., BRIERLEY, G. V., LOCKETT, T., GIBBS, P. & TIE, J. 2015. Blood-based protein biomarker panel for the detection of colorectal cancer. *PloS one,* 10**,** e0120425.

GAN, N., JIA, L. & ZHENG, L. 2011. A Sandwich Electrochemical Immunosensor Using Magnetic DNA Nanoprobes for Carcinoembryonic Antigen. *International Journal of Molecular Sciences,* 12**,** 7410.

GAO, Y.-S., XU, J.-K., LU, L.-M., ZHU, X.-F., WANG, W.-M., YANG, T.-T., ZHANG, K.-X. & YU, Y.-F. 2015. A label-free electrochemical immunosensor for carcinoembryonic antigen detection on a graphene platform doped with poly (3, 4-ethylenedioxythiophene)/Au nanoparticles. *RSC Advances,* 5**,** 86910-86918.

GARCIA, M., SEIGNER, C., BASTID, C., CHOUX, R., PAYAN, M. & REGGIO, H. 1991. Carcinoembryonic antigen has a different molecular weight in normal colon and in cancer cells due to N-glycosylation differences. *Cancer research,* 51**,** 5679-5686.

GEISE, R. J., ADAMS, J. M., BARONE, N. J. & YACYNYCH, A. M. 1991. Electropolymerized films to prevent interferences and electrode fouling in biosensors. *Biosensors and Bioelectronics,* 6**,** 151-160.

GOLD, P. & FREEDMAN, S. O. 1965. Specific carcinoembryonic antigens of the human digestive system. *Journal of Experimental Medicine,* 122**,** 467-481.

GOMES, R. S., MOREIRA, F. T., FERNANDES, R. & SALES, M. G. F. 2018. Sensing CA 15-3 in point-of-care by electropolymerizing O-phenylenediamine (oPDA) on Au-screen printed electrodes. *PloS one,* 13**,** e0196656.

GONZALEZ-PONS, M. & CRUZ-CORREA, M. 2015. Colorectal cancer biomarkers: where are we now? *BioMed research international,* 2015.

GOODE, J., DILLON, G. & MILLNER, P. A. 2016. The development and optimisation of nanobody based electrochemical immunosensors for IgG. *Sensors and Actuators B: Chemical,* 234**,** 478-484.

GOODE, J. A. 2015. *Development of biosensors using novel bioreceptors; Investigation and optimisation of fundamental parameters at the nanoscale.* PhD PhD, University of Leeds.

GRAFF, C. P., CHESTER, K., BEGENT, R. & WITTRUP, K. D. 2004. Directed evolution of an anti-carcinoembryonic antigen scFv with a 4-day monovalent dissociation half-time at 37 degrees C. *Protein Eng Des Sel,* 17**,** 293-304.

GRAMMOUSTIANOU, A. & GIZELI, E. 2018. Chapter 9 - Acoustic Wave–Based Immunoassays. *In:* VASHIST, S. K. & LUONG, J. H. T. (eds.) *Handbook of Immunoassay Technologies.* Academic Press.

GRIESHABER, D., MACKENZIE, R., VOEROES, J. & REIMHULT, E. 2008. Electrochemical biosensors-sensor principles and architectures. *Sensors,* 8**,** 1400-1458.

GUPTA, V. K., YOLA, M. L., QURESHI, M. S., SOLAK, A. O., ATAR, N. & ÜSTÜNDAĞ, Z. 2013. A novel impedimetric biosensor based

on graphene oxide/gold nanoplatform for detection of DNA arrays. *Sensors and Actuators B: Chemical,* 188**,** 1201-1211.

HAMMARSTRÖM, S. The carcinoembryonic antigen (CEA) family: structures, suggested functions and expression in normal and malignant tissues. Seminars in cancer biology, 1999. Elsevier, 67-81.

HAMMOND, JULES L., FORMISANO, N., ESTRELA, P., CARRARA, S. & TKAC, J. 2016. Electrochemical biosensors and nanobiosensors. *Essays in Biochemistry,* 60**,** 69-80.

HAMZEH-MIVEHROUD, M., ALIZADEH, A. A., MORRIS, M. B., CHURCH, W. B. & DASTMALCHI, S. 2013. Phage display as a technology delivering on the promise of peptide drug discovery. *Drug discovery today,* 18**,** 1144-1157.

HARLOW, E., LANE, D. & HARLOW, E. 1999. Using antibodies: a laboratory manual.

HATAKEYAMA, K., WAKABAYASHI-NAKAO, K., OHSHIMA, K., SAKURA, N., YAMAGUCHI, K. & MOCHIZUKI, T. 2013. Novel protein isoforms of carcinoembryonic antigen are secreted from pancreatic, gastric and colorectal cancer cells. *BMC research notes,* 6**,** 381.

HAUPTMAN, N., GLAVA, #X010D & , D. 2017. Colorectal Cancer Blood-Based Biomarkers. *Gastroenterology Research and Practice,* 2017**,** 11.

HAYS, H. C. W., MILLNER, P. A. & PRODROMIDIS, M. I. 2006. Development of capacitance based immunosensors on mixed self-assembled monolayers. *Sensors and Actuators B: Chemical,* 114**,** 1064-1070.

HE, L., PAGNEUX, Q., LARROULET, I., SERRANO, A. Y., PESQUERA, A., ZURUTUZA, A., MANDLER, D., BOUKHERROUB, R. & SZUNERITS, S. 2017. Label-free femtomolar cancer biomarker detection in human serum using graphene-coated surface plasmon resonance chips. *Biosensors and Bioelectronics,* 89**,** 606-611.

HEICHMAN, K. A. 2014. Blood-Based Testing for Colorectal Cancer Screening. *Molecular Diagnosis & Therapy,* 18**,** 127-135.

HELMA, J., CARDOSO, M. C., MUYLDERMANS, S. & LEONHARDT, H. 2015. Nanobodies and recombinant binders in cell biology. *J Cell Biol,* 209**,** 633-44.

HIRST, N. A. 2014. *Development of biosensors for early detection of anastomotic leak and sepsis.* University of Leeds.

HOOGENBOOM, H. R., GRIFFITHS, A. D., JOHNSON, K. S., CHISWELL, D. J., HUDSON, P. & WINTER, G. 1991. Multi-subunit proteins on the surface of filamentous phage: methodologies for displaying antibody (Fab) heavy and light chains. *Nucleic Acids Res,* 19**,** 4133-7.

HOU, L., CUI, Y., XU, M., GAO, Z., HUANG, J. & TANG, D. 2013. Graphene oxide-labeled sandwich-type impedimetric immunoassay with sensitive enhancement based on enzymatic 4-chloro-1-naphthol oxidation. *Biosensors and Bioelectronics,* 47**,** 149-156.

HUANG, J.-Y., ZHAO, L., LEI, W., WEN, W., WANG, Y.-J., BAO, T., XIONG, H.-Y., ZHANG, X.-H. & WANG, S.-F. 2018. A high-sensitivity electrochemical aptasensor of carcinoembryonic antigen based on graphene quantum dots-ionic liquid-nafion nanomatrix and DNAzyme-assisted signal amplification strategy. *Biosensors and Bioelectronics,* 99**,** 28-33.

HUGHES, D. J., TIEDE, C., PENSWICK, N., TANG, A. A.-S., TRINH, C. H., MANDAL, U., ZAJAC, K. Z., GAULE, T., HOWELL, G., EDWARDS, T. A., DUAN, J., FEYFANT, E., MCPHERSON, M. J., TOMLINSON, D. C. & WHITEHOUSE, A. 2017. Generation of specific inhibitors of SUMO-1– and SUMO-2/3–mediated protein-protein interactions using Affimer (Adhiron) technology. *Science Signaling,* 10.

ILKHANI, H., RAVALLI, A. & MARRAZZA, G. 2016. Design of an Affibody-Based Recognition Strategy for Human Epidermal Growth Factor Receptor 2 (HER2) Detection by Electrochemical Biosensors. *Chemosensors,* 4**,** 23.

ILKHANI, H., SARPARAST, M., NOORI, A., ZAHRA BATHAIE, S. & MOUSAVI, M. F. 2015. Electrochemical aptamer/antibody based sandwich immunosensor for the detection of EGFR, a cancer biomarker, using gold nanoparticles as a signaling probe. *Biosensors and Bioelectronics,* 74**,** 491-497.

INTERLANDI, G., WETZEL, S. K., SETTANNI, G., PLÜCKTHUN, A. & CAFLISCH, A. 2008. Characterization and Further Stabilization of Designed Ankyrin Repeat Proteins by Combining Molecular Dynamics Simulations and Experiments. *Journal of Molecular Biology,* 375**,** 837-854.

IORDĂNESCU, A., TERTIS, M., CERNAT, A., SUCIU, M., SĂNDULESCU, R. & CRISTEA, C. 2018. Poly-(pyrrole-3-carboxylic acid) Based Nanostructured Platform for the Detection of Carcinoembryonic Antigen. *Electroanalysis,* 30**,** 1100-1106.

JACKSON, Z. 2017. *Production of a novel Affimer based biosensor for the detection of porcine reproductive and respiratory syndrome virus nucleocapsid protein.* University of Leeds.

JEUKEN, L. J. C. 2016. Structure and Modification of Electrode Materials for Protein Electrochemistry. *Adv Biochem Eng Biotechnol,* 158**,** 43-73.

JOHNSON, A., SONG, Q., KO FERRIGNO, P., BUENO, P. R. & DAVIS, J. J. 2012. Sensitive Affimer and Antibody Based Impedimetric Label-Free Assays for C-Reactive Protein. *Analytical Chemistry,* 84**,** 6553-6560.

JOST, C., SCHILLING, J., TAMASKOVIC, R., SCHWILL, M., HONEGGER, A. & PLÜCKTHUN, A. 2013. Structural Basis for Eliciting a Cytotoxic Effect in HER2-Overexpressing Cancer Cells via Binding to the Extracellular Domain of HER2. *Structure,* 21**,** 1979-1991.

KAISTI, M. 2017. Detection principles of biological and chemical FET sensors. *Biosensors and Bioelectronics,* 98**,** 437-448.

KANG, D.-H., GHO, Y.-S., SUH, M.-K. & KANG, C.-H. 2002. Highly sensitive and fast protein detection with coomassie brilliant blue in sodium dodecyl sulfate-polyacrylamide gel electrophoresis. *Bulletin of the Korean Chemical Society,* 23**,** 1511-1512.

KATO, K., ASAI, S., TAGA, H., TOMINAGA, Y., ISHIKAWA, K. & ARAKAWA, Y. 1997. Affinity and kinetic studies for the evaluation of lectin-reactive α-fetoprotein with a biosensor based on surface plasmon resonance. *Hepatology Research,* 8**,** 95-105.

KATSAMBA, P. S., NAVRATILOVA, I., CALDERON-CACIA, M., FAN, L., THORNTON, K., ZHU, M., BOS, T. V., FORTE, C., FRIEND,

D., LAIRD-OFFRINGA, I., TAVARES, G., WHATLEY, J., SHI, E., WIDOM, A., LINDQUIST, K. C., KLAKAMP, S., DRAKE, A., BOHMANN, D., ROELL, M., ROSE, L., DOROCKE, J., ROTH, B., LUGINBUHL, B. & MYSZKA, D. G. 2006. Kinetic analysis of a high-affinity antibody/antigen interaction performed by multiple Biacore users. *Anal Biochem,* 352**,** 208-21.

KAUFMAN, H. L., HÖRIG, H., MEDINA, F. A., GOLDING, S. & CONKRIGHT, W. A. 2000. Strategies for cancer therapy using carcinoembryonic antigen vaccines. *Expert reviews in molecular medicine,* 2**,** 1-24.

KIM, J. Y., KIM, N. K., SOHN, S. K., KIM, Y. W., KIM, K. J., HUR, H., MIN, B. S. & CHO, C. H. 2009. Prognostic value of postoperative CEA clearance in rectal cancer patients with high preoperative CEA levels. *Ann Surg Oncol,* 16**,** 2771-8.

KOIDE, A., BAILEY, C. W., HUANG, X. & KOIDE, S. 1998. The fibronectin type III domain as a scaffold for novel binding proteins1. *Journal of molecular biology,* 284**,** 1141-1151.

KOIDE, A., WOJCIK, J., GILBRETH, R. N., HOEY, R. J. & KOIDE, S. 2012. Teaching an old scaffold new tricks: monobodies constructed using alternative surfaces of the FN3 scaffold. *Journal of molecular biology,* 415**,** 393-405.

KOIDE, S. & SIDHU, S. S. 2009. The importance of being tyrosine: lessons in molecular recognition from minimalist synthetic binding proteins. *ACS Chem Biol,* 4**,** 325-34.

KOKKINOS, C., ECONOMOU, A. & PRODROMIDIS, M. I. 2016. Electrochemical immunosensors: Critical survey of different architectures and transduction strategies. *TrAC Trends in Analytical Chemistry,* 79**,** 88-105.

KONCKI, R. 2007. Recent developments in potentiometric biosensors for biomedical analysis. *Analytica Chimica Acta,* 599**,** 7-15.

KOUTSOUMPELI, E., TIEDE, C., MURRAY, J., TANG, A., BON, R. S., TOMLINSON, D. C. & JOHNSON, S. 2017. Antibody Mimetics for the Detection of Small Organic Compounds Using a Quartz Crystal Microbalance. *Analytical Chemistry,* 89**,** 3051-3058.

KRAFT, A. 2007. Doped Diamond: A Compact Review on a New, Versatile Electrode Material. *Int. J. Electrochem. Sci,* 2**,** 355-385.

KUMAR, S., KUMAR, S., PANDEY, C. M. & MALHOTRA, B. D. Conducting paper based sensor for cancer biomarker detection. Journal of Physics: Conference Series, 2016. IOP Publishing, 012010.

KUMMER, L., HSU, C.-W., DAGLIYAN, O., MACNEVIN, C., KAUFHOLZ, M., ZIMMERMANN, B., DOKHOLYAN, NIKOLAY V., HAHN, KLAUS M. & PLÜCKTHUN, A. 2013. Knowledge-Based Design of a Biosensor to Quantify Localized ERK Activation in Living Cells. *Chemistry & Biology,* 20**,** 847-856.

KUROKI, M., MURAKAMI, M., WAKISAKA, M., KROP-WATOREK, A., OIKAWA, S., NAKAZATO, H., KOSAKI, G. & MATSUOKA, Y. 1992. Epitopes Predominantly Retained on the Carcinoembryonic Antigen Molecules in Plasma of Patients with Malignant Tumors but Not on Those in Plasma of Normal Individuals. *Japanese Journal of Cancer Research,* 83**,** 505-514.

KYLE, H. F., WICKSON, K. F., STOTT, J., BURSLEM, G. M., BREEZE, A. L., TIEDE, C., TOMLINSON, D. C., WARRINER, S. L., NELSON, A., WILSON, A. J. & EDWARDS, T. A. 2015. Exploration of the HIF-1alpha/p300 interface using peptide and Adhiron phage display technologies. *Mol Biosyst,* 11**,** 2738-49.

LABIANCA, R., NORDLINGER, B., BERETTA, G. D., BROUQUET, A., CERVANTES, A. & GROUP, E. G. W. 2010. Primary colon cancer: ESMO Clinical Practice Guidelines for diagnosis, adjuvant treatment and follow-up. *Ann Oncol,* 21 Suppl 5**,** v70-7.

LANGAN, R. C., MULLINAX, J. E., RAIJI, M. T., UPHAM, T., SUMMERS, T., STOJADINOVIC, A. & AVITAL, I. 2013. Colorectal cancer biomarkers and the potential role of cancer stem cells. *J Cancer,* 4**,** 241-50.

LANGE, K., RAPP, B. E. & RAPP, M. 2008. Surface acoustic wave biosensors: a review. *Anal Bioanal Chem,* 391**,** 1509-19.

LECH, G., SLOTWINSKI, R., SLODKOWSKI, M. & KRASNODEBSKI, I. W. 2016. Colorectal cancer tumour markers and biomarkers: Recent therapeutic advances. *World J Gastroenterol,* 22**,** 1745-55.

LEE, J. H. & LEE, S.-W. 2017. The roles of carcinoembryonic antigen in liver metastasis and therapeutic approaches. *Gastroenterology research and practice,* 2017.

LEVI, Z., BIRKENFELD, S., VILKIN, A., BAR-CHANA, M., LIFSHITZ, I., CHARED, M., MAOZ, E. & NIV, Y. 2011. A higher detection rate for colorectal cancer and advanced adenomatous polyp for screening with immunochemical fecal occult blood test than guaiac fecal occult blood test, despite lower compliance rate. A prospective, controlled, feasibility study. *Int J Cancer,* 128**,** 2415-24.

LI, G. & MIAO, P. 2013. Theoretical Background of Electrochemical Analysis. *Electrochemical Analysis of Proteins and Cells.* Berlin, Heidelberg: Springer Berlin Heidelberg.

LI, J., LI, S. & YANG, C. F. 2012. Electrochemical biosensors for cancer biomarker detection. *Electroanalysis,* 24**,** 2213-2229.

LI, X., YU, M., CHEN, Z., LIN, X. & WU, Q. 2017. A sensor for detection of carcinoembryonic antigen based on the polyaniline-Au nanoparticles and gap-based interdigitated electrode. *Sensors and Actuators B: Chemical,* 239**,** 874-882.

LIAO, H.-I., OLSON, C. A., HWANG, S., DENG, H., WONG, E., BARIC, R. S., ROBERTS, R. W. & SUN, R. 2009. mRNA display design of fibronectin-based intrabodies that detect and inhibit severe acute respiratory syndrome coronavirus nucleocapsid protein. *Journal of Biological Chemistry,* 284**,** 17512-17520.

LIPOVSEK, D. 2011. Adnectins: engineered target-binding protein therapeutics. *Protein Eng Des Sel,* 24**,** 3-9.

LISDAT, F. & SCHÄFER, D. 2008. The use of electrochemical impedance spectroscopy for biosensing. *Analytical and Bioanalytical Chemistry,* 391**,** 1555.

LIU, Z. & MA, Z. 2013. Fabrication of an ultrasensitive electrochemical immunosensor for CEA based on conducting long-chain polythiols. *Biosensors and Bioelectronics,* 46**,** 1-7.

LOFBLOM, J., FELDWISCH, J., TOLMACHEV, V., CARLSSON, J., STAHL, S. & FREJD, F. Y. 2010. Affibody molecules: engineered proteins for therapeutic, diagnostic and biotechnological applications. *FEBS Lett,* 584**,** 2670-80.

LÖFBLOM, J., FREJD, F. Y. & STÅHL, S. 2011. Non-immunoglobulin based protein scaffolds. *Current opinion in biotechnology,* 22**,** 843-848.

LONG, F., ZHU, A. & SHI, H. 2013. Recent advances in optical biosensors for environmental monitoring and early warning. *Sensors (Basel),* 13**,** 13928-48.

LOPATA, A., HUGHES, R., TIEDE, C., HEISSLER, S. M., SELLERS, J. R., KNIGHT, P. J., TOMLINSON, D. & PECKHAM, M. 2018. Affimer proteins for F-actin: novel affinity reagents that label F-actin in live and fixed cells. *Sci Rep,* 8**,** 6572.

LU, W., CAO, X., TAO, L., GE, J., DONG, J. & QIAN, W. 2014. A novel label-free amperometric immunosensor for carcinoembryonic antigen based on Ag nanoparticle decorated infinite coordination polymer fibres. *Biosensors and Bioelectronics,* 57**,** 219-225.

LV, H., LI, Y., ZHANG, X., GAO, Z., ZHANG, C., ZHANG, S. & DONG, Y. 2018. Enhanced peroxidase-like properties of Au@Pt DNs/NG/Cu2+ and application of sandwich-type electrochemical immunosensor for highly sensitive detection of CEA. *Biosensors and Bioelectronics,* 112**,** 1-7.

LVOVICH, V. F. 2012. *Impedance spectroscopy: applications to electrochemical and dielectric phenomena*, John Wiley & Sons.

MACDONALD, D. D. 2006. Reflections on the history of electrochemical impedance spectroscopy. *Electrochimica Acta,* 51**,** 1376-1388.

MAGDALENA, M., TAREK, B., LINDVI, G., MARTIN, L., Y., F. F., STEFAN, S. & JOHN, L. 2014. Engineering of a bispecific affibody molecule towards HER2 and HER3 by addition of an albumin-binding domain allows for affinity purification and in vivo half-life extension. *Biotechnology Journal,* 9**,** 1215-1222.

MAHATNIRUNKUL, T. 2017. *One-step gold nanoparticle size-shift assay using synthetic binding proteins and dynamic light scattering.* University of Leeds.

MARSHALL, K. W., MOHR, S., KHETTABI, F. E., NOSSOVA, N., CHAO, S., BAO, W., MA, J., LI, X. J. & LIEW, C. C. 2010. A blood-based biomarker panel for stratifying current risk for colorectal cancer. *Int J Cancer,* 126**,** 1177-86.

MCCREERY, R. L. 2008. Advanced carbon electrode materials for molecular electrochemistry. *Chem Rev,* 108**,** 2646-87.

MIAO, J., WANG, X., LU, L., ZHU, P., MAO, C., ZHAO, H., SONG, Y. & SHEN, J. 2014. Electrochemical immunosensor based on hyperbranched structure for carcinoembryonic antigen detection. *Biosensors and Bioelectronics,* 58**,** 9-16.

MICHEL, M. A., SWATEK, K. N., HOSPENTHAL, M. K. & KOMANDER, D. 2017. Ubiquitin Linkage-Specific Affimers Reveal Insights into K6-Linked Ubiquitin Signaling. *Molecular Cell,* 68**,** 233-246.e5.

MILLNER, P. A., HAYS, H. C., VAKUROV, A., PCHELINTSEV, N. A., BILLAH, M. M. & RODGERS, M. A. 2009. Nanostructured transducer surfaces for electrochemical biosensor construction--interfacing the sensing component with the electrode. *Semin Cell Dev Biol,* 20**,** 34-40.

MIRANDA, F. F., BRIENT-LITZLER, E., ZIDANE, N., PECORARI, F. & BEDOUELLE, H. 2011. Reagentless fluorescent biosensors from artificial families of antigen binding proteins. *Biosensors and Bioelectronics,* 26**,** 4184-4190.

MOLGAARD, K., COMPTE, M., NUNEZ-PRADO, N., HARWOOD, S. L., SANZ, L. & ALVAREZ-VALLINA, L. 2017. Balanced secretion of anti-CEA x anti-CD3 diabody chains using the 2A self-cleaving peptide maximizes diabody assembly and tumor-specific cytotoxicity. *Gene Ther,* 24**,** 208-214.

NAVEEN, M. H., GURUDATT, N. G. & SHIM, Y.-B. 2017. Applications of conducting polymer composites to electrochemical sensors: A review. *Applied Materials Today,* 9**,** 419-433.

NDIEYIRA, J. W., WATARI, M. & MCKENDRY, R. A. 2013. Nanomechanics of drug-target interactions and antibacterial resistance detection. *J Vis Exp***,** e50719.

NGUYEN, H. H., PARK, J., KANG, S. & KIM, M. 2015. Surface plasmon resonance: a versatile technique for biosensor applications. *Sensors (Basel),* 15**,** 10481-510.

NI, X., CASTANARES, M., MUKHERJEE, A. & LUPOLD, S. E. 2011. Nucleic acid aptamers: clinical applications and promising new horizons. *Current Medicinal Chemistry,* 18**,** 4206-4214.

NORD, K., NILSSON, J., NILSSON, B., UHLEN, M. & NYGREN, P. A. 1995. A combinatorial library of an alpha-helical bacterial receptor domain. *Protein Eng,* 8**,** 601-8.

NYGREN, P.-Å. & SKERRA, A. 2004. Binding proteins from alternative scaffolds. *Journal of immunological methods,* 290**,** 3-28.

O'KENNEDY, R., FITZGERALD, S. & MURPHY, C. 2017. Don't blame it all on antibodies – The need for exhaustive characterisation, appropriate handling, and addressing the issues that affect specificity. *TrAC Trends in Analytical Chemistry,* 89**,** 53-59.

O'NEILL, P. M., FLETCHER, J. E., STAFFORD, C. G., DANIELS, P. B. & BACARESE-HAMILTON, T. 1995. Use of an optical biosensor to measure prostate-specific antigen in whole blood. *Sensors and Actuators B: Chemical,* 29**,** 79-83.

OHWADA, A., TAKAHASHI, H., NAGAOKA, I., IWABUCHI, K., MIKAMI, O. & KIRA, S. 1995. Effect of cigarette smoke on the mRNA and protein expression of carcinoembryonic antigen (CEA), a possible chemoattractant for neutrophils in human bronchioloalveolar tissues. *Thorax,* 50**,** 651-657.

PARK, K. S. 2018. Nucleic acid aptamer-based methods for diagnosis of infections. *Biosensors and Bioelectronics,* 102**,** 179-188.

PAVONI, E., FLEGO, M., DUPUIS, M. L., BARCA, S., PETRONZELLI, F., ANASTASI, A. M., D'ALESSIO, V., PELLICCIA, A., VACCARO, P., MONTERIU, G., ASCIONE, A., DE SANTIS, R., FELICI, F., CIANFRIGLIA, M. & MINENKOVA, O. 2006. Selection, affinity maturation, and characterization of a human scFv antibody against CEA protein. *BMC Cancer,* 6**,** 41.

PENG, H. P., LEE, K. H., JIAN, J. W. & YANG, A. S. 2014. Origins of specificity and affinity in antibody-protein interactions. *Proc Natl Acad Sci U S A,* 111**,** E2656-65.

PILEHVAR, S., DIERCKX, T., BLUST, R., BREUGELMANS, T. & DE WAEL, K. 2014. An Electrochemical Impedimetric Aptasensing Platform for Sensitive and Selective Detection of Small Molecules Such as Chloramphenicol. *Sensors,* 14**,** 12059-12069.

PISOSCHI, A. M. 2012. Glucose Determination by Biosensors. *Biochem. Anal. Biochem.,* 1**,** 1-2.

PLUCKTHUN, A. 2015. Designed ankyrin repeat proteins (DARPins): binding proteins for research, diagnostics, and therapy. *Annu Rev Pharmacol Toxicol,* 55**,** 489-511.

PRITCHARD, C. C. & GRADY, W. M. 2011. Colorectal cancer molecular biology moves into clinical practice. *Gut,* 60**,** 116-29.

PRODROMIDIS, M. I. 2010. Impedimetric immunosensors—A review. *Electrochimica Acta,* 55**,** 4227-4233.

QURESHI, A., GURBUZ, Y. & NIAZI, J. H. 2015. Label-free capacitance based aptasensor platform for the detection of HER2/ErbB2 cancer biomarker in serum. *Sensors and Actuators B: Chemical,* 220**,** 1145-1151.

RAHMAN, M. M., AHAMMAD, A. J. S., JIN, J.-H., AHN, S. J. & LEE, J.-J. 2010. A Comprehensive Review of Glucose Biosensors Based on Nanostructured Metal-Oxides. *Sensors,* 10**,** 4855.

RAINA, M. 2013. *Development of an impedimetric biosensor using a non-antibody based biological recognition molecule*, University of Leeds.

RAINA, M., SHARMA, R., DEACON, S. E., TIEDE, C., TOMLINSON, D., DAVIES, A. G., MCPHERSON, M. J. & WALTI, C. 2015. Antibody mimetic receptor proteins for label-free biosensors. *Analyst,* 140**,** 803-810.

RANDLES, J. E. B. 1947. Kinetics of rapid electrode reactions. *Discussions of the Faraday Society,* 1**,** 11-19.

RANDVIIR, E. P. & BANKS, C. E. 2013. Electrochemical impedance spectroscopy: an overview of bioanalytical applications. *Analytical Methods,* 5**,** 1098-1115.

RANJAN, R., ESIMBEKOVA, E. N. & KRATASYUK, V. A. 2017. Rapid biosensing tools for cancer biomarkers. *Biosensors and Bioelectronics,* 87**,** 918-930.

RAVALLI, A., DA ROCHA, C. G., YAMANAKA, H. & MARRAZZA, G. 2015. A label-free electrochemical affisensor for cancer marker detection: The case of HER2. *Bioelectrochemistry,* 106**,** 268-275.

RAWLINGS, A. E., BRAMBLE, J. P., TANG, A. A. S., SOMNER, L. A., MONNINGTON, A. E., COOKE, D. J., MCPHERSON, M. J., TOMLINSON, D. C. & STANILAND, S. S. 2015. Phage display

selected magnetite interacting Adhirons for shape controlled nanoparticle synthesis. *Chem Sci,* 6**,** 5586-5594.

REIMERS, M. S., ZEESTRATEN, E. C., KUPPEN, P. J., LIEFERS, G. J. & VAN DE VELDE, C. J. 2013. Biomarkers in precision therapy in colorectal cancer. *Gastroenterol Rep (Oxf),* 1**,** 166-83.

RENBERG, B., NORDIN, J., MERCA, A., UHLÉN, M., FELDWISCH, J., NYGREN, P.-Å. & ERIKSSON KARLSTRÖM, A. 2007. Affibody Molecules in Protein Capture Microarrays: Evaluation of Multidomain Ligands and Different Detection Formats. *Journal of Proteome Research,* 6**,** 171-179.

RENBERG, B., NYGREN, P.-Å., EKLUND, M. & KARLSTRÖM, A. E. 2004. Fluorescence resonance energy transfer-based detection of analytes using antiidiotypic affinity protein pairs. *Analytical Biochemistry,* 334**,** 72-80.

RENBERG, B., SHIROYAMA, I., ENGFELDT, T., NYGREN, P.-Å. & KARLSTRÖM, A. E. 2005. Affibody protein capture microarrays: Synthesis and evaluation of random and directed immobilization of affibody molecules. *Analytical Biochemistry,* 341**,** 334-343.

ROBINSON, J. I., BAXTER, E. W., OWEN, R. L., THOMSEN, M., TOMLINSON, D. C., WATERHOUSE, M. P., WIN, S. J., NETTLESHIP, J. E., TIEDE, C., FOSTER, R. J., OWENS, R. J., FISHWICK, C. W. G., HARRIS, S. A., GOLDMAN, A., MCPHERSON, M. J. & MORGAN, A. W. 2018. Affimer proteins inhibit immune complex binding to FcγRIIIa with high specificity through competitive and allosteric modes of action. *Proceedings of the National Academy of Sciences,* 115**,** E72-E81.

ROMER, T., LEONHARDT, H. & ROTHBAUER, U. 2011. Engineering antibodies and proteins for molecular in vivo imaging. *Current opinion in biotechnology,* 22**,** 882-887.

RONKAINEN, N. J., HALSALL, H. B. & HEINEMAN, W. R. 2010. Electrochemical biosensors. *Chem Soc Rev,* 39**,** 1747-63.

ROSS, J. S., TORRES-MORA, J., WAGLE, N., JENNINGS, T. A. & JONES, D. M. 2010. Biomarker-based prediction of response to therapy for colorectal cancer: current perspective. *Am J Clin Pathol,* 134**,** 478-90.

RUSHWORTH, J., AHMED, A. & MILLNER, P. 2013a. Midland Blotting: A Rapid, Semi-Quantitative Method for Biosensor Surface Characterization. *J Biosens Bioelectron,* 4**,** 146.

RUSHWORTH, J. V., AHMED, A., GRIFFITHS, H. H., POLLOCK, N. M., HOOPER, N. M. & MILLNER, P. A. 2014. A label-free electrical impedimetric biosensor for the specific detection of Alzheimer's amyloid-beta oligomers. *Biosens Bioelectron,* 56**,** 83-90.

RUSHWORTH, J. V., HIRST, N. A., GOODE, J. A., PIKE, D. J., AHMED, A. & MILLNER, P. A. 2013b. Impedimetric biosensors for medical applications current progress and challenges. *Biomedical and nanomedical technologies.*

SANIZ PASTOR, N. 2008. *Generation and characterisation of designed ankyrin repeat proteins for targeting carcinoembryonic antigen.* Ph.D Ph.D, University College London.

SANTOSH, B. & YADAVA, P. K. 2014. Nucleic acid aptamers: research tools in disease diagnostics and therapeutics. *Biomed Res Int,* 2014**,** 540451.

SCHILLING, J., SCHÖPPE, J. & PLÜCKTHUN, A. 2014. From DARPins to LoopDARPins: Novel LoopDARPin Design Allows the Selection of Low Picomolar Binders in a Single Round of Ribosome Display. *Journal of Molecular Biology,* 426**,** 691-721.

SCHÜTZ, M., BATYUK, A., KLENK, C., KUMMER, L., DE PICCIOTTO, S., GÜLBAKAN, B., WU, Y., NEWBY, G. A., ZOSEL, F., SCHÖPPE, J., SEDLÁK, E., MITTL, P. R. E., ZENOBI, R., WITTRUP, K. D. & PLÜCKTHUN, A. 2016. Generation of Fluorogen-Activating Designed Ankyrin Repeat Proteins (FADAs) as Versatile Sensor Tools. *Journal of Molecular Biology,* 428**,** 1272-1289.

SCOTT, A. M., WOLCHOK, J. D. & OLD, L. J. 2012. Antibody therapy of cancer. *Nature Reviews Cancer,* 12**,** 278.

SEOKHEUN, C. & JUNSEOK, C. 2010. Methods of reducing non-specific adsorption in microfluidic biosensors. *Journal of Micromechanics and Microengineering,* 20**,** 075015.

SHA, F., SALZMAN, G., GUPTA, A. & KOIDE, S. 2017. Monobodies and other synthetic binding proteins for expanding protein science. *Protein Sci,* 26**,** 910-924.

SHAH, R., JONES, E., VIDART, V., KUPPEN, P. J., CONTI, J. A. & FRANCIS, N. K. 2014. Biomarkers for early detection of colorectal cancer and polyps: systematic review. *Cancer Epidemiol Biomarkers Prev,* 23**,** 1712-28.

SHAHIDAN, M. A. 2012. *Development of impedimetric biosensors for carbohydrate detection.* University of Leeds.

SHAN, W., PAN, Y., FANG, H., GUO, M., NIE, Z., HUANG, Y. & YAO, S. 2014. An aptamer-based quartz crystal microbalance biosensor for sensitive and selective detection of leukemia cells using silver-enhanced gold nanoparticle label. *Talanta,* 126**,** 130-135.

SHARMA, R., DEACON, S. E., NOWAK, D., GEORGE, S. E., SZYMONIK, M. P., TANG, A. A. S., TOMLINSON, D. C., DAVIES, A. G., MCPHERSON, M. J. & WÄLTI, C. 2016a. Label-free electrochemical impedance biosensor to detect human interleukin-8 in serum with sub-pg/ml sensitivity. *Biosensors and Bioelectronics,* 80**,** 607-613.

SHARMA, S., BYRNE, H. & O'KENNEDY, R. J. 2016b. Antibodies and antibody-derived analytical biosensors. *Essays Biochem,* 60**,** 9-18.

SHARMA, S., BYRNE, H. & O'KENNEDY, R. J. 2016c. Antibodies and antibody-derived analytical biosensors. *Essays in biochemistry,* 60**,** 9-18.

SHARMA, S., ZAPATERO-RODRÍGUEZ, J., SAXENA, R., O'KENNEDY, R. & SRIVASTAVA, S. 2018. Ultrasensitive direct impedimetric immunosensor for detection of serum HER2. *Biosensors and Bioelectronics,* 106**,** 78-85.

SHEKARI, Z., ZARE, H. R. & FALAHATI, A. 2017. Developing an Impedimetric Aptasensor for Selective Label–Free Detection of CEA as a Cancer Biomarker Based on Gold Nanoparticles Loaded in Functionalized Mesoporous Silica Films. *Journal of The Electrochemical Society,* 164**,** B739-B745.

SHOICHI, I., MASAHIDE, K., MASATORA, H., SHINZO, O., HIROSHI, N., GORO, K. & YUJI, M. 1992. Epitope mapping of the carcinoembryonic antigen with various related recombinant proteins expressed in chinese hamster ovary cells and 25 distinct monoclonal antibodies. *Molecular Immunology,* 29**,** 229-240.

SKERRA, A. 2007. Alternative non-antibody scaffolds for molecular recognition. *Curr Opin Biotechnol,* 18**,** 295-304.

STADLER, L. K. J., HOFFMANN, T., TOMLINSON, D. C., SONG, Q., LEE, T., BUSBY, M., NYATHI, Y., GENDRA, E., TIEDE, C., FLANAGAN, K., COCKELL, S. J., WIPAT, A., HARWOOD, C., WAGNER, S. D., KNOWLES, M. A., DAVIS, J. J., KEEGAN, N. & KO FERRIGNO, P. 2011. Structure−function studies of an engineered scaffold protein derived from Stefin A. II: Development and applications of the SQT variant. *Protein Engineering, Design and Selection,* 24**,** 751-763.

STAHL, S., GRASLUND, T., ERIKSSON KARLSTROM, A., FREJD, F. Y., NYGREN, P. A. & LOFBLOM, J. 2017. Affibody Molecules in Biotechnological and Medical Applications. *Trends Biotechnol,* 35**,** 691-712.

STEELAND, S., VANDENBROUCKE, R. E. & LIBERT, C. 2016. Nanobodies as therapeutics: big opportunities for small antibodies. *Drug Discov Today,* 21**,** 1076-113.

SU, B. B., SHI, H. & WAN, J. 2012. Role of serum carcinoembryonic antigen in the detection of colorectal cancer before and after surgical resection. *World J Gastroenterol,* 18**,** 2121-6.

SUN, X., HUI, N. & LUO, X. 2017. Reagentless and label-free voltammetric immunosensor for carcinoembryonic antigen based on polyaniline nanowires grown on porous conducting polymer composite. *Microchimica Acta,* 184**,** 889-896.

TAGHDISI, S. M., DANESH, N. M., RAMEZANI, M., EMRANI, A. S. & ABNOUS, K. 2018. A Novel Electrochemical Aptasensor for Carcinoembryonic Antigen Detection Based on Target-induced Bridge Assembly. *Electroanalysis,* 30**,** 1734-1739.

TAMASKOVIC, R., SIMON, M., STEFAN, N., SCHWILL, M. & PLÜCKTHUN, A. 2012. Chapter five - Designed Ankyrin Repeat Proteins (DARPins): From Research to Therapy. *In:* WITTRUP, K. D. & VERDINE, G. L. (eds.) *Methods in Enzymology.* Academic Press.

TAMAYO, J., KOSAKA, P. M., RUZ, J. J., SAN PAULO, A. & CALLEJA, M. 2013. Biosensors based on nanomechanical systems. *Chem Soc Rev,* 42**,** 1287-311.

TANAKA, T. 2009. Colorectal carcinogenesis: review of human and experimental animal studies. *Journal of carcinogenesis,* 8.

TANG, H., CHEN, J., NIE, L., KUANG, Y. & YAO, S. 2007. A label-free electrochemical immunoassay for carcinoembryonic antigen (CEA) based on gold nanoparticles (AuNPs) and nonconductive polymer film. *Biosensors and Bioelectronics,* 22**,** 1061-1067.

TCHOUPA, A. K., SCHUHMACHER, T. & HAUCK, C. R. 2014. Signaling by epithelial members of the CEACAM family – mucosal docking sites for pathogenic bacteria. *Cell Communication and Signaling,* 12**,** 27.

THEURILLAT, J.-P., DREIER, B., NAGY-DAVIDESCU, G., SEIFERT, B., BEHNKE, S., ZÜRRER-HÄRDI, U., INGOLD, F., PLÜCKTHUN, A. & MOCH, H. 2010. Designed ankyrin repeat proteins: a novel tool for testing epidermal growth factor receptor 2 expression in breast cancer. *Modern Pathology,* 23**,** 1289.

THOMAS, P., TOTH, C. A., SAINI, K. S., JESSUP, J. M. & STEELE JR, G. 1990. The structure, metabolism and function of the carcinoembryonic antigen gene family. *Biochimica et Biophysica Acta (BBA)-Reviews on Cancer,* 1032**,** 177-189.

TIEDE, C., BEDFORD, R., HESELTINE, S. J., SMITH, G., WIJETUNGA, I., ROSS, R., ALQALLAF, D., ROBERTS, A. P., BALLS, A., CURD, A., HUGHES, R. E., MARTIN, H., NEEDHAM, S. R., ZANETTI-DOMINGUES, L. C., SADIGH, Y., PEACOCK, T. P., TANG, A. A., GIBSON, N., KYLE, H., PLATT, G. W., INGRAM, N., TAYLOR, T., COLETTA, L. P., MANFIELD, I., KNOWLES, M., BELL, S., ESTEVES, F., MAQBOOL, A., PRASAD, R. K., DRINKHILL, M., BON, R. S., PATEL, V., GOODCHILD, S. A., MARTIN-FERNANDEZ, M., OWENS, R. J., NETTLESHIP, J. E., WEBB, M. E., HARRISON, M., LIPPIAT, J. D., PONNAMBALAM, S., PECKHAM, M., SMITH, A., FERRIGNO, P. K., JOHNSON, M., MCPHERSON, M. J. & TOMLINSON, D. C. 2017. Affimer proteins are versatile and renewable affinity reagents. *Elife,* 6.

TIEDE, C., TANG, A. A. S., DEACON, S. E., MANDAL, U., NETTLESHIP, J. E., OWEN, R. L., GEORGE, S. E., HARRISON, D. J., OWENS, R. J., TOMLINSON, D. C. & MCPHERSON, M. J. 2014. Adhiron: a stable and versatile peptide display scaffold for molecular recognition applications. *Protein Engineering Design & Selection,* 27**,** 145-155.

TIERNAN, J. P., INGRAM, N., MARSTON, G., PERRY, S. L., RUSHWORTH, J. V., COLETTA, P. L., MILLNER, P. A., JAYNE, D. G. & HUGHES, T. A. 2015. CEA-targeted nanoparticles allow specific in vivo fluorescent imaging of colorectal cancer models. *Nanomedicine (Lond),* 10**,** 1223-31.

TOTHILL, I. E. 2009. Biosensors for cancer markers diagnosis. *Semin Cell Dev Biol,* 20**,** 55-62.

TUCCERI, R. 2013. Non-Conducting Poly (O-Aminophenol) Films in the Field of the Bioelectrochemistry. *American Journal of Analytical Chemistry,* 4**,** 13-26.

TULLIUS, R. M. 2017. *High-throughput biosensing using chiral plasmonic nanostructures.* University of Glasgow.

TURNER, A. P. 2013. Biosensors: sense and sensibility. *Chem Soc Rev,* 42**,** 3184-96.

ULUDAG, Y. & TOTHILL, I. E. 2012. Cancer Biomarker Detection in Serum Samples Using Surface Plasmon Resonance and Quartz Crystal Microbalance Sensors with Nanoparticle Signal Amplification. *Analytical Chemistry,* 84**,** 5898-5904.

VANEYCKEN, I., GOVAERT, J., VINCKE, C., CAVELIERS, V., LAHOUTTE, T., DE BAETSELIER, P., RAES, G., BOSSUYT, A., MUYLDERMANS, S. & DEVOOGDT, N. 2010. In vitro analysis and in vivo tumor targeting of a humanized, grafted nanobody in mice using pinhole SPECT/micro-CT. *J Nucl Med,* 51**,** 1099-106.

VASHIST, S. K. & VASHIST, P. 2011. Recent Advances in Quartz Crystal Microbalance-Based Sensors. *Journal of Sensors,* 2011**,** 13.

VELASCO-GARCIA, M. N. 2009. Optical biosensors for probing at the cellular level: a review of recent progress and future prospects. *Semin Cell Dev Biol,* 20**,** 27-33.

VUSA, C. S. R., VENKATESAN, M., K, A., BERCHMANS, S. & ARUMUGAM, P. 2017. Tactical tuning of the surface and interfacial properties of graphene: A Versatile and rational electrochemical approach. *Sci Rep,* 7**,** 8354.

WANG, H., MENG, A. M., LI, S. H. & ZHOU, X. L. 2017a. A nanobody targeting carcinoembryonic antigen as a promising molecular probe for non-small cell lung cancer. *Mol Med Rep,* 16**,** 625-630.

WANG, J. 2008. Electrochemical Glucose Biosensors. *Chemical Reviews,* 108**,** 814-825.

WANG, J., RIVAS, G., CAI, X., CHICHARRO, M., PARRADO, C., DONTHA, N., BEGLEITER, A., MOWAT, M., PALECEK, E. & NIELSEN, P. E. 1997. Detection of point mutation in the p53 gene using a peptide nucleic acid biosensor. *Analytica Chimica Acta,* 344**,** 111-118.

WANG, R., CHEN, X., MA, J. & MA, Z. 2013. Ultrasensitive detection of carcinoembryonic antigen by a simple label-free immunosensor. *Sensors and Actuators B: Chemical,* 176**,** 1044-1050.

WANG, T., GREEN, R., NAIR, R., HOWELL, M., MOHAPATRA, S., GULDIKEN, R. & MOHAPATRA, S. 2015. Surface Acoustic Waves (SAW)-Based Biosensing for Quantification of Cell Growth in 2D and 3D Cultures. *Sensors,* 15**,** 29909.

WANG, W., GUO, Y., TIEDE, C., CHEN, S., KOPYTYNSKI, M., KONG, Y., KULAK, A., TOMLINSON, D., CHEN, R., MCPHERSON, M. & ZHOU, D. 2017b. Ultraefficient Cap-Exchange Protocol To Compact Biofunctional Quantum Dots for Sensitive Ratiometric Biosensing and Cell Imaging. *ACS Applied Materials & Interfaces,* 9**,** 15232-15244.

WANG, Y., ZHANG, Z., JAIN, V., YI, J., MUELLER, S., SOKOLOV, J., LIU, Z., LEVON, K., RIGAS, B. & RAFAILOVICH, M. H. 2010. Potentiometric sensors based on surface molecular imprinting: Detection of cancer biomarkers and viruses. *Sensors and Actuators B: Chemical,* 146**,** 381-387.

WECKMAN, N. E., MCRAE, C., KO FERRIGNO, P. & SESHIA, A. A. 2016. Comparison of the specificity and affinity of surface immobilised Affimer binders using the quartz crystal microbalance. *Analyst,* 141**,** 6278-6286.

WEIDLE, U. H., AUER, J., BRINKMANN, U., GEORGES, G. & TIEFENTHALER, G. 2013. The emerging role of new protein scaffold-based agents for treatment of cancer. *Cancer Genomics-Proteomics,* 10**,** 155-168.

WELCH, N. G., SCOBLE, J. A., MUIR, B. W. & PIGRAM, P. J. 2017. Orientation and characterization of immobilized antibodies for improved immunoassays (Review). *Biointerphases,* 12**,** 02D301.

WEN, W., HUANG, J.-Y., BAO, T., ZHOU, J., XIA, H.-X., ZHANG, X.-H., WANG, S.-F. & ZHAO, Y.-D. 2016. Increased electrocatalyzed performance through hairpin oligonucleotide aptamer-functionalized gold nanorods labels and graphene-streptavidin nanomatrix: Highly selective and sensitive electrochemical biosensor of carcinoembryonic antigen. *Biosensors and Bioelectronics,* 83**,** 142-148.

WOLFE, C. A. & HAGE, D. S. 1995. Studies on the rate and control of antibody oxidation by periodate. *Analytical biochemistry,* 231**,** 123-130.

WU, H. H., LIN, W. C. & TSAI, K. W. 2014. Advances in molecular biomarkers for gastric cancer: miRNAs as emerging novel cancer markers. *Expert Rev Mol Med,* 16**,** e1.

WU, X.-Z., MA, F. & WANG, X.-L. 2010. Serological diagnostic factors for liver metastasis in patients with colorectal cancer. *World journal of gastroenterology: WJG,* 16**,** 4084.

XIE, C., TIEDE, C., ZHANG, X., WANG, C., LI, Z., XU, X., MCPHERSON, M. J., TOMLINSON, D. C. & XU, W. 2017. Development of an Affimer-antibody combined immunological diagnosis kit for glypican-3. *Sci Rep,* 7**,** 9608.

XU, S., ZHANG, R., ZHAO, W., ZHU, Y., WEI, W., LIU, X. & LUO, J. 2017. Self-assembled polymeric nanoparticles film stabilizing gold nanoparticles as a versatile platform for ultrasensitive detection of carcino-embryonic antigen. *Biosensors and Bioelectronics,* 92**,** 570-576.

XUE, X., WANG, B., DU, W., ZHANG, C., SONG, Y., CAI, Y., CEN, D., WANG, L., XIONG, Y., JIANG, P., ZHU, S., ZHAO, K.-N. & ZHANG, L. 2016. Generation of affibody molecules specific for HPV16 E7 recognition. *Oncotarget,* 7**,** 73995-74005.

YARMAN, A., TURNER, A. & SCHELLER, F. 2014. Electropolymers for (nano-) imprinted biomimetic biosensors. *Nanosensors for chemical and biological applications.* Elsevier.

YAZAKI, P. J., LEE, B., CHANNAPPA, D., CHEUNG, C.-W., CROW, D., CHEA, J., POKU, E., LI, L., ANDERSEN, J. T. & SANDLIE, I. 2012. A series of anti-CEA/anti-DOTA bispecific antibody formats evaluated for pre-targeting: comparison of tumor uptake and blood clearance. *Protein Engineering, Design & Selection,* 26**,** 187-193.

YEH, C.-H., SU, K.-F. & LIN, Y.-C. 2016. Development of an impedimetric immunobiosensor for measurement of carcinoembryonic antigen. *Sensors and Actuators A: Physical,* 241**,** 203-211.

YIN, T. & QIN, W. 2013. Applications of nanomaterials in potentiometric sensors. *TrAC Trends in Analytical Chemistry,* 51**,** 79-86.

YIU, A. J. & YIU, C. Y. 2016. Biomarkers in Colorectal Cancer. *Anticancer Res,* 36**,** 1093-102.

YOUNG, P. E. & WOMELDORPH, C. M. 2013. Colonoscopy for colorectal cancer screening. *J Cancer,* 4**,** 217-26.

YU, X., YANG, Y. P., DIKICI, E., DEO, S. K. & DAUNERT, S. 2017. Beyond Antibodies as Binding Partners: The Role of Antibody Mimetics in Bioanalysis. *Annu Rev Anal Chem (Palo Alto Calif),* 10**,** 293-320.

YU, Y., ZHANG, Q., BUSCAGLIA, J., CHANG, C.-C., LIU, Y., YANG, Z., GUO, Y., WANG, Y., LEVON, K. & RAFAILOVICH, M. 2016. Quantitative real-time detection of carcinoembryonic antigen (CEA) from pancreatic cyst fluid using 3-D surface molecular imprinting. *Analyst,* 141**,** 4424-4431.

YUQING, M., JIANRONG, C. & XIAOHUA, W. 2004. Using electropolymerized non-conducting polymers to develop enzyme amperometric biosensors. *Trends Biotechnol,* 22**,** 227-31.

ZHANG, X., ZOU, Y., AN, C., YING, K., CHEN, X. & WANG, P. 2015. Sensitive detection of carcinoembryonic antigen in exhaled breath condensate using surface acoustic wave immunosensor. *Sensors and Actuators B: Chemical,* 217**,** 100-106.

ZHANG, Y. & HELLER, A. 2005. Reduction of the Nonspecific Binding of a Target Antibody and of Its Enzyme-Labeled Detection Probe Enabling Electrochemical Immunoassay of an Antibody through the 7 pg/mL−100 ng/mL (40 fM−400 pM) Range. *Analytical Chemistry,* 77**,** 7758-7762.

ZHANG, Y., ZHANG, M., WEI, Q., GAO, Y., GUO, L., AL-GHANIM, K. A., MAHBOOB, S. & ZHANG, X. 2016. An easily fabricated electrochemical sensor based on a graphene-modified glassy carbon electrode for determination of octopamine and tyramine. *Sensors,* 16**,** 535.

ZHURAUSKI, P., ARYA, S. K., JOLLY, P., TIEDE, C., TOMLINSON, D. C., KO FERRIGNO, P. & ESTRELA, P. 2018. Sensitive and selective Affimer-functionalised interdigitated electrode-based capacitive biosensor for Her4 protein tumour biomarker detection. *Biosensors and Bioelectronics,* 108**,** 1-8.

Appendix

Appendix 1: List of buffers used

Name	Ingredients	pH	Application
PBS	137 mM NaCl, 2.7 mM KCl, 10 mM Na_2HPO_4, 1.8 mM KH_2PO_4	7.4	Genereal use
PBST	PBS + 0.1% Tween-20	7.4	ELISA
LB	Yeast extract (5 g.l^{-1}); tryptone (10 g.l^{-1}) ; NaCl (5 g.l^{-1})	7.4	Bacterial cell culture media
2TY	Yeast extract (10 g.l^{-1}); tryptone (16 g.l^{-1}) ; NaCl (5 g.l^{-1})	7.4	Bacterial cell culture media
Glycine elution buffer	200mM Glycine	2.2	Bio-panning
Tris-Hcl neutralization buffer	1M Tris-Hcl	9.1	Bio-panning
Tris-Hcl neutralization buffer	1M Tris-Hcl	7	Bio-panning
Triethylamine	100mM Triethylamine		Bio-panning
SOB medium	Yeast extract (5 g.l^{-1}); tryptone (20 g.l^{-1}) ; NaCl (0.5 g.l^{-1}), 1M $MgCl_2$ and 1M $MgSO_4$	7	Bacterial Transformation
SOC medium	SOB + 20mM Glucose	7	Bacterial Transformation
Lysis buffer	50 mM NaH_2PO_4; 300 mM NaCl; 30 mM Imidazole; 10% Glycerol	7.4	Protein extraction
Wash buffer	50 mM NaH_2PO_4; 500 mM NaCl; 30 mM Imidazole	7.4	Protein extraction
Elution buffer	50mM NaH_2PO_4, 500 mM NaCl; 300 mM Imidazole; 20% Glycerol	7.4	Protein extraction
Tris-Glycine-SDS Running buffer	25 mM Tris, 192 mM glycine, 0.1% SDS	8.3	SDS-PAGE
Tris-Glycine Transfer buffer	26 mM Tris, 192 mM glycine	8.3	Western blot
0.1 % TBST	TBS + 0.1% Tween-20	7.4	Western blot
0.3 % TBST	TBS + 0.3% Tween-20	7.4	Western blot

Appendix 2 : Composition of PCR mixture

Component	Final concentration	Volume (μL)
5X Phusion buffer	1X	5
25 mM dNTPs mix	200 μM	0.2
DMSO	3%	0.75
Forward Primer (10μM)	0.8 μM	2
Reverse Primer (10μM)	0.8 μM	2
Phusion DNA Polymerase	0.02 units/μl	0.25
Template DNA	< 250 ng	1
Nuclease free water		13.8

Appendix 3: Poster presented at the NIHR Colorectal Therapies HTC'S National meeting 2016-Technologies driving precision medicine

Development of Affimer-based Impedimetric Biosensor for Colorectal Cancer Biomarker Detection

Shazana Hilda Shamsuddin[1*], Darren Tomlinson[2], Michael McPherson[2] and Paul Millner[1]
[1]The Leeds Bionanotechnology Group, School of Biomedical Sciences, [2]Bioscreening Technology Group, School of Molecular and Cellular Biology
*bsshs@leeds.ac.uk

UNIVERSITY OF LEEDS

1 Introduction

Carcinoembryogenic antigen (CEA)

- Secreted in the blood by the tumour
- Clinically used as a **prognostic biomarker** after diagnosis & **surveillance biomarker** for tumour recurrence in post-operative CrC patients.

Colorectal cancer (CrC) [1,2]
2nd leading killer in the UK in 2014.

Advantage of biosensor devices
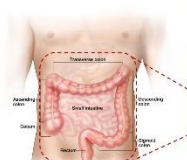
- Point-of-care (POC) devices
- Highly sensitive and specific
- Rapid response time
- User friendly & low cost
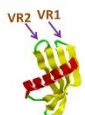
Affimer[3] - artificial binding protein scaffolds

- Synthetic binding protein that possess similar functions to antibody but is small in size and highly thermostable.

2 Aims of the study

Development of electrochemical affinity biosensor using artificial binding proteins (Affimers) as bioreceptors for colorectal cancer.

DropSens gold electrode
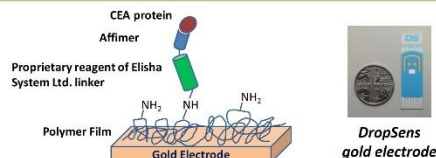
3 Results & Discussion

3.1 Screening of CEA binders using Affimer libraries
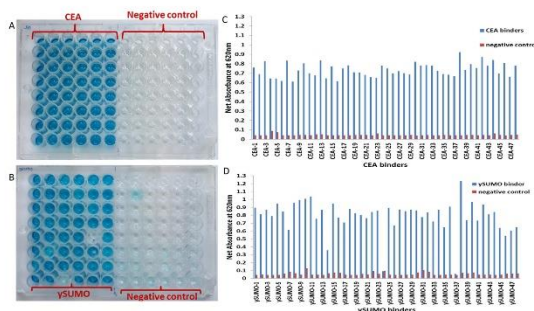
CEA protein was biotinylated for phage display using the Affimer libraries. After three panning rounds , 48 Affimer clones were isolated and investigated for binding to CEA using phage ELISA (Fig. 3.1 A and C). ySUMO was used as positive control (Fig. 3.1 B and D). The phage ELISA showed a 85% positive hit rate and three unique Affimer binders were isolated.

3.2 Characterization of CEA protein secreted from LoVo cells using Affimers as monoclonal reagent
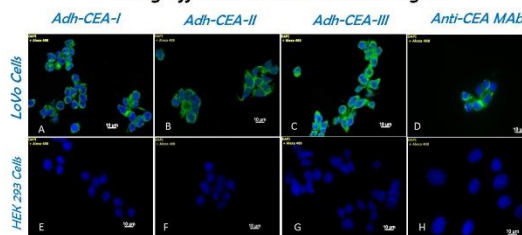
Immunofluorescence staining using Affimers (Fig. 3.2 A-C) as monoclonal reagent showed that CEA protein presents on the cell membrane of LoVo cells which coincides with CEA being membrane–anchored glycoprotein. Similar expression was seen when using anti-CEA monoclonal antibody as positive control (Fig. 3.2 D). No expression of CEA protein was found in the HEK 293 cells which were used as a negative control (Fig. 3.2 E-H).

3.3 Immobilization of Affimers onto gold electrode
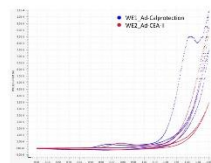
Specific (Ad-CEA-II) and non-specific (Ad-Calprotectin) Affimers were deposited onto gold electrode using a proprietary reagent of Elisha System Ltd. Linker via cyclic voltammery.

3.4 CEA detection
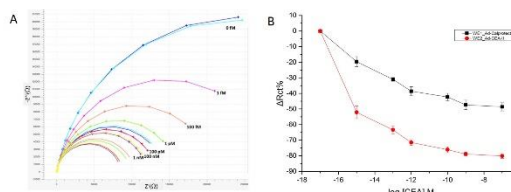
Sensor interrogation was done by measuring the impedance signal from 0.25 to 2.5 KHz which is plotted as Nyquist plot (Fig. 3.4 A). The percentage change in Rct showed that the sensor was highly sensitive with limit of detection (LOD) at 1 fM which is significantly lower than the basal clinical levels of 25 pM. The detection range is 1 fM -100 nM.

4 Future works

The performance of Affimer-based biosensor will be compared with whole antibody based sensor. The sensitivity, specificity and efficiency of these sensors will be compared with the gold standard technique which is the ELISA.

5 References and Acknowledgments

1. The website of the National Cancer Institute (http://www.cancer.gov)
2. http://www.cancerresearchuk.org/cancer-info/cancerstats/types/bowel
3. Tiede, C. et al., 2014. Adhiron: a stable and versatile peptide display scaffold for molecular recognition applications. Protein Engineering Design & Selection, 27, 145-155.
SHS is sponsored by the Malaysian Government scholarship.
Special thanks to all Millner's group for their invaluable assistance.

Development of an electrochemical affinity biosensor using Affimer as biorecognition element for colorectal cancer biomarker detection

Shazana Hilda Shamsuddin[1*], Darren Tomlinson[2], Michael McPherson[2] and Paul Millner[1]
[1]The Leeds Bionanotechnology Group, School of Biomedical Sciences, [2]Bioscreening Technology Group, School of Molecular and Cellular Biology
*bsshs@leeds.ac.uk

UNIVERSITY OF LEEDS

1 Introduction

Carcinoembryogenic antigen (CEA)

> Secreted in the blood by the tumour
> Clinically used as a **prognostic biomarker** after diagnosis & **surveillance biomarker** for tumour recurrence in post-operative CrC patients.

Colorectal cancer (CrC) [1,2]
2nd leading killer in the UK in 2014

Advantage of biosensor devices
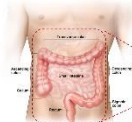
- Point-of-care (POC) devices
- Highly sensitive and specific
- Rapid response time

Affimer[3]- artificial binding protein scaffolds

> Synthetic binding protein that possess similar functions to antibody but is small in size and highly thermostable.
> Easy to produce in large quantities inexpensively

2 Aims of the study

Development of electrochemical affinity biosensor using artificial binding proteins (Affimers) as bioreceptors for colorectal cancer detection.

DropSens gold electrode
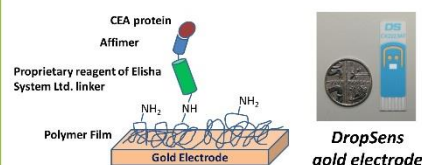
3 Results & Discussion

3.1 Characterization of CEA protein secreted from LoVo cells using Affimers as monoclonal reagent
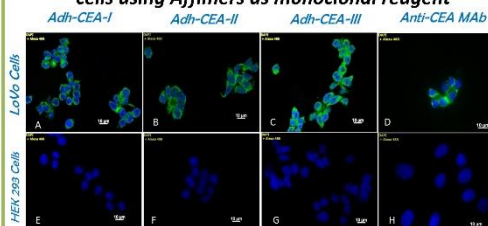
Three unique Affimer binders against CEA were screened and isolated from phage display libraries. The specificity of these binders were evaluated via immunofluorescence staining. Results showed that Anti-CEA-Affimers (Fig. 3.1 A-C) recognized CEA protein presents on the cell membrane of LoVo cells which coincides with CEA being membrane–anchored glycoprotein. Similar expression was seen when using anti-CEA monoclonal antibody as positive control (Fig. 3.1 D). No expression of CEA protein was found in the HEK 293 cells which were used as a negative control (Fig. 3.1 E-H).

3.2 Immobilization of Affimers onto screen printed gold electrode
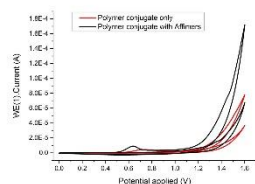
Specific (Anti-CEA Affimer) and non-specific (Anti-Calprotectin Affimer) were deposited onto screen printed gold electrode using proprietary reagent of Elisha System Ltd. Linker via cyclic voltammery (black line) .

3.3 CEA detection
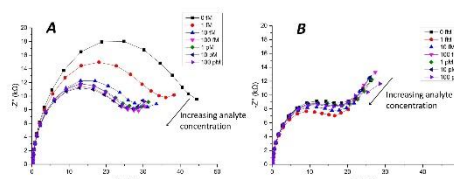
Sensor interrogation was done by measuring the impedance signal from 0.25 to 2.5 KHz which is plotted as Nyquist plot (Fig. 3.3 (A) shows the Nyquist plot of CEA-Affimer sensor and (B) Calprotectin-Affimer sensor as negative control).
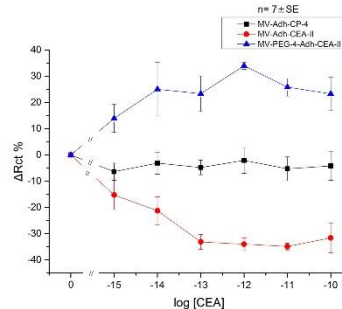
The percentage change in Rct showed that the sensor was highly sensitive with limit of detection (LOD) at 1 fM which is significantly lower than the basal clinical levels of 25 pM. The detection range is 1 fM -100 pM. A decrease in resistance were observed upon addition of analyte (red line). In contrast, increase in resistance (blue line) were seen when the bioreceptors were distance from the sensor interfaces.

4 Future works

The performance of Affimer-based biosensor will be compared with whole antibody based sensor. The sensitivity, specificity and efficiency of these sensors will be compared with the gold standard technique which is the ELISA.

5 References and Acknowledgments

1. The website of the National Cancer Institute (http://www.cancer.gov)
2. http://www.cancerresearchuk.org/cancer-info/cancerstats/types/bowel
3. Tiede, C. et al., 2014. Adhiron: a stable and versatile peptide display scaffold for molecular recognition applications. *Protein Engineering Design & Selection*, 27, 145-155.